POLITECNICO DI MILANO

Facoltà di Ingegneria Industriale

Dipartimento di Ingegneria Energetica

Master of Science in Energy Engineering

Process modeling of an innovative system for power generation
by Solid Oxide Fuel Cell (SOFC) and Chemical Looping Combustion (CLC)

Advisor: Prof. Matteo Carmelo ROMANO

Co-advisor: Doct. Vincenzo SPALLINA

Thesis of:

Pasquale NOCERINO
ID 823984

Academic Year 2015 - 2016

Acknowledgements

This work has been carried out in the group of Chemical Process Intensification (**SPI**) of the Technische Universiteit of Eindhoven (**TU/e**) with the supervision of Prof. Martin van Sint Annaland, Prof. Fausto Gallucci and Doct. Vincenzo Spallina.
The author is grateful to the people that contributed to the successful conclusion of the work.

Ringraziamenti

Un sentito ringraziamento va al Professor Matteo Romano per avermi dato la possibilità di svolgere questa tesi e per aver reso possibile la mia esperienza ad Eindhoven. Grazie per i consigli e per il prezioso sostegno nel lavoro nonostante la distanza.
Ringrazio il mio supervisore ad Eindhoven, il Dott. Vincenzo Spallina. Grazie per avermi seguito costantemente e per avermi consigliato di rimanere ad Eindhoven in primavera, periodo nel quale l'Olanda da il meglio di sé.

Grazie a Marco, più di un semplice amico, il mio compagno di viaggio senza il quale non avrei mai pensato di cimentarmi in questa esperienza.
Grazie a Filippo per l'ospitalità e l'amicizia, senza Hoogstraat 167C il primo periodo ad Eindhoven sarebbe stato di gran lunga più difficile.
Grazie alle tante persone che ho conosciuto ad Eindhoven. Grazie a voi la mia esperienza è stata eccezionale. Grazie in particolare a Maria, Nadia e Vincenzo perché con voi è nato un rapporto speciale. Grazie al gruppo SMR della TU/e ed ai ragazzi della student room perché grazie a voi lavorare (e non solo) è stato un piacere.

Il ringraziamento più grande va a mio papà Filippo che non mi ha mai fatto mancare nulla nonostante le difficoltà. Sei il eroe ed il mio modello da seguire. Grazie a mia mamma Maria per l'amore che mi dona ogni giorno. Grazie a mio fratello Francesco per il sostegno e per l'esempio di forza e tenacia. Grazie ai miei nonni, Antonietta e Pasquale, che mi sono sempre vicini con il cuore nonostante la distanza.

Ringrazio tutti i compagni di università per aver reso meno faticosi questi anni al Politecnico. Grazie a Giovanni, Francesco, Marco, Pierluigi e Rocco, il gruppo studi di energetica, e grazie al gruppo studi del primo anno. Un ringraziamento particolare va a Giulio, diventato un amico davvero prezioso negli ultimi anni.

Grazie agli amici di sempre di Cremona. Grazie per il sostegno e le tante esperienze che abbiamo condiviso. Siete una certezza. Ringrazio in particolare Lorenzo che negli anni di università mi è stato vicino costantemente e con il quale ho condiviso tanti momenti importanti.

Ringrazio i tanti allenatori e compagni di calcio di questi anni. Grazie per le soddisfazioni conquistate sul campo e per lo svago che mi ha distratto dagli impegni universitari. Grazie anche per le innumerevoli baraccate. Ringrazio in particolare Daniele, amico da una vita, oltre che Filippo, Marco, Michele e Valentino, diventati grandi amici fuori dal campo.

Ultimo ma non ultimo, un ringraziamento speciale va ad Alice, la mia anima gemella. Nonostante io sia una persona piena di difetti a cui è molto difficile stare vicino, mi scegli ogni giorno. Mi sopporti e mi supporti, sempre, come è stato per la tesi ad Eindhoven. Mi dai forza e mi dai serenità anche e soprattutto nei momenti peggiori. Ciò che abbiamo è unico, è e sarà sempre il mio (e nostro) più grande successo.

Extended summary

Scope of the work

Reduction of greenhouse gas emissions is one of the most important challenges that the power industry will face in the next decades [3]. Solid Oxide Fuel Cells (SOFCs) are electrochemical devices able to convert a fuel into electricity, promoting a direct oxy-combustion in which the anode exhaust is a CO_2-rich stream that can be separated and sent to the final storage. SOFCs act as an air separation device in which O_2 migrates from cathode to anode generating electricity and therefore several configurations have been proposed for CO_2 capture [3]. However, the SOFC voltage drops to zero if the fuel is completely consumed at the anode therefore some unburnt species are always present in the anode off-gas. In the recent years, integration of CO_2 capture technologies has been presented using natural gas and coal as primary feedstock [62-65]. The majority of these studies consider hybrid cycles, where high temperature fuel cells are integrated with a simple or modified Brayton cycle, in some cases adding a bottoming cycle (e.g. based on steam or ORC). Natural gas integrated SOFC plants have demonstrated to reach already more than 60% electric efficiency, even at few kW scale [44]. Moreover, when applied to electric power generation, SOFC hybrid cycles (hundreds MW plants) can reach an impressive electrical efficiency (up to 75-78%) approaching the theoretical efficiency. In case of coal and the integrated gasification fuel cells (IGFC), a net electric efficiency of 52-54% was calculated, showing a remarkable increase with respect to state-of-the-art advanced IGCCs [66] which is reduced to about 47% (with anode off-gas oxy-combustion) up to 52% [63] when also CO_2 capture is considered.
Recently Campanari et al. [41] have presented a revised study on natural gas hybrid cycles using advanced SOFC operated at 800°C with fuel utilization of 85% and cell voltage of 0.86 V reflecting the best available technology of different manufacturers [42]. The overall performance is 75.2% where 89.5% of the gross power output is produced from the SOFC. In this case, the anode off-gas and the O_2 depleted air from the cathode outlet are burnt in a combustor to provide the heat duty to air – preheating up to the cathode inlet temperature (>730°C). The CO_2 specific emission of this plant is 273.59 gCO_2/kWh. In order to implement the CO_2 capture technology, this work proposed a system in which the anode off-gas is first sent to a HT-WGS to consume CO (more than 80%) increasing the CO_2 gas fraction and the resulting syngas is then sent to a CO_2 cryogenic unit to recovery the H_2 in the gas stream (35% content vol. dry basis) and separate the CO_2 at high purity (98.8%). This system leads to an efficiency penalty of 3.78 percentage points with a CO_2 avoidance of 82.14% (where the resulting SPECCA is 1.11 $MJ/kgCO_2$).
The integration of CLC and SOFC has been already discussed by Chen at al. [67] for an integrated coal gasification plant. The authors suggested using syngas for coal gasification at the anode of SOFC while the compressed air is sent to the cathode. The two streams, leaving the pressurized SOFC, are sent to the CLC unit where the anode off-gas is completely oxidized while the air is heated up to 950°C and sent to the gas turbine. The sensitivity analysis shows that the efficiency is in the range of 46 to 51.2%. This system presents some complexity in the heat management of the SOFC: air is fed at 424 °C with a ΔT across the cell of 475°C, extremely challenging for the

durability of the SOFC, and the syngas pre-heating to SOFC inlet temperature (800°C) is carried out using the syngas coolers.
This work proposes the integration of chemical looping combustion at atmospheric pressure for both large and small scale applications. In this work, current state-of-the-art technologies are used. Atmospheric SOFC is operated at 800°C with natural gas and the interconnected fluidized bed reactors for the CLC is working at mild conditions (500-800°C) and 1 bar. Large scale application plant is designed according to the work from Campanari et al. [41], where the fuel power input has been fixed to 100 MWth (based on natural gas LHV). For small scale application, the size of the plant is selected according to CO_2 utilization plant (145 kg/h of CO_2) which corresponds to a hybrid power plant of about 500 kWel. Both technologies, SOFC and CLC, have been already demonstrated for small size and therefore the scale-up and implementation of this technology (for CO_2 utilization) does not present any specific limitations.

Configurations of SOFC power cycles integrated with CLC

The schematic layout of one of the proposed fuel cell plants integrated with chemical looping combustion is shown in Figure 1.

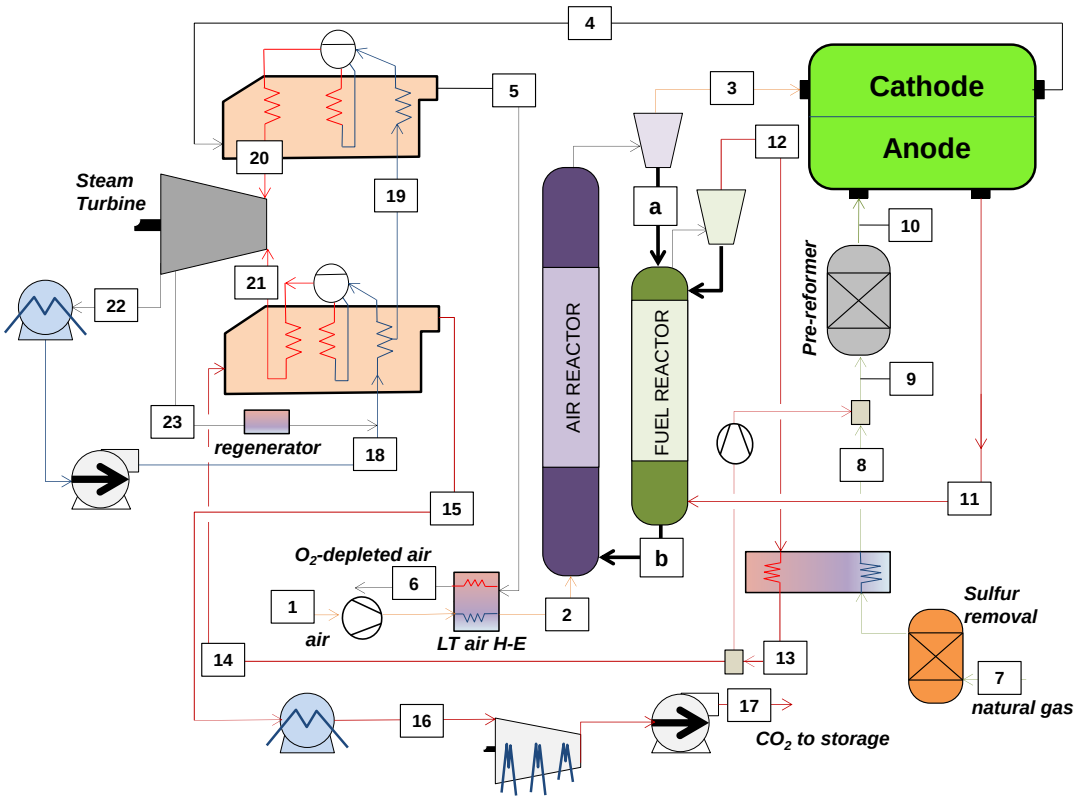

Figure 1: Schematic layout of SOFC integrated with chemical looping combustion (cold recycle).

Before the SOFC module, the natural gas pre-treatment section consists of a low temperature desulphurisation reactor to reach below 0.1 ppm of total sulphur content in order to not poison the catalyst of the SOFC. The SOFC thermal management is carried out using an Indirect Internal Reforming (IIR) with a dedicated unit prior the

cell stack where part the C_{2+} are cracked to avoid excessive temperature drop at the cell inlet. The natural gas dilution is carried out in two different ways: the first case consists of recycling part of the anode exhaust stream (hot recycle) while, in the second strategy, part of exhausts at the fuel reactor (FR) outlet (mostly CO_2 and H_2O) is recirculated to the system (cold recycle). The exhaust recycle can be obtained by a blower (as in the case of cold recycle) or by an ejector driven by higher pressure fuel (cold recycle). The dilution rate is based on a steam-to-carbon ratio (S/C) equal to 2. However, a sensitivity analysis has been carried out. At the outlet of the SOFC stack, the off-gas (#11) is sent to the fuel reactor (FR) where the oxygen carriers (#a) is reduced. The resulting gas is then cooled down to ambient temperature providing heat for the centralized steam bottoming cycle.
At the cathode side, air (#1) is sent to system from a blower and heated up to 450°C with a low temperature heat exchanger (LT air H-E). At the air reactor (AR), the OC (#b) is oxidized and the air is also heated up to the inlet temperature of SOFC above 730°C (#3). With this configuration, the O_2 content at the cathode inlet is lower than in the conventional configuration. Hot gases exiting the modules at around 800°C (#4) are sent to a heat recovery boiler to producing intermediate pressure steam (T=400°C, p=40 bar) for additional power generation. The bottoming cycle turns out to be a medium-scale steam cycle similar to waste-to-energy Rankine cycles; its thermodynamic conditions and plant configuration are consistent with those reported by Consonni et al. [45] for a similar arrangement.
The air (U_{ox}) and fuel (U_f) utilization are varied in order to obtain the temperature of the air at SOFC inlet higher than 730°C. The air flow rate is therefore varied accordingly so that the final temperature in the SOFC is equal to 800°C.

Air utilization $$U_{ox} = \frac{\dot{m}_{O_2,in} - \dot{m}_{O_2,out}}{\dot{m}_{O_2,in}}$$

Fuel utilization $$U_f = \frac{\dot{m}_{H_{2,eq,in}} - \dot{m}_{H_{2,eq,out}}}{\dot{m}_{H_{2,eq,in}}}$$

SOFC model

A co-current mono-dimensional SOFC model has been implemented to calculate the SOFC polarization losses and their effect in the design of the SOFC.
The current model is based on the following simplified assumptions:

- all the kinetics and material properties are assumed calculated at constant temperature;
- the kinetics model for the heterogeneous reactions of steam methane reforming and water gas shift is based on Numaguchi and Kikuchi equations [15];
- only current from the H_2 oxidation is considered according to the electrochemical model proposed in Aguiar et al. [16];
- concentration overpotentials in the cell are neglected as well as the mass transfer limitations from the bulk to the electrode.

A cell voltage of 0.8 V has been considered. However, a sensitivity analysis has been carried out on this parameter.

Cell Voltage $$V_{cell} = E_{rev,H_2} - \eta_{ohm}(i) - \eta_{act,an}(i) - \eta_{act,cat}(i) \quad (1)$$

Nernst Voltage $$E_{rev,H_2} = E_0^{H_2} - \frac{RT}{2F} ln\left(\frac{p_{H_2O}}{p_{H_2}\left(p_{O_2}/101325\right)^{0.5}} \right) \quad (2)$$

Ohmic Losses $$\eta_{ohm} = R_{TOT}\, i \quad (3)$$

Activation Losses

Cathode $$i_{0,cat} = \frac{RT}{n_e F} k_{cat} \cdot e^{\frac{-E_{cat}}{RT}}; \qquad i = i_{0,cat}\left[e^{\frac{n_e \eta_{act,cat} F}{RT}\alpha} - e^{\frac{n_e \eta_{act,cat} F}{RT}(\alpha - 1)} \right]$$

(4)

Anode $$i_{0,an} = \frac{RT}{n_e F} k_{an} \cdot e^{\frac{-E_{an}}{RT}}; \qquad i = i_{0,an}\left[e^{\frac{n_e \eta_{act,an} F}{RT}\alpha} - e^{\frac{n_e \eta_{act,an} F}{RT}(\alpha - 1)} \right] \quad (5)$$

$$P = i \cdot A \cdot V_{cell}$$

Chemical Looping

The chemical looping combustion process is assumed to be operated at the chemical equilibrium. Three different oxygen carriers have been considered: Cu, Fe and Ni based OC. Zirconia (ZrO_2) has been assumed as support material (60% wt. basis) and therefore its properties have been used to solve the energy balance of the system. In case of Cu-based material, both Cu_2O/Cu are considered during the reduction. In case of Fe-based OC, all the different Fe species are considered in the equilibrium (Fe_2O_3, Fe_3O_4, FeO and Fe). However, only Fe_2O_3/Fe_3O_4 pair is present in the system because of low operating temperature and the high dilution of CO_2 and H_2O of the anode off-gas at the fuel reactor inlet. In case of Ni-based OC, only Ni/NiO species participate to the redox reactions.
For the simulation of the interconnected fluidized beds, the maximum solid circulation of 20 kg/s/m^2 is considered.

Results

The details about stream thermodynamic conditions and chemical compositions for the case cold recycle are reported in Table 1. In this configuration, the cell voltage has been fixed to 0.8 V with a U_f of 81%. In the chemical looping unit, the 8% of the oxygen is consumed during the oxidation, while, in the SOFC, the U_{ox} is equal to 35%.

	T	***p***	***N***	***m***	***Composition, %mol***								
#	°C	bar	kmol/s	kg/s	**CH_4**	**C_{2+}**	**CO_2**	**H_2O**	**N_2**	**O_2**	**H_2**	**CO**	**Ar**
1	15.0	1.01	2.79	80.51	-	-	0.04	1.00	77.30	20.70	-	-	0.90
2	450.0	1.28	2.79	80.51	-	-	0.04	1.00	77.30	20.70	-	-	0.90
3	734.6	1.12	2.74	79.02	-	-	0.04	1.00	78.60	19.40	-	-	0.90
4	800.0	1.09	2.54	72.56	-	-	0.04	1.10	84.80	13.00	-	-	1.00
5	525.6	1.04	2.54	72.56	-	-	0.04	1.10	84.80	13.00	-	-	1.00

6	80.0	1.02	2.54	72.56	-	-	0.04	1.10	84.80	13.00	-	-	1.00
7	15.0	19.40	0.12	2.15	89.00	8.10	2.00	-	0.90	-	-	-	-
8	85.0	19.38	0.12	2.15	89.00	8.10	2.00	-	0.90	-	-	-	-
9	600.0	1.13	0.51	12.72	20.80	1.80	27.00	49.80	0.40	-	-	-	-
10	442.3	1.13	0.56	12.72	18.40	-	27.80	38.10	0.40	-	14.10	1.20	-
11	800.0	1.10	0.76	19.18	-	-	30.60	56.90	0.30	-	8.20	4.00	-
12	757.7	1.13	0.76	20.68	-	-	34.70	65.10	0.30	-	-	-	-
13	563.6	1.13	0.76	20.68	-	-	34.70	65.10	0.30	-	-	-	-
14	400.0	1.08	0.37	10.11	-	-	34.70	65.10	0.30	-	-	-	-
15	87.9	1.06	0.37	10.11	-	-	34.70	65.10	0.30	-	-	-	-
16	30.0	1.06	0.13	5.73	-	-	99.00	0.20	0.80	-	-	-	-
17	37.6	110.0	0.13	5.73	-	-	99.00	0.20	0.80	-	-	-	-
18	110.0	5.60	0.61	10.96	-	-	-	100.0	-	-	-	-	-
19	201.2	40.00	0.52	9.44	-	-	-	100.0	-	-	-	-	-
20	398.5	36.67	0.52	9.44	-	-	-	100.0	-	-	-	-	-
21	398.5	36.67	0.12	2.20	-	-	-	100.0	-	-	-	-	-
22	32.2	0.05	0.61	10.97	-	-	-	100.0	-	-	-	-	-
23	152.2	3.79	0.04	0.68	-	-	-	100.0	-	-	-	-	-
a	734.6	1.28	9.18	926.8	*weight fraction*: CuO 40%; ZrO_2 60%								
b	757.7	1.28	9.08	925.34	*weight fraction*: CuO 38.6%; Cu_2O 1.4%; ZrO_2 60%								

Table 1: Thermodynamic conditions and chemical compositions of the main streams (referred to Figure 1).

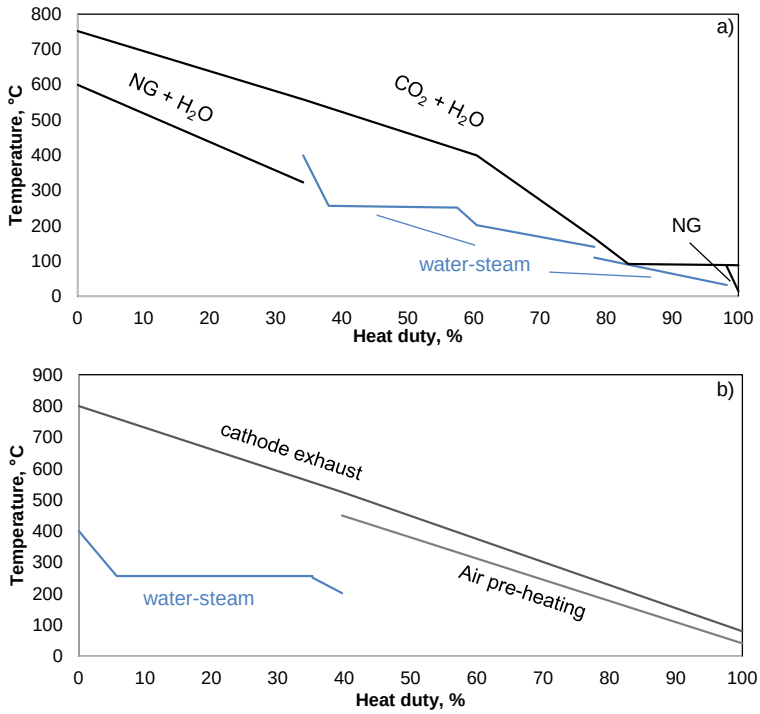

Figure 2: Cumulative grant curves for the heat recovery: a) FR exhaust cooling; b) cathode exhaust cooling.

More than 85% of the gross electric power is coming from the SOFC for the different cases presented in Table 2. These results are mostly from the high fuel utilization and cell voltage used. Compared to the other configurations (with and without CO_2 capture), the CLC-based hybrid cycle always show a higher gross electric power due to the higher steam turbine production. However, the higher air flow rate required (for the case at 0.8 V in Table 2) for the case with CLC increases also the auxiliaries consumptions (forced draft fan). The lower efficiencies of the SOFC-CLC respect to

the benchmark hybrid cycle are due to the CO_2 compression up to 110 bar for the final storage. When comparing hybrid SOFC integrated with CO_2 capture technology (CLC vs WGS/cryogenic separation), the net electric efficiency increases up to 2 percentage points. Moreover, the carbon capture rate (CCR) is 100% in case of CLC while only 82% can be achieved in case of cryogenic separation due to the presence of some CO and CO_2 in the cryogenic off-gas. In terms of specific primary energy consumption for CO_2 avoided (SPECCA), the combination of SOFC and CLC is more advantageous (0.3 vs 1.11 MJ/kgCO_2).
In case of hot recycle configuration is considered, the result does not change significantly. Since the syngas dilution is carried out by recirculating the anode off-gas, the single passage fuel utilization is 58% (overall 81% as in the other case). In terms of performance, a slightly improvement is obtained due to the lower auxiliaries consumptions (no CO_2-H_2O recirculation blower is required). However, due to the off-gas recirculation, the anode-SOFC inlet flow rate increases from 12.72 kg/s (#9 in Figure 1) to 20.61 kg/s.

Plant Performance		Cell Voltage 0.8 V			Cell voltage 0.86 V		
		Hybrid SOFC	SOFC	SOFC	Hybrid SOFC[41]	Hybrid SOFC[41]	SOFC
CO_2 capture			CLC cold-rec	CLC hot-rec	-	WGS+ cryogenic	CLC cold-rec
Natural Gas, inlet	MW_{th}	100	100	100	100	100	100
SOFC, AC power	MW_E	56.40	60.50	60.53	68.06	68.06	69.8
cell voltage	V	0.8	0.8	0.8	0.86	0.86	0.86
Fuel Utilization, U_f		75.7%	81.3%	81.3%	85.0%	85.0%	87.3%
Air Utilization, O_{ox}		69.7%	38.0%	39.5%	21.8%	20%	58.7%
Steam Turbine	MW_E	12.42	10.84	10.69	8.06	7.68	7.90
aux FD Fan	MW_E	-0.10	-2.29	-2.22			-1.59
aux water pumps	MW_E	-0.09	-0.08	-0.08	-0.91	-4.24	-0.06
aux CO_2 compressors	MW_E		-1.85	-1.85			-1.85
aux CO_2/H_2O rec blower	MW_E		-0.18	-			-0.18
Gross electric power	MW_E	68.82	71.34	71.22	76.12	75.74	77.7
Net electric power	MW_E	68.20	66.76	66.91	75.2	71.49	73.90
net el. efficiency, LHV	%	68.2%	66.7%	66.8%	75.2%	71.5%	73.9%
CO_2 specific emissions, E_{CO2}	kg MWh^{-1}	301.92	0	0	273.59	48.86	0.00
CCR	%	-	100%	100	-	82%	100%
SPECCA	MJ kg_{CO2}^{-1}	-	0.38	0.34	-	1.11	0.31

Table 2: Energy balance of the systems and comparison with benchmark technologies.

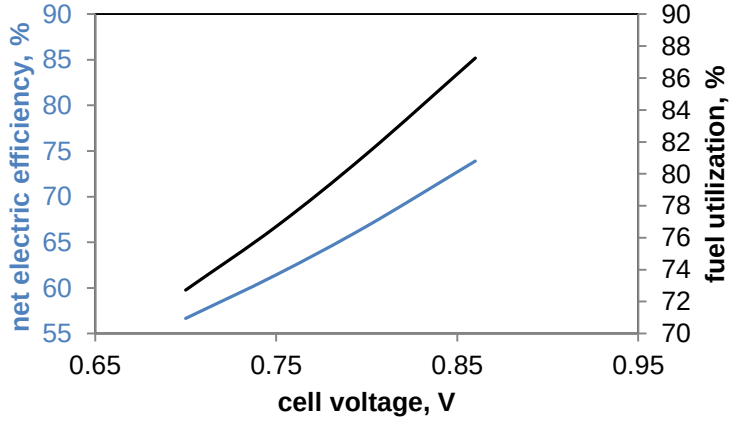

Figure 3: Net electric efficiency and fuel utilization curves by varying the cell voltage.

The cell voltage plays an important role in the overall performance of the plant due to the high power share associated to the SOFC. Increasing the cell voltage, more electricity is produced from the SOFC ($P_{SOFC} = i_{cell} \cdot A \cdot V_{cell}$), where i_{cell} is the current density (A/m^2) and A is the electrode surface. At increased cell voltage, higher fuel utilization is required to keep the SOFC at 800°C. Increasing the cell voltage, less heat is available at the electrode and therefore higher fuel conversion is required.
Based on the SOFC model, an average current density of 2915.4 A/m^2 is calculated for the cold recycle case. The molar concentration and the overpotential losses along the cell are showed in Figure 4.

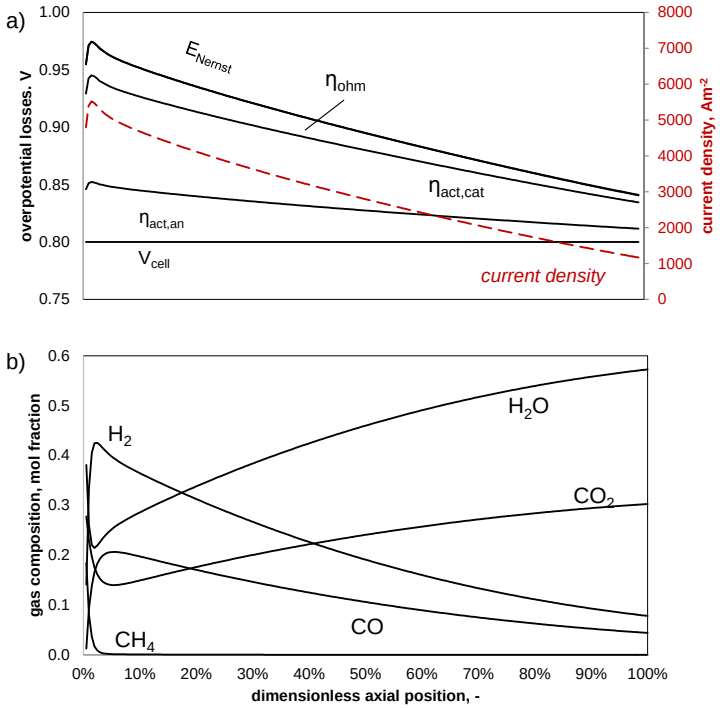

Figure 4: a) overpotential losses profile and b) and gas composition along the SOFC for the system in Figure 1 operated at 0.8 V.

Effect of steam-to-carbon ratio (S/C)

In the hybrid SOFC-CLC, the natural gas humidification is not carried out using steam from the steam cycle but either the off-gas (hot recycle) or the FR exhausts (cold recycle) recirculation. Therefore the increase of the S/C does not penalize the performance of the thermodynamic cycle.
In case of cold recycle configuration, an increase of S/C from 2 to 3 corresponds to an increase in the overall net electric efficiency from 66.76% to 68.07%. Due to the higher amount of gasses at the anode side, the U_f slightly increases (from 81% to 83.4%) in order to maintain the fuel cell at 800 °C increasing the SOFC power production as well as the CO_2-H_2O blower consumption (+20%).
In case of hot recycle, since everything occurs within the SOFC module, the system performance does not change. However, due to the higher amount of H_2O required at the anode inlet, the fuel flow rate increases up to 39.5 kg/s (at S/C equal to 3).

Sensitivity on the oxygen carriers

The solid circulation between the AR and FR is used to control the temperature of the air at the cathode inlet. The higher is the solid circulation rate (Gs), the closer are the temperature of the gases leaving the AR and FR (dashed line in Figure 4). In case of Cu-based oxygen carrier, the temperature at the fuel reactor is always higher than in the air reactor due to the fact that also the reduction is a fairly strong exothermic reaction. Therefore, high solid circulation is always required in order to reach the temperature higher than 730°C at the AR outlet.

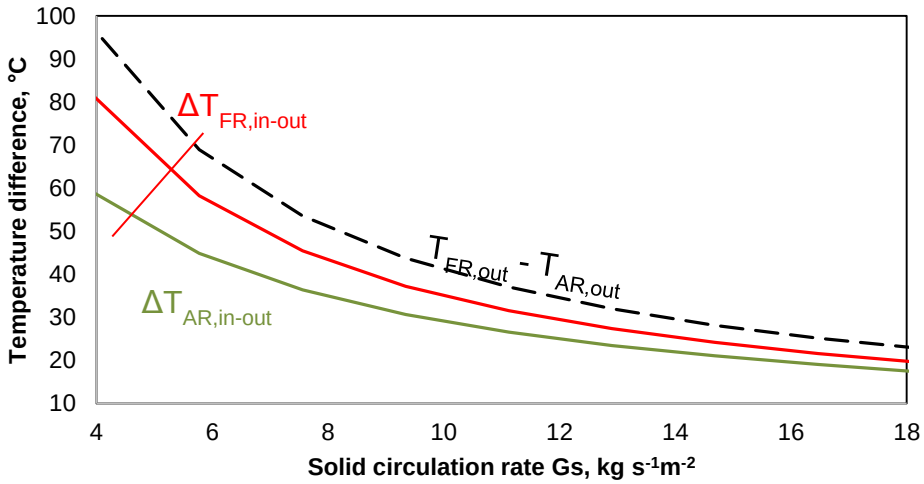

Figure 5: Temperature differences of the gases leaving the chemical looping reactors.

When using Fe-based OC, the amount of solid to circulate between AR and FR can decrease also to 200 kg/s (corresponding to 3.94 kg/s/m^2) while, in case of Ni, the amount of solid required is 886.5 kg/s (corresponding to 17.4 kg/s/m^2).
Based on this sensitivity, the pair Fe_3O_4/Fe_2O_3 OC results to be the best option in order to decrease the chemical looping reactors size and cost. However, the kinetics of Ni and Cu based OC is usually faster than in the case of Fe-based, especially at intermediate temperature (500-800°C) which is the operating range of the hybrid SOFC-CLC. Therefore the selection of the oxygen carrier and the reactor design needs to be properly carried out.

Small scale application performance

As already anticipated, SOFCs have been commercialize in the last years in the range of 100-1000 kW power size from CHP applications. For CLC, the demonstration as already reached 1 MWth scale [68]. Therefore, the combination of both systems can also be considered for small scale application as in the case of CO_2 production plant (typically higher than 145 kg/h). In this case, a different arrangement should be considered for the heat recovery. The thermal input required is 712 kWth (corresponding to a NG feeding flow rate of 55.13 kg/h). An organic Rankine cycle (ORC) can be adopted for the heat recovery of the system (using Toluene as operating fluid, as in the case of Triogen generator [59]). In this case, the SOFC power output is 450 kWel while the ORC would provide about 50 kWel (based on turbine isentropic

efficiency of 85% inlet turbine pressure of 32 bar and maximum turbine inlet temperature of 300°C) which are produced from the overall heat duty of 183.6 kWth. Such system can also be considered without ORC producing IP-LP steam for industrial processes.

Conclusions

This work presented the thermodynamic analysis of SOFC power cycles designed for electricity generation using natural gas as a fuel integrated with CLC. The plant has been described and analysed in detail. The hybrid cycle is based on atmospheric SOFC following the state-of-the-art SOFC and CLC process, reaching a net electrical efficiency of 66.7% (with SPECCA of 0.34-0.38 $MJ_{LHV}/kgCO_2$). Compared to the conventional hybrid cycle without CO_2, capture the efficiency penalty is exclusively associated to the CO_2 compression. Very similar performance are obtained by varying the SOFC humidification system (cold and hot recycle), as well as the S/C. In case higher cell voltage (0.86 V) is considered the efficiency rises of 6 percentage points showing also a reduction in SPECCA compared with hybrid cycle with cryogenic CO_2 separation (0.3 vs 1.1 MJLHV/kgCO2) due to the combination of high CCR (+18%) and higher electric efficiency (+2.5%). By using Cu-based OC, high solid circulation (about 20 $kg/s/m^2$) is required to heat-up the air stream to the SOFC inlet temperature. However, the solid circulation significantly decreases by using Fe-based oxygen carrier due the different heat of reaction. Finally, the integrated SOFC plant with CLC also shows very promising performance at small scale where all the single technologies have been already developed with the intention of producing pure CO_2 for other processes and applications.

[70] is based on the work of this thesis. The extended summary and the abstract refer to [70].

Riassunto esteso

Scopo del lavoro

La riduzione delle emissioni di gas serra è una delle sfide più importanti che l'industria dell'energia dovrà affrontare nei prossimi decenni [3]. Le celle a combustibile ad ossido solido (SOFC) sono dispositivi elettrochimici capaci di convertire combustibile in elettricità, promuovendo un ossi-combustione diretta in cui il flusso in uscita dall'anodo è ricco di CO_2 che può essere separata ed inviata allo stoccaggio finale. Le SOFC agiscono come un separatore in cui l'ossigeno migra dal catodo all'anodo generando elettricità. Sono state proposte diverse configurazioni per la cattura della CO_2 [3]. Alcune specie incombuste sono sempre presenti nel flusso in uscita dall'anodo in quanto, per consumare completamente il combustibile, sarebbe necessario portare a zero la tensione della SOFC. Negli ultimi anni, sono state applicate tecnologie di cattura della CO_2 integrate con sistemi che utilizzano gas naturale e carbone come materia primaria [62-65]. La maggior parte di questi studi considera cicli ibridi in cui le celle a combustibile ad alta temperatura sono integrate con un ciclo Brayton semplice o modificato o, invece, aggiungendo un ciclo 'bottoming' (ad esempio, cicli a vapore o ORC). E' stato dimostrato che impianti SOFC integrati a gas naturale sono in grado di raggiungere già oltre il 60% di efficienza elettrica, anche a pochi kW [44]. Inoltre, se applicato alla produzione di energia elettrica in larga scala, i cicli ibridi SOFC (a centinaia di MW) possono raggiungere un'impressionante efficienza elettrica teorica (fino a 75-78%). Nel caso di integrazione di celle a combustibile con processi di gassificazione (IGFC), è stato calcolato un rendimento elettrico netto del 52-54%, mostrando un notevole incremento rispetto allo stato dell'arte avanzata degli IGCCs [66] che si riduce a circa 47% (con l'ossi-combustione del flusso in uscita dall'anodo) [63].
Recentemente Campanari et al. [41] hanno presentato uno studio sui cicli ibridi a gas naturale utilizzando una SOFC avanzata a 800 ° C con fattore di utilizzo del combustibile del 85% e tensione di cella di 0.86 V, condizioni operative che riflettono le migliori tecnologie disponibili dai diversi produttori [42]. La performance complessiva è del 75.2%, dove l'89.5% della potenza lorda è prodotto dalla SOFC. In questo caso, il flusso in uscita dall'anodo ed il flusso di aria impoverita dall'ossigeno proveniente dal catodo sono bruciati in un combustore per fornire all'aria il calore necessario al pre-riscaldamento fino alla temperatura di ingresso al catodo (> 730 °C). Le emissioni specifiche di CO_2 di questo impianto sono 273.6 gCO_2/kWh. Al fine di implementare la tecnologia di cattura della CO_2, in [41] viene proposto un sistema in cui il flusso in uscita dall'anodo viene prima inviato ad un HT-WGS in modo da consumare la CO presente (più dell'80%) ed aumentare la frazione di CO_2; il syngas risultante viene poi inviato ad un'unità criogenica in grado di recuperare l'idrogeno presente nella corrente di gas (35% vol. su base secca) e separare CO_2 ad elevata purezza (98.8%). Questo sistema porta ad una perdita di efficienza di 3.78 punti percentuali, con un fattore di cattura della CO_2 del 82.14% ed uno SPECCA uguale a 1.11 $MJ/kgCO_2$.
L'integrazione di SOFC e CLC è già stata discussa da Chen et al. [67] per un impianto di gassificazione del carbone. Gli autori hanno proposto di usare syngas da gassificazione del carbone per alimentare l'anodo della SOFC e inviare l'aria

compressa al catodo. Le due correnti in uscita dalla SOFC pressurizzata vengono inviate all'unità CLC dove il flusso in uscita dall'anodo è completamente ossidato mentre l'aria viene riscaldata fino a 950 °C ed inviata alla turbina a gas. L'analisi di sensibilità mostra che l'efficienza del sistema si attesta nell'intervallo 46-51%. Questo sistema presenta una certa complessità nella gestione del calore della SOFC: l'aria viene alimentata a 424 ° C con una differenza di temperatura attraverso la cella di 475 °C, estremamente alta per la durabilità della SOFC, ed il pre-riscaldamento del syngas fino alla temperatura di ingresso alla SOFC (800 ° C) viene effettuato attraverso syngas coolers.
Questa tesi propone l'integrazione alla SOFC di un processo di Chemical Looping Combustione (CLC) a pressione atmosferica per applicazioni sia di grande che piccola scala. La SOFC a pressione atmosferica lavorerà a 800 ° C con gas naturale mentre i reattori interconnessi a letto fluido della CLC lavoreranno in condizioni blande (500-800 °C e 1 bar). L'impianto per applicazioni di larga-scala è progettato in contrapposizione al lavoro di Campanari et al. [41], in cui il combustibile alimentato è stato fissato a 100 MWth (basata sul PCI del gas naturale). Per l'applicazione su piccola scala, l'impianto è invece dimensionato sulla produzione di CO_2 (145 kg/h) che corrisponderà ad una centrale ibrida di circa 500 kWel. Entrambe le tecnologie, SOFC e CLC, sono già disponibile per applicazioni su piccola scala: l'implementazione di queste tecnologie per l'utilizzo della CO_2 non avrà quindi alcuna limitazione specifica.

Impianti di potenza con integrazione di SOFC e CLC

Uno degli schemi d'impianto con integrazione di SOFC e CLC è mostrato in Figura 1.

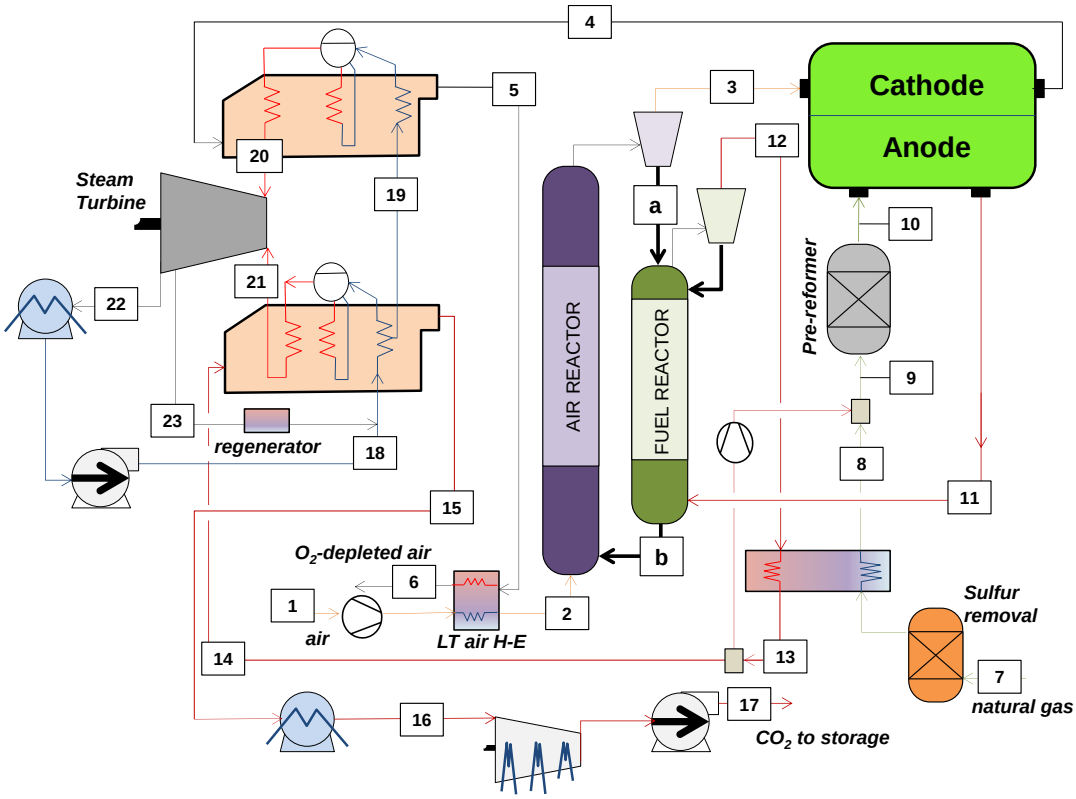

Figura 1: Schema d'impianto integrato SOFC-CLC, caso con ricircolo freddo.

Prima della SOFC è presente una sezione di pre-trattamento del gas costituita da un reattore a bassa temperatura di desolforazione per raggiungere valori di contenuto totale di zolfo inferiori alle 0.1 ppm in modo da non avvelenare il catalizzatore della SOFC. Il bilanciamento termico della SOFC prevede un reforming interno indiretto (IIR) con un'unità specifica prima della cella in modo da far reagire le specie C_{2+} ed evitare una caduta eccessiva della temperatura all'ingresso della cella (reazioni endotermiche). La diluizione del gas naturale può essere effettuata in due modi diversi: nel primo caso, si ha il ricircolo di parte del gas in uscita dal lato anodico (ricircolo caldo) mentre, nella seconda versione, viene ricircolato parte del flusso in uscita dal FR della CLC, flusso ricco di CO_2 e H_2O (ricircolo freddo). Il ricircolo ed il miscelamento possono avvenire grazie ad un fan (caso ricircolo freddo) o con un eiettore alimentato con combustibile ad alta pressione (caso ricircolo caldo). La diluizione è basata su un rapporto di vapore-carbonio (S/C) pari a 2. Tuttavia, in seguito, è effettuata un'analisi di sensitività su questo parametro operativo. All'uscita della SOFC, l'off-gas (#11) viene inviato al FR dove l'OC (#a) viene ridotto. Il gas risultante viene quindi raffreddato fino a temperatura ambiente fornendo calore al ciclo bottoming a vapore.
L'aria (#1) viene inviata al lato catodo grazie ad un fan e pre-riscaldata fino a 450 ° C con uno scambiatore di calore a bassa temperatura (LT dell'aria H-E). Nell'AR, l'OC (#b) viene ossidato mentre l'aria viene riscaldato alla temperatura di ingresso della SOFC, ovvero sopra i 730 ° C (# 3). Con questa configurazione, il contenuto di O_2 in ingresso al catodo è inferiore rispetto a quello della configurazione convenzionale. I gas caldi (#4) uscenti a 800 °C vengono inviati ad una caldaia a recupero di calore per la produzione di vapore a pressione intermedia (T = 400 ° C, p = 40 bar) per la generazione di energia supplementare. Il ciclo a vapore è un ciclo a media-scala con prestazioni simili a quelle dei cicli Rankine finalizzati al waste-to-energy; le sue condizioni termodinamiche e la configurazione dell'impianto sono coerenti con quelli riportati da Consonni et al. [45] per una disposizione simile.
Il fattore di utilizzo dell'aria (U_{ox}) e del combustibile (U_f) sono variati in modo da ottenere la temperatura dell'aria in ingresso alla SOFC superiore a 730 ° C. La portata dell'aria è variata di conseguenza in modo che la temperatura finale della SOFC sia pari a 800 °C.

Fattore di utilizzo dell'aria $$U_{ox} = \frac{\dot{m}_{O_2,in} - \dot{m}_{O_2,out}}{\dot{m}_{O_2,in}}$$

Fattore di utilizzo del combustibile $$U_f = \frac{\dot{m}_{H_2,eq,in} - \dot{m}_{H_2,eq,out}}{\dot{m}_{H_2,eq,in}}$$

Modello della SOFC

Al fine di calcolare le perdite di potenziale nella cella ed il loro effetto sulla progettazione della stessa, è stato implementato un modello della SOFC mono-dimensionale equicorrente.
Il modello è basato sulle seguenti assunzioni:

- tutte le cinetiche e le proprietà dei materiali sono calcolate considerando la temperatura della cella costante;

- il modello cinetico per le reazioni di steam methane reforming e water gas shift è basato sulle equazioni di Numaguchi e Kikuchi [15];
- è considerato solamente il contributo di corrente dovuto all'ossidazione dell'H_2, in accordo con il modello elettrochimico proposto da Aguiar et al. [16];
- le perdite di concentrazione sono state trascurate, così come le limitazioni allo scambio di massa fra il flusso principale e l'elettrodo.

E' stata considerata una tensione di cella di 0.8 V. Tuttavia, sarà condotta un'analisi di sensitività su questo parametro operativo.

Tensione della cella $$V_{cell} = E_{rev,H_2} - \eta_{ohm}(i) - \eta_{act,an}(i) - \eta_{act,cat}(i) \quad (1)$$

Potenziale di Nernst $$E_{rev,H_2} = E_0^{H_2} - \frac{RT}{2F} ln\left(\frac{p_{H_2O}}{p_{H_2}\left(p_{O_2}/101325\right)^{0.5}} \right) \quad (2)$$

Perdite ohmiche $$\eta_{ohm} = R_{TOT}\, i \quad (3)$$

Perdite di attivazione

Catodo $$i_{0,cat} = \frac{RT}{n_e F} k_{cat} \cdot e^{\frac{-E_{cat}}{RT}}; \qquad i = i_{0,cat}\left[e^{\frac{n_e \eta_{act,cat} F}{RT}\alpha} - e^{\frac{n_e \eta_{act,cat} F}{RT}(\alpha-1)} \right] \quad (4)$$

Anodo $$i_{0,an} = \frac{RT}{n_e F} k_{an} \cdot e^{\frac{-E_{an}}{RT}}; \qquad i = i_{0,an}\left[e^{\frac{n_e \eta_{act,an} F}{RT}\alpha} - e^{\frac{n_e \eta_{act,an} F}{RT}(\alpha-1)} \right] \quad (5)$$

$$P = i \cdot A \cdot V_{cell}$$

Chemical Looping

Si considera il processo di chemical looping in equilibrio chimico. Sono stati considerati tre diversi OC: a base Cu, Fe e Ni. E' stato assunto come materiale di supporto lo Zirconia (ZrO2) con una percentuale in peso del 60%. Le sue proprietà sono state utilizzate per risolvere il bilancio energetico del sistema. Nel caso di OC a base di Cu, sono stati considerati per la riduzione sia Cu_2O che Cu. Nel caso di OC a base di Fe, sono state considerate in equilibrio tutte le specie che si riferiscono a Fe (Fe2O3, Fe3O4, FeO e Fe). Tuttavia, a causa delle basse temperature di esercizio e dell'elevata diluizione del flusso in uscita dall'anodo (ricco di CO_2 e H_2O), sarà presente solo la coppia Fe_2O_3/Fe_3O_4. Nel caso di OC a base Ni, le uniche specie a partecipare alla riduzione sono Ni/NiO. Per i letti fluidizzati interconnessi, il fattore di ricircolo massimo considerato è stato 20 kg/s/m^2.

Risultati

In Tabella 1 sono riportate, in dettaglio, le condizioni termodinamiche e le composizioni chimiche di tutti i flussi nel caso SOFC-CLC ricircolo freddo (Figura

1). In questa configurazione, la tensione di cella è fissata a 0.8 V con un fattore di utilizzo del combustibile del 81%. Nell'unità di chemical looping, l'8% dell'ossigeno è consumato durante l'ossidazione mentre, nella SOFC, il fattore di utilizzo dell'ossidante uguale al 35%.

	T	***p***	***N***	***m***	***Composizione, %mol***								
#	°C	bar	kmol/s	kg/s	**CH_4**	**C_{2+}**	**CO_2**	**H_2O**	**N_2**	**O_2**	**H_2**	**CO**	**Ar**
1	15.0	1.01	2.79	80.51	-	-	0.04%	1.00%	77.30%	20.70%	-	-	0.90%
2	450.0	1.28	2.79	80.51	-	-	0.04%	1.00%	77.30%	20.70%	-	-	0.90%
3	734.6	1.12	2.74	79.02	-	-	0.04%	1.00%	78.60%	19.40%	-	-	0.90%
4	800.0	1.09	2.54	72.56	-	-	0.04%	1.10%	84.80%	13.00%	-	-	1.00%
5	525.6	1.04	2.54	72.56	-	-	0.04%	1.10%	84.80%	13.00%	-	-	1.00%
6	80.0	1.02	2.54	72.56	-	-	0.04%	1.10%	84.80%	13.00%	-	-	1.00%
7	15.0	19.40	0.12	2.15	89.00%	8.10%	2.00%	-	0.90%	-	-	-	-
8	85.0	19.38	0.12	2.15	89.00%	8.10%	2.00%	-	0.90%	-	-	-	-
9	600.0	1.13	0.51	12.72	20.80%	1.80%	27.00%	49.80%	0.40%	-	-	-	-
10	442.3	1.13	0.56	12.72	18.40%	-	27.80%	38.10%	0.40%	-	14.10%	1.20%	-
11	800.0	1.10	0.76	19.18	-	-	30.60%	56.90%	0.30%	-	8.20%	4.00%	-
12	757.7	1.13	0.76	20.68	-	-	34.70%	65.10%	0.30%	-	-	-	-
13	563.6	1.13	0.76	20.68	-	-	34.70%	65.10%	0.30%	-	-	-	-
14	400.0	1.08	0.37	10.11	-	-	34.70%	65.10%	0.30%	-	-	-	-
15	87.9	1.06	0.37	10.11	-	-	34.70%	65.10%	0.30%	-	-	-	-
16	30.0	1.06	0.13	5.73	-	-	99.0%	0.20%	0.80%	-	-	-	-
17	37.6	110.0	0.13	5.73	-	-	99.0%	0.20%	0.80%	-	-	-	-
18	110.0	5.60	0.61	10.96	-	-	-	100%	-	-	-	-	-
19	201.2	40.00	0.52	9.44	-	-	-	100%	-	-	-	-	-
20	398.5	36.67	0.52	9.44	-	-	-	100%	-	-	-	-	-
21	398.5	36.67	0.12	2.20	-	-	-	100%	-	-	-	-	-
22	32.2	0.05	0.61	10.97	-	-	-	100%	-	-	-	-	-
23	152.2	3.79	0.04	0.68	-	-	-	100%	-	-	-	-	-
a	734.6	1.28	9.18	926.8	*Frazione in massa*: CuO 40%; ZrO_2 60%								
b	757.7	1.28	9.08	925.34	*Frazione in massa*: CuO 38.6%; Cu_2O 1.4%; ZrO_2 60%								

Tabella 1: Condizioni termodinamiche e composizioni chimiche dei flussi principali (riferiti alla Figura 1).

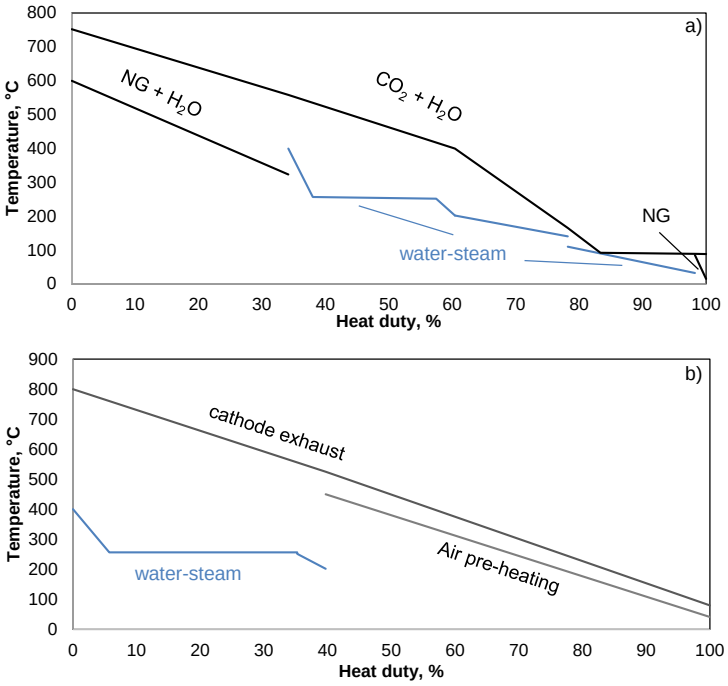

Figura 2: Curve di scambio termico: a) raffreddamento del flusso in uscita dal FR; b) raffreddamento del flusso in uscita dal catodo.

Più dell'85% della potenza elettrica lorda è prodotta dalla SOFC nei diversi casi presentati in Tabella 2. Questo risultato deriva per lo più dal fatto che alto è il fattore di utilizzo del combustibile come alta è la tensione di cella imposta. Rispetto ad altre configurazioni (con o senza cattura della CO_2), il ciclo ibrido basato su CLC mostra sempre alta produzione di potenza elettrica lorda grazie anche al ciclo a vapore. Tuttavia, l'alta portata di aria richiesta con la CLC fa aumentare il consumo degli ausiliari. Le più basse efficienze dei sistemi integrati SOFC-CLC rispetto al caso ibrido di riferimento sono dovute esclusivamente alla compressione della CO_2 fino a 110 bar per lo stoccaggio finale. Confrontando questi risultati con quelli di altri sistemi ibridi con integrazione di SOFC con tecnologie di cattura della CO_2 (CLC vs WGS/sistema di separazione criogenico), si può verificare come l'efficienza elettrica netta aumenti di circa 2 punti percentuali. Inoltre, nel caso con CLC, il CCR risulta uguale al 100% mentre nel caso con sistema di separazione criogenico il CCR si attesta all'82% a causa della presenza di CO e CO_2 nei flussi in uscita. Per quanto riguarda l'energia primaria specifica consumata per la CO_2 evitata (SPECCA), la combinazione SOFC e CLC è più vantaggiosa (0.3 vs 1.11 MJ/kgCO_2).
Nel caso di ricircolo caldo, le prestazioni non cambiano in modo rilevante. Dal momento che la diluizione del syngas avviene ricircolando parte del flusso in uscita dall'anodo, il fattore di utilizzo del combustibile del singolo passaggio risulta uguale al 58% (globale uguale al 81%, più o meno uguale al caso precedente). Si ha un lieve miglioramento in termini di prestazioni dovuto alla diminuzione dei consumi degli ausiliari (non è richiesto un compressore aggiuntivo per il ricircolo di CO_2-H_2O). Tuttavia, a causa del ricircolo del flusso in uscita dall'anodo, la portata in ingresso all'anodo aumenta da 12.72 kg/s (#9 in Figura 1) a 20.61 kg/s.

Plant Performance			Cell Voltage 0.8 V			Cell voltage 0.86 V		
		Hybrid SOFC	SOFC	SOFC	Hybrid SOFC[41]	Hybrid SOFC[41]	SOFC
CO_2 capture			CLC cold-rec	CLC hot-rec	-	WGS+ cryogenic	CLC cold-rec
Natural Gas, inlet	MW_{th}	100	100	100	100	100	100
SOFC, AC power	MW_E	56.40	60.50	60.53	68.06	68.06	69.8
cell voltage	V	0.8	0.8	0.8	0.86	0.86	0.86
Fuel Utilization, U_f		75.7%	81.3%	81.3%	85.0%	85.0%	87.3%
Air Utilization, O_{ox}		69.7%	38.0%	39.5%	21.8%	20%	58.7%
Steam Turbine	MW_E	12.42	10.84	10.69	8.06	7.68	7.90
aux FD Fan	MW_E	-0.10	-2.29	-2.22			-1.59
aux water pumps	MW_E	-0.09	-0.08	-0.08	-0.91	-4.24	-0.06
aux CO_2 compressors	MW_E		-1.85	-1.85			-1.85
aux CO_2/H_2O rec blower	MW_E		-0.18	-			-0.18
Gross electric power	MW_E	68.82	71.34	71.22	76.12	75.74	77.7
Net electric power	MW_E	68.20	66.76	66.91	75.2	71.49	73.90
net el. efficiency, LHV	%	68.2%	66.7%	66.8%	75.2%	71.5%	73.9%
CO_2 specific emissions, E_{CO2}	kg MWh^{-1}	301.92	0	0	273.59	48.86	0.00
CCR	%	-	100%	100	-	82%	100%
SPECCA	MJ kg_{CO2}^{-1}	-	0.38	0.34	-	1.11	0.31

Tabella 2: Bilancio energetico dei sistemi e confronto con le tecnologie di riferimento.

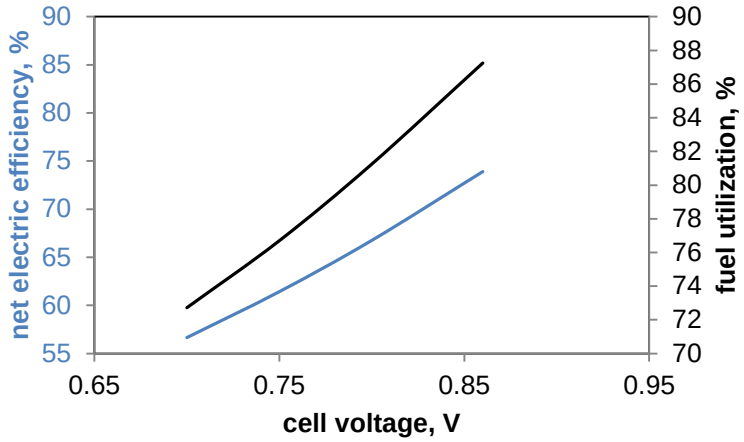

Figura 3: Variazione dell'efficienza elettrica netta e del fattore di utilizzo del combustibile variando la tensione di cella imposta.

La tensione di cella gioca un ruolo molto importante per le prestazioni globali dell'impianto a causa dell'alta frazione di potenza prodotta dalla SOFC. Aumentando la tensione di cella, la SOFC produce più potenza ($P_{SOFC} = i_{cell} \cdot A \cdot V_{cell}$, dove i_{cell} rappresenta la densità di corrente [A/m^2] e A la superficie di scambio). Un'altra conseguenza dell'aumento della tensione di cella è l'aumento del fattore di utilizzo del combustibile necessario per mantenere la temperatura in uscita dalla cella a 800°C.

Grazie al modello della SOFC, è stato possibile calcolare una densità di corrente media della cella di 2915.4 A/m^2 per il caso con ricircolo freddo. In Figura 4 sono mostrati gli andamenti delle concentrazioni molari e delle perdite di tensione nella cella.

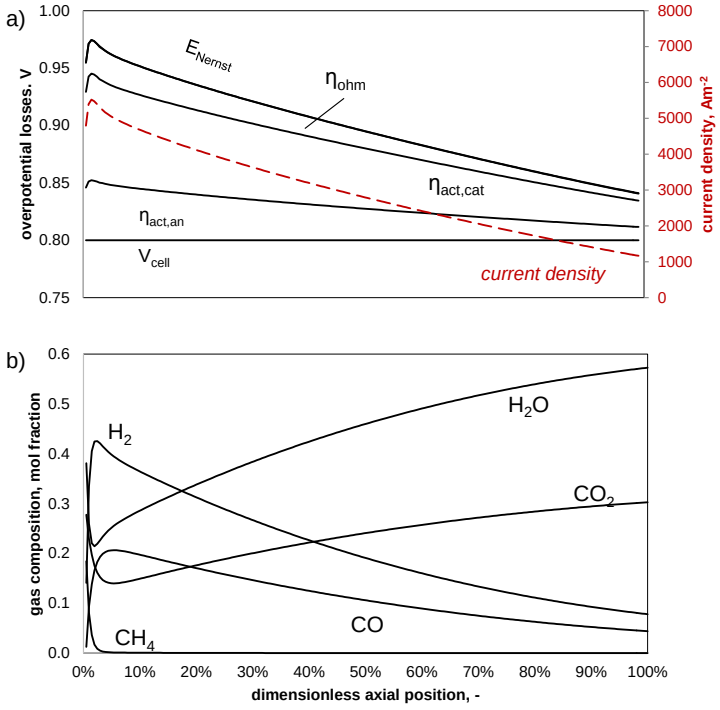

Figura 4: a) profilo delle perdite di tensione e della densità di corrente e b) profilo delle composizioni molari lato anodo, caso ricircolo freddo con tensione imposta uguale a 0.8 V.

Effetto del rapporto S/C

Nel sistema ibrido SOFC-CLC, il vapore non è fornito al gas naturale dal ciclo a vapore ma ricircolando parte del flusso in uscita dall'anodo (ricircolo caldo) o parte del flusso in uscita dal FR (ricircolo freddo). Di conseguenza, l'aumento di S/C non comporta una penalizzazione per le prestazioni termodinamiche del sistema.
Nel caso con ricircolo freddo, un aumento di S/C da 2 a 3 corrisponde ad un aumento dell'efficienza elettrica netta globale da 66.76% a 68.07%. Questo lieve miglioramento delle prestazioni è dovuto all'aumento della quantità di gas lato anodo con conseguente aumento del fattore di utilizzo del combustibile (da 81% a 83.4%)al fine di mantenere constante la temperatura in uscita dalla SOFC (800 °C). Questo effetto è più rilevante rispetto all'aumento del consumo del fan di ricircolo (+20%).
Nel caso con ricircolo caldo, le prestazioni globali del sistema non cambiano perché i cambiamenti riguardano solo il componente SOFC. Tuttavia, a causa dell'aumento del vapore richiesto, la portata in ingresso all'anodo aumenta fino a 39.5 kg/s (con S/C uguale a 3).

Analisi di sensibilità sull'OC

Il ricircolo di solidi fra AR e FR della CLC è funzionale al mantenimento della temperatura dell'aria in ingresso al catodo. Più sarà alto il fattore di ricircolo dei solidi fra i reattori (Gs), più vicine saranno le temperature dei flussi in uscita dai due reattori (linea tratteggiata in Figura 4). Nel caso di Cu come base per l'OC, la temperature in uscita dal FR sarà sempre più alta rispetto a quella . Therefore, high solid circulation is always required in order to reach the temperature higher than 730°C at the AR outlet.

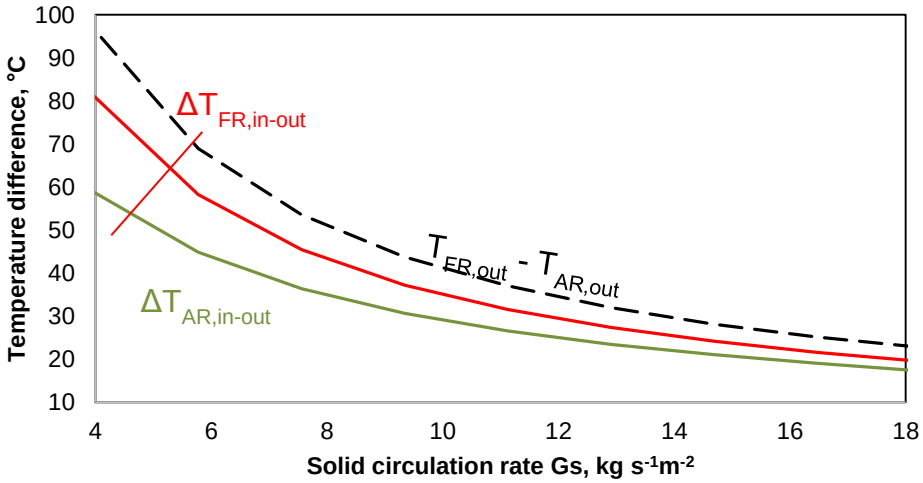

Figura 5: Differenza di temperatura del flusso a cavallo di FR e AR, caso Cu.

Usando OC a base Fe, la quantità di solidi ricircolati tra AR e FR può diminuire anche fino a 200 kg/s (condizione che corrisponde ad un fattore di ricircolo uguale a 3.94 kg/s/m^2) mentre, con OC a base Ni, la quantità di solidi necessario è 886.5 kg/s (fattore di ricircolo 17.4 kg/s/m^2).

A conclusione di questa analisi di sensitività, la coppia Fe_3O_4/Fe_2O_3 OC risulta essere la migliore opzione al fine di diminuire la dimensione dei reattori di chemical looping, oltre che i relative costi. Tuttavia, le cinetiche degli OC a base Ni e Cu sono spesso più veloci di quelle del caso Fe, specialmente a temperature di lavoro intermedie (500-800°C), le temperature operative dei sistemi ibridi SOFC-CLC. Di conseguenza, la scelta dell'OC e la progettazione del reattore necessita un'apposita analisi.

Prestazioni per applicazioni su piccola scala

Come già anticipato, negli ultimi anni le SOFC sono state già commercializzate nel range di potenza 100-1000. Per la CLC, già esistono prototipi di scala 1 MWth [68]. Di conseguenza, la combinazione dei due sistemi può anche essere presa in considerazione per applicazioni in piccolo scala come il caso di un impianto per la produzione di CO_2 (tipicamente maggiore di 145 kg/h). In questo caso sarò necessario un altro tipo di sistema per il recupero dell'energia. L'input termico richiesto per avere 712 kWth (corresponding to a NG feeding flow rate of 55.13 kg/h). An organic Rankine cycle (ORC) can be adopted for the heat recovery of the system (using Toluene as operating fluid, as in the case of Triogen generator [59]). In this case, the SOFC power output is 450 kWel while the ORC would provide about 50 kWel (based on turbine isentropic efficiency of 85% inlet turbine pressure of 32 bar and maximum turbine inlet temperature of 300°C) which are produced from the overall heat duty of 183.6 kWth. Such system can also be considered without ORC producing IP-LP steam for industrial processes.

Conclusioni

Questo lavoro presenta l'analisi termodinamica di un sistema integrato SOFC-CLC finalizzato alla produzione di potenza elettrica a partire da gas naturale. L'impianto è stato descritto ed analizzato in dettaglio. Il sistema ibrido è basato su una SOFC atmosferica le cui condizioni operative rispecchiano quelle dello stato dell'arte ed in grado di raggiungere un'efficienza elettrica netta del 66.7% (con SPECCA di 0.34-0.38 $MJ_{PCI}/kgCO_2$). In confronto a cicli ibridi convenzionali senza cattura della CO_2, la penalizzazione sull'efficienza è esclusivamente dovuta alla compressione della CO_2. Prestazioni molto simili sono state ottenute modificando la modalità con la quale viene fornito il vapore alla cella (ricircolo caldo o freddo), così come variando il rapporto S/C in ingresso al pre-reformer. Con una tensione di cella maggiore (0.86 V), l'efficienza dell'impianto cresce di circa 6 punti percentuali con una conseguente riduzione dello SPECCA a valori certamente comparabili con quelli di un ciclo ibrido con impianto criogenico di separazione della CO_2 (0.3 vs 1.1 $MJ_{PCI}/kgCO_2$), risultato che è combinazione di un più alto CCR (+18%) e di una più alta efficienza elettrica (+2.5%). Usando un OC a base Cu, è necessario un alto fattore di ricircolo dei solidi (circa 20 $kg/s/m^2$) al fine di pre-riscaldare l'aria alla temperatura di ingresso al catodo. Tuttavia, la circolazione dei solidi diminuisce significativamente con l'utilizzo di OC a base Fe a causa dei differenti calori di reazione dei. Infine, l'impianto integrato SOFC-CLC presenta ottime prestazioni anche su piccola scala per le quali queste tecnologie sono già ben sviluppate. L'obiettivo di questo impianto,

oltre che la produzione di energia elettrica, è la produzione di $CO_{2,}$ utile per altri processi o applicazioni.

L'articolo [70] è basato su questo lavoro. Il riassunto esteso e l'estratto di questa tesi fanno riferimento a [70].

Table of contents

Abstract

Solid Oxide Fuel Cells (SOFCs) are electrochemical devices able to convert fuel into electricity, promoting a direct oxy-combustion. The anode exhaust is a CO_2-rich stream that can be separated and sent to the final storage. SOFCs act as an air separation device in which O_2 migrates from cathode to anode generating electricity. The efficiency of the SOFC decreases by increasing the fuel utilization and some unburnt species are present in the anode off-gas. Chemical Looping Combustion (CLC) could be integrated in a SOFC plant with different configurations. In this work, two novel configurations are proposed using natural gas as primary feedstock. The SOFC operates at atmospheric pressure with an operating temperature of 800°C. Air is heated up to the cathode inlet temperature with a regenerative heat exchanger (up to 450°C) and then further heated in the air reactor without requiring high temperature gas-gas heat exchangers or additional burners leading to some CO_2 emissions. At the fuel reactor, the unconverted fuel species (anode off-gas) are completely oxidized to CO_2 and H_2O. The electric efficiencies of the integrated plant approach 67% (based on NG_{LHV}) with carbon capture rate of 100% where the CLC plant is operated at mild conditions (atmospheric pressure and temperature of 500-700°C). Two different scenarios are studied: in the first case, the SOFC is designed for large scale application in which a heat recovery steam generator is used to increase the power production. In the second case, the system is designed for small applications, possibly integrated in a plant with CO_2 utilization, where the integrated SOFC+CLC are combined with an ORC. The main parameters affecting the plant performance are studied. The S/C ratio at pre-reformer inlet, the SOFC voltage (ΔV) and fuel utilization (U_f) are varied to assess the electricity production. Three different OCs (Ni, Fe and Cu based) are compared to see the effect in the thermal balance of the plant and the gas conversion efficiency. The SOFC exchange area, current density and voltage losses are studied varying the different operating conditions.

Keywords: SOFC power cycle, hybrid cycle, CO_2 capture, high efficiency, performance evaluation.

Estratto

Le celle a combustibile ad ossido solido (SOFC) sono dispositivi elettrochimici capaci di convertire combustibile in energia elettrica, promuovendo un'ossi-combustione diretta. Il flusso in uscita dall'anodo è ricco di CO_2 che può essere separata ed inviata a stoccaggio. Le SOFC agiscono come un dispositivo di separazione dell'aria grazie alle quali l'ossigeno migra dal catodo all'anodo generando elettricità. L'efficienza della SOFC diminuisce aumentando il fattore di utilizzo del combustibile ed alcune specie incombuste saranno presenti nel flusso in uscita dall'anodo. Il processo di Chemical Looping Combustion (CLC) potrebbe essere integrato in un impianto SOFC in modi differenti. In questo lavoro, sono proposte due configurazioni innovative che utilizzano gas naturale come materia prima principale. La SOFC opera a pressione atmosferica con una temperatura di esercizio di 800 °C. L'aria è riscaldata fino alla temperatura di ingresso al catodo con uno scambiatore rigenerativo (fino a 450 ° C) e poi riscaldata ulteriormente nell'air reactor della CLC senza richiedere scambiatori aggiuntivi di calore gas-gas ad alta temperatura o bruciatori supplementari con relative emissioni di CO_2. Nel fuel reactor della CLC, le specie combustibili non convertite (il flusso in uscita dall'anodo) sono completamente ossidate a CO_2 e H_2O. Le efficienze elettriche del sistema integrato si attestano intorno al 67% (sulla base del PCI del gas naturale) con un'efficienza di cattura della CO_2 del 100% e CLC che lavora in condizioni blande (pressione atmosferica e temperatura di 500-700 ° C). Sono studiate due diverse configurazioni: nel primo caso, la SOFC è progettata per applicazione su larga scala con una caldaia a recupero di calore, utilizzata per aumentare la produzione di energia. Nel secondo caso, il sistema è progettato per piccole applicazioni in un impianto finalizzato alla produzione di CO_2, dove SOFC e CLC sono integrate con un ORC. Verranno studiati i principali parametri che influenzano le prestazioni dell'impianto. Il rapporto S/C all'ingresso pre-reformer, la tensione (ΔV) ed il fattore di utilizzo del combustibile (U_f) della SOFC verranno variati con l'obiettivo di valutare la loro influenza sulla produzione di elettricità. Tre diversi OC (a base Ni, Fe e Cu) verranno confrontati per valutarne l'effetto sul bilancio termico dell'impianto e sull'efficienza di conversione del gas. L'area di scambio, la densità di corrente e le perdite di tensione della SOFC verranno studiate variando le diverse condizioni operative.

Parole chiave: cicli di potenza con SOFC, cicli ibridi, cattura della CO_2, alta efficienza, valutazione delle prestazioni.

Introduction

Nowadays, the issues in energy and environmental matters are many. In particular, these three are among the main questions.

- Greenhouse gas emissions.
  It is the principal cause of the recent climate changes and global warming, according to the most opinions within the scientific international community. Carbon Capture and Storage (CCS) is a middle-term solution. It consists in the reduction of CO_2 emissions thanks to the separation of CO_2 from the exhaust gas of the energy production processes and the consequent CO_2 storage underground, in order to not release it in atmosphere.

- Depletion of fossil fuels stocks.
  Oil and natural gas are finishing, according to the scientific common opinion. Indeed, the years pass and the valued time before the end of fossil fuels stocks remains almost the same. This is due to the continuous increment of the proven reserves of fossil fuels. In fact, the assessment of the time remained before the end of the stocks is based on the proven reserves and the reserves that are already being exploited.
  Anyway, fossil fuels are sources not renewable so, it is important to find systems and processes able to use it more efficiently as possible. In the middle term, another way to solve this problem is a better integration with the energy production by renewable sources. However, in a close future, it will not be easily possible to produce the most of energy by renewable sources because of technical problems, related to their randomness and their low efficiency of conversion.

- Increment of world energy needs.
  This is due to the population increment and to the growth of the developing countries, in population but, mostly, in technology. It will be necessary more energy and more energy in large size.

The purpose of this thesis is to study an innovative process for power production using two of the technologies most studied nowadays in energy and chemical field: fuel cells and Chemical Looping Combustion (CLC).
In fuel cells, the conversion from chemical energy to electricity is direct: the process results more efficient because the conversion in mechanical and/or thermal energy is skipped.
On the other hand, CLC can be exploited for two interesting objectives: heating and CO_2 separation. In particular, the CO_2 separation occurs very easily, without large technological complications and large energy expenses.

The integration of these two technologies could generate an innovative system, able to fit the three main questions explained before.

In this work will be studied the perspective and the strength of this integration, as well as the performance of the system with different operating conditions and configurations.

This thesis is structured as follows:

- *Chapter 1: CO_2 emissions problem*
  Overview of CO_2 emissions problem, CCS systems description and efficiency question.
- *Chapter 2: Solid Oxide Fuel Cell (SOFC)*
  SOFC technology overview and description of its state-of-art.
- *Chapter 3: Chemical Looping Combustion (CLC)*
  CLC technology overview and description of its state-of-art.
- *Chapter 4: Methodology of calculation*
  Description of the main assumptions used to build the plants and definition of the most important process evaluation indexes.
- *Chapter 5: Comparison between the systems with and without CO_2 capture*
  Analysis of two innovative plants for large-size power generation with CO_2 and comparison with a more traditional similar plant without CO_2 capture and proposed in literature.
- *Chapter 6: Sensitivity analysis*
  Sensitivity analysis for the two innovative systems in order to find out the influence of operating conditions on the performance and new possible best working conditions.
- *Chapter 7: SOFC analysis*
  Specific study of the SOFC, the main component of the systems, in order to study the features and the future feasibility.
- *Chapter 8:Models for small-size power generation*
  Description and analysis of different plants proposed for small-size power production with CO_2 capture.
- *Chapter 9: Conclusions and recommendations.*
  Summary of the final results, conclusions and indications for future studies in the same field.

Chapter 1

CO_2 emissions problem

1.1 Greenhouse effect and CO_2 emissions

The energy sector allowed reaching and guarantees exceptional levels of well-being and health typical of modern industrial company. A continuous technological improvement in almost all sectors was possible with increased availability of energy resources. The systems of production and conversion of energy have been changed over the years in order to improve the efficiency and reduce the environmental impact. These are still two important challenges. Just in response to environmental problem, scientific research deals the study of systems able to optimize efficiency and reduce emissions of pollutants and greenhouse gas effect. In fact, within the scientific international community, there is a great agreement about increment of greenhouse gas emissions as the biggest reason for the actual global warming.

CO_2 is not classified as a pollutant but its overproduction can be dangerous. CO_2 tends to accumulate in the top layer of the troposphere and, together with other gases, it is directly responsible for the increase of the greenhouse effect, very important to maintain the equilibrium of our planet's climate. This molecule is transparent to short-wave radiation coming from the sun (visible range) but absorbs wider wavelength reflected from the lands and from the water (infrared range). This property is generally positive because it allows mitigating the temperature and allows life on Earth. However, the excessive increase of CO_2 in the atmosphere could affect the heat balance of the ecosystem, causing an abnormal growth in the average temperature of the globe.

Scholars do not agree among themselves on the real effects of an excessive increase of greenhouse gases in the atmosphere but it is common the need to achieve an effective solution to reduce emissions and avoid understatements of the situation. In this purview, there are the studies on CCS and on efficiency optimization.

1.1.1 Greenhouse effect and use of fossil fuels

Today, it is generally accepted that the increase of CO_2 concentration in the atmosphere is mainly due to human activities. Since the industrial revolution, mankind started burning fossil fuels to produce energy without caring about the consequences. Only recently, men started to think about the relation between their activities and climate changes.

In 1998, Intergovernmental Panel on Climate Change (IPCC) has been found by two organization of United Nations (UN): the World Meteorological Organization (WMO) and the United Nations Environment Programme (UNEP). IPCC is a scientific group that monitors climate changes and periodically publishes reports

about it. The last IPCC report is of 2014, the Fifth Assessment Report [2]. The most important findings of these studies are three.

Carbon dioxide (CO_2), methane (CH_4) and nitrous oxide (N_2O) concentration in the atmosphere increased in comparison to the level of 1750 (before industrial revolution). In 2011, the concentrations of these greenhouse gases were, respectively, 391 ppmv (part per million in volumes), 1803 ppm (part per billion in volumes) and 324 ppmv, increased by 40%, 150% and 20%. In particular, Figure 1.1 shows the CO_2 increment in the periods 850 – 2000 (Figure 1A) and in the last years (Figure 1B).

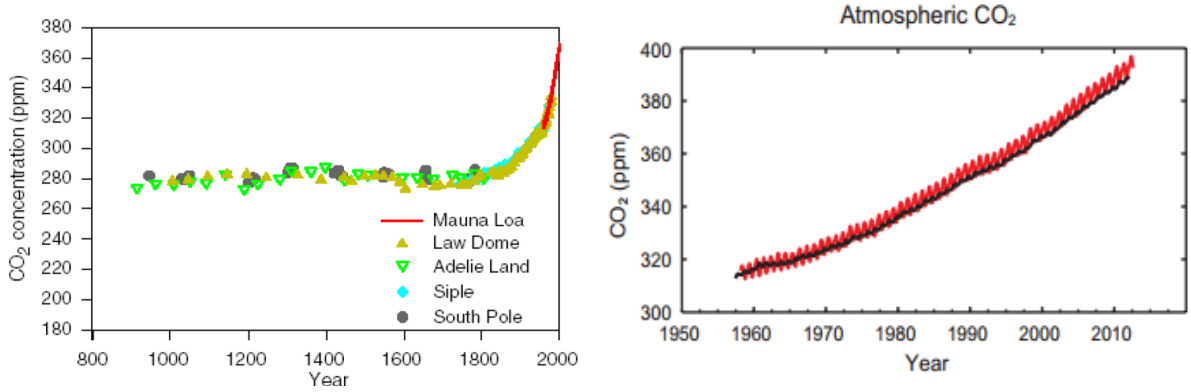

Figure 1: a) CO_2 concentration profile during the years [1]. b) CO_2 concentration profile in the last years (1958-2011) for Mauna Loa (red line) and South Pole (black line) [2].

Ocean acidity and partial pressure of dissolved CO_2 in the superficial ocean increased. The increase of acidity of ocean water is demonstrated by the reduction of its ph, expressed in situ ph (Figure 2).

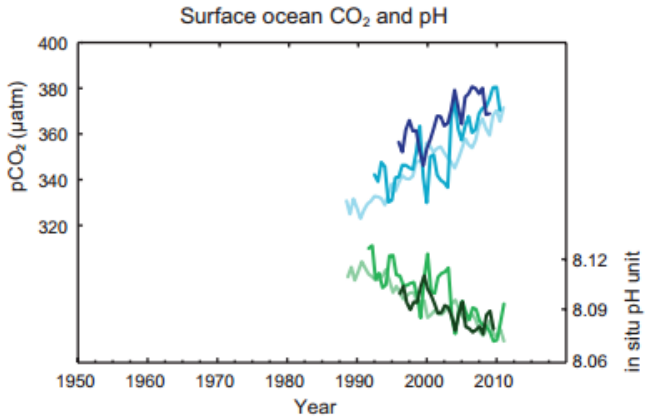

Figure 2: Partial pressure of dissolved CO_2 in the superficial ocean and trend of ocean acidity in the period 1988-2011 (3 colours = 3 measurements of 3 different oceanic stations) [2].

Land and ocean temperature increased. The combined data of the global mean surface temperature of the earth and ocean, calculated with a linear trend, show a heating equal to 0.85 [0.65 - 1.06] °C in the period 1880-2012 (Figure 3).

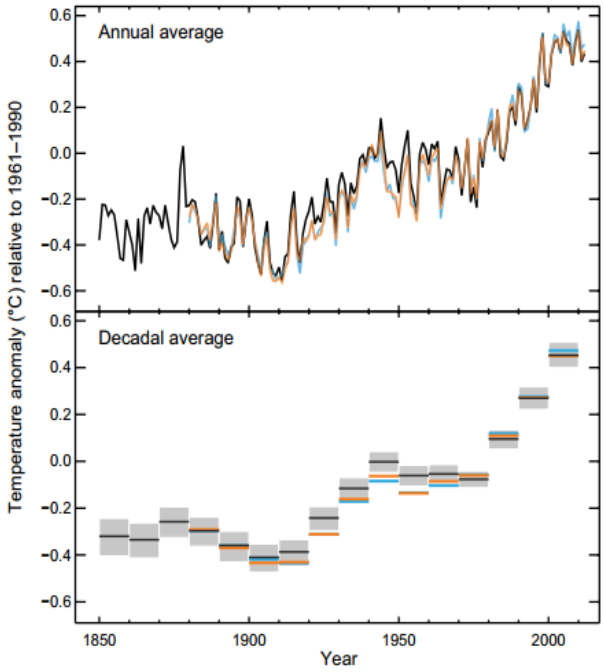

Figure 3: Combination of land and ocean surface temperature anomalies (1850-2012) [2].

The increase of CO_2 concentration in the atmosphere is related to the higher consumption of fossil fuels.

International Energy Agency (IEA) is a Paris-based autonomous intergovernmental organization established in the framework of the Organization for Economic Co-operation and Development (OECD) in 1974, in the wake of the 1973 oil crisis. IEA publishes reports every year about utilization of different energy sources.

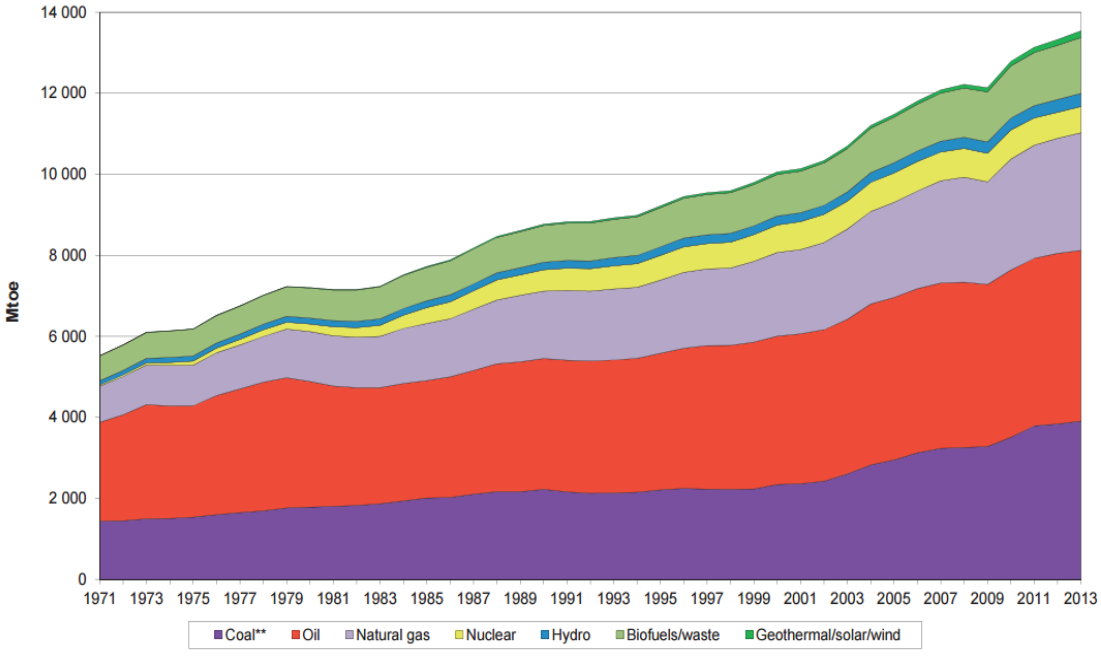

Figure 4: World Total Primary Energy Supply (TPES) in Mtoe, from 1971 to 2013 by fuel [3].

Figure 4 shows that, in 2013, approximately 80% of the primary energy supplies were provided by burning fossil fuels and their consumption was constantly increased during the years.

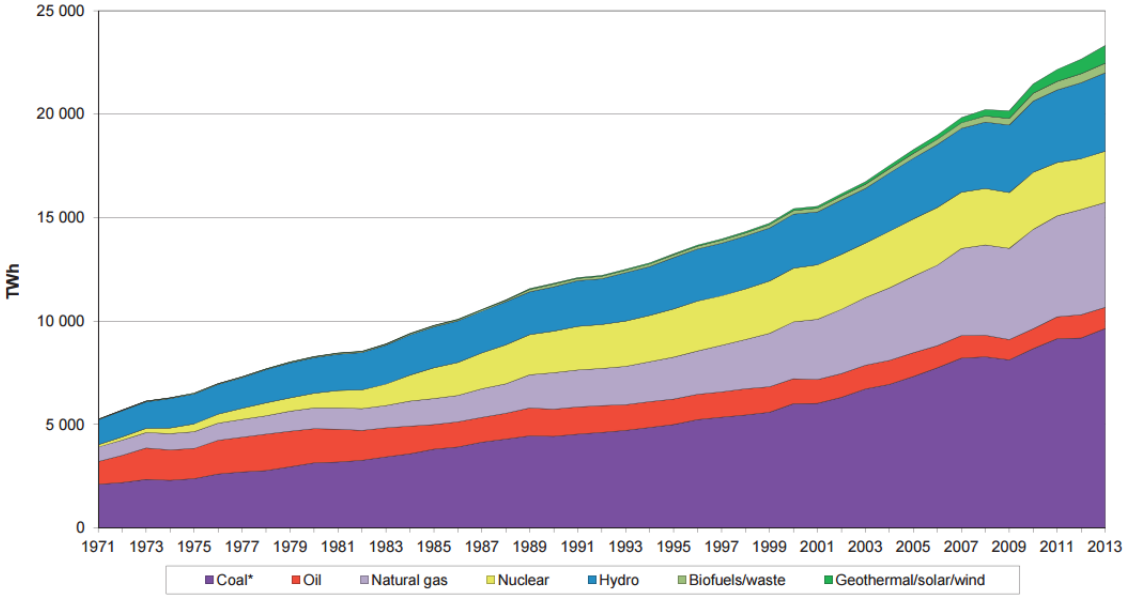

Figure 5: Electricity generation from 1971 to 2013 by fuel (Mtoe) [3].

Figure 5 shows the same for the electricity generation. The energy mix consists for the most part in fossil fuels (approximately 70%) and the need for electricity is steadily increasing since 1971, except for the period around 2008 when the reduction in consumption was due to the economic crisis. This negative drop can also be seen for TPES in Figure 4.

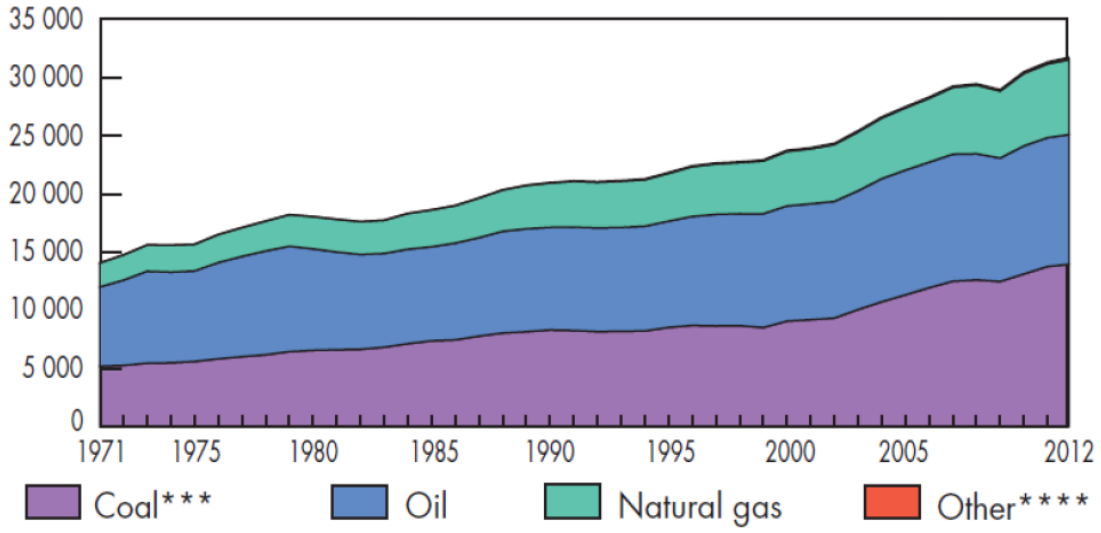

Figure 6: World CO_2 emissions profile from 1971 to 2012 by fuel (Mt of CO_2) [4].

Carbon dioxide emissions have more than doubled in the last 40 years and almost the totalities of these are due to fossil fuels (Figure 6).

These trends demonstrate that there is a great connection between emissions, human activities and the use of fossil fuels. Against this background, it is essential to study systems for utilizing fossil fuels efficiently with an appropriate emissions treatment. This is the idea that underlies this thesis.

1.1.2 Environmental policies

The consciousness of the connection between human activities, CO_2 emissions and climate changes forced the international community to think about environmental policy measures.

The first and most important measure in environmental issues has been the Kyoto Protocol, released in 1997 by more than 180 countries, those which attended the United Nations Framework Convention on Climate Change (UNFCCC).
The most important target stipulated by Kyoto Protocol is a global reduction of greenhouse gas emissions by 5.3 % compared to 1990 emissions level, to be achieved in the period between 2008 and 2012. The Kyoto Protocol entered into force on 16 February 2005, ratified by at least 55 shares (countries or groupings of countries like EU), representing, approximately, 55% of global emissions of CO_2 equivalent in 1990. The countries which applied the binding reduction targets are called countries Annex I. Every country participating in the Protocol has a specific objective of binding; for Italy, it was a reduction of 6.5% compared to 1990.
Emissions allowed to the countries are called Assigned Amounts Units (AAU), measured in tons of CO_2 equivalent. These units are tradable securities and are assigned by UNFCCC. At the end of the reporting period, all the countries have to return to the international authorities many carbon credits how many their actual emissions recorded during the period.

In order to reduce emissions and achieve their objectives, countries Annex I can use two kinds of measures. Internal measures, such as:

- seeking improvements in energy efficiency for system of energy production in order to reduce fuel consumptions;
- promoting the spread of co-generation plants;
- changing fossil fuels mixture giving priority to natural gas, nuclear and renewable sources;
- limiting emissions of methane from landfills;
- reducing emissions in the transport sector;
- promoting agriculture with low environmental impact by restricting the use of substances which can release greenhouse gases;
- integrating power plants with CO_2 capture (CCS);

External measures, such as:

- Joint Implementation (JI) - Annex I countries can invest in emission reduction projects in other Annex I countries, in particular, in countries with economy in transition. For every ton of CO_2 equivalent avoided, countries earn credits called ‘Emission Reduction Units’ (ERUs). The emission reduction remains in Annex I. Consequently, ERUs are only AAUs converted;

- Clean Development Mechanism (CDM) - The idea is the same of JI but investments have to be made in developing countries. CDM gives credits called 'Certified Emissions Reductions' (CERs) for every ton of CO_2 equivalent avoided. CER is only a greater benefit in terms of reducing emissions to an adherent country. For the other countries (non-adherent), there is no interest, if not the benefit of receiving the project;
- International Emission Trading System (ETS) - Annex I countries can trade with each other (buy or sell) carbon credits to cover any emissions that exceed the limit assigned by the Kyoto Protocol;
  To facilitate the achievement of the target, European member countries have agreed to adopt the 'European Union Emissions Trading Scheme' (EU ETS) that covers only industrial plants belonging to some specific manufacturing sectors (energy and energy-intensive).

In this way, the objectives of Kyoto Protocol become global matter and not only a local problem.

After 2012, the effects of Kyoto Protocol are finished. Consequently, in the beginning of March 2007, European Council has set new objectives to reach by the 2020:

- reducing emissions of greenhouse gases by, at least, 20% compared to 1990, with the proposal to increase the target to 30%, if the international agreement was ratified by other developed or developing;
- 20% share of renewables in total gross energy consumption in the European Union, with a minimum contribution of 10% of biofuels to the consumption of transport fuels in each of the member countries;
- savings in the energy consumption of European Union by 20%, compared to the forecasts of the European Commission in the recent Green Paper about energy efficiency (forecasts if not environmental measures). This goal is not binding because it is implicit in the other two.

Following these decisions, it was implemented the European climate and energy agreement, approved in December 2008.
Furthermore, in October 2014, European Council has set the new objectives for 2030, respectively increased to 43% compared to 2005 (30% for sectors not belonging to ETS), 27% and 27%. These should be achieved without new environmental measures.

It has also to consider the strong energy dependence on oil and its importance about emissions. In sight of it, European Union has set the following strategic targets:

- sustainability, through the reduction of greenhouse gas emissions;
- security, pursued by diversifying the sources, developing the renewable sources and the energy efficiency in order to depend less on imported fuels;
- competitiveness, pursued by diversifying the sources, developing the renewable sources and the energy efficiency, in order to be less affected by the volatility in oil price.

Now, the cost for emitting CO_2 has been lowered and the companies have not so many interests to invest in reducing emissions. It can be seen thanks to the trend of

CO_2 price in EU ETS. In Appendix A, all the features of the three periods of EU ETS are described specifically and the CO_2 price trend during the years is shown.

Some considerations have to be made about EU ETS:

- the economic and financial crisis, that began in 2008, involved a significant reduction of activities and therefore of the emissions. It has caused the establishment of a reservoir of bankable permits and international credits and a strong decline in the price of CO_2 (offer >> request);
- the incentives for renewable sources and energy efficiency, applied at national level, involved a reduction of the effectiveness of the instrument. Currently, EU ETS occupies a role marginal in the investment plans of the companies;
- the strengthening of the ETS requires the adoption of policies on extended horizons.

Therefore, the reform of the system ETS consists of actions in order to reduce the excess allowances:

- in the short term, the decision to withdraw about 900 million allowances from the auctions of three-year period 2014-2016 to increase its price (called 'back loading'). The allowances withdrawn should be auctioned at the end period (2019-2020) or transferred to reserves;
- in the long term, the proposal for the introduction from 2021 of a Stability Reserve Market at the auction system in order to make the system more flexible to possible external shocks; in situations of significant surplus, the shares to be offered at auction would partly transferred to the reserve in order to be used in periods of deficit, according to predefined rules.

Finally, the last measure on environment theme was the EU climate and energy policy post 2020 that fixed objectives and tools until 2030. The European Council of 23-24 October 2014 has approved the new climate and energy targets for 2030:

- the reduction of 40% of greenhouse gas emissions with binding targets for member countries for non-ETS sectors;
- the increase of 27% of renewable on final consumption of energy, binding European level but without binding targets for all member countries;
- 27% of energy efficiency, non-binding but subject to reviews in order to be increased to 30%.

1.2 CO_2 capture systems

The utilization of biofuels and renewable sources is not the only way to reduce CO_2 emissions. Nowadays, only renewable energy for power production is not a possible scenario in short time and it would require a radical change in systems and distribution. Therefore, it is necessary to find middle-term solutions, such as to integrate conventional plants with CCS systems. It allows using the same plants and sources with lower CO_2 emissions and without big changes in the facilities.
It has two negative consequences on the plants: lower efficiency and increment in total cost. It is due to additional components with an additional cost and electrical consumption.

The principal techniques used in industry to separate CO_2 are three:

- pre-combustion systems
- post-combustion systems
- oxy fuel systems

1.2.1 Pre-combustion systems

CO_2 derives from the carbon (C) contained in the fuel. Therefore, one solution to have less CO_2 after combustion is to remove the carbon in the fuel.
First step is to produce CO from the C contained in the fuel. There are two possible reactions: the coal gasification process (Equation 1.1) and the steam reforming reaction (SMR, 1.2).

$$C_nH_m + \frac{n}{2}O_2 \implies nCO + \frac{m}{2}H_2 \quad (1.1)$$

$$C_nH_m + nH_2O \implies nCO + (n + m/2)H_2 \quad (1.2)$$

The second step is to convert the CO in H_2 using the Water Gas Shift reaction (WGS, 1.3).

$$CO + H_2O \Leftrightarrow CO_2 + H_2 \quad (1.3)$$

The large amount of H_2 can be burned without any emissions. Instead, the CO_2 has to be separated from the other products by an absorption unit (third step).

In the absorption, a gaseous mixture is brought in contact with a phase liquid (the solvent) able to absorb preferentially one or more of its components. The separation assumes a transfer of material between contacting fluid phases (gas-liquid, liquid-vapour or liquid-liquid). This transfer takes place at the interface between the phases and it is favoured by a large contact surface. Therefore, the equipment are configured to allow high surface at the interface between the phases.

Different kind of solvent can be used in absorption. According to the different qualities, the solvents can be divided into two main groups, physical or chemical.

- Physical solvents profit by the physical interaction to absorb CO_2. The trend of absorption in relation to the partial pressure of CO_2 is a straight line (Figure 7); they are able to separate a lot of CO_2 when partial pressure is high, if not, their efficacy is low;
- Chemical solvents profit by chemical interaction and the trend of absorption is logarithmic (Figure 7), different in comparison to the previous case. They are better at low CO_2 partial pressure but, if it increases, the efficiency goes down; gradually, chemical bonds are saturated and the solvent is no longer able to separate further CO_2.

There is a special solvent, the MDEA (Methyl Diethanolamine), which has intermediate properties.

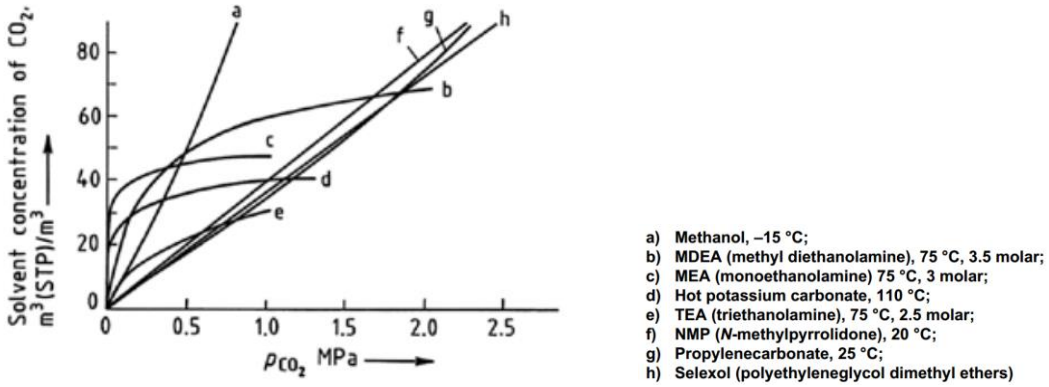

Figure 7: Trend of absorption for different kinds of solvent [7].

The solvent is chosen according to the partial pressure of the contaminant in the gaseous mixture: physical solvents for high partial pressure, chemical solvents for low partial pressure.

Another factor that influences the choice of the solvent is the energy required for regeneration of the solvent. After the absorption, the solvent is full of contaminants and it is necessary to regenerate it by desorption, favoured at high temperatures and low pressures, unlike absorption. Consequently, a physical solvent can be regenerated with an expansion and a chemical solvent increasing the temperature. Therefore, if the regeneration and the capture efficiency is great, it could be preferable a physical solvent in order to save the energy consumption to raise the temperature.

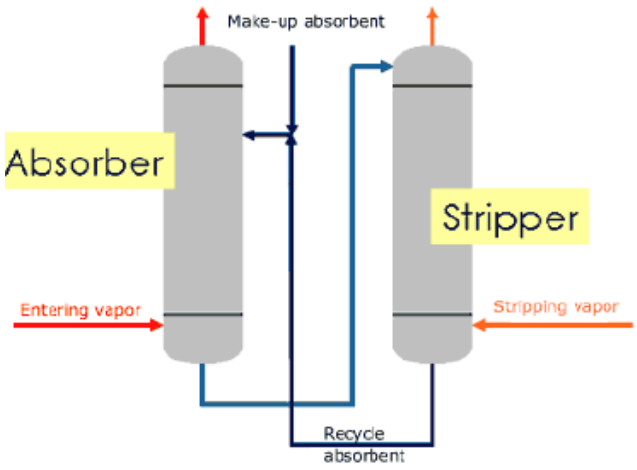

Figure 8: Generic absorption + regeneration plant [7].

In general, the stream at the outlet of WGS is available at high pressure; therefore, it is better to use MDEA or a physical solvent.

1.3.2 Post-combustion systems

CO_2 is separated using absorption after the combustion. In general, the flue gas is at atmospheric pressure and CO_2 is diluted with air nitrogen in order to have low CO_2 molar fraction (5-15%) and partial pressure. The preferable solvent is chemical (e.g. MEA, Mono Ethanol Amine).

The advantage of this system is the easy installation in operative plants. The disadvantage is the reduction of global efficiency because of the heat required to regenerate the solvent and the cost of compression.

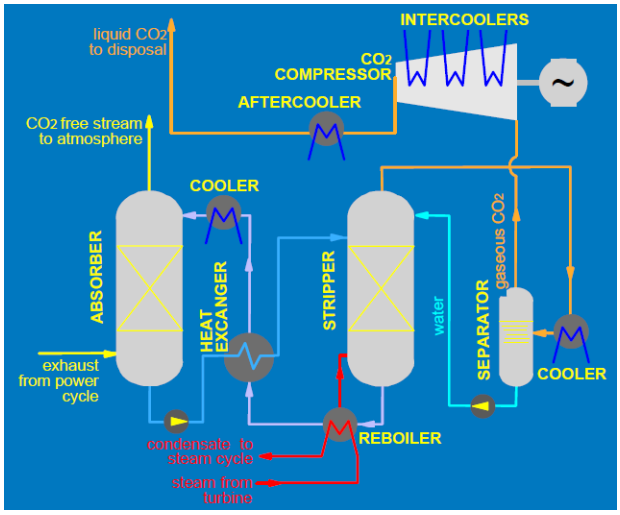

Figure 9: Generic post-combustion system [8].

1.3.3 Oxy fuel systems

Oxy fuel combustion uses pure oxygen to burn the fuel. The most of flue gas is CO_2 and H_2O and CO_2 can be easily separated by condensing the water.
The separation is simple but the disadvantage is the additional component, the Air Separation Unit (ASU), necessary to produce pure oxygen from air and which requires a big electrical consumption (0.21 kWh/kg_{O2}). ASU is not suitable for small size plants because it is very sensitive to scale economies. ASU is not able to produce really pure oxygen but only 95-98% O_2 with traces of Ar and N_2. The flow produced by the combustion has an excess of oxidant and it is composed by 90% CO_2 and 10% of incondensable gasses (O_2, Ar, N_2), separable with a cryogenic system, reaching almost zero emissions.

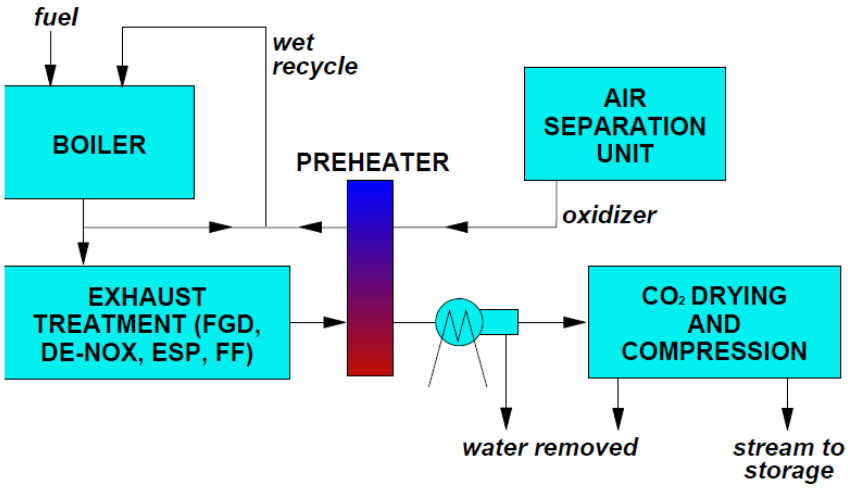

Figure 10: An oxy fuel combustion system [8].

1.3.4 Chemical Looping Combustion (CLC)

CLC is an innovative system and belongs to Oxy Fuel Systems. In CLC case, O_2 is fed by an oxygen carrier. It is a solid metal recirculated between a Fuel Reactor (FR), where it reacts with the fuel and loses O_2, and an Air Reactor (AR), where it is regenerated thanks to air which provides the O_2. The flue gas contains only CO_2 and H_2O and CO_2 can be separated easily by condensing the water.
The two biggest problems of this technique are the oxygen carrier circulation and the metal resistance at high temperature.

1.3 CO_2 storage systems

The CO_2 separated has to be stored so as to prevent it from being released into atmosphere. It is necessary to compress the CO_2 in order to have it liquid. In this way, it can be transported and stored. CO_2 has critical point at 30.38 °C and 73.77 bar, therefore, to become liquid, it has to reach 80-150 bar. An intercooled compressor can be used to make it. Its power consumption is not negligible and reduces the total efficiency of the plant: CO_2 separation and storage is a disadvantage from an energetic point of view.

Storages could be divided in two different types:

- underground geological storages, similar to the natural storages. In nature, there is accumulation of CO_2 in some places in upper layers of Earth's surface (e.g. natural deposit). The two most common underground geological storages are deep saline aquifers and the Enhance Oil Recovery (EOR).
  The deep saline aquifers are characterized by big thickness and porosity of the permeable layer sufficient to have a good capability. They have above an additional impermeable layer made of rock (called 'cap rock') necessary to avoid the permeation of CO_2. Deep saline aquifers have a good stability.
  EOR allows CO_2 storage and increase the productivity of the oilfield (economic advantage) if CO_2 is put inside the oil and gas reservoirs;
- oceans are natural deposits of CO_2. CO_2 is absorbed and reacts with water to produce acid carbonate that is separated into ions. The consequence is the reduction of oceans water ph of 0.1 in comparison to the preindustrial values. CO_2 is stored at great depth below the oceans (more than 1000m).

Nowadays, geological storage are preferred because CO_2 is not in equilibrium with the environment in the oceans and it is released in atmosphere, even if very slowly. It could bring some problems to the marine ecosystem.

It is important to underline the different view about the CO_2: some years ago, it was only waste, now it has an economic value. The only problem is the availability of the storages, limited just in some areas.

1.4 Energy efficiency

Energy efficiency means getting the same results with saving primary energy. This concept can be analysed from three different points of view:

- energy intensity (amount of energy used per unit of output);
- level of energy service;
- time distribution of savings.

An increase of energy efficiency can be made in two different ways:

- reduction of final consumption (DSM, Demand Side Management), with measures which produce an energy service level equal or greater through the use of a smaller amount of energy. These interventions are normally of long duration and allow a saving of energy in different time periods;
- optimization of the overall energy system (DR, Demand Response), interventions aimed to reshaping over time in energy demand without necessarily lead to a reduction of the amount of energy.

Increment of energy efficiency involves public benefits, as reduction in national energy consumption, less dependence from abroad, less risk of blackouts and lower greenhouse gas emissions, and also private benefits like reduced fuel bills and reduction of maintenance and improvement costs.
The problem is that some barriers prevent that the market generates alone stimuli to interventions of this type: bad information, uncertainty, marketing that drives the increase in consumption, types and timing of costs and benefits.

Below, a list of some of the possible energy promotion tools:

- regulatory measures (e.g., imposition of quality standards/performance): it is a command and control tool;
- financial tools (e.g., tax breaks, subsidies on interest);
- market tools (e.g., marketable securities, competitive procedures for the selection of the energy efficiency measures): it is an economic quantity tool;
- voluntary agreements (e.g., unilateral commitments by firms/associations, voluntary public schemes);
- energy audit (eg., audit, monitoring, analysis of energy use);
- information for end customers.

Chapter 2

Solid Oxide Fuel Cell (SOFC)

Solid Oxide Fuel Cells (SOFCs) operate at high temperatures (873-1273 K) and their project design is consolidated and reliable. These features and the possibility to reach high efficiency make SOFC ideal for stationary applications. The most important objective that can be reached with this technology is the production of electric power with high efficiency and low pollution by using fuels like natural gas or syngas.

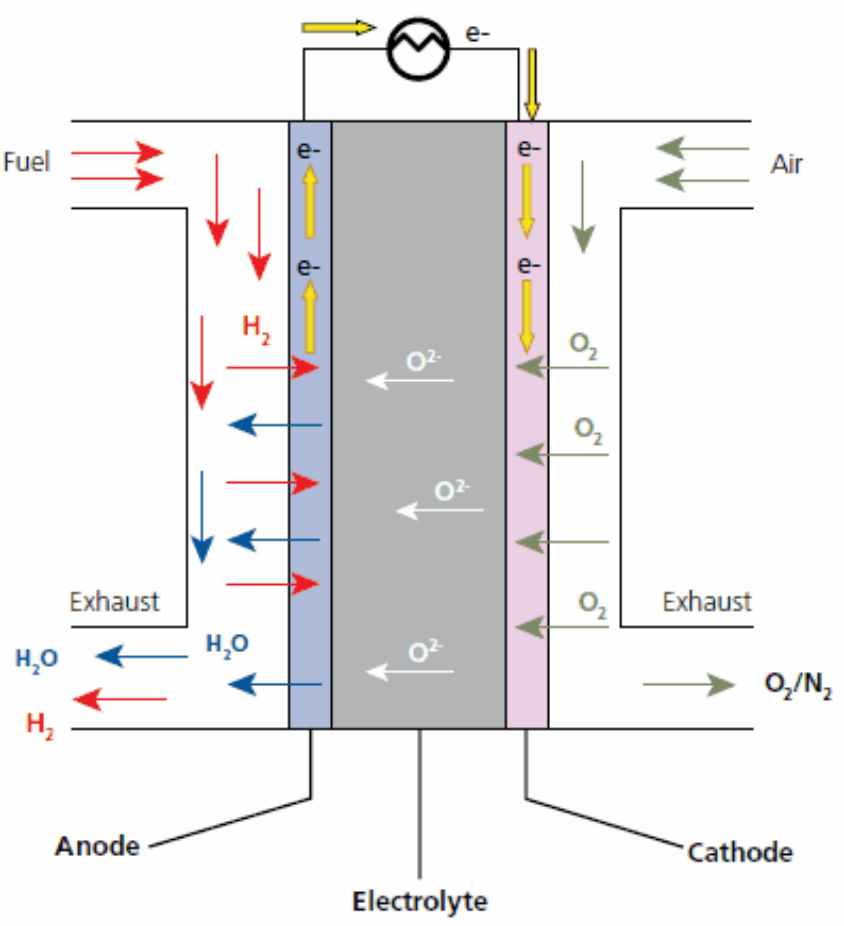

Figure 11: General scheme of a SOFC.

The second law of thermodynamic explains that the amount of energy is important but also its quality. It is possible to define the Exergy like the part of energy to be converted in high value work, while 'Anergy' is the competitive part. The most of the power generation processes get high value work (electricity) from chemical energy passing through combustion and thermal energy. This process has a good efficiency from a quantitative point of view (I° law of thermodynamic) but not from a qualitative point of view (II° law) because it is a very irreversible mechanism with

important exergy lost due to the combustion. With fuel cells, it is possible to skip the combustion and have direct conversion of chemical energy into electricity.
Exergy analysis was underestimated until it was linked to an economic point of view thanks to the thermo economic analysis: every different kind of exergetic unit has a money value and the money value of exergy losses is calculated by a cost balance between inputs and outputs. In this way, the second law of thermodynamic acquired a practical meaning and it is taken into account for plant design and optimization.
Exergy balance unifies energy and entropy balances and depends on the states of the system and on the environment. Consequently, it considers thermal, mechanical and chemical processes. If changes in kinetic and potential energies are neglected, it is possible to write the energy balance between single inlet/outlet systems:

$$\sum_j(Q_j) \; - W = \; [\sum_i(m_i \; h_i)]_{inlet} \; - \; [\sum_i(m_i \; h_i)]_{outlet} \tag{2.1}$$

where W is positive if is made by the system and Q_j is positive when its direction is from environment to the system. m_i is the mass flow of every component i and h_i is the specific enthalpy for every component of mass flow.

It is possible to write also the entropy balance:

$$\frac{dS}{dt} = \; \sum_i \left(\frac{\dot{Q}_j}{T_j}\right) \; + \; [\sum_i(m_i \; s_i)]_{inlet} \; - \; [\sum_i(m_i \; s_i)]_{outlet} \; + \; \dot{S}_{irr} \tag{2.2}$$

where s_i is the specific entropy for every component i of mass flow; $\dot{S}_{irr}$ is the rate of production of entropy due to irreversible phenomena of the process; the first element at right side is the sum of entropy production due to the different heat transfers with environment and with other system at constant temperature (T_j).

Exergy balance is obtained by mixing the two previous balances:

$$\dot{E}x_{loss} = T_o \; s_{gen} = [\sum_i(m_i \; ex_i)]_{inlet} - [\sum_i(m_i \; ex_i)]_{outlet} + \sum_i \left[\left(1 - \frac{T_0}{T_j}\right) \dot{Q}_j\right] - W \tag{2.3}$$

where ex_i is the specific exergy for every component i of mass flow and it is the sum of two different part, physical (ex_i^{ph}) and chemical specific exergy (ex_i^{ch}):

$$ex_i^{ph} = (h - \; h_0)_i - \; T_0 \; (s - \; s_0)_i \tag{2.4}$$

$$ex_i^{ch} = -R \; T_0 \ln \frac{x_i^e \; p_i}{p_0} \tag{2.5}$$

with p_i equal to the partial pressure of the component i of mass flow; x_i^e the molar fraction of the component i in standard reference environment; T_0 and p_0 the environment condition (usually 298.15 K and 1.013 bar) ; h_0 and s_0, specific enthalpy and entropy of the component i of mass flow at environment condition (T_0 and p_0). In this way, it is possible to calculate $\dot{E}x_{loss}$, the rate of exergy destruction. The third element in Equation 2.3 represents the amount of exergy produced by heat transfers. If $\dot{Q}_j$ is positive (from the source at constant temperature to the system

analysed), this element is positive and it is as big as the difference between the temperature of the source (T_j) and the temperature of the environment is higher. An increment of this element is equal to an increment of $\dot{E}x_{loss}$.

It is possible to calculate an exergetic efficiency (η_{ex}) of a methane combustor at atmospheric pressure in order to understand the amount of exergy losses for a normal combustion. Considering 1 kmol/s of methane, a complete combustion, 19.4 kmol/s of air (x_{O_2}= 21%, x_{N_2}= 79%), 1 bar of outlet pressure, 1 bar and 298.15 K as environment condition, the result is:

$$\eta_{ex} = \frac{\dot{E}x_{out} + \dot{n}_{out}\, ex_{out}}{\sum_i (\dot{E}x_{out} + \dot{n}_{out}\, ex_{out})} \approx 60\% \qquad \Longrightarrow \qquad \Delta\eta_{II} = \frac{T_0\, \Delta s}{\dot{m}_f\, Ex_f} \approx 40\% \qquad (2.6)$$

where $\Delta\eta_{II,comb}$ is the loss of efficiency (of II° principle); $\dot{m}_c$ and Ex_f are, respectively, the fuel mass flow and its total exergy ($Ex_f \sim W_{rev,f} \sim LHV_f \sim HHV_f$).
Exergy losses can be reduced sensibly with direct conversion of chemical energy in electricity/high value work. In this way, the process will be more efficient.

2.1 General principles

SOFC profits by electrochemical oxidation process in order to have an energy conversion and produce electricity and heat directly from gaseous fuels. For the future, SOFC represents a very interesting solution for the reasons listed below:

- high efficiency, due to the high operating temperature, 1000 °C for the high temperature SOFCs (HT-SOFCs) and 700-800 °C for the intermediate SOFCs (IT-SOFCs);
- low emissions, because SOFC works like an oxygen separator and, at the anode side, produces a CO_2 rich stream to send to the separation;
- able to work in stand-alone units or integrated with different thermodynamics cycles;
- able to use some kind of fuels (e.g. natural gas, biogas, syngas), also if methane rich.

In particular, the case of IT-SOFCs has great potentialities. Their operating temperature allows using more and cheaper material with relative advantage for the effective cost of the fabrication. IT-SOFCs are usually electrode supported (more often, anode supported) with the goal to minimize the electrolyte ohmic losses.

Materials used to make the different part of the SOFC are:

- Yttria-stabilized Zirconia (YSZ) for the electrolyte;
- Nickel-Zirconia alloy for the anode electrode, which guarantees excellent electrochemical performance and allows to have fuel conversion and oxidation in the same process;
- Perovskite material for the cathode electrode, like Strontium doped Lanthanum Manganite (LSM).

At the working temperature of IT-SOFCs, direct internal reforming (DIR) at the anode side allows to use efficiently natural gas, biogas and all the fuels methane-rich. This kind of SOFC can also use fuels rich of H_2 and CO (e.g. syngas). In this way, H_2 rich streams can be used as fuel and O_2 of the air as oxidant. The presence of CO is not a problem because the poisoning happens at lower temperature and CO is electrochemically converted.

The direct oxidation of CH_4, a solution not yet feasible to date, is represent by the following reaction:

$$CH_4 + 2O_2 + 8e^- \Longrightarrow CO_2 + 2H_2O + 8e^- \quad (2.7)$$

Thermodynamic efficiency conversion of even η = 99.7% can be reached with this kind of solution: it is the reason for which direct oxidation of CH_4 in SOFC is very interesting.
This reaction must be approximated for a SOFC by a Steam Methane Reforming (SMR) reaction together with a CO-shift reaction (Equation 2.9):

$$CH_4 + H_2O \Longrightarrow 3H_2 + CO \quad (2.8)$$

$$CO + H_2O \Longrightarrow H_2 + CO \quad (2.9)$$

The products of the reactions 2.8 and 2.9 will be allocated to the following ones:

Cathode $$O_2 + 4e^- \Longrightarrow O^{2-} + O^{2-} \quad (2.10)$$

Anode $$H_2 + O^{2-} \Longrightarrow H_2O + 2e^- \quad (2.11)$$
$$CO + O^{2-} \Longrightarrow CO_2 + 2e^- \quad (2.12)$$

Consequently, the total reaction of the process is:

$$H_2 + \frac{1}{2}O_2 + 2e^- \Longrightarrow H_2O + 2e^- \quad (2.13)$$
$$CO + \frac{1}{2}O_2 + 2e^- \Longrightarrow CO_2 + 2e^- \quad (2.14)$$

The reforming reaction (2.8) is much endothermic: the specific molar enthalpy difference at 1000 °C is ΔH = +227.5 kJ/mol [12]. The heat necessary is given in an irreversible way by the reactions 2.13 and 2.14. These reactions, at 1000 °C, provides more energy than the sufficient one (Q_{irr} = -325.54 kJ/mol) [12]. The surplus energy heats the air flow in the cathode side.

This process is basically less efficient than the direct oxidation of CH_4 because there is the loss of free energy for the steam reforming process. The free energy available at 1000 °C is [12]

$$\Delta G = 3\,\Delta G_{(2.11)}^{\circ} + \Delta G_{(2.12)}^{\circ} = -704.41\ \frac{kJ}{mol} \quad (2.15)$$

lower by 12.3% in comparison to the free energy of the direct oxidation of CH_4 $\left(\Delta G = -802.55\ \frac{kJ}{mol}\right)$ with a thermodynamic efficiency of η_{th} = 87.7%, higher than η_{th} = 71.1% of pure H_2 oxidation [12].

The cooling effect by the endothermic reaction (DIR configuration) allows feed less air at the cathode side. Consequently, the components are less and the consumptions of the auxiliaries are lower. The thermodynamic efficiency is thus higher.

2.2 Model description

There are many works in literature about SOFC modelling. Each of these has a different approach. It involves in different kinetics and electrochemical models. These models are based on different literature data, so they are valid regardless of the type of cell used, IT-SOFC or HT-SOFC. These models refer to a co-flow planar cell configuration (anode and cathode channels with same direction). It is possible to study the effects on the SOFC performance for different operating conditions or inlet fuel composition. The possibility to make a detailed simulation of SOFC internal behaviour is important in order to develop new cell design and investigate different operating conditions such as temperature, total pressure and flow composition. The objective is the optimization of the power plant performance.

2.2.1 Kinetic model

SOFC are able to use directly different kind of fuels. Generally, an external process to obtain a H_2-rich stream is required only by low temperature fuel cells (e.g. PEMFC, AFC, etc.).
Considering a humidified CH_4-rich syngas, the process analysed includes a Steam Methane Reforming reaction (2.8) and a Water Gas Shift reaction (2.9).

$$CH_4 + H_2O \Leftrightarrow 3H_2 + CO \quad \left(\Delta H° = 206\ \frac{kJ}{mol}\right)$$
$$CO + H_2O \Leftrightarrow H_2 + CO \quad \left(\Delta H° = -41.6\ \frac{kJ}{mol}\right)$$

There are a forward and a reverse reaction rate constants for both the reaction: k_w^+ and k_w^- for WGS, k_r^+ and k_r^- for SMR. The model used in literature for these constants are different.
The kinetic model, proposed by Divisek [13], calculates the kinetic from the operating condition of the cell (T, p) and from the partial pressure of products and reactants in the feed flows. The rate constants of the reactions (R_w and R_r) are calculated in Arrhenius form, while forward and reverse reaction rates constants are obtained by polynomial equations. Equations 2.16 of the model are provided from articles [13] and [14].

$$R_r = \frac{d\dot{N}_{CH_4}}{dt}\left[\frac{mol}{m^3\ s}\right] = k_r^+\left(p_{CH_4} \cdot p_{H_2O}\right) - k_r^-\left(p_{CO} \cdot p_{H_2}^3\right)$$
$$R_w = \frac{d\dot{N}_{CO}}{dt}\left[\frac{mol}{m^3\ s}\right] = k_w^+\left(p_{CO} \cdot p_{H_2O}\right) - k_w^-\left(p_{CO_2} \cdot p_{H_2}\right)$$

$$k_r^+ = k_o \exp\left(\frac{-E_a}{RT}\right) = (1.942)\,(2395) \exp\left(\frac{-231266}{RT}\right)$$

$$k_w^+ = (1.185)\,(0.0171) \exp\left(\frac{-103191}{RT}\right)$$

$$K_{eq}^{SMR} = \frac{k_r^+}{k_r^-} = \frac{p_{CO} \cdot p_{H_2}^3}{p_{CH_4} \cdot p_{H_2O}} \qquad K_{eq}^{WGS} = \frac{k_w^+}{k_w^-} = \frac{p_{CO_2} \cdot p_{H_2}}{p_{CO} \cdot p_{H_2O}}$$

(2.16)

K_{eq}^{SMR} and K_{eq}^{WGS} are the equilibrium constant of the reactions, functions of temperature or partial pressure of the components. With the previous equations, it is possible to have the molar rates of formation for the various species [14]:

$$\frac{d\dot{N}_{CH_4}}{dt} = -R_r \;;\; \frac{d\dot{N}_{CO}}{dt} = R_r + R_w \;;\; \frac{d\dot{N}_{CO_2}}{dt} = R_w \;;$$
$$\frac{d\dot{N}_{H_2}}{dt} = 3R_r + R_w \;;\; \frac{d\dot{N}_{H_2O}}{dt} = -R_r - R_w \qquad (2.17)$$

In this case, WGS is not considered at equilibrium, as in the most literature models, and SMR considers the effect of pressure.

The values of the reaction rate calculated using the model proposed by Divisek could generate a very slow kinetic of the reactions. In sight of this, it is suggested also the Numaguchi and Kikuchi model [15], which takes in account the interaction with the catalyst.

$$k_r^+ = k_o \exp\left(\frac{-E_a}{RT}\right) = (2.62 \cdot 10^2) \exp\left(\frac{-106900}{RT}\right)$$

$$k_w^+ = (2.45 \cdot 10^2) \exp\left(\frac{-54500}{RT}\right)$$

$$K_{eq}^{SMR} = \exp\left(\frac{-20009}{T} + 22.82\right) \qquad K_{eq}^{WGS} = \exp\left(\frac{4400}{T} - 4.036\right)$$

$$R_r = \frac{d\dot{N}_{CH_4}}{dt}\left[\frac{mol}{m^3\,s}\right] = \frac{k_r^+\left(p_{CH_4} \cdot p_{H_2O}\right) - \frac{k_r^+}{K_{eq}^{SMR}}\left(p_{CO} \cdot p_{H_2}^3\right)}{p_{H_2O}^{\,1.596}} \cdot \rho_{cat}\,(1-\varepsilon)$$

$$R_w = \frac{d\dot{N}_{CO}}{dt}\left[\frac{mol}{m^3\,s}\right] = \frac{k_w^+\left(p_{CO} \cdot p_{H_2O}\right) - \frac{k_w^+}{K_{eq}^{WGS}}\left(p_{CO_2} \cdot p_{H_2}\right)}{p_{H_2O}} \cdot \rho_{cat}\,(1-\varepsilon)$$

(2.18)

Temperatures are expressed in Kelvin. R is the universal gas constant $\left(8.314472\ \frac{J}{K\ mol}\right)$, k_o is the pre-exponential factor, E_a the activation energy typical of an Arrhenius law, ρ_{cat} is the catalyst density and ε the void factor of the catalyst (generally, equal to 0.6).

There are two different types of steam reforming in a SOFC: direct and indirect. Direct steam reforming occurs in the anode side channel; indirect steam reforming occurs before the anode side. Both the solutions have the advantage to move more the reaction to the products: the more is the H_2 fed, the more is the produced H_2O. Consequently, it is possible to feed less CH_4 fuel because the heat is used to reform and produce a more valuable fuel.
In the indirect steam reforming, the feed channel is next to the anode side and the catalyst is not useful to remove directly H_2 but to transfer heat from a channel to the other. If the heat removed is excessive, it is possible to increase the oxidant mole flow in order to consume more heat and maintain constant the SOFC operating temperature. The problem of indirect steam reforming is the mechanical resistance of the material and its chemical stability. Differently, for the direct steam reforming, it is difficult to manage the temperature in the anode side channel because the two reactions are, respectively, endothermic and exothermic.

2.2.2 Electrochemical model

The electrochemical models proposed by the literature are two. The difference is about the mechanism to describe the O^{--} consumption at the anode side (generally referred to the current): the 'H_2-CO' model considers the contribution of H_2 and CO to the produced current; the 'H_2-only' model considers only the hydrogen contribution.

SOFCs works with open-circuit and it is possible to calculate the maximum cell voltage really achievable ($V_{OC,cell}$), which is very close to the Nernst potential (E_{rev}), the reversible voltage, function of total pressure, temperature and composition of the flow and obtainable only if the current output is zero. The difference between E_{rev} and $V_{OC,cell}$ is very small and depends on the SOFC design and manufacture. This difference is due to internal parasitic currents and it can be neglected for this modelling [14].

$$V_{OC,cell} = E_{rev} = -\frac{-\Delta G_r^\circ}{n_e F} - \frac{R\,T}{n_e F} \ln \prod p_k^{v_k} \qquad (2.19)$$

n_e is the available number of electrons; F is the Faraday constant equal to 96485.3365 $C \cdot mol^{-1}$; ΔG_r° is the available Gibbs free energy of the reaction; p_k is the partial pressure of the component k elevated to its stoichiometric factor v^k.

E_{rev} can be calculated from the solid structure temperature (T_{ss}) and it is function of temperature, total pressure and composition.

$$E_0^{H_2} = 1.2729 - (2.7632 \cdot 10^{-4})\,T_{ss} \qquad E_0^{CO} = 1.4671 - (4.5292 \cdot 10^{-4})\,T_{ss}$$

$$E_{rev,H_2} = E_0^{H_2} - \frac{R\,T}{2\,F}\ln\left(\frac{p_{H_2O}}{p_{H_2}\left(\frac{p_{O_2}}{p_{amb}}\right)^{0.5}}\right)$$
$$E_{rev,CO} = E_0^{CO} - \frac{R\,T}{2\,F}\ln\left(\frac{p_{CO}}{p_{CO}\left(\frac{p_{O_2}}{p_{amb}}\right)^{0.5}}\right) \quad (2.20)$$

The two models (H_2-only and H_2-CO) are both from [14], respectively referred to Aguiar model [16] and Suwanwarangkul one [17].

In a real application, it is not possible to achieve this reversible potential because of losses. These losses can be called overpotentials η_i and can be divided in 3 different groups: activation, ohmic and concentration overtpotentials.
The operating cell voltage is

$$V_{cell} = E_{rev} - \eta_{ohm}(i) - \eta_{act,an}(i) - \eta_{act,cat}(i) - \eta_{conc,an}(i) - \eta_{conc,cat}(i) \quad (2.21)$$

where i is the density current.

It is possible to write a system of non-linear equations from the electrochemical model.

$$V_{cell} = E_{rev,H_2} - \eta_{ohm}(i) - \eta_{act,H_2}(i_{H_2}) - \eta_{act,cat}(i) - \eta_{conc,H_2}(i_{H_2}) - \eta_{conc,cat}(i)$$
$$V_{cell} = E_{rev,CO} - \eta_{ohm}(i) - \eta_{act,CO}(i_{CO}) - \eta_{act,cat}(i) - \eta_{conc,CO}(i_{CO}) - \eta_{conc,cat}(i)$$
$$i = i_{H_2} + i_{CO} \quad (2.22)$$

i_{H_2} and i_{CO} are the density currents, respectively related to H_2 and CO oxidation.

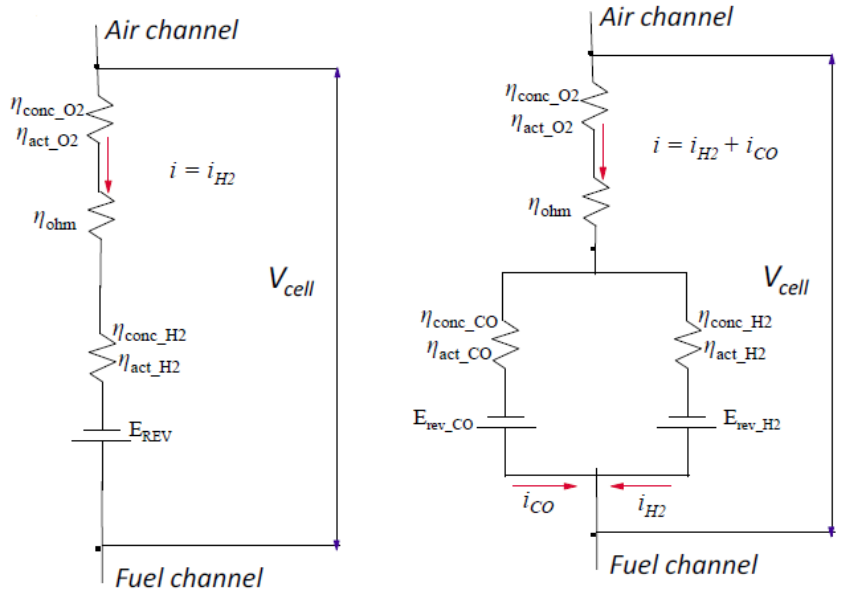

Figure 12: Equivalent electric circuit for H_2-only oxidation model (left) and for H_2-CO oxidation model (right) [14].

2.2.3 Overpotentials model

Ohmic overpotentials η_{ohm} are due to the surfaces resistivity of electrodes, interconnections and electrolyte. These losses are linked to the movement of electrons and oxygen ions. The total resistance can be separated in 3 different contributions: air channel interconnection, fuel channel interconnection and solid structure (SS) resistance composed by anode, cathode and electrolyte layers. To calculate the total resistance, the first step is to consider the single unit element of the cell (Figure 13) and divide the resistance of the interconnections as suggested by Campanari et al. (Figure 14) [14] [18].

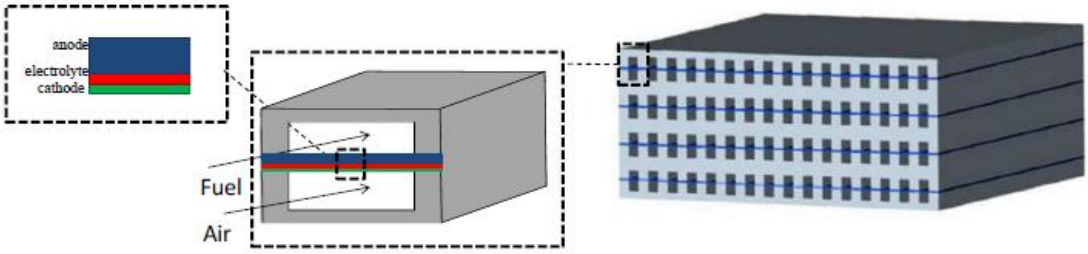

Figure 13: Unit cell element in co-flow configuration of a SOFC stack [14].

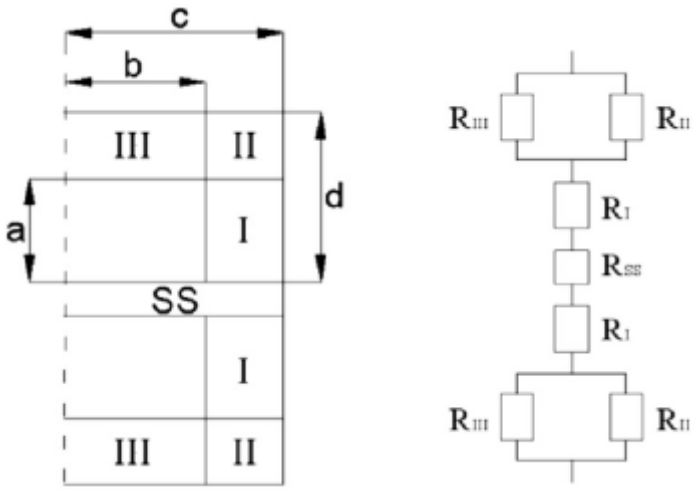

Figure 14: Geometric model of the ohmic overpotential (left) and equivalent electric circuit (right) of an unit single element of a SOFC stack [14].

The interconnections with 'L-shaped' are divided in three rectangular elements (I, II, III). The resistance of the solid structure is calculated from the resistivity of the layers, which depends on the temperature and the material. Solved the equivalent electric circuit, it is possible to calculate the total resistance of the unit cell element with Ohm's law approach, as proposed in [14] and [18].

$$R_{SS} = \frac{\sum_{k=an,cat,el} \rho_k \, \delta_k}{A}$$

$$R_I = \frac{a \, \rho_{ic}}{z \, (c-b)} \qquad R_{II} = \frac{(d-a) \, \rho_{ic}}{z \, (c-b)} \qquad R_{III} = \frac{\rho_{ic}}{z} \frac{1}{0.41 \left[1 - \exp\left(-1.2 \, \frac{b}{d-a}\right)\right]}$$

$$R_{TOT} = \frac{R_{III}\,R_{II}}{R_{III}+R_{II}} + R_I + \frac{R_{SS}}{2} \qquad \eta_{ohm} = R_{TOT}\; i \tag{2.23}$$

where a, b, c and d are the geometrical dimensions of the unit single element (Figure 14), ρ_k and δ_k resistivity and thickness of the different layers of the solid structure (anode, cathode and electrolyte), z and A the length and the passage area of the unit single element.

Activation overpotentials $\eta_{act,el}$ are relative to the energy required to activate the two main reactions at anode and cathode side, respectively the combination of oxygen ions with hydrogen/carbon monoxide and the reduction of oxygen and electrons. The calculation of these losses starts from the Butler-Volmer relationship, an implicit form for the current density [14].

$$i = i_o \left[exp\left(\frac{n_e\,\eta_{act,el}\,F}{R\,T}\;\alpha\right) - exp\left(\frac{n_e\,\eta_{act,el}\,F}{R\,T}\;(\alpha-1)\right)\right] \tag{2.24}$$

i_o is the calculated current density for both the electrodes; α is the transfer coefficient, considered equal to 0.5; F is the Faraday constant; n_e is the number of permeated electrons at the anode side (equal to 2); i_o is calculated with an Arrhenius equation. This definition changes model to model and depends on a pre-exponential factor A_{el} and on an activation energy E_{el}, as well as on the operating conditions of the SOFC. This kind of loss is small at high temperature (e.g. 1000 °C) because the electrode reaction is fast. On the contrary, at lower temperatures, the activation overpotentials are the most of the losses.

For simplicity, it will be used only the H_2-only model for this modelling. For brevity, Equations 2.25, report only the expressions for this electrochemical model [14] [16].

Cathode

$$i_{o,cat} = \frac{RT}{n_e\,F}\;k_{cat}\;e^{\frac{-E_{cat}}{R\,T}}$$

$$i = i_{o,cat}\left[e^{\frac{n_e\,\eta_{act,cat}\,F}{R\,T}\alpha} - e^{\frac{n_e\,\eta_{act,cat}\,F}{R\,T}(\alpha-1)}\right]$$

$k_{cat} = 2.35 \cdot 10^{11}\ \Omega\, m^{-2}$ $\qquad$ $E_{cat} = 137 \cdot 10^{3}\ \mathrm{J}\, mol^{-1}$

Anode

$$i_{o,an} = \frac{RT}{n_e\,F}\;k_{an}\;e^{\frac{-E_{an}}{R\,T}}$$

$$i = i_{o,an}\left[\frac{x_{H_2}^{TPB}}{x_{H_2}^{bulk}}\;e^{\frac{n_e\,\eta_{act,an}\,F}{R\,T}\alpha} - \frac{x_{H_2O}^{TPB}}{x_{H_2O}^{bulk}}\;e^{\frac{n_e\,\eta_{act,an}\,F}{R\,T}(\alpha-1)}\right]$$

$k_{an} = 6.54 \cdot 10^{11}\ \Omega\, m^{-2}$ $\qquad$ $E_{an} = 140 \cdot 10^{3}\ \mathrm{J}\, mol^{-1}$

(2.25)

x_i^{TPB} is the molar fraction of the component i at cell reaction sites and x_i^{bulk} is the bulk flow molar fraction of the component i. The ratio between these is necessary to consider the effect on current density of the lower reactant concentration at cell reaction sites.

Concentration overpotentials $\eta_{conc,el}$ are relative to the current density: the more is the current density, the more is the consumption of fuel; the higher is the production rate, the lower is partial pressure of the reactants at the reaction sites.
Equations 2.26 are proposed in [14] and [19] to calculate concentration overpotentials for both the models, depending on the different concentrations at TPB and in the bulk flow.

$$\eta_{conc,cat} = \frac{RT_{SS}}{4\,F}\, ln\left(\frac{x_{O_2}^{bulk}}{x_{O_2}^{TPB}}\right)$$

$$\eta_{conc,H_2} = \frac{RT_{SS}}{2\,F}\, ln\left[\left(\frac{x_{H_2O}^{bulk}}{x_{H_2O}^{TPB}}\right)\left(\frac{x_{H_2}^{bulk}}{x_{H_2}^{TPB}}\right)\right] \qquad \eta_{conc,CO} = \frac{RT_{SS}}{2\,F}\, ln\left[\left(\frac{x_{CO}^{bulk}}{x_{CO}^{TPB}}\right)\left(\frac{x_{CO_2}^{bulk}}{x_{CO_2}^{TPB}}\right)\right]$$

(2.26)

Gas species concentration can be calculated, as reported by Campanari et al. [19], using the Dusty Gas Model. This law takes into account the Knudsen diffusion phenomena and the different molecular weight and modifies the Stephan-Maxwell Model, the most used model for multicomponent systems.
In general, the contribution of the concentration overpotentials to the cell voltage is low. For this reason, it is not useful a more detailed mass transfer model because the results are not so influenced.

2.2.4 Thermal model and energy balance

The electrochemical model system is solved with a finite volume approach for every part of the SOFC: anode, cathode and the solid structure. This model needs a link to the internal temperature profile. A thermal model will consider the convective heat transfer between the flowing gas and the solid structure and the absolute enthalpy at the inlet of anode and cathode side. The radiative heat transfer is neglected because it is demonstrated in [20] that its influence on the heat transfer and the solid structure temperature profile is not relevant.
Equations 2.27, proposed by Campanari et al. [18], are related to the thermal model.

$$\sum_i^n \left(n_i^{in}\, h_i^{in}\right) - \sum_i^n \left(n_i^{out}\, h_i^{out}\right) + \lambda_f\, A_f \left(T_{ss} - T_{f,bulk}\right)$$

$$\sum_k^n \left(n_k^{in}\, h_k^{in}\right) - \sum_k^n \left(n_k^{out}\, h_k^{out}\right) + \lambda_a\, A_a \left(T_{ss} - T_{a,bulk}\right)$$

$$\int_x k_{ss}\, A_x\, \frac{\partial^2 T_{ss}}{\partial x^2}\, dx + \int_y k_{ss}\, A_x\, \frac{\partial^2 T_{ss}}{\partial y^2}\, dy + \lambda_a A_a \left(T_{ss} - T_{a,bulk}\right) + \lambda_f A_f \left(T_{ss} - T_{f,bulk}\right) + W_{el} + Q_{loss} = 0 \tag{2.27}$$

The first equation is related to the anode side, therefore i is relative to H_2, H_2O, CO, CO_2, CH_4 and N_2; the second equation to the cathode side, therefore i is relative to O_2 and N_2. The third equation is the energy balance of the solid structure: k_{ss} is the thermal conductivity, W_{el} the electric power and Q_{loss} the thermal power losses for dissipation.

The electric power can be obtained from the permeated oxygen moles $n_{O_{2,perm}}$:

$$W_{el} = i \cdot A = n_e \cdot F \cdot \frac{\left(\dot{m}_{IN} - \dot{m}_{OUT}\right)_{comb}}{MM_{comb}} = n_e \cdot F \cdot n_{O_{2,perm}} \tag{2.28}$$

where A is the electrode surface and n_e is the number of charges/electrons for every permeated ions of oxygen. A reduction factor ε_F, called Faraday factor, can be added to the Equation 2.28: it considers that not all the permeated electrons reach the electric circuit.

Chapter 3

Chemical Looping Combustion (CLC)

The first studies about the Chemical Looping Combustion (CLC) are of the first years after the Second World War. In 1946, there was the first patent about something similar to the Chemical Looping: the researchers of Standard oil Development Company proposed a system where two fluidized beds are used to produce syngas (Figure 15) [21].

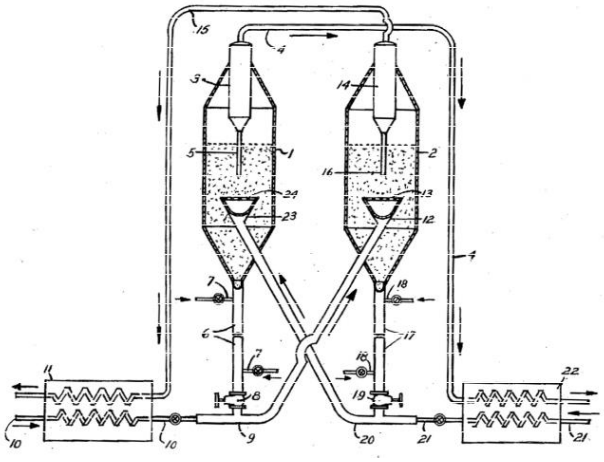

Figure 15: Picture of the patent n◦ 2.665.199 of 10th December 1946 by Homer Z. Martin and Charles E. Heminger for the Standard Oil Development Company [21].

In 1950, Lewis and Gilliland designed a fluidized bed to produce pure CO_2 using the reduction and the oxidation of a recirculated solid metal [22]. In 1983, Karl F. Knoche from Aachen and Horst J. Richter from Hannover published an article, ‘’Reversibility of combustion processes’’: they tried to demonstrate that combustion with an intermediate medium is able to reduce the irreversibility in comparison to the direct contact between air and fuel [23]. This intermediate medium could be a metal oxide which reacts consequently with fuel and air, transferring the atomic oxygen. This solution is the first study very close to the actual CLC and the metal oxide can be called Oxygen Carrier (OC) of the CLC. In 1987, the name Chemical Looping Combustion was used for the first time by Ishida [24].

Nowadays, Chemical Looping is one of the most studied processes because it can be used to generate heat and to separate easily CO_2 from an exhaust gas of a power production process that uses fossil fuels. These are two objectives with great industrial interest.
Several CLC prototypes have been presented in literature. The biggest testing prototype (1 MWth) is in Darmstadt and uses coal as fuel [26].

3.1 General Principles

In a general scheme (Figure 16), CLC uses two reactors with different functions:

- in a Fuel Reactor (FR), fuel and metal oxide are fed and react;
- in an Air Reactor (AR), the regeneration of metal oxide occurs and the air provides the missing O_2.

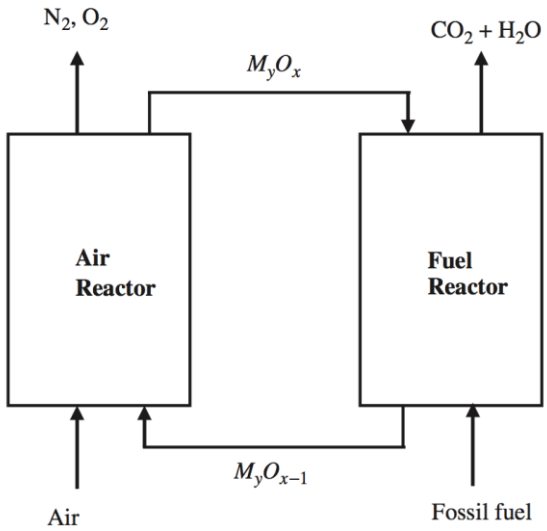

Figure 16: General scheme of CLC [25].

The products of this system are two:

- from FR, a flow rich of H_2O and CO_2, sometimes with a little amount of H_2 or CO, depending on the type of fuel;
- from AR, oxygen-depleted air, generally to send to a power plant.

In the beginning, the goal of CLC was to improve the efficiency of the power plant and all the studies were focus about that. However, during these studies, it was evident that CLC could be more useful for CO_2 separation and capture. The possibility to obtain a flow rich of H_2O and CO_2 allows to separate CO_2 easily with water condensation, taking advantage of the different point of condensation of H_2O and CO_2. In turn, no additional systems for CO_2 separation are required. It is a benefit for the global energy balance because it is a process with very low thermodynamic losses and a benefit from an economic point of view (fewer components to buy). The capture efficiency can be very close to 100%. The CO_2 flow is obtained almost pure and it can be sent to compression and storage/sell.

Reactions 3.1 can summarize the reactions in the FR:

$$(2n+m)M_yO_x + C_nH_{2m} \Leftrightarrow (2n+m)M_yO_{x-1} + mH_2O + nCO_2$$

$$CO + MeO_a \Leftrightarrow CO_2 + MeO_{a-1}$$

$$H_2 + MeO_a \Leftrightarrow H_2O + MeO_{a-1} \quad (3.1)$$

Reaction 3.2 can summarize the reactions in the AR:

$$M_y O_{x-1} + \frac{1}{2} O_{2\,(air)} \Leftrightarrow M_y O_x + \left(N_{2\,(air)} + unreacted\ O_2\right) \qquad (3.2)$$

(3.2) is always exothermic because it is an oxidation/regeneration; (3.1) can be exothermic or endothermic, depending on the oxygen carrier and the fuel. The sum of the two reactions is a direct combustion between fuel and air: the energy released by a single CLC loop has to be the same of the direct combustion one. It can be calculated using the standard enthalpy of formation of the reactants, the specific heat of the single components and the operating temperature.

In general, the advantages of CLC process are:

- low additional energy required to separate CO_2 and, consequently, less penalties unlike the other separation systems;
- less NO_x because of the lower temperature of the thermodynamic cycle and the lower oxygen in the oxidant.

Conversely, the disadvantages are:

- an integrated gas turbines would not work at the maximum because the operating temperature would be limited by the maximum operating temperature of the metal oxide;
- oxidation processes at high temperature are very complex because of circulation, chemical stability and mechanical resistance;
- CLC is a technology not industrial/commercial but only available as small size prototype.

The difficulties of the utilization of this technology is relative to the need to know the chemical behaviour, the specific kinetic, the energy balance of the reactors and the fluid dynamic regime to design very well the system. All these aspects have been studied a lot about small size prototype and the next step is to applicate this technology and these studies on industrial plants.

3.2 Oxygen carriers

The type of oxygen carrier is very important to design the reactors and for the configuration of the integrated thermodynamic cycle.

The general features of the oxygen carrier have to be the following:

- high reactivity with the fuel (reduction) and with the air (oxidation) in order to have the maximum oxygen transport capacity between the two reactors;
- high fuel conversion capacity in order to have at minimum fuel conversion losses;
- high oxygen transport capacity, calculable as

$$R_{OC} = \frac{\dot{m}_{ox} - \dot{m}_{red}}{\dot{m}_{ox}} \qquad (3.3)$$

where $\dot{m}_{ox}$ is the mass flow of the oxidized OC and $\dot{m}_{red}$ is the mass flow of the reduced OC. The more is the oxygen transport capacity, the fewer is the mass flow necessary to transport the same amount of oxygen and the energy consumed to move the metal oxide (fluidized beds) or the smaller is the size of the reactors (fixed beds);

- low agglomeration at the high temperature, in order to avoid the coalescence of the particles and the consequent reduction of fluidity and reactivity, depending on the ratio surface/volume;
- as few expensive as possible and no environment problems;
- high mechanical resistance to frictional stress, linked to the circulation of the particles in fluidized beds.

Iron (Fe), Copper (Cu) and Nickel (Ni) are the principal components used as base of the metal oxide. The results of the previous works have shown that their features match with the perfect ones. Conversely, Cobalt (Co) has problem of agglomeration and Manganese (Mn) does not allow a full conversion of the fuel and not work at temperature higher than 1000 °C. Another interesting material is Ilmenite, an oxide of Iron and Titanium, which seems optimum for the syngas case.

These materials have to be studied with the relative support, made of another metallic material. Previous works have shown that the combination with the support improves the performance of the metal oxide. Generally, the support is made of a derivate of Alumina (Al_2O_3), ZrO_2, YSZ, Silicon and Titanium oxide, Bentonite or Sepiolite.

In Appendix B, there is a summary of all OCs studied with their principal features.

3.2.1 Nickel oxides

Pure Nickel oxides have very good behaviour but the performance gets worse fast because of agglomeration. The support is necessary to increase the mechanical resistance, leaving unchanged the thermodynamic properties of the metal oxide and promoting the reactions.
The supports more studied are: Alumina (Al_2O_3), $MgAl_2O_4$ and YSZ. The first has a good stability, in particular with syngas at high temperature but has not a good mechanical resistance and tends to produce Nickel aluminate ($NiAl_2O_4$) at temperature higher than 1000 °C. The second has the best performance with syngas: good mechanical resistance, high reactivity and good stability. The third has very good reactivity and regenerability and the best oxidation velocity with the couple NiO-YSZ but it is too expensive. Other supports studied are SiO_2, ZrO_2 and TiO_2.
References of these considerations are the articles [25], [27], [28], [29] and [39].

3.2.2 Iron oxides

The principal advantage of Iron is to be very common and, consequently, cheap. The iron oxides are three, depending on the level of oxidation: Ematite (Fe_2O_3), Magnetite (Fe_3O_4) and Wustite (FeO). These different levels of oxidation allow using more than two reactors, with a particular scheme with three reactors.

Alumina is the best material as support of Iron. In particular, the couple Fe_2O_3/Al_2O_3 has shown an increase of the reactivity going ahead with the cycles. It is due to the expansion of the pores that increases the diffusivity of the reactant gases. The mechanical resistance is very good and the agglomeration does not occur, also at high temperature (T > 1000 °C). However, the reactivity is lower than Nickel.
$MgAl_2O_4$ with iron oxides shows agglomeration going ahead with the cycles while TiO_2 has a reduction of available oxygen due to the formation of Ilmenite ($FeTiO_3$). SiO_2 has the same problem of TiO_2 because of formation of inert iron silicates. Instead, YSZ reduces directly Ematite in Wustite with the consequent formation of Fe_3C.
References of these considerations are the articles [25], [30], [31], [32], [33], [34] and [39].

3.2.3 Copper oxides

Copper has different advantages in comparison to the other materials:

- the highest oxygen transport capacity ($R_{OC} \sim 0.5$);
- the reduction of CuO is particularly efficient and it is able to guarantee the total conversion of gas fuels, like syngas and natural gas;
- high reactivity in reduction and oxidation.

The big problem relative to Copper is the low fusion temperature (1083 °C). It limits the maximum operating temperature (850 °C) and it is a problem in case of integration with a combined cycle. Furthermore, it was demonstrated that Copper performance decreases fast at temperature like 850 °C because of agglomeration. However, for its cheapness, Copper is the material most attractive to industrial application. The combination with a support can increase a lot the performance of the Copper. The most studied materials as support are Alumina, ZrO_2 and YSZ.
References of these considerations are the articles [25], [33], [34], [35] and [39].

3.2.4 Ilmenite

Ilmenite is a mineral of Iron and Titanium, very common in nature and cheap. Its more oxidized state is Pseudobrookite (Fe_2TiO_5) + Rutile (TiO_2) while the more reduced is Fe_2O_3. An advantage of Ilmenite is the possibility to produce it from TiO_2 and Fe_2O_3. Ilmenite is able to convert CO and H_2 with high efficiency (respectively, $CO/(CO + CO_2)$ and $H_2/(H_2 + H_2O)$ are equal to 0.0006 and 0.0004) and it has a good behaviour in case of direct combustion of solid fuel. It tends to maintain a good reactivity going ahead with the cycles, in particular in the first cycles the reactivity increases because of growth of the porosity and the consequent increment of the contact surface between reactants (Figure 17).

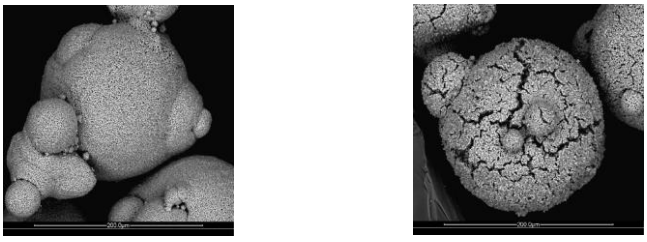

Figure 17: Ilmenite before (left) and after (right) 30 cycles of CLC. The increase of porosity is evident [36].

Ilmenite has a good oxygen transport capacity but lower than Nickel and Copper. Furthermore, in comparison to the other materials, it does not need an inert support (it has a Titanium part) and it has a good mechanical resistance which increases with the Titanium composition.
References of these considerations are the articles [36] and [37].

3.3 Reactors design

The design of the reactors is one of the most important parameter to achieve the optimum performance. The reactors have to guarantee a good contact between gas species and the OC. A good contact allows few energy losses and fast time of reduction and oxidation. The design is complex because of the dependence in relation to a lot of parameters.

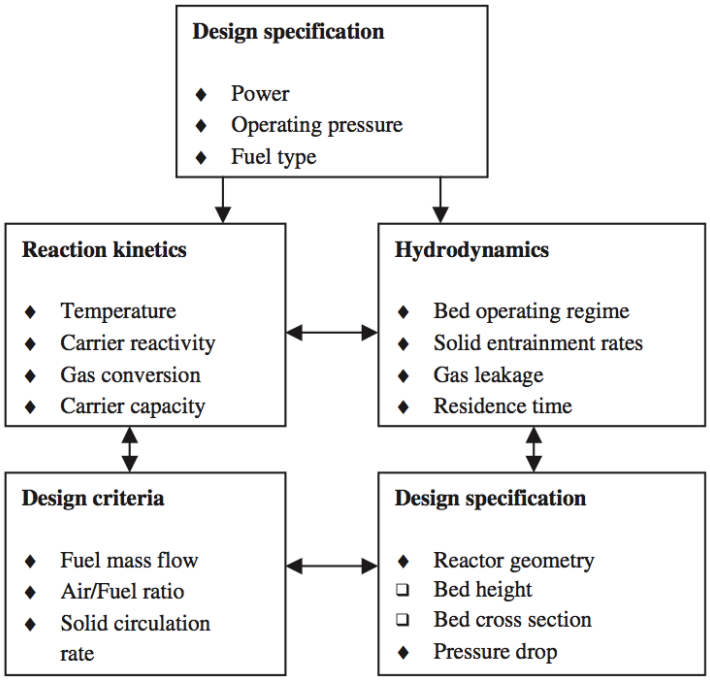

Figure 18: Block diagram, proposed by Kronberger, for the design of CLC reactors [38].

Kronberger [38] proposed a cycle to follow for the design of CLC. His scheme (Figure 18) shows how difficult is the design of CLC reactors: it is necessary to consider together mechanical-structural, kinetic-chemical and hydrodynamic aspects.

In particular, the most important parameters for the design are:

- the operating temperature: if it raises, the reaction is faster and it reaches easily the chemical equilibrium. But the reactions of CLC can be endothermic or exothermic: endothermic reactions are promoted at high temperature while exothermic at low temperature. In relation of these considerations, the choice of the OC will be done and it is fundamental;
- OC reactivity: if high, the kinetic of reaction is fast, otherwise it will be necessary a catalyst to achieve high degree of progress and to maintain an adequate excess of metal oxide;
- maximum conversion of the gas;

- oxygen ratio;
- OC stability: it is the capacity to maintain the same thermodynamic and chemical-mechanical properties after some cycles of working. A task of the inert support is to improve this property.

Considering these parameters, it is possible to calculate the fuel mass flow, the air-fuel ratio, the amount of solid and the velocities of recirculation. The geometry of the reactors (height and transversal section) and the energy losses is determined by the analysis of the fluid dynamic regime, the rate of solid entrainment (if fluidized bed), the rate of residence and the gas leakage. As shown in Figure 18, all these aspects are interconnected each other.

The first important thing to decide is the kind of reactors, fixed beds or fluidized beds.

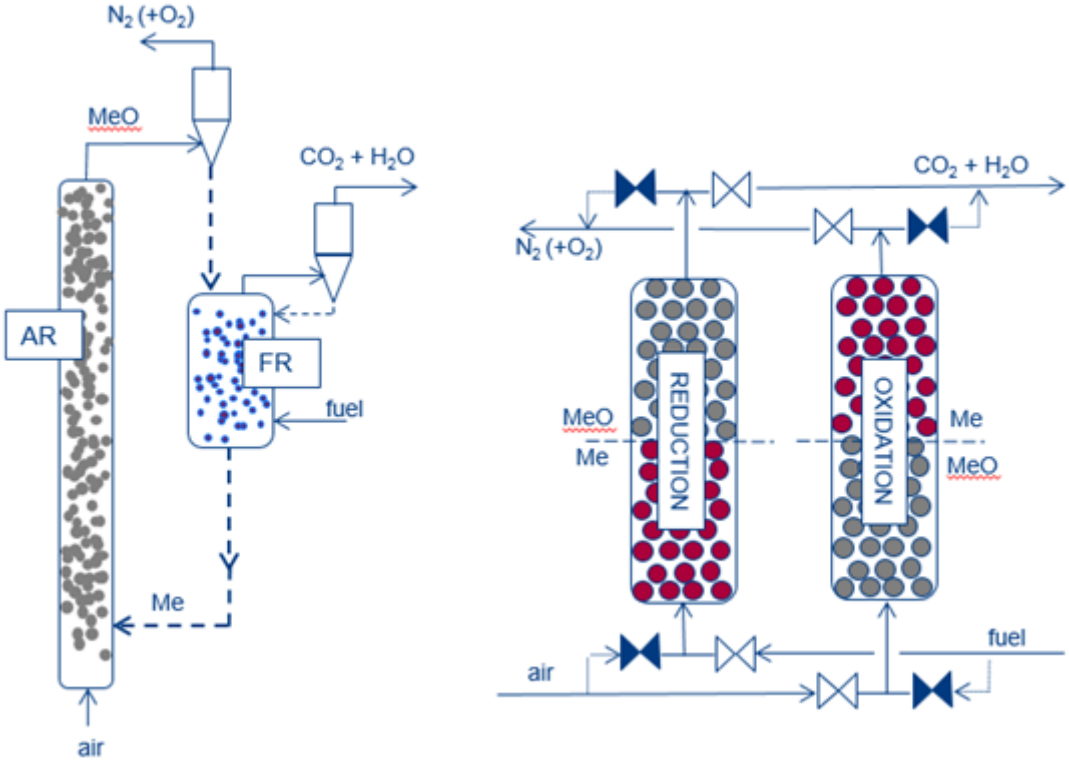

Figure 19: Schemes of the two types of reactors for CLC: a) fluidized beds and b) fixed beds [26].

The fluidized bed is the most used in literature and the most adequate for industrial application. In a fluidized bed, the solid particles are dragged on by the air in the AR (typically, a riser). Then, the solid particles reach the reduction reactor, a boiling bed where the OC is reduced by the fed fuel from the base (Figure 19). The advantage of fluidized beds in comparison to fixed ones is to work continuously. At the same time, it is necessary to move the solid metal oxide and separate the solid with a cyclone. All the particles have to be removed because these can be dangerous for the components of a following power plant or for CO_2 treatment. This operation is difficult at high temperature and high pressure but not at atmospheric pressure. Fluidized beds are favoured in comparison to fixed beds because easier to design and manage because of the smaller dimensions.

In a fixed bed, the problem of the solid movement is solved with a periodic control on the inlet and outlet valves: in this way, it is possible to work with two (usually more than two) beds which work alternatively in oxidation and reduction. It can be an advantage because the reactors will work at different pressure, saving the energy for the CO_2 compression. However, in fixed beds, it is more important the problem of carbon deposition and sulphur solid compounds formation and it is more difficult the temperature control in comparison to the fluidized beds, which work at stationary condition.

3.4 Carbon deposition

Carbon deposition is one of the most common problems in the FR of CLC. It is important to avoid it for two reasons:

- if the beds are interconnected, carbon can go into the AR, reacts with the oxygen and produces CO_2 with a consequent reduction of the capture efficiency;
- production of lampblack reduces the energy efficiency because of the filling of the active sites, in particular for fixed beds. The energy/pressure losses rise and the metal oxide is not all reduced.

The reactions of lampblack generation are two: the pyrolysis of the methane and the inverse Boudouard reaction:

$$\begin{aligned} CH_4 &\Leftrightarrow C + 2H_2 \\ 2CO &\Leftrightarrow C + CO_2 \end{aligned} \tag{3.4}$$

The first one is endothermic, promoted at higher temperature. The second one is exothermic, promoted at lower temperature. The kinetics of these two reactions is very slow in absence of catalyst but some reduced metal oxides works as catalyst. It is important to make a good study about the OC and check its behaviour in relation with carbon deposition.
The amount of available oxygen by the metal oxides, the operating temperature, the reactor pressure and the composition of the feed (more hydrogen and oxygen is better) are the principal factors that influence the carbon deposition.
It is possible to define an oxygen added ratio(ζ), equal to the ratio between the available oxygen by the OC ($n_{O,added}$) and the stoichiometric oxygen necessary to convert all the fuel in CO_2 and H_2O ($n_{O,stoich}$).

$$\zeta = \frac{n_{O,added}}{n_{O,stoich}} \tag{3.5}$$

As shown in Figure 20:

- at temperature higher than 900 °C, carbon deposition is not possible if the oxygen is more than 25% of the stoichiometric amount;
- the influence of pressure is opposite in comparison to the temperature influence: if temperature is high, an increase of pressure reduces the carbon deposition, vice versa promotes it. This behaviour is due to the different nature of the two carbon deposition reactions: the first is endothermic with increment of mole number (favourite at low pressure), the second one is exothermic with reduction of mole number (favourite at high pressure).

- for methane, an increment of temperature with a reduction of pressure or an increment of the amount of steam water, reduces the possibility of carbon deposition.

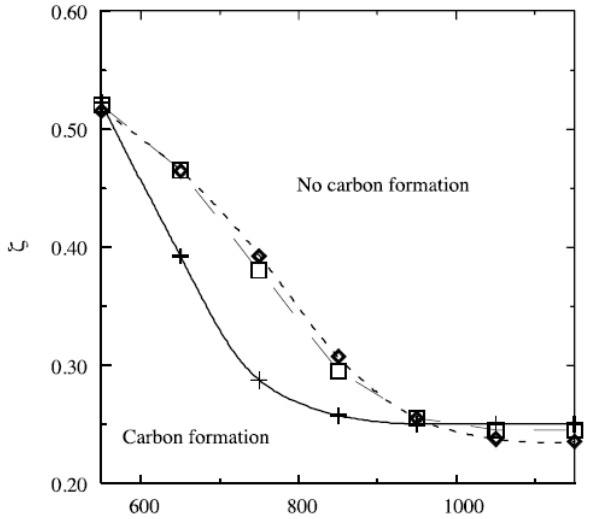

Figure 20: Relation between oxygen added ratio (ζ) and temperature at different constant pressure (1 bar +, 15 bar □, 30 bar ◊) with natural gas. It is shown the zone where carbon formation is possible [27].

The previous diagram is valid for all the cases (different feed and oxygen carrier). The only difference with the syngas case is that there is a limit temperature above which there is not carbon formation, also for oxygen added ratio equal to zero. This temperature is strongly dependent by CO and H_2O concentration in the syngas.

Chapter 4

Methodology of calculation

The purpose of this work is to study the strength and the prospective of a large size integrated system of an IT-SOFC and a CLC reactor. The objectives of the plant are to produce electricity as efficiently as possible and separate and compress the CO_2 produced by the utilization of a fossil fuel, as well to store it.

The work pursues different goals:

- create a model with an integrated system of SOFC and CLC, able to produce electricity in large-size and separate the CO_2 produced;
- design an adequate thermal integration;
- analyse the performance of the model and compare the results with the benchmark plant, without CO_2 capture and more traditional;
- make a sensitivity analysis and analyse the influence on performance of changes in operating conditions and/or in the configuration of the model;
- study specifically the SOFC and, using the available models, get the trends of compositions in the fuel cell, calculate its dimensions and evaluate all its features, such as current density and voltage losses trends;
- propose a small-size model with an adequate thermal integration and analyse its performance.

The models are realized using Aspen Plus, a software that includes many chemical and mechanical components and able to make rigorous mass and energy balance. Excel is used to integrate some specific calculation in the Aspen Plus models, analyse the trend of sensitivity analysis and build the SOFC model.

The comparison of the results of the SOFC+CLC model with the results of a more traditional and simpler system without CO_2 separation and storage is fundamental to validate the model and understand if this kind of integration can be interesting. The reference plant is the plant proposed by Campanari et al. [41]. This plant consists in a SOFC without chemical looping, without CO_2 capture and storage, with an easy combustor to pre-heat the air to be sent to the cathode side. The combustor burns the flows from the SOFC outlet. This plant will be re-modelled in Aspen Plus, as rigorous as possible; the objective is to have results as close as the ones had in [41], in order to have a comparison even more valid. For the same reason, the assumptions of the two models have to be the same or, at least, as close as possible.

The large-size model is the main topic of this work; from here, whole the discussion will be about this. The small-size model will be discussed separately in Chapter 8.

4.1 SOFC: state-of-art

It is possible to refer to four of the most important manufactures in the world to explain IT-SOFCs state-of-art, as made by Campanari et al. [41]: Ceramic Fuel Cell Ltd (CFCL, Australia), Fuel Cell Energy Inc. (USA), Solid Power (Italy) and Bloom Energy (USA). In particular, [41] reports the simulation model of one of the best example of latest generation IT-SOFC. This is proposed by CFCL [42][43] and it is a micro-CHP unit (1.5-2 kW range), rated at 60% net LHV efficiency (AC) and fed with natural gas. The cell can work at about 750°C with low excess of air and a limited steam-to-carbon ratio in the reforming process.
In Figure 21, this SOFC plant layout is reported while, in Figure 22, there is its energy balance.

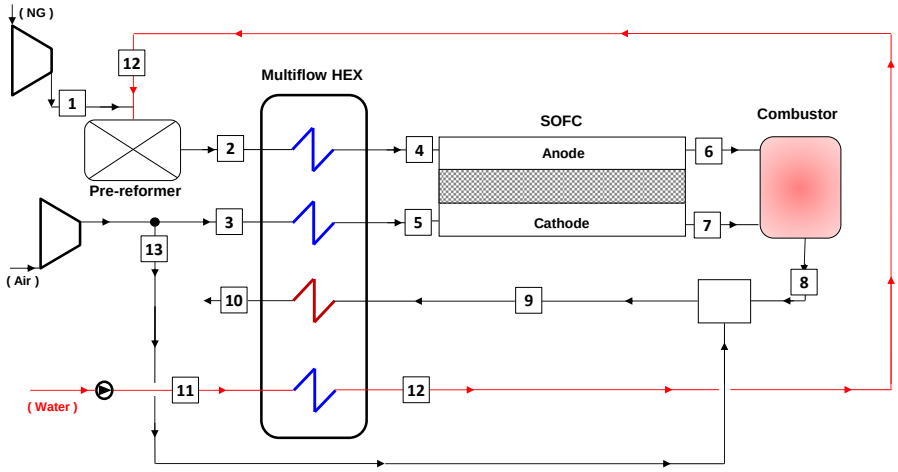

Figure 21: Layout of IT-SOFC stack manufactured by CFCL [41][42][43].

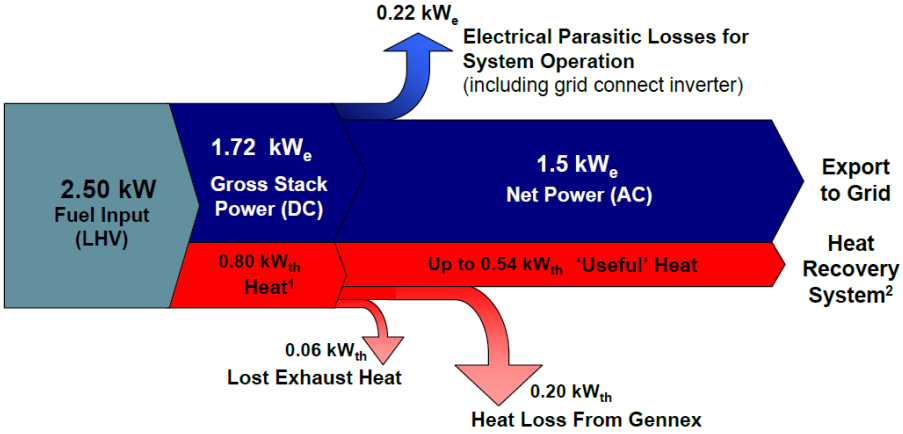

Figure 22: Energy balance of IT-SOFC proposed by CFCL [41][42][43].

In Appendix C, there are all the assumptions and the results about the simulation model made by Campanari et al. [41] using the software GS. GS is a proprietary simulation code originally developed at Princeton University for the analysis of gas/steam power cycles and then extended at the Department of Energy of Politecnico di Milano [41].

The fuel utilization (Paragraph 4.3) achieved in this system is 85% and the increment of air temperature through the cathode side is approximately 40 °C (from 735°C and 774°C). The average cell voltage is 0.86 V, reached through 51 cells operating at 43.7 V. Fuel temperature at anode side inlet is 500°C, while 380°C is its temperature after the pre-reformer. The steam-to-carbon is imposed equal to 2.16. The air utilization (Paragraph 4.3) is set to 30.5%, in order to have a temperature of 830 °C at the outlet of the burner. The thermal power input is 2452 kWth (LHV-based) and the SOFC power output achieved is 1713 W. Inverter and auxiliaries losses are 221 W. The net electrical efficiency obtained is 61.2% (LHV), very close to the one presented in Figure 4.2, 61.3%.
All these results and assumptions made by Campanari et al. [41] are very close to the manufacturer's ones; the same performances and operating conditions are reported for other 60%-class efficient SOFCs (with different plant layout) and confirmed by similar works in literature [41][43][44][45][46].

The purpose of this work is to use similar operating conditions for a large-size SOFC system, with and without CO_2 capture. It is not a gamble. One of the most important advantages of this technology is to be highly modular, have flexible working conditions and efficiency independent of the load and the size. Furthermore, it is a technology of high reliability and availability due to the absence of moving parts (with the resulting performance decline). Obviously, a large-size plant will show an improved efficiency of the auxiliaries (e.g. DC/AC conversion losses) due to scale effects but, at the same time, different kind of thermal integration or new specific losses (e.g. piping thermal and pressure losses) [41].

In Figure 23, a general scheme of the obtainable electrical efficiency in state-of-art, depending on the size, fuel and power generation solution [41][42][43].

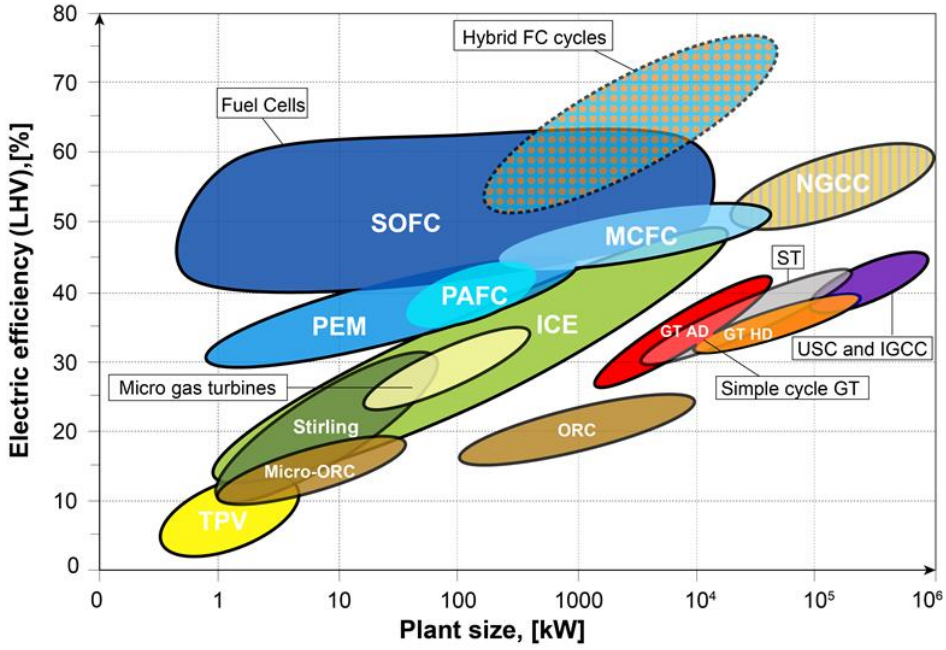

Figure 23: Scheme of state of art electrical efficiency in different power production systems (PEM = Polymeric Electrolyte Fuel Cell; PAFC = Phosphoric Acid fuel cells; MCFC = Molten

Carbonate Fuel Cells; ORC = Organic Rankine Cycle; ICE = Internal Combustion Engines; TPV = Thermo-Photovoltaic units; GT AD/HD = Aero-Derivative or Heavy Duty gas turbines; ST = conventional Steam Turbine cycles; USC = Ultra Super-Critical steam cycles; NGCC = Natural Gas Combined cycles; IGCC = Integrated Gasification Combined Cycles).

4.2 Main assumptions

It is possible to summarize all inputs and outputs of the model with a simple diagram (Figure 24), regardless of the operating conditions.

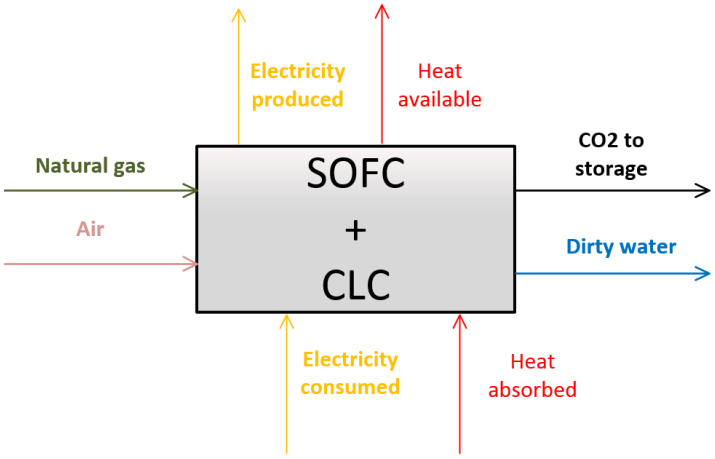

Figure 24: Schematic process description for SOFC+CLC plant.

One of the SOFC advantage is to have low environmental impact because of the use of high-grade fuels. The fuel of this model is natural gas: a clean fuel, available by the pressurized network (20 bar), able to provide a good amount of energy (46.482 MJ/kg). The composition used for the natural gas is the standard one, considering methane and heavier hydrocarbons. Another feature of natural gas is not to need particular processes to be produced or treated before use (in comparison to syngas). The amount of natural gas to feed in the model in all the cases (2.151 kg/s) will be the same and will be equal to a thermal input of 100 MW, reasonable for a large-size plant.
SOFC is used to produce electricity efficiently, without combustion; CLC to pre-heat the air flow and to separate CO_2 produced in the SOFC by the oxidation of CO and H_2. The heated air feeds the cathode side from AR of CLC while the flow at the outlet of FR of CLC, rich of H_2O and CO_2, has to be cooled: due to the different point of condensation of H_2O and CO_2, CO_2 separation occurs very easily and without a big energy expense. The fuel of CLC will be the flow at the exit of anode side that contains the remaining CO and H_2, not reacted in the SOFC.
The thermal integration plays very important rule. It is available a good amount of heat from the flow at high temperature to be cooled. This waste energy can be used to produce additional electricity with the integration of a thermodynamic process. The integrated thermodynamic cycle has to be the right one in relation to the amount of available heat and its temperature. In this case, a simple steam cycle, without re-heats, can be the perfect solution. The reasons will be explained better later.
The reference plant differs from the SOFC+CLC system for the absence of CLC and for the presence of a combustor to pre-heat the air burning the flows from the SOFC

outlet. The integrated thermodynamic cycle is the same of the SOFC+CLC system, a steam cycle with the same operating conditions and assumptions.

In Table 4.1, there are the main assumptions adopted for all the models, with and without CO_2 capture.

Ambient conditions		
Temperature [°C]	15.0	
Pressure [bar]	1.013	
Relative Humidity [%]	60.0	
Natural Gas		
Molar composition [%vol]	CH_4: 89.0, CO_2: 2.0, C_2H_6: 7.0, C_3H_8: 1.0, N_2: 0.89, C_4H_{10}: 0.11	
LHV [MJ/kg]	46.482	
Fuel power input [MW_{th}]	100.0	
Feed network pressure [bar]	20.0	
SOFC		
Minimum air inlet temperature [°C]		735.0
Minimum fuel inlet temperature [°C]		600.0
Anode and cathode outlet temperature [°C]		800.0
Cell voltage [V]		0.80
Minimum O_2 molar fraction at SOFC outlet [%v/v]		5.0
Air and fuel channels pressure losses [%]		3.0
Pressure drop of air filter [bar]		0.01
Heat loss [% of fuel LHV]		2.0
DC/AC electrical efficiency [%]		97.0
Steam Cycle		
Evaporation pressure [bar]		40.0
Maximum steam temperature [°C]		400.0
Subcooling ΔT at evaporator drum inlet [°C]		5.0
Pressure drop in steam superheater [%]		3.5
Pressure drop in economiser [bar]		10.0
Pressure drop at turbine inlet [%]		5.0
Gas pressure drop in recovery boiler [bar]		0.05
Temperature drop in superheater to turbine piping [°C]		2.0
Minimum condensing pressure [bar]		0.048
Turbine isentropic efficiency [%]		85.0
Feed water pump hydraulic efficiency [%]		85.0
Turbine mechanical efficiency [%]		99.60
Generator electric efficiency [%]		98.50
Minimum O_2 molar fraction at combustor outlet [%v/v]		1.50
Pre-reformer		
Pre-reformer inlet S/C ratio* [-]		2.0
Low Temperature Sulphur removal		
Operating temperature [°C]	15.0	
Fuel pressure loss Δp/pin [%]	3.0	
Heat Exchangers		
Hot and cold side $\Delta p/p_{in}$ [%]		2.0
LT and HT air regenerators $\Delta p/p_{in}$ [%]		3.0
Heat losses [% of heat transferred]		0.7
Minimum gas - evaporating water ΔT (pinch-point)[°C]		10.0
Minimum ΔT in gas - water heat exchangers [°C]		15.0
Minimum ΔT in gas - gas heat exchangers [°C]		30.0
Minimum ΔT in liquid – evaporating/condensing liquid exchangers [°C]		2.0

Chemical Looping	
Minimum air inlet temperature at AR [°C]	400.0
SOFC exhaust gas inlet temperature [°C]	800.0
Minimum outlet temperature from AR [°C]	735.0
Fuel reactor outlet temperature [°C]	800.0
Maximum GS factor [kg/s/m^2]	20.0
Gas pressure drop in FR and AR [bar]	0.15
Minimum exhaust temperature at stack [°C]	80.0
Minimum exhaust pressure at stack [bar]	1.013
Air fan isentropic efficiency [%]	94.0
Air fan mechanical-electrical efficiency [%]	80.0
Auxiliaries for heat rejection [% of heat rejected]	0.8
CO_2 compression and storage	
Minimum CO_2 pressure to storage [bar]	110.0
Maximum pressure ratio/intercooled compressor stage [-]	2.0
CO_2 pressure at compressor outlet [bar]	80.0
Intercooled compressor stage isentropic efficiency [%]	82.0
Intercooled compressor stage mechanical efficiency [%]	94.0
Temperature at outlet of each cooling stage [°C]	30.0
Pressure drop in each cooling stage [% of p at inlet]	2.0
Pump isentropic efficiency [%]	75.0
Pump mechanical efficiency [%]	95.0
Minimum CO_2 dry purity [%v/v]	95.0

Table 1: Main assumptions, in common to all the models (benchmark case and SOFC+CLC).

The main reference taken into account for these assumptions is [41]. In turn, it takes as references the assumptions of IT-SOFC plant proposed by CFCL [42][43] and by [45]. Another reference for these assumptions is [47].

Some of these assumptions need a more specific explanation.

- It is necessary a minimum tolerable O_2 molar fraction at cathode outlet because there can be some problems of permeability if O_2 is less in the channel.
- Outlet temperature is considered equal to a typical value for IT-SOFCs, the kind of SOFC considered in this work. The reason of this choice is the easier management and cheaper cost of the material for the IT-SOFCs in comparison to the HT-SOFCs, as explained in Chapter 2. The difference of temperature is more critics across the cathode side (air) than across the anode side (fuel).
- The value of minimum air feed temperature is typical of this kind of SOFC [41] and the task of CLC and heat management will be to provide air at this temperature.
- The operating cell voltage of the SOFC (0.80 V) is different in comparison to the one used in the reference work [41] and by CFCL (0.86 V). The reasons of this choice will be explained in detail in Chapter 7 and are linked to the SOFC model, in particular to its design.
- The operating conditions selected for the steam cycle are typical values and equal to the values reported in [41]. In industry, it is common to find steam cycle more performing, with one or more re-heats, higher pressure or higher temperature (for example, USC steam cycle) but, in this case, the steam cycle

will be used only to recover electricity from waste energy and it will produce less than 10 MW: nowadays, from an economic point of view, it is not convenient to build a steam cycle more critic for this size and, from a plant engineering point of view, it is important to have a configuration for the energy recovery as simple as possible.

- The isentropic efficiency of the steam turbine has to be chosen carefully because it determines the power output, the vapour fraction at the outlet and the temperature of any bleedings. In particular, the vapour fraction at turbine outlet is important to design the steam turbine: the increase of steam density during the expansion increases the volume flow rate. According to [41], it has been chosen a value of 85% for the isentropic efficiency of the steam turbine. It is a typical value for the big size steam cycle plant designed to achieve high efficiency and it is normal that it is higher than the ones used by Consonni et el. [45], related to older energy recovery plants.
- About CLC, it is important to underline the limit for the temperature at FR outlet and for Gs factor. The first depends on the type of oxygen carrier used, Copper in this case. Its melting point is 1085 °C (Appendix B), therefore it is preferable to operate below this value. The second limit is about the solid recirculation between AR and FR. Equation 4.1 defines the Gs factor, or solid recirculation factor.

$$\boldsymbol{Gs}\ \left[\frac{\boldsymbol{kg}}{\boldsymbol{s\ m^2}}\right] = \frac{\dot{\boldsymbol{m}}_{\boldsymbol{sol}}}{\boldsymbol{A}} = \frac{\dot{\boldsymbol{m}}_{\boldsymbol{sol}}}{\frac{\dot{\boldsymbol{m}}_{\boldsymbol{gas}}}{\boldsymbol{\rho\ v}}} \tag{4.1}$$

  where $\dot{m}_{sol}$ is the solid mass flow at AR outlet, $\dot{m}_{gas}$ is the gas mass flow at AR outlet, A is the transversal area of the AR reactor calculable as the ratio between $\dot{m}_{gas}$ and the product of $\dot{m}_{gas}$ density and gas velocity. The velocity used for this calculation is 4 m/s, a typical value used in these processes [26].
- About CO_2 separation and storage, the main reference is [47]. The goal of intercooled compressor is to get liquid CO_2 while the pump has to compress the CO_2 until reaching the pressure of storage (Chapter 1). The minimum CO_2 dry purity depends on the maximum amount of incondensable species [8]. An intercooled compressor is necessary to reduce the consumption (not negligible for the total energy efficiency of the plant). Because of the limits imposed, 7 stages will be necessary for the intercooled compressor to achieve the target temperature and pressure.
- In addition to the assumptions of [41], additional pressure losses are considered at the inlet of cathode side and at the inlet of the steam turbines, respectively due to the admission filter and valves.

4.3 Aspen model

In this paragraph, the Aspen model of the main components of the integrated system (SOFC and CLC) will be shown, in order to explain the methodology of calculation.

4.3.1 SOFC model in Aspen

Figure 25 shows the Aspen model of the SOFC in the 'hot-recycle' configuration of the integrated system (see Chapter 5). The stream called 'PROD0' is the mixture of

the fed natural gas and the recycle. To build the SOFC model in Aspen, six components were needed:

- 'PREREF' is the pre-reformer reactor before the SOFC. In Aspen, it is an adiabatic Gibbs reactor: the Gibbs free energy of the reactants is minimized without heat exchanges;
- 'STRE' is the first component of the SOFC modelling. It is a stoichiometric reactor where reactions of SMR and WGS (Equations 2.8 and 2.9) occur with complete conversion of the reactants. In this way, all the species in 'STRE' are converted in hydrogen and there will be in 'PROD2' the maximum amount of possible hydrogen. The imposed operating temperature of 'STRE' is 700 °C but it is not influential: the reactor is not adiabatic and the heat released by the reactions is sent to the component 'ANODE' where the SOFC energy balance will be solved;
- 'SPLIT0' is a simple mixer through which it is possible to impose the SOFC fuel utilization (single passage). The stream 'PROD3' will be the only amount oxidized in the SOFC;
- 'CATHODE' is a simple separator. This component is used in order to separate the amount of oxygen necessary to oxidize the fuel from the air stream. This amount ('O2') is sent to the component called 'ANODE';
- 'ANODE' is the main component of the SOFC modelling. Through this component, the SOFC energy balance is solved and the SOFC outlet composition is calculated. It is an adiabatic Gibbs reactor. The heat streams at the inlet are: 'Q0' (the heat released by the reactions in 'STRE'), 'EL' (it is the gross electric power output of the SOFC, calculated with the Equation 2.28) and 'Q1' (the heat from 'COOLER1', it represents the cooling effects of the O_2-depleted air);
- 'COOLER1' is a fake heat exchanger and it is necessary to implement the cooling effect of the O_2-depleted air. Its operating temperature is equal to the temperature imposed at the SOFC outlet (800 °C).

The mass flow rate of the air is varied by Aspen in order to have the temperature of the stream at the anode outlet ('PROD4') equal to the temperature imposed at the SOFC outlet (800 °C).

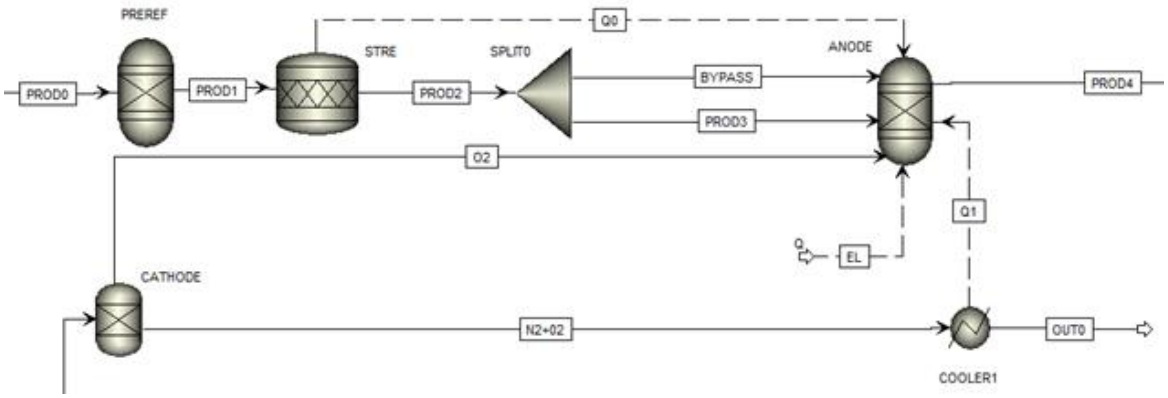

Figure 25: Aspen model of the SOFC.

4.3.2 CLC model in Aspen

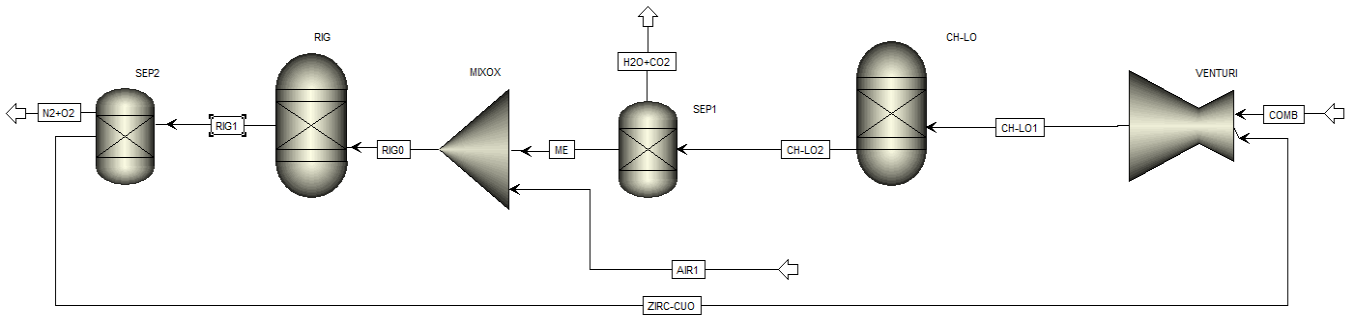

Figure 26: Aspen model of the CLC.

Figure 26 shows the Aspen model of the CLC. The stream called 'COMB' is the flow from the SOFC anode outlet (see Chapter 5). To build the CLC model in Aspen, six components were needed:

- 'CH-LO' is the FR of CLC where the fuel (stream 'COMB') and the OC (stream 'ZIRC-CUO') react. It is an adiabatic Gibbs reactor: the Gibbs free energy of the reactants is minimized without heat exchanges;
- 'SEP1' is the separator/cyclone through which the gas flow at FR outlet (stream 'H2O+CO2') is separated from the solid part (stream 'ME');
- 'RIG' is the AR of the CLC. It is an adiabatic Gibbs reactor;
- 'SEP2' is the separator/cyclone through which the gas flow at AR outlet (stream 'N2+O2') is separated from the solid part (stream 'ZIRC-CUO').

In the stream 'ZIRC-CUO', the mass fractions of the metal oxide (e.g. CuO) and the support (e.g. ZrO_2) are imposed (see Chapter 5). The mole flow rate of the stream 'ZIRC-CUO' is calculated in order to have a certain oxygen added ratio ζ (freely imposed) in relation to the fuel contained in the stream from the anode outlet ('COMB'). The stream 'ZIRC-CUO' represents the regenerated solid oxide. Varying the mole flow rate of the regenerated solid oxide, the solid recirculation will be different. It is calculated after the component 'SEP2' (Equation 4.1).
In the AR and in the FR, it will be possible to have all the possible metal oxides in relation to the kind of solid oxide considered (e.g. for the Cu-based case, $CuO/Cu_2O/Cu$).

4.4 Parameters to evaluate the system

Different parameters can be defined to analyse and evaluate the performance of the model. The parameters will be the same for the different models and for the different cases.
The main objective of the work is to find a plant able to produce electricity more efficiently as possible. Equation 4.2 defines the total energy efficiency of the plant.

$$\eta = \frac{P_{el,net}}{\dot{m}_{NG,in} \cdot LHV_{NG}} \tag{4.2}$$

η is the total efficiency of the plant; $P_{el,net}$ is the electric net power produced; $\dot{m}_{NG,in}$ is the natural gas mass flow fed to the system.

$P_{el,net}$ is not only the net electric power output of the SOFC but the result of a sum of different contributions (Equation 4.3).

$$P_{el,net} = P_{el,net,SOFC} + P_{el,net,th} - P_{el,cons,CO_2} - P_{el,cons,th} - P_{el,cons,other} \quad (4.3)$$

$P_{el,net,SOFC}$ is the net electric power output of the SOFC, therefore considering the conversion from the providing Direct Current (DC) to Alternating Current (AC); $P_{el,net,th}$ is the net electric power obtained by the energy recovery using the waste heat of the system; $P_{el,cons,CO_2}$ is the electric consumption to compress the CO_2; $P_{el,cons,th}$ is the electric consumption required by the thermodynamic cycle used to exploit the waste heat; $P_{el,cons,other}$ represents all the other consumption.

In addition to the total energy efficiency, it is possible to define different energy efficiency (Equations 4.4) not considering the consumption of CO_2 compression. In this way, the comparison between the two models, with and without CO_2 separation and storage, can be more focused on the efficiency of the power production process.

$$\eta_{no\ CO_2} = \frac{P_{el,net,no\ CO_2}}{\dot{m}_{NG,in} \cdot LHV_{NG}}$$

$$P_{el,net,no\ CO_2} = P_{el,net,SOFC} + P_{el,net,th} - P_{el,cons,th} - P_{el,cons,other} \quad (4.4)$$

The second main objective of the model is to separate and compress CO_2 produced by the power production system, as easily and efficiently as possible. In this way, it is possible to define a specific CO_2 emissions index (Equation 4.5).

$$e\left[\frac{g_{CO_2}}{MJ_{el}}\right] = \frac{\dot{m}_{CO_2,em}}{P_{el,net}} \quad (4.5)$$

$\dot{m}_{CO_2,em}$ is the emitted CO_2 mass flow. If the plant is more efficient, with the same fuel fed, the power output will be higher and, consequently, e will be lower. Consequently, e depends on the efficiency of the plant/technology and the cleaning of the fuel.

In case of CO_2 capture and storage, it is possible to define a second parameter called Carbon Capture Ratio (CCR). CCR evaluates the quality of CO_2 capture. Equation 4.6 defines this index: it is the ratio between the mass flow rate of CO_2 sent to storage and the mass flow rate of CO_2 associated to the natural gas fed to the plant, calculated using e_{NG}, the specific CO_2 emission per unit of energy input of natural gas, equal to 57 gCO_2/MJ_{LHV} [47].

$$CCR = \frac{\dot{m}_{CO_2,st}}{\dot{m}_{NG} \cdot LHV_{NG} \cdot e_{NG}} \quad (4.6)$$

Another parameter is defined to analyse the influence of the presence of CO_2 capture and storage on the plant performance. As explained in Chapter 1 and 3, adding components to treat CO_2 is energy and economic costs. The consumption of these

components is not negligible and reduces the plant performance. SPECCA (Specific Primary Energy Consumption for CO_2 Avoided) is an energy index that calculates the additional primary energy consumption due to the CCS system installation [47] compared to a benchmark technology without CO_2 capture. Equation 4.7 defines the SPECCA. Subscript 'CCS' is related to the values of the plant with CO_2 separation and storage while 'ref' is related to the values of the reference plant, without CO_2 treatment.

$$SPECCA = \frac{HR_{CCS} - HR_{ref}}{e_{ref} - e_{CCS}} \cdot 1000 = \frac{\frac{1}{\eta} - \frac{1}{\eta_{ref}}}{e_{eq,ref} - e_{eq}} \cdot 1000 \left[\frac{MJ}{kg_{CO_2}}\right] \tag{4.7}$$

The lower is the SPECCA, the higher is the efficiency of the process because the less is the additional energy consumed to separate CO_2. With these two parameters, it is possible to compare different technologies and plants in relation to CO_2 treatment question.

It is possible to define useful parameters to analyse how much the SOFC profits by the fed fuel. Equations 4.8 present two indices called, respectively, fuel utilization (U_{fuel}) and oxidant utilization (U_{ox}).

$$U_{fuel} = \frac{\dot{m}_{H_2,in} - \dot{m}_{H_2,out}}{\dot{m}_{H_2,in}} \qquad U_{ox} = \frac{\dot{m}_{ox,in} - \dot{m}_{ox,out}}{\dot{m}_{ox,in}} \tag{4.8}$$

$\dot{m}_{ox,in}$ and $\dot{m}_{ox,out}$ are the mass flows of the oxidant; $\dot{m}_{H_2,in}$ and $\dot{m}_{H_2,out}$ the mass flows of equivalent hydrogen; subscripts 'in' and 'out' are related to inlet and outlet of the control volume considered. Equivalent hydrogen is not only the amount of hydrogen in the anode flow but it is the maximum amount of H_2 that would be obtained if all the species (C_xH_y and CO) were converted into H_2 by steam reforming and WGS reactions (Equation 2.9). Equation 4.9 shows the amount of equivalent hydrogen related to a generic hydrocarbon.

$$C_xH_y + x \cdot H_2O \implies (y-1) \cdot H_2 + x \cdot CO \tag{4.9}$$

Chapter 5

Comparison between the systems with and without CO_2 capture

5.1 Benchmark plant without CO_2 capture

The benchmark plant proposed in [41] is obtained with the integration of three main components: an atmospheric SOFC, a combustor and a steam cycle. Natural Gas (NG) at 20 bar from the network and air are the only two input streams of the system. This plant configuration has been calculated according to Campanari et al. [41].

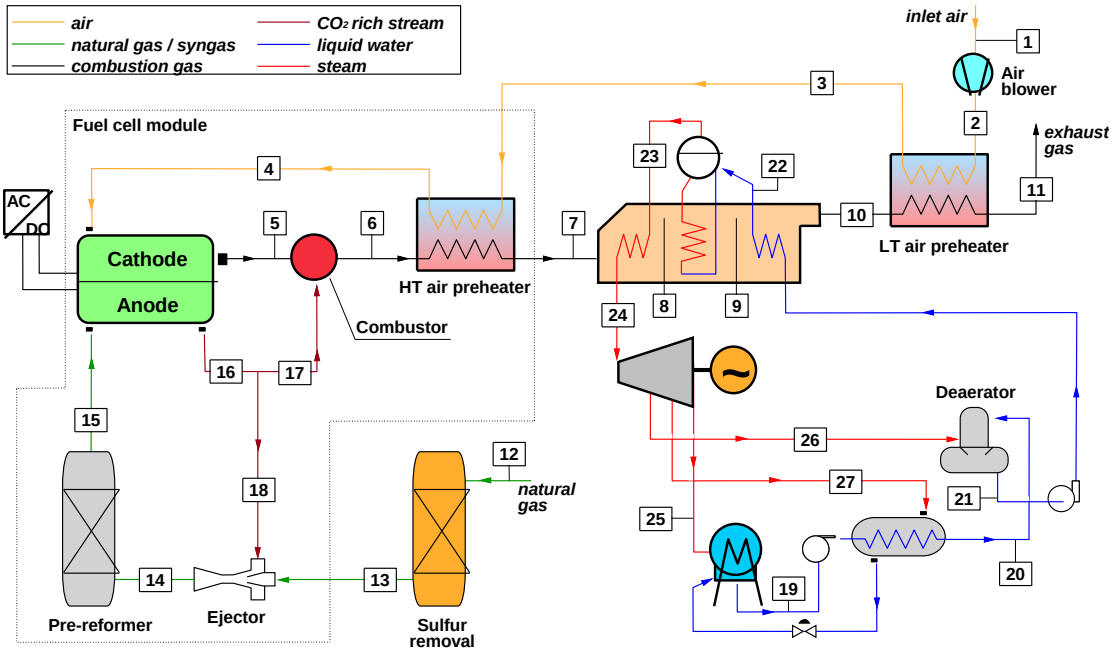

Figure 27: Layout of the benchmark plant [41].

NG is pre-treated by a section of desulphurization. It consists of a low temperature desulphurization reactor, necessary to remove traces of H_2S and odorants (mercaptans, tiophenes); SOFC catalytic materials, generally Ni-based, need to work below 0.1 ppm of total Sulphur content. This kind of reactor is a commercial technology [48] and consists of a fixed bed. NG, at ambient temperature, flows through the sulphur-selective adsorbent. When the sulphur compound front reaches the end of the bed, NG is switched to a different column while the spent bed undergoes the temperature-based regeneration process. Sorbent is typically regenerated at 300°C with a purge stream (e.g. air, nitrogen) [41].
After desulphurization treatment, NG is fed to the SOFC by an ejector. It has two objectives: exploit NG high pressure to sustain the flow across the SOFC and mix efficiently NG with a recycle from the outlet of anode side. The recycle is necessary

to heat the NG, initially at ambient temperature, and to provide the S/C ratio (Equation 5.1). The recycle is a flow with a various composition: it is composed by the fuel not reacted in the SOFC and H_2O and CO_2 produced by the reactions. The S/C ratio has to be high enough to avoid carbon deposition in the SOFC and to feed the H_2O necessary to sustain the reactions expressed in Equations 2.8 and 2.9 (SMR and WGS).

$$\frac{S}{C} = \frac{\dot{n}_{H_2O}}{\dot{n}_{CO} + \dot{n}_{CH_4} + 2 \cdot \dot{n}_{C_2H_6} + 3 \cdot \dot{n}_{C_3H_8} + 4 \cdot \dot{n}_{C_4H_{10}}} \tag{5.1}$$

This S/C ratio does not consider the CO_2.
Before the SOFC, there is a pre-reformer. Its task is to crack the fuel molecules heavier than methane present in NG (propane, etc.).
The air is pre-heated in two exchangers. The air has to reach the minimum temperature required at the inlet of cathode side (735 °C), necessary to avoid excessive mechanical stress to the SOFC.
The High Temperature (HT) air pre-heater comes after a combustor. In this exchanger, the two hot flows from SOFC outlet are mixed and react. The flow from anode side (Point #17) will contain a part of the fuel not reacted in the SOFC and it will be burned using the O_2-depleted air at the cathode outlet (#5).
The hot flow coming from the combustor, after being cooled in HT pre-heater and in HRSG (Heat Recovery Steam Generator), is finally cooled in a Low Temperature (LT) pre-heater and released from the stack.
The steam produced by the HRSG is exploited by a steam cycle to produce additional electricity. The steam cycle works with the operating conditions indicated in Table 4.1. As shown in Figure 27, the steam cycle uses also a LT regenerator and a deaerator.
The choice made for this model is to use as low air as possible and have the minimum O_2 molar fraction at the outlet of cathode side and combustor. In this way, the energy and the fuel spent to heat up the air will be lower and the rest of the fuel can be used to produce electricity.

In comparison to Campanari et al. [41], the cell voltage considered is 0.8 V instead of 0.86 V. This change will result in a sensible reduction of the performance. Before, to verify the assumptions, it is necessary a comparison between the results of the Aspen model with 0.86 V and the results are shown in [41] (see Appendix D).

The operating conditions are mostly taken from [41]. In addition to the voltage, also the air temperature at the SOFC inlet (#4) has been changed from 753.8 °C to 735 °C (Table 4.1) to obtain the highest fuel utilization possible in the SOFC.

The task of the thermal integration is heating the flows before SOFC and CLC and producing additional electricity as efficiently as possible. For a large-size power generation plant, Steam Rankine Cycle is the typical technology used to recover energy. The reasons are its operating temperature and the high specific power of the steam.

A diagram Temperature – Heat Duty (T-Q) is useful to analyse the efficiency of the heat transfer and to check the minimum difference of temperature in the heat recovery

system. The lower is the minimum difference of temperature between hot and cold side, the higher is the efficiency of the heat transfer. In particular, in HRSG, the lower is the minimum difference of temperature between hot flow and water/steam, the higher is the mass flow of generated steam and, consequently, the turbine power output.
In Figure 28, there is the diagram T-Q for the new benchmark case.

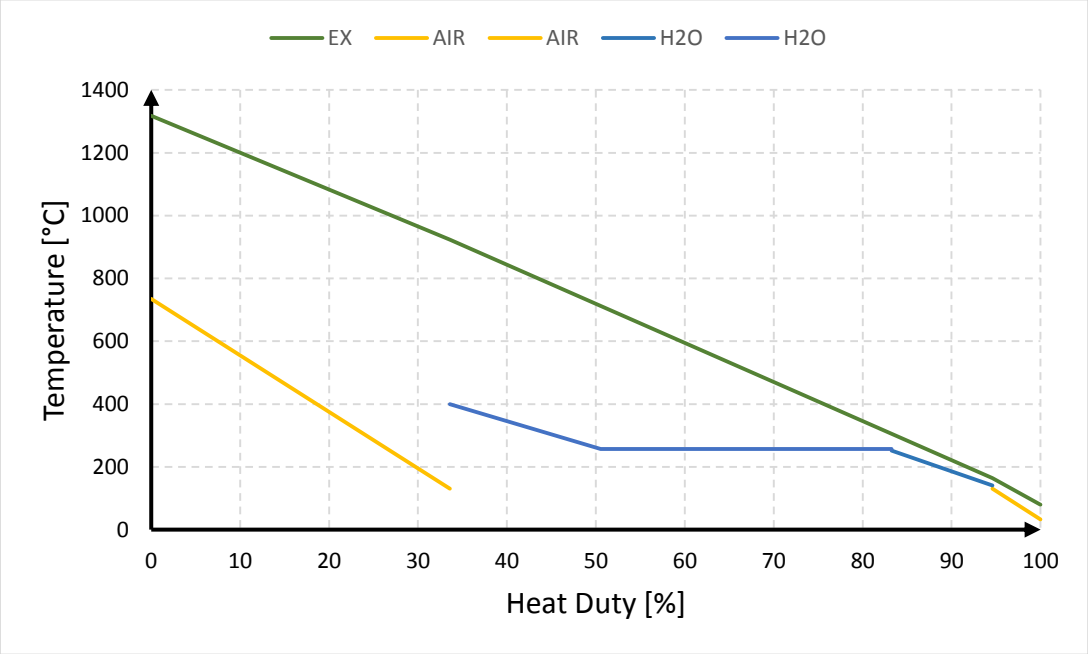

Figure 28: T-Q for the new benchmark case (EX = Exhaust gas from the burner).

The minimum temperature difference is located at the outlet of HRSG and it is approximately 25 °C, more than the minimum allowable difference of temperature gas – water (15 °C) but close enough. Furthermore, the horizontal line relative to water evaporation is close enough to the hot flow cooling line. The heat transfer can be considered efficient.
In Appendix E, the properties of the streams for the new benchmark case are shown.

5.2 Systems SOFC + CLC with CO_2 capture

5.2.1 'Hot recycle' configuration

The IT-SOFC system with CLC integration can be developed in two different ways which can be called, respectively, hot and cold recycle configuration. The difference is the fuel humidification, mixed with NG and necessary to feed H_2O and CO_2 to the SOFC.

The first configuration analysed is the 'Hot Recycle' one (H-R). It is based on the benchmark plant and consists in a recycle from the outlet of the anode side, made with an ejector.

In Figure 29, there is the complete plant layout of this kind of integration.

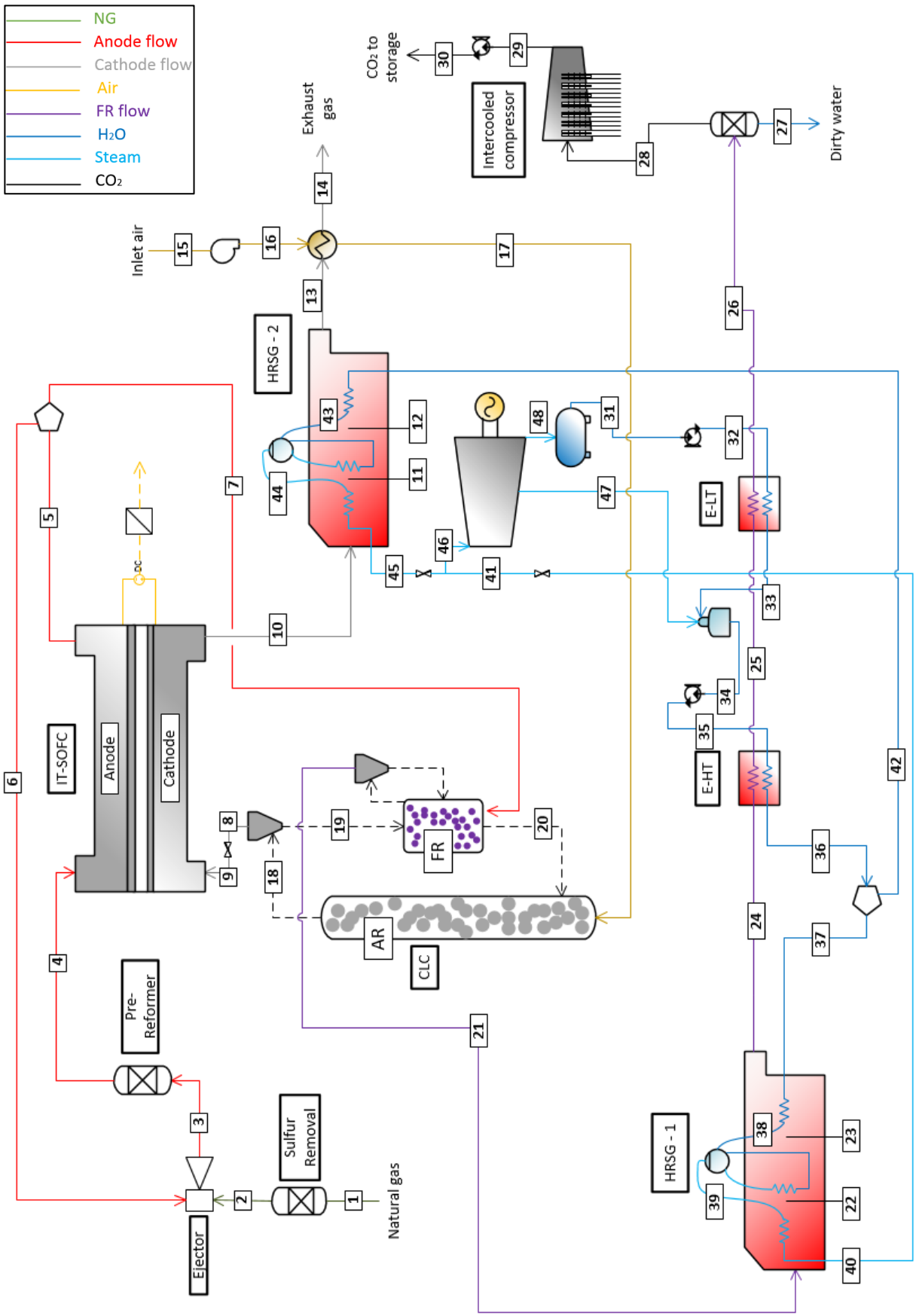

Figure 29: Layout of the system SOFC + CLC, 'H-R' configuration.

The main differences in comparison to the benchmark case are four:

- the burner is replaced by a CLC reactor to pre-heat, partially, the air. The oxygen carrier used is Copper ($Cu/Cu_2O/CuO$), an adequate material for the operating temperature of the system (max 800 °C) supported with Zirconia (ZrO_2). The solid composition is set at #19 based on literature data [49]: respectively, a mass fraction of 0.4 (CuO) and 0.6 (ZrO_2). The total molar flow of oxygen carrier + inert is set at #19 in order to have a certain value of oxygen added ratio (ζ, Equation 3.5);
- two HRSGs are required for the heat recovery;
- the presence of a section to compress and sent to storage the CO_2, composed by an intercooled compressor and a pump;

The objective of the model is to optimize the electric efficiency according to the assumptions (Table 1). The more critical points are:

- respecting the minimum inlet temperature at the cathode inlet (#9), achievable by increasing the air temperature at the outlet of the exchanger between #16 and #17 or by increasing the solid recirculation among the CLC reactors. Initially the air temperature at CLC inlet was set to 400 °C. Then, it has been set equal to 450 °C in order to use more fuel in the SOFC;
- the fuel utilization factor (single pass), relative to the SOFC. This value is fundamental because SOFC power output is strongly dependent on it and the same goes for the air temperature at the cathode inlet: the more is the fuel used by SOFC, the less is the fuel available for the CLC to pre-heat the air and the less critical is the solid recirculation. The choice made for this work is to consider the recirculation as close as possible to a critical value of 20 $kg/s/m^2$. In this way, the air outlet temperature will be higher with equal fuel fed to CLC. As explained in Chapter 3, the design of CLC reactors is specific for each case and the design can be expensive, in terms of cost and engineering, if the objective is to build a component for an high efficiency and large-size plant;
- respecting the minimum difference of temperature allowable in all the points of the model, depending on the phase of the fluids involved in each heat exchange.

In Appendix F, there are all the streams properties for the 'H-R' configuration.

As in the benchmark case, Figure 30 shows the T-Q diagrams relative to the system SOFC + CLC 'H-R' configuration, in order to analyse the efficiency of the heat transfer.

About the diagrams in Figure 30, it is possible to make some comments:

- the minimum difference of temperature related to the FR flow cooling, after the deareator, is imposed and relieved at the outlet of the exchanger E-HT (Exchanger – Hot Temperature). The difference between #25 and #35 is 24.3 °C, more than the minimum difference of temperature allowable for a heat transfer gas – water (15 °C) but small enough. With a lower outlet temperature, there will be an intersection between the heat transfer curves in the exchanger E-LT (Exchanger – Low Temperature). Indeed, in this

exchanger, it is relieved the minimum temperature difference of all the plant exchangers and it has to be more than the minimum allowable for this kind of heat transfer (liquid-condensing/evaporating liquid 2 °C). Figure 30a is not enough to appreciate this minimum temperature difference but, thanks to Aspen, it is possible to make a zone analysis for each exchanger with a maximum of 5000 zones. Every critical exchanger has set its analysis to be sure that there is not intersection between the heat transfer curves. In Figure 30c, in detail, the heat exchange curves about E-LT, made with the data of the relative Aspen zone analysis. The curve of FR flow cooling will be similar to a parabola, if it considers all the cooling to ambient temperature because the water in the flow starts to condense since 92 °C and the heat rate increases in relation to the amount of condensed. The minimum difference of temperature calculated is 2.19 °C, between 75% and 80% of heat duty;

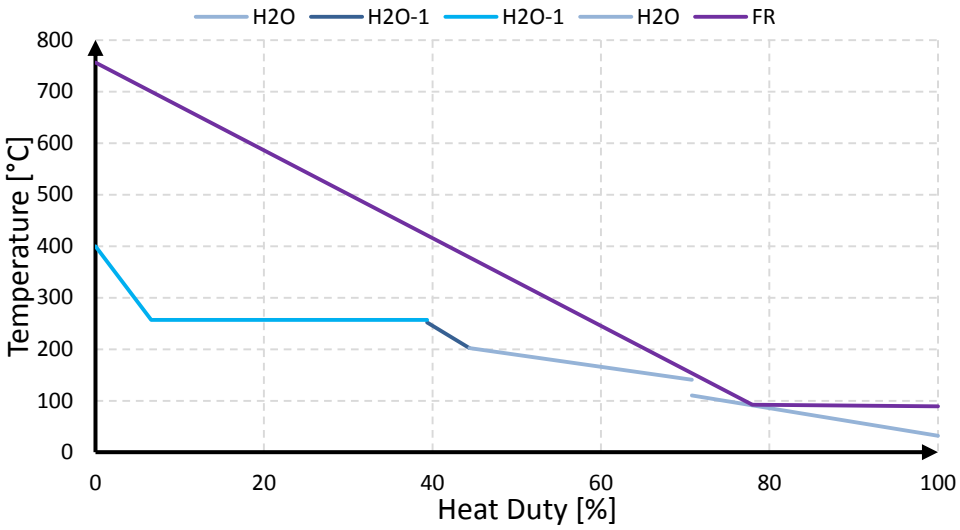

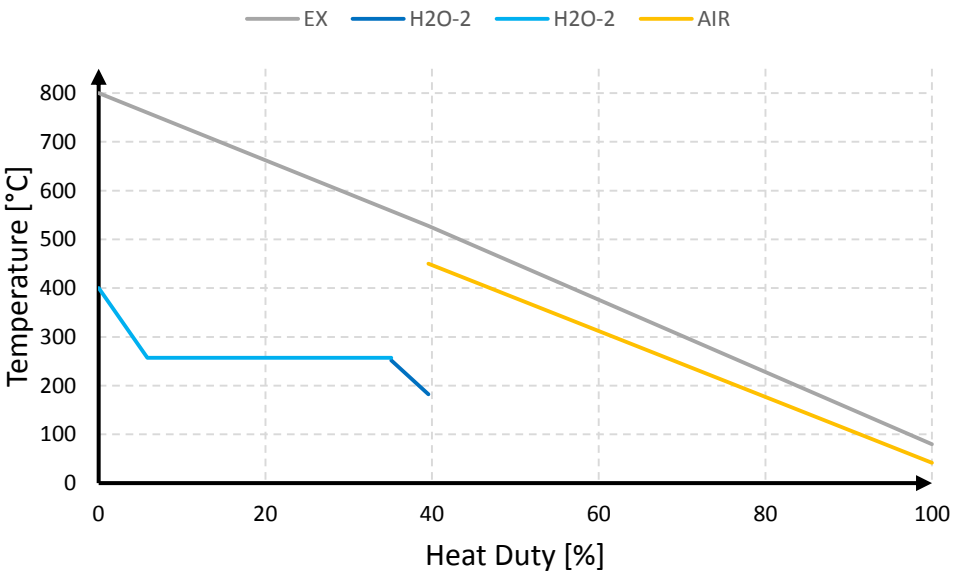

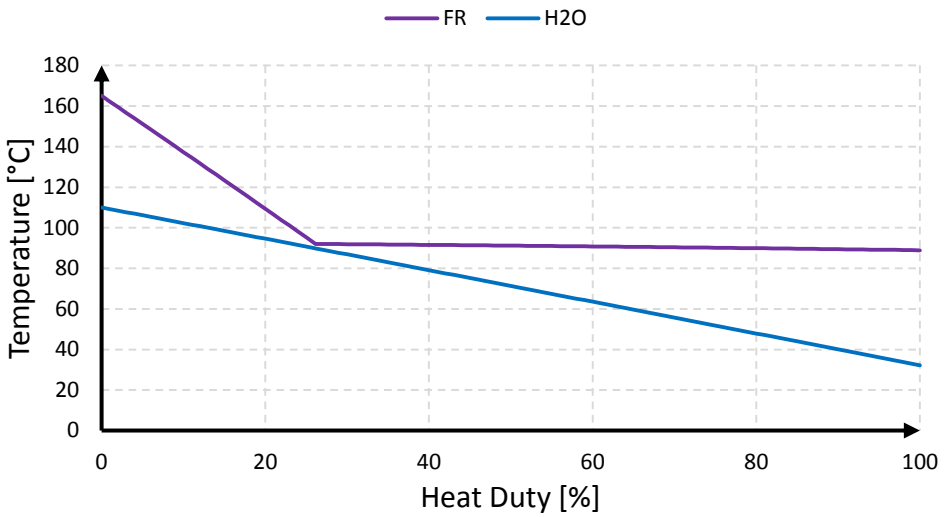

Figure 30: T-Q diagrams for SOFC + CLC 'H-R' configuration. a) The heat exchange relative to the cooling of the flow from the FR of CLC; b) the cooling of the flow from cathode; c) in detail, the heat transfer curves of E-LT (EX = Exhaust gas of the cathode; FR = flow from Fuel Reactor; H_2O = relative to the total flow of water; H_2O-1 = water mass flow from #37 to #41; H_2O-2 = water mass flow from #42 to #45)

- the final part of FR flow cooling is not reported in the diagrams because not particularly insightful. It is made using ambient water (15 °C) to 30 °C;
- in Figure 30a, it is observable the rate of the deareator to the water heating. The deareator acts also as regenerator. This rate is represented by the gap in the water curve at about 70% of heat duty;
- after the split to the two HRSG, it is observable a different inclination for the curves: the more is the mass flow, the less is the inclination. The difference is not sensible after the deareator since the added mass flow from the steam turbine is low in comparison to the principal flow;
- it is possible to set freely the outlet temperature of the FR flow from HRSG-1. Its change does not involve change of total efficiency of the system. It was decided to impose a temperature more or less intermediate in order to have exchangers less critical after and before this point.

In conclusion, the heat transfer in the system SOFC + CLC 'H-R' can be considered efficient and respects the restrictions.

5.2.1 'Cold recycle' configuration

The second configuration of the system SOFC + CLC presents a recycle by the flow from FR outlet. The temperature of this flow will be lower in comparison to 800 °C, the temperature at the SOFC outlet: for this reason, the configuration is called 'Cold Recycle' (C-R).

In Figure 31, it is shown the complete layout of this configuration of the system while, in Appendix G, all the streams properties.

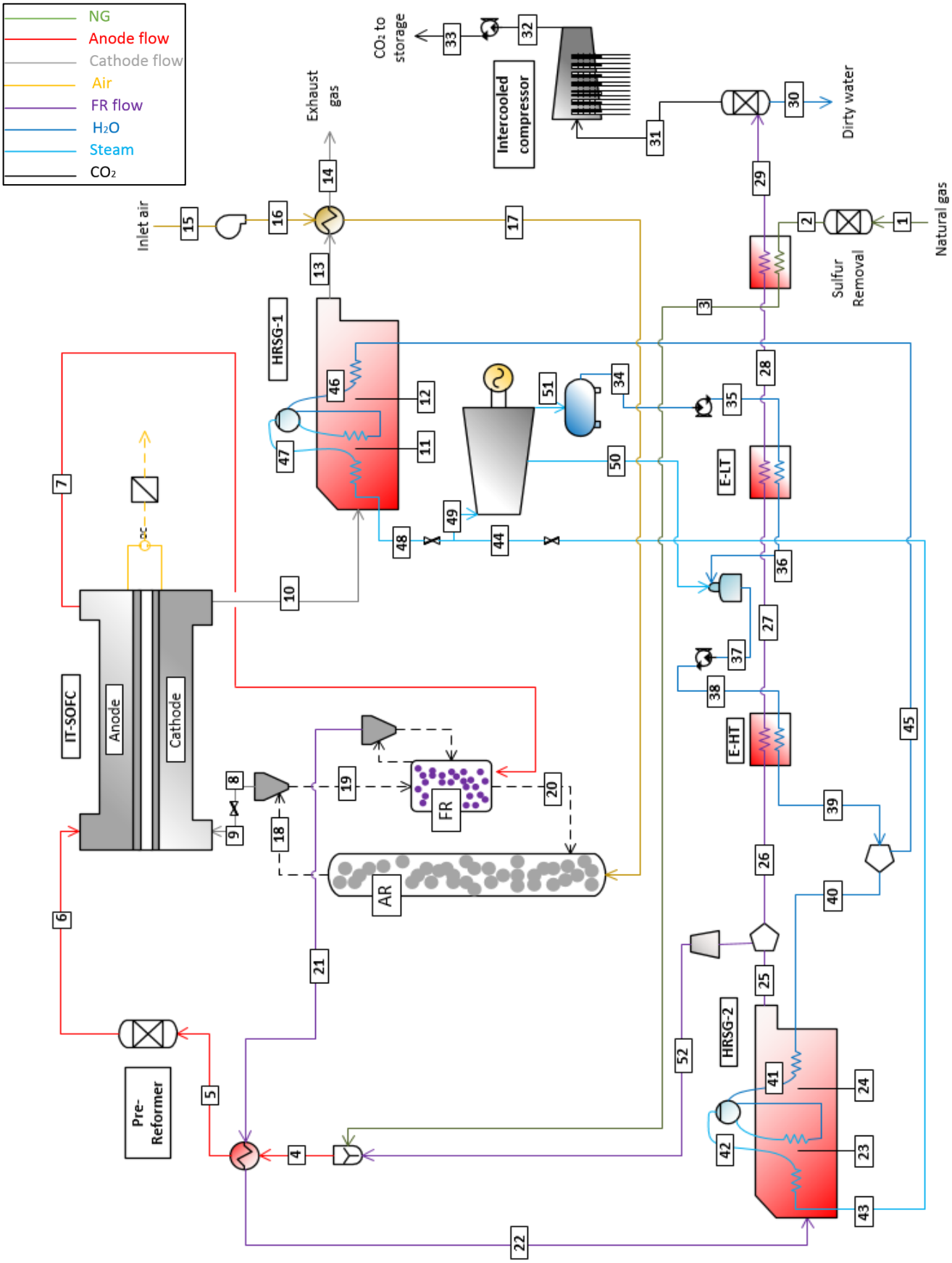

Figure 31: Layout of the system SOFC + CLC, 'C-R' configuration.

There are six main differences in comparison to the previous cases:

- the absence of the ejector. The recycle is mixed to the fuel through a simple mixer. An exhaust fan is used to increase the pressure after the CLC reactors;
- the composition of the recycle is different. In this case, the flow is richer of H_2O and CO_2, the two products of the oxidation that occurs in the SOFC and in the CLC reactors. The consequence is that the necessary recycle, in terms of mass flow and split fraction, is lower because the required S/C is achieved more easily;
- the fuel temperature at SOFC inlet is set 600 °C, the minimum allowable temperature. In this way, an higher difference of temperature can be exploited and the fuel utilization of the SOFC can be higher, with the other operating condition unchanged;
- an exchanger for the NG is added before the mixing with the recycle. FR flow has to be cooled to separate CO_2 therefore it is important to recover more energy as possible. Furthermore, FR flow is a condensing fluid and can provide a great amount of heat;
- the colder temperature of the recycle involves colder temperature of the fuel at the SOFC inlet. The recycle cannot be made directly after CLC because the consumption of the related compressor will be high. For a compressor, the higher is the temperature, the higher is the consumption. As in the configuration 'H-R', it was decided to set 400 °C as temperature at the outlet of HRSG-1. In this way, the consumption of the compressor is lower;

Thanks to the diagrams in Figure 32, it is possible to analyse the efficiency of the heat transfer and the energy recovery. The considerations about these are not so different in comparison to the considerations made for the 'H-R' case. Furthermore, it is possible to say:

- in the diagram 32a, there are two additional lines, the red one for the fuel heating and the green one for the NG heating;
- the minimum difference of temperature is located in the exchanger E-LT, as in the case 'H-R'. In Figure 32c, it is possible to check that there is not intersection between the curves, which is confirmed also thanks to Aspen zone analysis. The exact minimum difference of temperature is 2.07 °C, at about 80% - 85% of the heat duty;
- another critical point is the outlet of the NG pre-heater. The temperature imposed is 85 °C (#3) and the difference of temperature respect the FR flow (#29) is about 3 °C;
- the temperature set at #28 is the same of 'H-R' (165 °C), for the same reason;
- the temperature set at #25 is 400 °C for the reasons already explained.

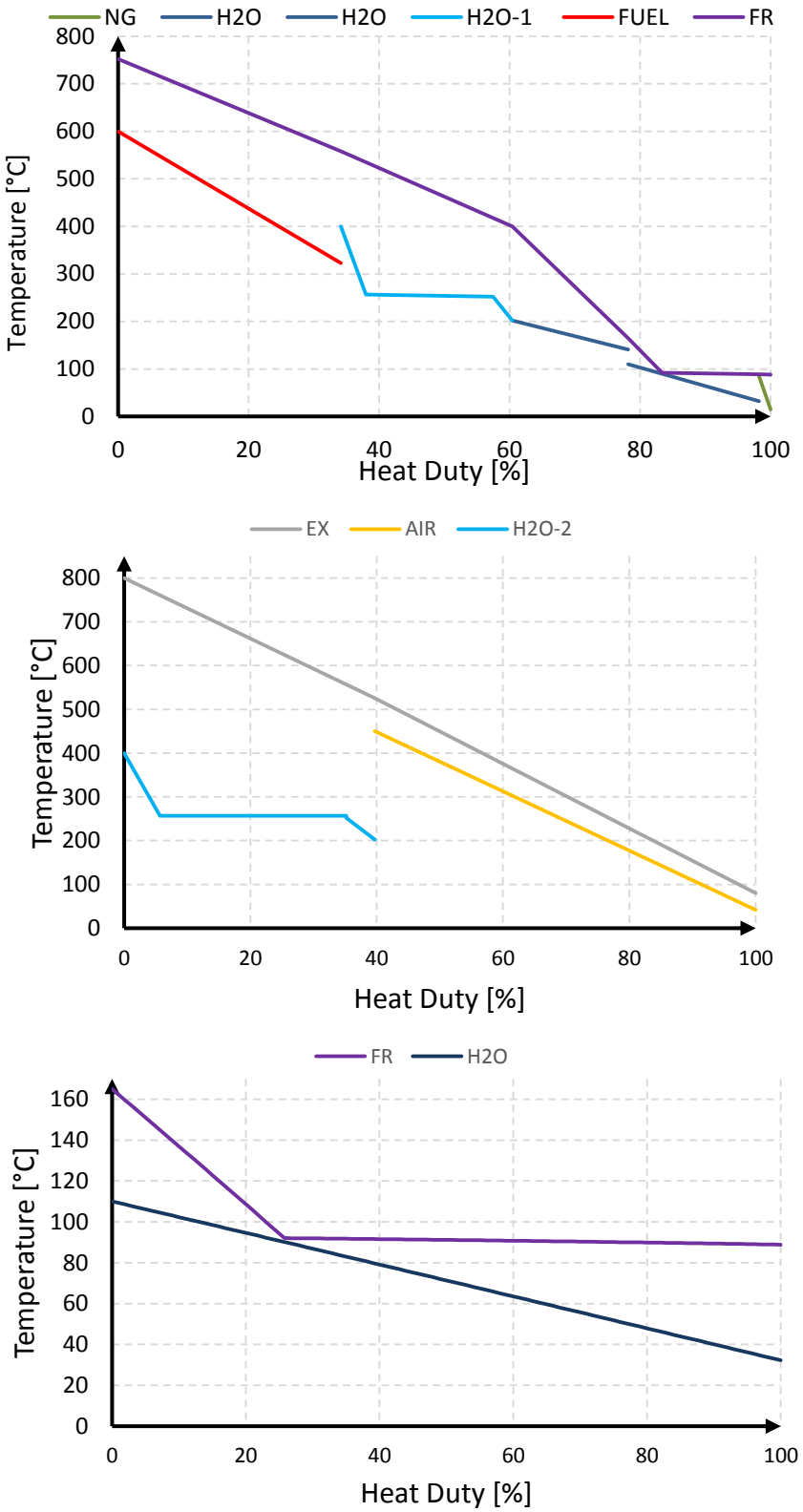

Figure 32: T-Q diagrams for SOFC + CLC 'C-R' configuration. a) The heat exchange relative to the cooling of the flow from the FR; b) the cooling heat exchange of the flow from the cathode; c) in detail, the heat transfer curves of E-LT (EX = Exhaust gas of the cathode; FR = flow from Fuel Reactor; H2O = total flow of water; H2O-1 = water mass flow from #37 to #41; H2O-2 = water mass flow from #42 to #45).

5.3 Performance comparison

The results regarding the performance of the 3 plants are summarized in Table 2 and Table 3.

Item	No CO_2 capture	With CO_2 capture	
	Benchmark case	H-R	C-R
$P_{el,net}$ [MW]	68.203	66.907	66.758
$P_{el,net,no\ CO_2}$ [MW]	68.203	68.753	68.613
η [%]	68.203	66.907	66.758
$\eta_{no\ CO_2}$[%]	68.203	68.753	68.613
Recycle split fraction [%]	75.562	68.089	51.120
U_{fuel} [%] (overall)	75.743	81.294	81.250
U_{fuel} [%] (single pass)	43.282	58.100	81.250
U_{ox}[%] (overall)	92.021	44.543	43.020
U_{ox}[%] (single pass)	69.711	39.484	38.020
Gs $\left[\frac{kg}{s\ m^2}\right]$	-	19.588	18.192
e $[g_{CO_2}/MJ_{el}]$	83.867	-	-
e $[g_{CO_2}/MWh]$	301.921	-	-
$SPECCA$ [MJ/kg_{CO_2}]	-	0.33864	0.37843
CCR [%]	-	100.0	100.0

Table 2: Parameters of performance for the 3 plants.

	Benchmark case	H-R	C-R
Fuel Inlet [MW]	100.000	100.000	100.000
SOFC net power [MW]	56.402	60.529	60.497
Steam cycle net power [MW]	12.420	10.690	10.841
CO_2 compressor [MW]	-	-1.810	-1.810
Recycle fan [MW]	-0.719	-	-0.181
FD fan [MW]	-0.104	-2.215	-2.292
Water pumps [MW]	-	-0.080	-0.081
CO_2 pump [MW]	24.602	-0.036	-0.036
Condensation heat [MW]	-	22.606	22.924
H2O+CO2 cooling heat [MW]	-0.197	8.866	8.467
Auxiliaries work for heat rejection [MW]	-0.197	-0.252	-0.251

Table 3: Energy balances of the 3 plants.

There are two types of U_{fuel}. The 'single pass' is related only to the single passage through the SOFC: the compositions considered as input and output are, respectively, #4 and #5 for 'H-R', #6 and #7 for 'C-R'. Instead, the 'overall'U_{fuel} considers also the recycle, if it is made from the outlet of the anode side: the compositions as input and output are, respectively, #4 and #6 for 'H-R', #6 and #7 for 'C-R'. For this reason, the two U_{fuel} are equal in the 'C-R' configuration and different in the 'H-R' configuration.

There are also two types of U_{ox}. The 'single pass' is related to the oxidant consumed in the single passage through the SOFC: the compositions considered as input and output are, respectively, #4 and #5 for the base case, #9 and #10 for both configuration with CLC. The 'overall' U_{fuel} considers also the oxidant consumed in th burner (base case) or in the CLC: the compositions considered as input and output are, respectively, #4 and #6 for the base case, #17 and #10 for both configuration with CLC.
The SPECCA is calculated in relation to the benchmark case.

Some considerations about the results can be done:

- the total energy efficiency of the benchmark case is higher than the total energy efficiency of the SOFC + CLC cases but, if the consumption for CO_2 treatment is not considered, is lower of about 0.5%: it means that the integrated system produces and recovers energy in an efficient way;
- 'H-R' configuration results slightly more efficient in comparison to the benchmark case and the 'C-R' configuration because the U_{fuel} is higher in the 'H-R' case and the consumption of the exhaust fan recycle in the 'C-R' case is not negligible;
- the steam cycle performance is slightly better for the 'C-R' case. This result could be due to the mass flow sent from FR to cooling: it is higher in comparison the mass flow of the 'H-R' case (approximately, 19 kg/s vs 8.5 kg/s);
- the higher steam flow rate increases the related pumps consumption;
- the system with integrated SOFC + CLC allows to have lower air utilization factor. It is an important result since the more is the oxygen in cathode side, the less difficult is its permeation and the less critical is the SOFC design. On the other hand, the higher is the air mass flow, the higher is the consumption of the compression and the energy stack losses;
- Gs factor, about solid recirculation in CLC, achieves a value close to the limit in both case;
- the consumptions to pressurize are not negligible and its influence on the efficiency is about 2-3%. The pressure losses increase because of CLC and the higher number of exchangers. For this reason, the efficiency of 'C-R' case (that has more components) is lower but the 'C-R' configuration allows to use the system SOFC + CLC also if NG is not fed pressurized by the network;
- the CO_2 emissions of the benchmark case are not so high compared to conventional NGCC (approximately 360 g_{CO_2}/MWh [8]) because of the higher electric efficiency;
- values obtained for SPECCA are very low compared to literature and other technologies (approximately 0.4 MJ/kg_{CO_2} respect to 2-3 [MJ/kg_{CO_2}] for plants, more or less, conventional [50]).

In conclusion, it was possible to demonstrate that an integrated system of SOFC + CLC can be a valid alternative in comparison to more conventional system. Power output and efficiency reach values very high and the treatment of CO_2 occurs without a large additional consumption of energy.

Chapter 6

Sensitivity analysis

After having demonstrated the efficiency and the feasibility of an integrated system IT-SOFC + CLC to produce electricity and treat the CO_2 produced, it is possible to carry out a sensitivity analysis in order to find the dependence of the performance parameters in relation to the operating conditions. Furthermore, it will be possible to find more performing structure of the model.
Sensitivity analysis will be divided in three different sections regarding the part of the system changed: SOFC, CLC or steam cycle.

6.1 IT-SOFC

6.1.1 Effect of cell voltage

The performance of the system is very sensible to the operating cell voltage. Cell voltage influences the SOFC power output, the most important output of the system. Furthermore, a different cell voltage requires different fuel utilization. Consequently, the mole flows will be changed because of the changes in composition due to the different fuel utilization: the amount of heat and its conditions will be different in comparison to the base case with 0.8 V.

The operating cell voltage will be decreased to 0.7 V, one of most used value in literature, and increased to 0.86 V, the value used by Campanari et al. [41] in the reference work.
Firstly, it is analysed the 'H-R' configuration. In Table 4, the results for the performance parameters in the different cases are shown. Table 5 shows the energy balances and the changes for other interesting properties for this sensitivity analysis.

Item	0.7 V	0.75 V	0.8 V	0.86 V
$P_{el,net}$ [MW]	56.932	61.638	66.907	74.151
$P_{el,net,no\ CO_2}$ [MW]	58.777	63.484	68.753	75.997
η [%]	56.932	61.638	66.907	74.151
$\eta_{no\ CO_2}$[%]	58.777	63.484	68.753	75.997
Recycle split fraction [%]	80.054	73.389	68.089	61.353
U_{fuel} [%] (overall)	72.918	76.893	81.294	87.466
U_{fuel} [%] (single pass)	34.930	46.490	58.100	72.950
U_{ox}[%] (overall)	30.936	36.164	44.543	65.370
U_{ox}[%] (single pass)	24.184	30.342	39.484	62.280
Gs $\left[\frac{kg}{s\ m^2}\right]$	19.715	19.664	19.588	19.280

Table 4: Results for the performance parameters ('H-R' configuration) varying the operating cell voltage of the SOFC.

Item	0.7 V	0.75 V	0.8 V	0.86 V
Fuel inlet [MW]	100.0	100.0	100.0	100.0
SOFC net power [MW]	47.502	53.673	60.529	70.010
Steam cycle net power [MW]	14.775	12.821	10.690	7.704
SOFC power output ratio [%]	76.275	80.719	84.990	90.087
CO_2 compressor [MW]	-1.810	-1.810	-1.810	-1.810
FD fan [MW]	-3.188	-2.727	-2.215	-1.509
Water pumps [MW]	-0.111	-0.096	-0.080	-0.058
CO_2 pump [MW]	-0.036	-0.036	-0.036	-0.036
Condensation heat [MW]	31.243	27.112	22.606	16.291
H2O+CO2 cooling heat [MW]	7.633	8.281	8.866	9.802
Auxiliaries work for heat rejection [MW]	-0.311	-0.283	-0.252	-0.209
Fuel temperature #3 [°C]	720.1	693.9	668.5	637.8
FR flow temperature #21 [°C]	755.0	755.3	756.1	756.2
FR flow temperature #25 [°C]	182.0	178.0	165.0	155.0
$\dot{m}_{air}$ [kg/s]	111.857	95.688	77.719	52.935
$\dot{m}_{H_2O}$ [kg/s]	15.856	13.760	11.473	8.268

Table 5: Energy balances and results for other interesting parameters (H-R configuration), varying the operating cell voltage of the SOFC.

In Figure 33, there are the diagrams about the trend of the overall fuel utilization, total energy efficiency and the ratio of SOFC on net power output.

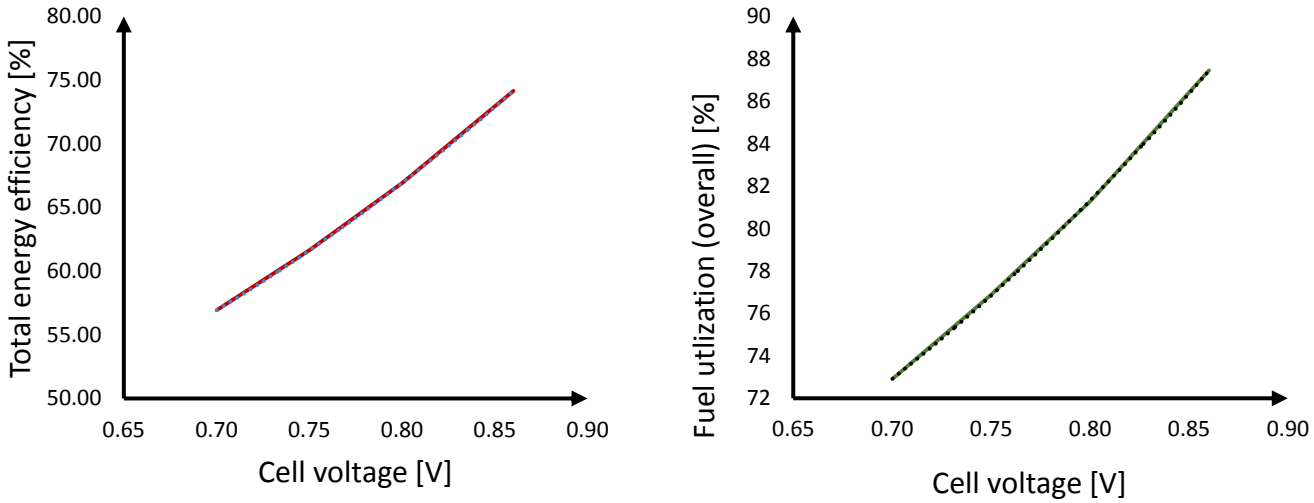

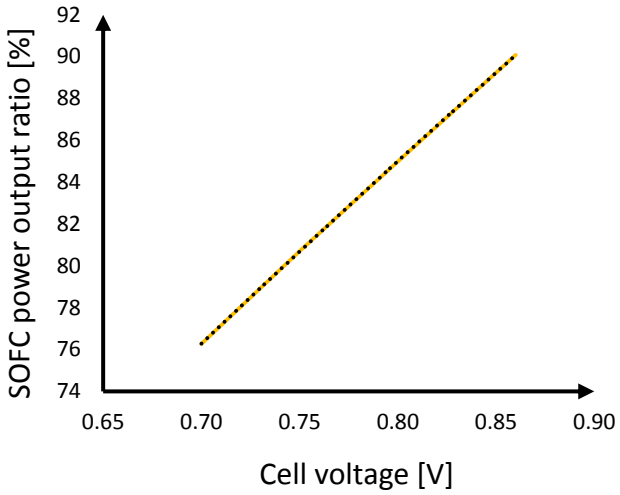

Figure 33: Sensitivity analysis regarding the operating cell voltage of the SOFC (H-R case). a) Trend of the total energy efficiency η; b) trend of the fuel utilization factor (overall) U; c) trend of the ratio of SOFC on the system net power output.

Some considerations can be made about this sensitivity analysis:

- as expected, the influence of SOFC operating voltage is really important. For example, from 0.86 V to 0.8 V, η decreases of almost 10%. In Figure 33a-33b, it is shown the dependence trend between the imposed cell voltage and η and U_f (overall), which are the most important performance parameters; these represent how the fuel is used in efficient way by the system. The same goes for the SOFC weight on the total net power output: if it is low, it means that SOFC is less efficient and the steam cycle has to produce more energy. In fact, the lower is the cell voltage, the higher is the power output of the steam cycle and, consequently, the steam mass flow and the pumps consumption;
- if cell voltage decreases, it is necessary to increase the recycle split factor because the anode outlet flow is less rich of products and it is more difficult to reach the S/C imposed at the pre-reformer inlet. Furthermore, the higher is the hot recycle, the higher is the temperature at SOFC inlet;
- if cell voltage decreases, both U_f and U_{ox} increase;
- the lower is the cell voltage, the higher is the air mass flow. The influence of U_f reduction and the related less need of oxygen is less strong than the higher fuel inlet temperature: the higher is the inlet temperature, the more air is necessary to cool the cell ;
- it was not necessary to change the ζ relative to the oxygen carrier of CLC since the limit about solid recirculation is respected. Consequently, Gs factor is almost the same value in every case, as the temperature at FR outlet;
- it was necessary to change the temperature at the outlet of exchanger E-LT to avoid intersection between the heat transfer curves and respect the limit about the minimum difference of temperature (2 °C). The lower is the cell voltage, the higher is this temperature because the higher is the water/steam mass flow and, consequently, the higher is the gradient of its heating curve and the more probable is the intersection;
- the higher is the cell voltage, the lower is the consumption for the auxiliaries because the stronger is the influence of the water/steam mass flow to

condense. The heat for FR flow cooling increases with the cell voltage because the temperature at E-LT outlet is slightly higher. In fact, the lower is the water/steam mass flow, the higher is the temperature at E-LT outlet;

- the consumption of CO_2 treatment section remains constant because constant is the amount of CO_2 sent to storage and its working conditions.

After the sensitivity analysis regarding the operating cell voltage of the 'H-R' configuration, it is analysed the 'C-R' case.
In Table 6, the results for the performance parameters are shown. Table 7 shows the energy balance and the changes for other interesting properties for this sensitivity analysis.
In Figure 34, there are the diagrams regarding the trend of the overall fuel utilization, the total energy efficiency and the ratio of SOFC on the net power output.

Item	0.7 V	0.75 V	0.8 V	0.86 V
$P_{el,net}$ [MW]	56.653	61.430	66.758	73.903
$P_{el,net,no\ CO_2}$ [MW]	58.507	63.284	68.613	75.757
η [%]	56.653	61.430	66.758	73.903
$\eta_{no\ CO_2}$[%]	58.507	63.284	68.613	75.757
Recycle split fraction [%]	51.112	51.112	51.112	51.112
U_{fuel} [%] (overall)	72.720	76.700	81.250	87.250
U_{fuel} [%] (single pass)	72.720	76.700	81.250	87.250
U_{ox}[%] (overall)	30.152	35.086	43.020	61.939
U_{ox}[%] (single pass)	23.891	29.306	38.020	58.675
Gs $\left[\frac{kg}{s\ m^2}\right]$	18.550	18.432	18.192	17.891

Table 6: Results for the performance parameters (case C-R) varying the operating cell voltage of the SOFC.

Item	0.7 V	0.75 V	0.8 V	0.86 V
Fuel inlet [MW]	100.0	100.0	100.0	100.0
SOFC net power [MW]	47.378	53.540	60.497	69.837
Steam cycle net power [MW]	14.893	13.019	10.841	7.903
SOFC power output ratio [%]	76.084	80.440	84.803	89.834
CO_2 compressor [MW]	-1.818	-1.818	-1.818	-1.818
Recycle fan [MW]	-0.182	-0.182	-0.182	-0.182
FD fan [MW]	-3.271	-2.811	-2.292	-1.592
Water pumps [MW]	-0.111	-0.097	-0.081	-0.059
CO_2 pump [MW]	-0.036	-0.036	-0.036	-0.036
Condensation heat [MW]	31.494	27.531	22.924	16.711
H2O+CO2 cooling heat [MW]	7.430	7.822	8.467	9.385
Auxiliaries work for heat rejection[MW]	-0.311	-0.283	-0.251	-0.209
FR flow temperature #21 [°C]	757.0	757.1	757.4	759.1
FR flow temperature #27 [°C]	195.0	175.0	165.0	155.0

$\dot{m}_{air}$ [kg/s]	114.766	98.626	80.438	55.868
$\dot{m}_{H_2O}$ [kg/s]	15.984	13.972	11.634	8.481

Table 7: Energy balances and other interesting parameters (case C-R) varying the operating cell voltage of the SOFC

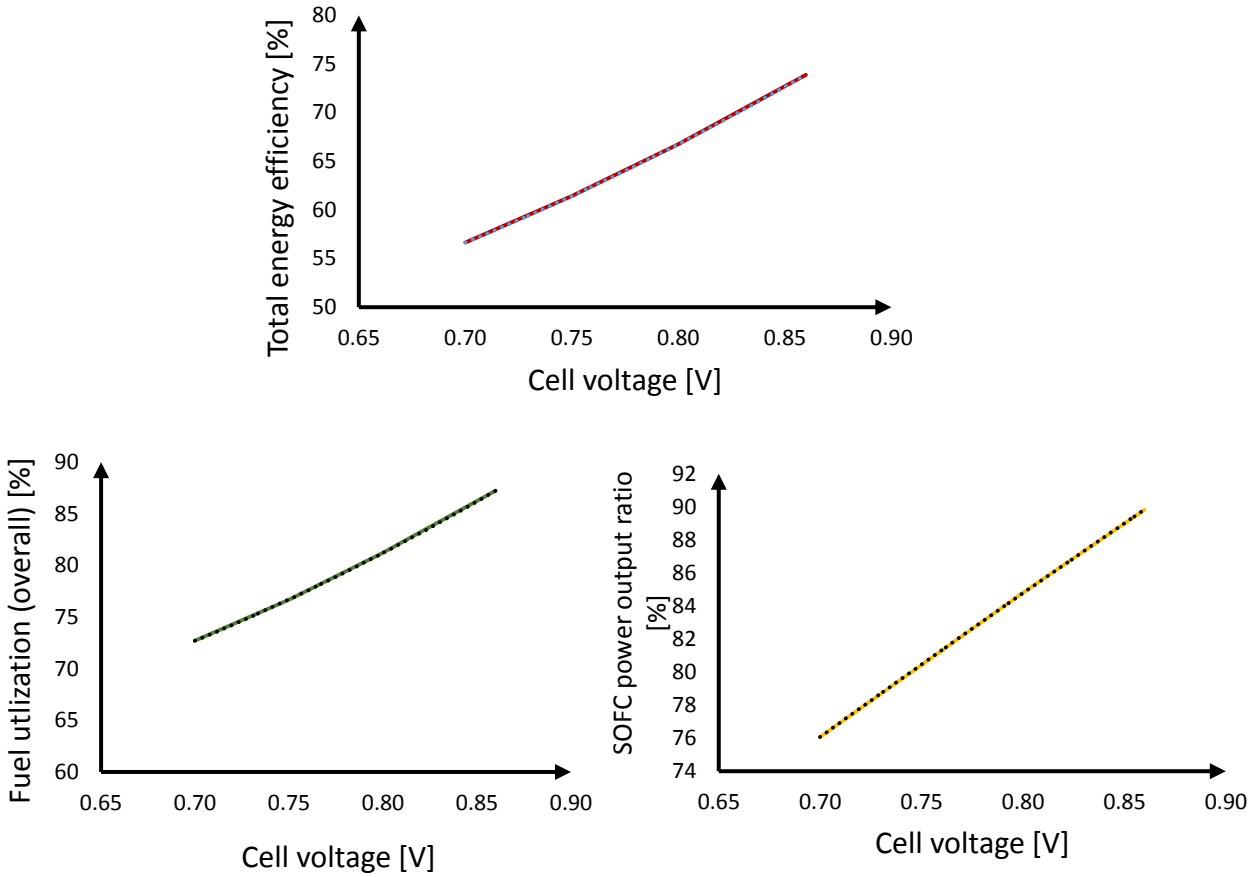

Figure 34: Sensitivity analysis regarding the operating cell voltage of the SOFC (C-R case). a) Trend of the total energy efficiency η; b) trend of the fuel utilization factor (overall) U; c) trend of the ratio of SOFC on the net power output of the system.

The considerations about 'C-R' case are the same of 'H-R' case regarding the trend lines, the total energy efficiency, the SOFC ratio on total power output, the solid recirculation, the FR flow temperatures, the steam cycle, the fuel and oxidant utilization factor, the mass flows considered and the CO_2 section. In addition, it is possible to say:

- the recycle split factor does not change with a different cell voltage. FR flow is not influenced by the air mass flow and depends on the fuel and its mass flow;
- in 'C-R' case, the fuel temperature at SOFC inlet is imposed and does not depend on the amount of recycle. In this way, the temperature difference through the anode side will be the same;
- for both case, the cell voltage lowering involves higher air mass flow. The lower is the cell voltage, the lower is the fuel utilization of the SOFC.

Consequently, the higher is the fuel available to the CLC, the higher is the air mass flow in order to guarantee the same SOFC inlet temperature (735 °C);

- the system 'H-R' remains always the more performing configuration between the two with SOFC and CLC integrated. Thanks to the case 0.86 V, it is possible to compare the performance of the systems with the benchmark case of Campanari et al. [41] (Appendix D). The considerations regarding the total energy efficiencies of the plants remain the same.

In conclusion, as expected, the influence of cell voltage on the performance is high. Furthermore, the most of the considerations made for a case, will be done also for the other ones.

6.1.2 Effect of S/C

Have a certain S/C is important to avoid carbon deposition in the SOFC. With this operating condition (S/C = 2, SOFC outlet temperature 800 °C, fuel SOFC inlet temperature 400-700 °C) the risk of carbon deposition is low. Phenomena of carbon deposition are explained in Paragraph 3.4 and it is expressed by the Reactions 3.4.

Takeguchi et al. [51] discuss about the results of carbon deposition in SOFC, with Ni-YSZ cermet and NG as fuel. In [51], ternary mixture (C, H, O) are shown respect carbon deposition at four different temperatures: 400 °C, 600 °C, 800 °C and 1000 °C. The risk of carbon deposition is higher at the inlet where temperature is lower and there is not the oxygen permeated, that disadvantages carbon deposition.

In Appendixes E, F and G, it is possible to find the compositions of the different SOFC inlet flows. In every of each one, the composition is approximately 55% hydrogen, 30% oxygen and 15% carbon. In Figure 35, the cases at 400 °C and 600 °C are shown and the green lines indicate the composition of interest. The composition of interest is close to the boundary, in particular in Figure 35a. Carbon deposition is not considered risky in the case of this work because the temperature of the inlet flow is higher than 400 °C (in every point, also after the pre-reformer).

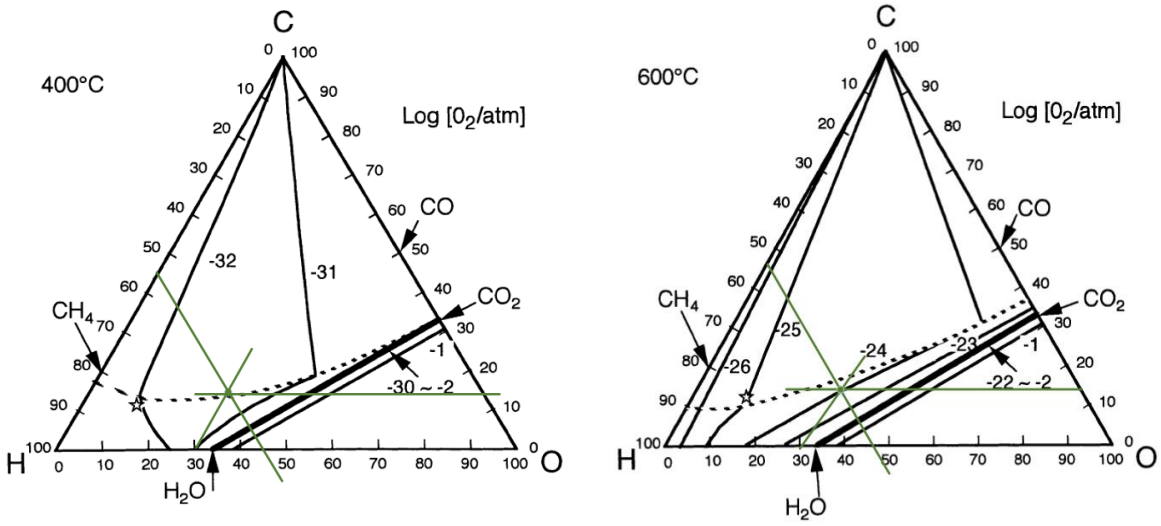

Figure 35: Boundary of carbon deposition region in gas mixtures (C–H–O) diagram at 400 °C (35a) and 600 °C (35b). Dotted lines show the boundary of carbon deposition region; therefore, carbon deposition is expected in carbon-rich composition beyond the lines [51]

S/C influences also the properties of all the streams in the system because S/C involves change in the recycle mass flow. In particular, different recycle mass flow involves different operating temperatures and compositions.

Firstly, it is analysed the 'H-R' configuration. In Table 8, the results for the performance parameters in the different S/C cases are shown. Table 9 shows the energy balances and the changes for other interesting properties for this sensitivity analysis.

Item	2.0	2.5	3.0
$P_{el,net}$ [MW]	66.907	66.939	66.914
$P_{el,net,no\ CO_2}$ [MW]	68.753	68.785	68.760
η [%]	66.907	66.939	66.914
$\eta_{no\ CO_2}$[%]	68.753	68.785	68.760
Recycle split fraction [%]	68.089	75.316	81.186
U_{fuel} [%] (overall)	81.294	81.354	82.170
U_{fuel} [%] (single pass)	58.100	51.850	48.100
U_{ox}[%] (overall)	44.543	44.566	44.524
U_{ox}[%] (single pass)	39.484	39.541	39.486
Gs $\left[\frac{kg}{s\ m^2}\right]$	19.588	19.539	19.660

Table 8: Results for the performance parameters (case H-R) varying the S/C imposed at the pre-reformer inlet.

Item	2.0	2.5	3.0
Fuel inlet [MW]	100.000	100.000	100.000
SOFC net power [MW]	60.529	60.574	60.538
Steam cycle net power [MW]	10.690	10.675	10.688
SOFC power output ratio [%]	84.990	85.017	84.994
CO_2 compressor [MW]	-1.810	-1.810	-1.810
FD fan [MW]	-2.215	-2.213	-2.215
Water pumps [MW]	-0.080	-0.080	-0.080
CO_2 pump [MW]	-0.036	-0.036	-0.036
Condensation heat [MW]	22.606	22.609	22.601
H2O+CO2 cooling heat [MW]	8.866	8.870	8.868
Auxiliaries work for heat rejection [MW]	-0.252	-0.247	-0.252
Fuel SOFC inlet temperature #3 [°C]	668.5	702.2	727.7
$\dot{m}_{air}$ [kg/s]	77.719	77.648	77.721
$\dot{m}_{H_2O}$ [kg/s]	11.473	11.457	11.470

Table 9: Results for the energy balances and for other interesting parameters (case H-R) varying the S/C imposed at the pre-reformer inlet.

Performance of the systems does not change significantly. The small difference in some values can be a result of a different mathematical calculation/approximation of Aspen Plus, because the fuel utilization (single pass) is imposed manually to reach 735 °C at the cathode inlet or because there will be some little difference in any heat capacity due to the different compositions.
The only three parameters that change significantly are the fuel temperature after the ejector (#3), the fuel utilization of the single pass and the split factor of the recycle. The three properties are strongly linked each other: if S/C imposed is higher, higher will be the hot recycle and, consequently, the temperature at #3. U_{fuel} overall remains almost the same (a little increment by increasing the S/C but it can be due to little difference in approximations and heat capacity) while U_{fuel} single pass decreases with S/C.

Figure 36 shows the trend lines of the three main performance parameters in relation to the S/C imposed at the pre-reformer inlet.

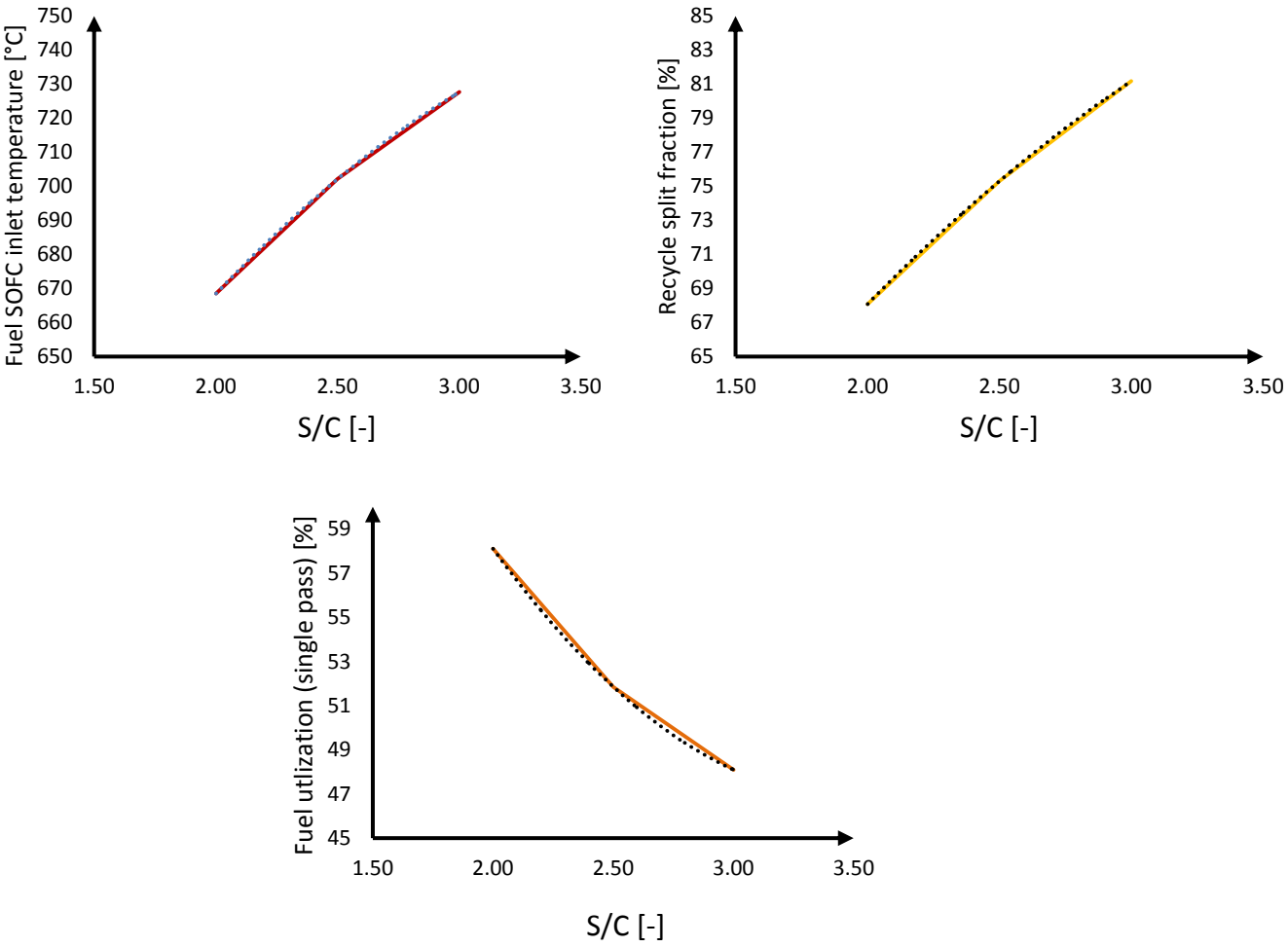

Figure 36: Sensitivity analysis regarding S/C, H-R case. a) Trend of fuel utilization factor (single pass) U; b) trend of the fuel temperature after the ejector (#3); c) trend of the recycle split factor.

In conclusion, in this sensitivity analysis it is demonstrated that in the integrated system SOFC + CLC 'H-R' configuration, a change in the S/C imposed at the pre-reformer inlet allows to reach almost the same general performance (in particular the same for the SOFC) with two advantages:

- lower difference of temperature through the anode side, which can be useful for the materials resistance;
- lower risk of carbon deposition, even if the risk is low with 2 as S/C.

After the sensitivity analysis regarding the S/C for 'H-R' configuration, it is analysed the 'C-R' case. In Table 10, the results for the performance parameters with the different S/C are shown. Table 11 shows the energy balances and the changes for other interesting properties for this sensitivity analysis.

Item	**2.0**	**2.5**	**3.0**
$P_{el,net}$ [MW]	66.758	67.399	68.067
$P_{el,net,no\ CO_2}$ [MW]	68.613	69.254	69.922
η [%]	66.758	67.399	68.067
$\eta_{no\ CO_2}$[%]	68.613	69.254	69.922
Recycle split fraction [%]	51.112	56.660	61.071
U_{fuel} [%] (overall)	81.250	82.300	83.400
U_{fuel} [%] (single pass)	81.250	82.300	83.400
U_{ox}[%] (overall)	43.020	82.300	47.695
U_{ox}[%] (single pass)	38.020	82.300	43.197
Gs $\left[\frac{kg}{s\ m^2}\right]$	18.192	18.036	17.838

Table 10: Results for the performance parameters (case C-R) varying the S/C imposed at the pre-reformer inlet.

Item	**2.0**	**2.5**	**3.0**
Fuel inlet [MW]	100.0	100.0	100.0
SOFC net power [MW]	60.497	61.279	62.098
Steam cycle net power [MW]	10.841	10.630	10.409
SOFC power output ratio [%]	84.803	85.217	85.645
CO_2 compressor [MW]	-1.818	-1.818	-1.818
Recycle fan [MW]	-0.182	-0.227	-0.273
FD fan [MW]	-2.292	-2.181	-2.062
Water pumps [MW]	-0.081	-0.081	-0.081
CO_2 pump [MW]	-0.036	-0.036	-0.036
Condensation heat [MW]	22.924	22.481	22.011
H2O+CO2 cooling heat [MW]	8.467	8.542	8.622
Auxiliares work for heat rejection [MW]	-0.251	-0.248	-0.245
$\dot{m}_{air}$ [kg/s]	80.438	76.541	72.553
$\dot{m}_{H_2O}$ [kg/s]	11.634	11.409	11.171

Table 11: Energy balances and results for other interesting parameters (case C-R) varying the S/C imposed at the pre-reformer inlet.

The results for 'C-R' configuration of the system are more interesting. An increment of S/C imposed involves an increment of all the performance parameters, in particular of the total net power output and the fuel utilization. Furthermore, the air mass flow is lower (due to the higher H_2O/CO_2 which contributes to the SOFC cooling), as well as the related consumption (FD fan).

In conclusion, in this sensitivity analysis it is demonstrated that an increment of S/C involves a slight improvement of the performance with also lower risk of carbon deposition.

Another question can be the influence of the different S/C on the size of the SOFC: a change of S/C involves change of composition at SOFC anode inlet and of the SOFC chemical processes. Consequently, the velocity of the reactions and the necessary dimensions of the SOFC component will be different. All these aspects will be discussed in Chapter 7.

6.2 CLC

The analysis of CLC reactors is important to understand how the result is achieved, not to explain the result itself, because most of input and output conditions are imposed:

- air is fed to AR at 450 °C and has to go out at 735 °C;
- the fuel, fed at 800 °C, arrives from the anode outlet and the amount of reagent species depends on SOFC fuel utilization and the totality of these will react in CLC.

Consequently, the free variables of the system are two:

- the amount of solid recirculated, limited by the solid recirculation factor (Equation 4.1) that has to be lower than 20 kg/s/m^2. In the model, this amount is calculated in order to have a certain ζ;
- the temperature at FR outlet, which depends on the solid recirculation, has to be lower than a certain temperature in order to be far enough in comparison to the melting point of the oxygen carrier used.

If the amount of oxygen fed increases, the solid recirculated increases and the temperatures at AR and FR outlet are closer. The temperature at FR outlet is higher than the temperature at the AR outlet so, in the case of this work, it is useful to have high solid recirculation in order to achieve more easily 735 °C for the air temperature.

The sensitivity analysis about CLC is made only for a model case ('C-R') because the influence of CLC on the total system performance is the same for both cases: if sensitivity analysis led to interesting results, possible modifications will be applied on both configurations.

6.2.1 Effect of solid recirculation

As explained in Paragraph 4.3.2 and in Chapter 5, the model calculates the solid mass flow recirculated in order to have certain ζ in relation to the available fuel and have a Gs factor as close as possible to the limit value (20 kg/s/m^2).

The objectives of this sensitivity analysis are to investigate the influence of ζ and solid recirculation on the temperatures at the reactors outlet, on the temperature difference through the reactors and on the mass flows. Table 12 and Figure 37 show the results for C-R case.

ζ [-]	Gs [kg/s/m^2]	T-AR-in [°C]	T-AR-out [°C]	ΔT-AR [°C]	$\dot{m}_{air}$ [kg/s]	A [m^2]	$\sqrt{A}$ [m]
50	18.192	717.1	734.5	17.4	80.438	50.811	7.128
45	16.465	715.3	734.4	19.1	80.239	50.675	7.119
40	14.685	713.1	734.2	21.1	79.989	50.504	7.107
35	12.905	710.4	733.9	23.5	79.673	50.287	7.091
30	11.124	706.9	733.5	26.6	79.260	50.005	7.071
25	9.342	702.3	733.0	30.7	78.696	49.618	7.044
20	7.558	695.9	732.3	36.4	77.886	49.063	7.005
15	5.772	686.2	731.1	44.9	76.605	48.186	6.942
10	3.978	670.1	728.9	58.8	74.305	46.611	6.827

ζ [-]	Gs [kg/s/m^2]	T-FR-in [°C]	T-FR-out [°C]	ΔT-FR [°C]	$\dot{m}_{sol}$ [kg/s]
50	18.192	737.8	757.4	19.6	924.855
45	16.465	738.0	759.6	21.6	834.353
40	14.685	738.2	762.4	24.2	741.647
35	12.905	738.5	765.9	27.4	648.941
30	11.124	739.0	770.6	31.6	556.234
25	9.342	739.6	776.8	37.2	463.528
20	7.558	740.4	785.9	45.5	370.822
15	5.772	741.8	800.1	58.3	278.115
10	3.978	744.4	825.5	81.1	185.408

Table 12: Results for the sensitivity analysis regarding solid recirculation of the CLC in the C-R case. a) The influence on AR; b) the influence on FR.

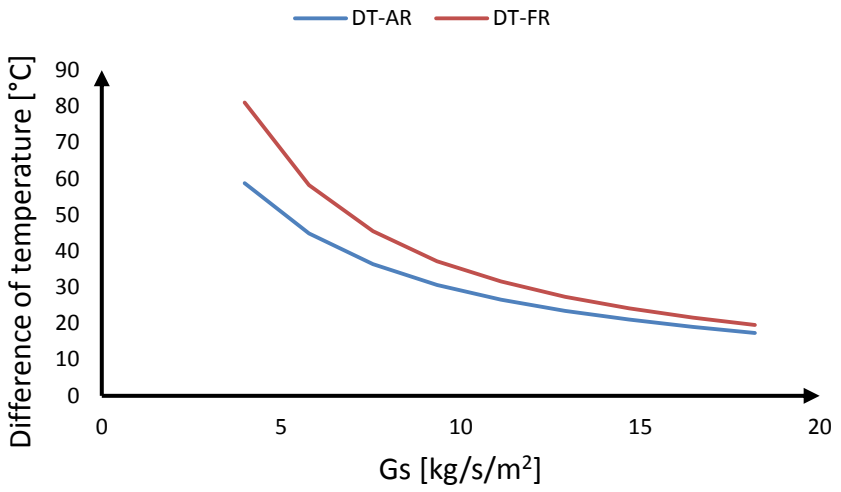

Figure 37: Dependence of difference of temperature through the reactors in relation to the solid recirculation factor Gs.

There are some considerations to be made about the results:

- the air mass flow slightly decreases with a lower solid recirculation because it involves a lower temperature at AR outlet. In fact, the higher is the difference of temperature through the SOFC (with equal outlet SOFC temperature), the lower is the air necessary. Obviously, the passage area (A) of AR, calculated as explained in Paragraph 4.2, decreases in the same way;
- as expected, the higher is the solid recirculation, the closer are the temperatures at the outlet of the two reactors;
- the solid mass flow is very high. The higher is the solids inventory, the higher is the pressure drop through the reactors. In this work, the CLC pressure drop for the gas flows is constant for each case (15 kPa): in literature, there is not a relation that correlates the pressure drop and the solid recirculation for a 3D reactor or the relation is not so reliable (standard deviation of the results of 40% [52]). Furthermore, the relation is strongly dependent on the specific features of the case: oxygen carrier, particle size, porosity, etc. (Paragraph 3.3). The value chosen for the pressure drop is reliable and common in literature. The pressure drop is due to the need of a depression at the base of AR: in this way, the air is able to drag the solid recirculated to the top of the reactor (Figure 19a);
- the temperature at the AR outlet, with a reduction of solid recirculation, decreases but not consistently.

A reduction of solids inventory will involve a lower pressure drop in a real application. Consequently, the consumption for the FD-Fan to pressurize the air at the inlet will be lower (positive for the total energy efficiency) but the temperature at AR outlet will be lower too. Therefore, it will be necessary to reduce the SOFC fuel utilization (reducing its power output) to reach the desired temperature and give more fuel to CLC in order to be able to heat more. A lower solid recirculation will turn out higher temperature at FR outlet: it means more heat at high temperature to use in the waste energy recovery system (increasing the steam cycle output).

In general, the effect of a variation of solids inventory on the total energy efficiency of the system is not so important because the possible additional consumption for the FD-fan at the inlet will be more influential in comparison to the reduction of SOFC performance (the consumption of a gas compressor is not negligible, the energy balances demonstrate it).

In conclusion, this sensitivity analysis has been demonstrated that a reduction of solid recirculation involves no changes (or not so strong changes) of the performance of the system with major simplifications of the CLC design. The best solution could be to operate with a solid recirculation borderline between the limits of allowable temperature at the FR outlet and the possible consequent reduction of fuel utilization.

6.2.2 Effect of oxygen carrier

In the models built in this work until this point, copper is the only OC used and it was never questioned. This sensitivity analysis is carried out to demonstrate if there is an OC better in comparison to copper for the case of this work. Better, in this case, means higher difference of temperature in the AR, lower solid recirculation to parity of performance or lower mass flow, with operating condition more similar as possible.

Nickel and Iron are the other considered OCs because they are two of the most studied and consolidated, in particular for these operating temperatures. Table 13 shows the most important properties of these materials.

Oxygen carrier	Mm [kg/kmol]	c [J/kg °C]	ρ [kg/m^3]	Melting point [°C]
Copper	63.6	385	8920	1085
Iron	55.8	444	7874	1538
Nickel	58.6	440	8920	1455

Table 13: Physical properties of the OCs (Mm = Molecular mass; c = specific heat; ρ = density).

The mixtures considered for the comparison is the same: 0.4 of mass fraction for the oxide of the OC (CuO, Fe_2O_3, NiO) and 0.6 for the inert/support. The support considered for that analysis is also the same, zirconium dioxide (ZrO_2). In this way, the comparison will be more significant regarding the properties of the oxygen carrier. In [49][53][54][55], it is possible to find these mixtures among the ones studied in the past works.

For the copper case, it is necessary to consider CLOU (Chemical Looping with Oxygen Uncoupling) processes: at high temperature, it is favoured the endothermic reaction of decomposition of CuO in Cu_2O (Reaction 6.1) [53].

$$4CuO \implies 2Cu_2O + O_2(g) \qquad \Delta H_{850} = 263.3\ kJ/kmol_{O_2} \qquad (6.1)$$

Instead, for iron, it is necessary to consider all the kind of iron oxides like possible products of the FR, as previously explained in Paragraph 3.2.2.

Table 14 shows the main results regarding this sensitivity analysis. The analysis is carried out only for the C-R configuration.

Item	Copper	Iron	Nickel
ζ [-]	**50**	**50**	**50**
Gs [kg/s/m^2]	18.192	11.957	17.357
ΔT-AR [°C]	17.4	38.1	32.7
ΔT-FR [°C]	19.6	3.4	2.8
T FR flow #21[°C]	757.4	742.4	741.2
$\dot{m}_{air}$ [kg/s]	80.438	81.675	80.780
$\dot{m}_{sol}$ [kg/s]	924.855	617.504	886.547
U_{fuel} (overall)	0.81250	0.81300	0.80970
η	0.66758	0.66654	0.66481

Table 14: Results about OC comparison using same ζ.

The comparison presents very interesting results:

- with the same ζ, iron increases the SOFC fuel utilization and decreases the solid mass flow of approximately 33%;
- in iron case, it was possible to increase the SOFC fuel utilization because the air temperature at AR outlet was higher than 735 °C;
- nickel and iron cases have similar behaviour for the CLC. The reactions in FR are slightly exothermic while in AR the reactions are more exothermic in comparison to the copper case. This nature of the reactions is confirmed by the reaction enthalpies indicated in Appendix B. These results regarding the outlet temperature are important in relation to the objective of this work. In fact, the CLC has to heat up the air flow rate.
  Furthermore, the problem of melting point in nickel and iron case is less important. In fact, their melting points are higher and the temperatures at FR outlet are also lower;
- in nickel case, it was necessary to reduce the SOFC fuel utilization in order to reach the desired air temperature at AR outlet;
- copper and nickel have similar results regarding the solid mass flow because, to ζ parity, they feeds the same amount of oxygen. The solid mass flow for copper case is higher because of CLOU processes and because of the higher molecular mass;
- iron and nickel case presents an higher air mass flow. It involves in higher consumption of FD-Fan;
- to ζ parity, copper presents the highest efficiency but the difference, among all the cases, is very small (lower than 0.2%). Nickel suffers the lower SOFC fuel utilization. The reasons for a so little difference can be a lot: the higher FD-Fan consumption because of the higher air mass flow, the lower temperature at FR outlet, etc.

This sensitivity analysis has demonstrated that:

- the general performance of the three cases are very similar;

- iron allows to reach certain performance with less critical operating conditions for CLC (lower solid recirculation). Furthermore, iron has higher melting point in comparison to copper and, consequently, iron can have higher operating temperature;
- nickel case is less performing in comparison to the copper case and does not present advantage relevant regarding CLC operating conditions.

It will be possible to build models using iron with less critical operating conditions for CLC and similar system performing.

A sensitivity analysis regarding the influence of solid recirculation with iron can be useful to understand if really iron case can be better than copper case. Table 15 and Figure 38 show the results. This sensitivity analysis is made using the same value for SOFC fuel utilization: in this way, the comparison considers the same amount of fuel fed to the CLC. The fuel temperature at the inlet of FR is set 800 °C.

ζ [-]	Gs [kg/s/m^2]	T-AR-in [°C]	T-AR-out [°C]	ΔT-AR [°C]	$\dot{m}_{air}$ [kg/s]	A [m^2]	$\sqrt{A}$ [m]
85	20.330	711.9	735.5	23.6	81.988	51.877	7.203
70	16.760	707.2	735.4	28.2	81.914	51.822	7.199
65	15.569	705.3	735.4	30.1	81.884	51.801	7.197
60	14.379	703.0	735.4	32.4	81.843	51.774	7.195
55	13.189	700.4	735.4	35.0	81.798	51.743	7.193
50	11.998	697.3	735.3	38.0	81.745	51.706	7.191
45	10.808	693.7	735.3	41.6	81.680	51.662	7.188
40	9.618	689.2	735.2	46.0	81.596	51.605	7.184
35	8.426	683.8	735.1	51.3	81.497	51.536	7.179
30	7.236	676.8	735.0	58.2	81.362	51.444	7.172
25	6.045	667.8	734.8	67.0	81.178	51.318	7.164
20	4.853	655.5	734.6	79.1	80.909	51.134	7.151
15	3.661	637.8	734.3	96.5	80.479	50.840	7.130
10	2.467	610.1	733.6	123.5	79.696	50.304	7.093
8	2.145	596.6	724.8	128.2	74.727	46.787	6.840

ζ [-]	Gs [kg/s/m^2]	T-FR-in [°C]	T-FR-out [°C]	ΔT-FR [°C]	$\dot{m}_{sol}$ [kg/s]
85	20.330	737.9	739.9	2.0	1054.657
70	16.760	738.4	740.8	2.4	868.541
65	15.569	738.6	741.2	2.6	806.502
60	14.379	738.8	741.6	2.8	744.464
55	13.189	739.0	742.1	3.1	682.425
50	11.998	739.3	742.7	3.4	620.386
45	10.808	739.7	743.5	3.8	558.348
40	9.618	740.1	744.4	4.3	496.309
35	8.426	740.7	745.5	4.8	434.271

30	7.236	741.5	747.0	5.5	372.232
25	6.045	742.5	749.1	6.6	310.193
20	4.853	743.9	752.1	8.2	248.155
15	3.661	746.2	756.9	10.7	186.116
10	2.467	750.1	765.6	15.5	124.077
8	2.145	746.9	763.0	16.1	100.344

Table 15: Results for the sensitivity analysis about solid recirculation of CLC with iron (C-R case). a) The influence on AR; b) the influence on FR .

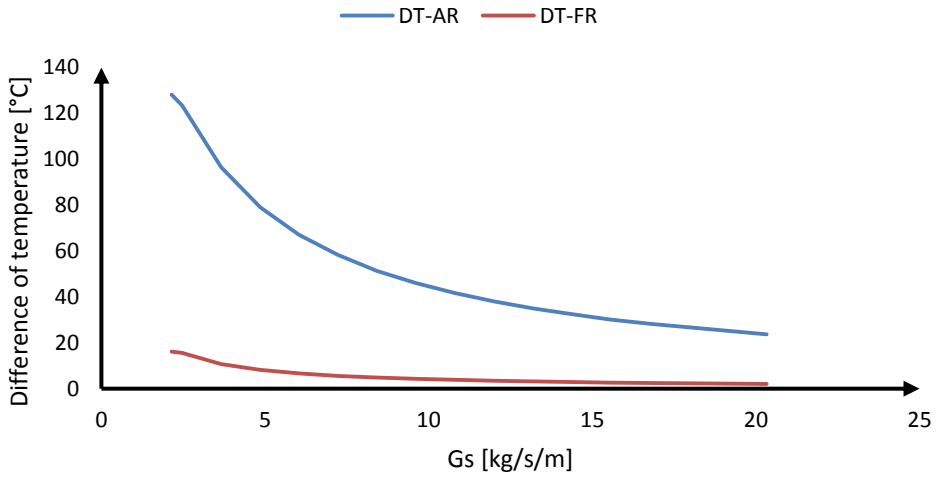

Figure 38: Dependence of difference of temperature through the reactors in relation to the solid recirculation factor Gs, C-R case with iron.

The results confirm that:

- with iron, the difference of temperature through the reactors is unbalanced (higher for AR) in comparison to the copper case (for AR, equal to FR or lower). The heat available by the fuel is distributed better among the reactors in relation to the thermal objectives of CLC in the system of this work (heat the air);
- with iron, it is possible for air to reach more easily 735 °C at AR outlet in comparison to the copper case (with a lower Gs): this result is evident comparing Table 15a (iron) and Table 12a (copper).

In order to have a further confirmation of these results, it will be made another comparison among the three OCs setting the same:

- air mass flow (80.438 kg/s);
- solid recirculated (200 kg/s);
- overall SOFC fuel utilization (81.25%), in order to have the same available fuel for CLC.

The air mass flow and the SOFC fuel utilization imposed are the same of the copper C-R base case; the amount of solid (200 kg/s) is imposed in order to have a value of solid recirculation less critical.

Table 16 shows the results of this comparison.

Item	Copper	Iron	Nickel
U_{fuel} (overall)	**0.81250**	**0.81250**	**0.81250**
$\dot{m}_{air}$ [kg/s]	**80.438**	**80.438**	**80.438**
$\dot{m}_{sol}$ [kg/s]	**200.0**	**200.0**	**200.0**
Gs [kg/s/m^2]	4.019	3.934	3.961
ΔT-AR [°C]	54.4	92.0	97.4
T AR flow #9[°C]	713.5	734.8	727.4
ΔT-FR [°C]	75.6	10.1	9.7
T FR flow #21[°C]	807.1	756.0	752.0

Table 16: Results of the comparison among the three OCs using same air, fuel and solid mass flow.

The solid recirculation is not the same since the reactions in the reactors are different case by case. In particular, in copper case, CLOU processes occur with consequent losses of oxygen capacity. This phenomenon is confirmed by the results in Appendix F and G since Cu_2O is present in the solid flow at FR outlet (#20) while, in the gas flow at FR outlet (#21), some traces of oxygen (lower than 10 ppm of molar fraction) are present. Instead, in iron case, the reaction of recombination occurs between the different iron oxides; at FR outlet (#20), Fe_2O3 and Fe_3O_4 are the only oxides present because FeO appears only at lower temperature.
Despite the same fuel utilization, the temperature at anode outlet is different because the mass flow rate at AR outlet is different case by case in relation to the different reactions of CLC and the need of oxygen.
In the model, it was added an additional exchanger at anode outlet in order to fix the temperature of the fuel fed to FR (800 °C).

The results of this comparison confirm the considerations made before regarding the CLC. This sensitivity analysis has been demonstrated that:

- the influence of CLC on the total system performance is small;
- iron and nickel could be more suitable to the objectives of CLC in the system proposed in this work;
- in iron and nickel cases, the reactions in FR are slightly exothermic and the outlet temperature results lower in comparison to the copper case. Furthermore, the melting points of nickel and iron are lower in comparison to copper case. Consequently, the problem of melting point becomes less important in iron and nickel cases;
- CLC operating conditions depend strongly on the specific features of the case, in particular regarding fluid dynamics and reactivity of the reactors: the best solution has to be found case by case.

6.2.3 Effect of inert/support

The total energy efficiency of the system is the main interest of this work. A parameter, which can influence the heat transfer and the reactions in CLC, is the material used as inert/support. Until this point, zirconium oxide is the only material considered as support because it is one of the most studied in literature and for its properties of resistance. Alumina (Al_2O_3) is among the most studied materials in

literature, in particular coupled with iron. It can be studied and compared with zirconium oxide. In literature, it is possible to find different mixtures of Alumina with the OCs studied, in particular: Fe_2O_3 (mass fraction of 0.6) – Al_2O_3 (0.4), Fe_2O_3 (0.4) – $MgAl_2O_4$ (0.6), CuO (0.6) - Al_2O_3 (0.4), etc. [49][53][54][55].

The choice of the support is influenced by some factors as, for example, the fluid dynamics, the relation between the oxygen carrier oxide and the support regarding the process of production, etc. In this work, it has been decided to leave the analysis of inert effect to work more specific since the conclusion would be not so interesting or not complete.

The results about CLC sensitivity analysis have demonstrated the advantages of iron as OC in comparison to copper. For this reason, two new models have been done using, in CLC, one of the most studied mixture in literature, that is Fe_2O_3 (0.6 wt%) – Al_2O_3 (0.4). The Gs factor is set approximately equal to 10 kg/s/m^2, a minimum limit value necessary to guarantee that reactions occur in the AR. The reactions in AR are faster in comparison to the reactions in FR; the lower is Gs, the lower is the amount of solids in AR, the more difficult is that reactions occur in AR.

Tables 17 show the results of these models and the comparison with the old configurations.

Item	H-R old	H-R new	C-R old	C-R new
$P_{el,net}$ [MW]	66.907	67.007	66.758	66.775
$P_{el,net,no\ CO_2}$ [MW]	68.753	68.853	68.613	68.630
η [%]	66.907	67.007	66.758	66.775
$\eta_{no\ CO_2}$[%]	68.753	68.853	68.613	68.630
Recycle split fraction[%]	68.089	67.900	51.120	51.120
U_{fuel} [%] (overall)	81.294	81.938	81.250	81.350
U_{fuel} [%] (single pass)	58.100	58.495	81.250	81.350
U_{ox}[%] (overall)	44.543	44.001	43.020	42.182
U_{ox}[%] (single pass)	39.484	39.023	38.020	37.246
Gs $\left[\frac{kg}{s\,m^2}\right]$	19.588	10.061	18.192	10.023

Item	H-R new	C-R new
Fuel Inlet [MW]	100.000	100.000
SOFC net power [MW]	60.646	60.573
Steam cycle net power [MW]	10.701	10.909

CO_2 compressor [MW]	-1.810	-1.818
Recycle fan [MW]	-	-0.182
FD fan [MW]	-2.241	-2.338
Water pumps [MW]	-0.080	-0.081
CO_2 pump [MW]	-0.036	-0.036
Condensation heat [MW]	22.628	22.897
H2O+CO2 cooling heat [MW]	8.862	8.471
Auxiliaries work [MW]	-0.252	-0.251

Table 17: Performance parameters and energy balances for the new cases with Iron and Alumina in CLC and comparison with the results of the old configurations of the models.

Iron and Alumina in CLC allow to have a slightly improvement of the performance of the plants with easier solid recirculation. In a real application, it means lower losses in CLC and lower consumption in order to recover the pressure losses. Another important advantage is that Al_2O_3 is much cheaper respect ZrO_2.
But the best OC is not only the OC that allows to achieve the theoretical best performance; all the aspects of CLC design have to be considered specifically.

6.3 Steam cycle

6.3.1 Effect of maximum pressure and temperature

It is a trivial energetic consideration that an increment in maximum pressure and temperature of the steam cycle brings to better performance. With external combustion, a higher maximum operating temperature allows to use energy at higher temperature and, consequently, this energy is more valuable. Furthermore, the higher is the evaporating pressure, the lower is the specific heat of evaporation.

The advantage of increasing the operating temperature is the performance improvement of the steam cycle and the easier design of the steam turbine. With other operating conditions unchanged (e.g. isentropic efficiency of turbine), the higher is the steam turbine inlet temperature, the higher is the vapour fraction at the outlet: it means less water condensed in the flow and easier management of the increment of volumetric flow rate due to the conservation of the mass flow.

The analysis of a system with different pressure and temperature can be useful to understand the really potentialities of the thermal integration (although the small size of the steam cycle imposes already some limitations). In future, with the improvement of the state-of-art, it will be possible (and cheaper) to apply more critical operating conditions (for example, as USC technology) to plant of smaller size.

‘H-R’ and ‘C-R’ configurations have been modified to build models more performing thanks to new steam cycle operating conditions. In Table 18, the new assumptions for the steam cycle are shown.

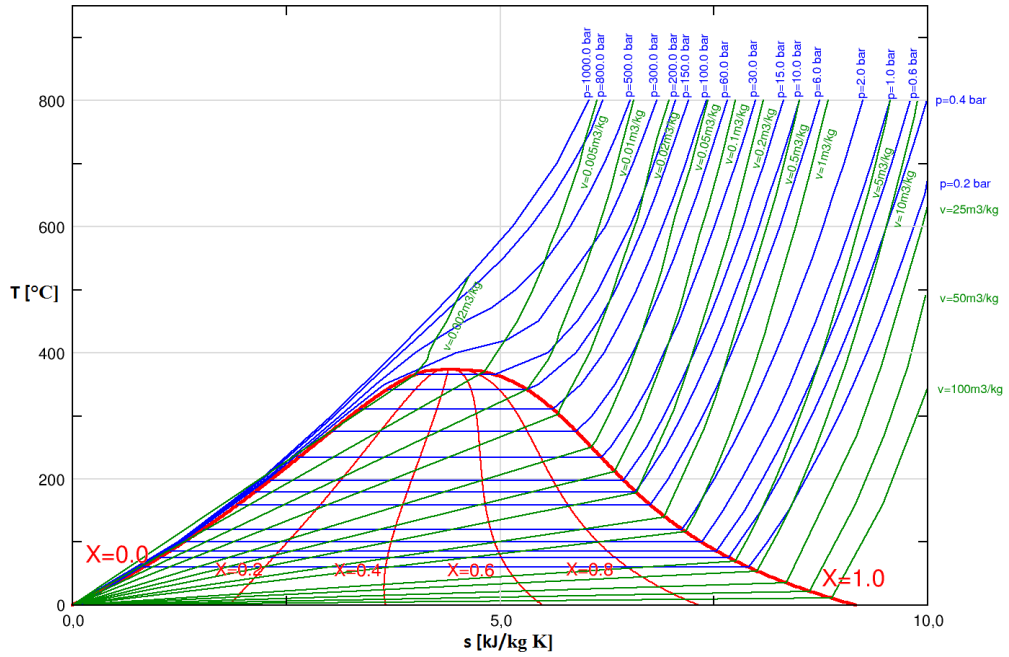

Figure 39: H_2O phase diagram Temperature [°C] – Entropy [kJ/kg K].

Steam Cycle	
Evaporation pressure [bar]	150.0
Maximum steam temperature [°C]	560.0
Steam temperature after reheat [°C]	560.0
Pressure of reheat [bar]	25.0
Subcooling ΔT at evaporator drum inlet [°C]	5.0
Pressure drop in steam superheater [%]	3.5
Pressure drop in steam reheat [%]	3.5
Pressure drop in economiser [bar]	30.0
Pressure drop at turbine inlet [%]	5.0
Gas pressure drop in recovery boiler [bar]	0.05
Temperature drop in superheater to turbine piping [°C]	2.0
Minimum condensing pressure [bar]	0.048
Turbine isentropic efficiency [%]	85.0
Feed water pump hydraulic efficiency [%]	85.0
Turbine mechanical efficiency [%]	99.60
Generator electric efficiency [%]	98.50

Table 18: New operating conditions for the integrated steam cycle of the SOFC + CLC systems.

There are four main modifications of the steam cycle:

- increment for the evaporating pressure from 40 bar to 150 bar;
- increment for the maximum steam temperature from 400 °C to 560 °C;
- addition of a reheat during the expansion: the RH heating is charged by the exhaust cathode flow (in the component HRSG-2 for both case, 'H-R' and 'C-R');
- the pressure drop in economizer is evaluated in proportion: in the base cases, the pressure losses are 10 bar out of 50 bar (20%) in order to have 40 bar in the evaporator; in the new case, 30 bar out of 180 bar (20%) in order to have 150 bar in the evaporator.

Table 19 shows the results for the performance parameters with the new steam cycle conditions compared to the base cases; Table 20 shows the comparison of the energy balances.

Item	H-R		C-R	
	Base	**New**	**Base**	**New**
$P_{el,net}$ [MW]	66.907	69.470	66.758	69.320
$P_{el,net,no\ CO_2}$ [MW]	68.753	71.316	68.613	71.174
η [%]	66.907	69.470	66.758	69.320
$\eta_{no\ CO_2}$[%]	68.753	71.316	68.613	71.174
Recycle split fraction [%]	68.089	68.089	51.120	51.120
U_{fuel} [%] (overall)	81.294	81.294	81.250	81.250
U_{fuel} [%] (single pass)	58.100	58.100	81.250	81.250
U_{ox}[%] (overall)	44.543	44.543	43.020	43.020
U_{ox}[%] (single pass)	39.484	39.484	38.020	38.020
Gs $\left[\frac{kg}{s\,m^2}\right]$	19.588	19.588	18.192	18.192

Table 19: Comparison about the performance parameters between the base case of integrated SOFC + CLC systems in comparison to the results of the new systems with improved operating conditions for the steam cycle.

Item	H-R		C-R	
	Base	**New**	**Base**	**New**
Fuel inlet [MW]	100.000	100.000	100.000	100.000
SOFC net power [MW]	60.529	60.529	60.497	60.497
Steam cycle net power [MW]	10.690	13.233	10.841	13.399
SOFC power output ratio [%]	84.990	82.060	84.803	81.868
CO_2 compressor [MW]	-1.810	-1.810	-1.818	-1.818
Recycle fan [MW]	-	-	-0.182	-0.197
FD fan [MW]	-2.215	-2.215	-2.292	-2.292
Water pumps [MW]	-0.080	-0.222	-0.081	-0.225
CO_2 pump [MW]	-0.036	-0.036	-0.036	-0.036
Condensation heat [MW]	22.606	19.670	22.606	19.917
H2O+CO2 cooling heat [MW]	8.866	9.562	8.866	9.158
Auxiliaries work for heat rejection [MW]	-0.252	-0.233	-0.252	-0.233
$\dot{m}_{air}$ [kg/s]	77.719	77.719	80.438	80.438
$\dot{m}_{H_2O}$ [kg/s]	11.473	8.973	11.634	9.087

Table 20: Energy balances of the base cases and the new cases with a more performing steam cycle.

About this sensitivity analysis, the things to underline are many:

- the changes in the steam cycle do not involve changes of SOFC and CLC performance;

- for both the new cases, it was possible to reach the minimum temperature for FR flow at the outlet of exchanger E-HT (155 °C, approximately 15 °C higher than water temperature, minimum difference of temperature allowable for an heat transfer gas – liquid). It is a consequence of the lower total mass flow of the water/steam;
- there is not intersection of curves in the exchanger E-LT for both the new case. It is confirmed by the zone analysis imposed in the Aspen model;
- in the new case 'C-R', it was necessary to increase the temperature of FR flow at outlet of HRSG-2 (#25) from 400 °C to 455 °C in order to respect the limit for the heat exchange gas – gas (30 °C) at the inlet of HRSG-2 (#22 at about 590 °C, #43 at 560 °C). It involves an hotter temperature of the recycle and a consequent little increment of the recycle fan consumption;
- the improvement of the total system performance is very important: for both the new cases, the net power output relative to the steam cycle rises of about 24% and the total energy efficiency η of 3.83% points. The improvement is slightly better for 'C-R' case;
- the improvement of performance could be also higher because it was not done a specific study regarding the heat transfer curves and the efficiency of heat transfer. Maybe, an additional simple regenerator at high temperature will be useful to reduce the difference of temperature between the evaporating water and the hot flow in order to make the heat transfer more efficiently;
- in the new case, the vapour fraction at steam turbine outlet is very high ($\sim$ 96%) in comparison to the base cases ($\sim$ 85%). This is an important advantage for the design of the steam turbine.

In conclusion, this sensitivity analysis has demonstrated that an improvement of steam cycle operating conditions involves important performance improvement for both the configurations of SOFC + CLC system.

Chapter 7

SOFC analysis

After having analysed performance and operating conditions of the system SOFC + CLC, it is necessary to study specifically the SOFC using the models presented in Chapter 2. In this way, it will be possible to have an idea of the future feasibility of this component and these plants. In fact, thanks to the models, it will be calculated the dimensions of the SOFC and all its features: the exchange area, the trend of current density, voltage losses, flow compositions, etc. The real behaviour of the SOFC is the main topic of this Chapter. Furthermore, it will be investigated possible variations of the SOFC in order to improve the performance.
The SOFC geometry supposed by the models is planar with co-flow configuration: the flows of air and fuel channels get in the SOFC from the same side and stream with the same direction towards the outlet.

7.1 Main assumptions

The model used for this analysis was already explained in detail in Chapter 2. It was built an Excel model able to calculate all the features of the SOFC starting from the inlet conditions taken from the Aspen model. The process followed by the Excel model is the subsequent:

- the SOFC inputs are given from the results of the Aspen model. For example, for the case H-R, the inlet conditions for the anode are the conditions of #4, at the pre-reformer outlet; conversely, for the inlet cathode conditions, the properties are the properties of #9;
- the dimensions of the unit cell elements are supposed. The reference is [14] and the assumptions are shown in Tables 21.

Width [mm]	1	**Anode thickness [μm]**	500
Fuel channel height [mm]	1	**Cathode thickness [μm]**	50
Air channel height [mm]	1	**Electrolyte thickness [μm]**	20
Length of control volume [mm]	100	**Interconnect thickness [μm]**	500

Table 21: Dimensions of the unit cell elements assumed in the model [14]

  The length of the control volume is supposed 0.1 m. The length has to be small enough to analyse precisely the reactions but not too small in order to not have too control volumes;
- the number of unit cell elements is supposed. The value does not influence the results of main interest (total exchange area, trend of current density, overpotentials, etc.);
- it is applied the kinetics model to the inlet compositions and new properties for the anode stream are obtained. The kinetic model is explained in Equations 2.16, 2.17 and 2.18. The model proposed by Divisek [13] was discarded because it generates a

kinetic too slowly, possibility already supposed in Paragraph 2.2.1. The kinetic model is the one by Numaguchi et al. [15];

- the electrochemical model is applied to the new anode stream properties in combination with the properties of the cathode flow, unchanged after the kinetic model. The model is explained in Chapter 2, Paragraphs 2.2.2 and 2.2.3. In order to calculate the resistivity of the unit cell elements, the correlations proposed by Spallina et al. in [14] are used. The correlations are shown in Table 22.

Layer	ρ [Ωm]	Material
Anode	1.25×10^{-5}	Ni-YSZ cermet
Cathode	1.25×10^{-5}	Perovskite materials
Electrolyte	$\left(33.4 \cdot 103 \cdot e^{\frac{-103000}{T(K)}}\right)^{-1}$	YSZ
Interconnect	$\left(\frac{9.3 \cdot 10^{6}}{T} \cdot e^{\frac{-1100}{T(K)}}\right)^{-1}$	Ceramic oxides with perovskite structure

Table 22: Correlations for the calculation of the resistivity of the SOFC materials.

It has been made some assumptions to simplify the model.

- The concentration overpotentials are neglected because its calculation is not easy and its contribution is not relevant.
- The thermal model, presented in Paragraph 2.2.4, is not used because too complicate for this kind of work. As explained in 2.2.4, it involves the calculation of temperature trend in the flows and in the solid structure. Consequently, it would be necessary the calculation of every specific coefficient of heat transfer, for conductive, convective and radiative heat transfer. Therefore, for simplicity, temperatures in the model are supposed constant and equal to the value of the SOFC outlet (800 °C).
- The electrochemical model used is the 'H_2-only' proposed by Aguiar [16] and not the 'H_2-CO' model proposed by Suwanwarangkul [17]. As demonstrated in [14] by Spallina et al., when the WGS reaction is at chemical equilibrium, the Nerst voltage of H_2 oxidation and CO oxidation reactions are the same ($E_{H_2} = E_{CO}$). This condition is reached fast and, consequently, the utilization of the simpler model 'H_2-only' is justified.
- The electrochemical model gets new properties for anode and cathode flows. The objective of the electrochemical model is to find the overpotentials and the current density in order to obtain the imposed operating cell voltage (e.g. 0.8 V) for every control volume. In this way, all the desired trends are obtained (current density, activation and ohmic overpotentials, etc.).
- The new properties of anode and cathode flows are used as inputs for the next control volume and the same process will be applied again. The iterative process continues until the total current produced by the SOFC is equal to the total current calculated by the Aspen model.
- Reached the total current calculated by the Aspen model, it is possible to calculate the total SOFC exchange area (*A*, Equation 7.1) as the product of the total SOFC

length obtained (l) to the unit cell element weight (w) and the total number of unit elements (n):

$$A = l \cdot w \cdot n \tag{7.1}$$

- At the last SOFC unit element, it is difficult that the total current calculated by the Excel model is perfectly equal to the total current calculated by the Aspen model due to the discretization. For this reason, it is used a linear proportion between the two last unit elements in order to calculate all the SOFC outlet properties. Equations 7.2 show this method.

$$\text{With } x \;/\; I_x < I_{Aspen} \;\&\; I_{x+1} > I_{Aspen} \implies a = \frac{I_{Aspen} - I_x}{I_{x+1} - I_x}$$

$$p_{out} = p_x + (p_{x+1} - p_x) \cdot a \tag{7.2}$$

where x is the number of an iteration; subscripts 'x' and 'x+1' is relative to the value, respectively, at the 'x' and 'x+1' iteration; p is a general property of the model (e.g. length, CO molar fraction, current density, etc.); subscript 'out' is relative to the SOFC outlet value.

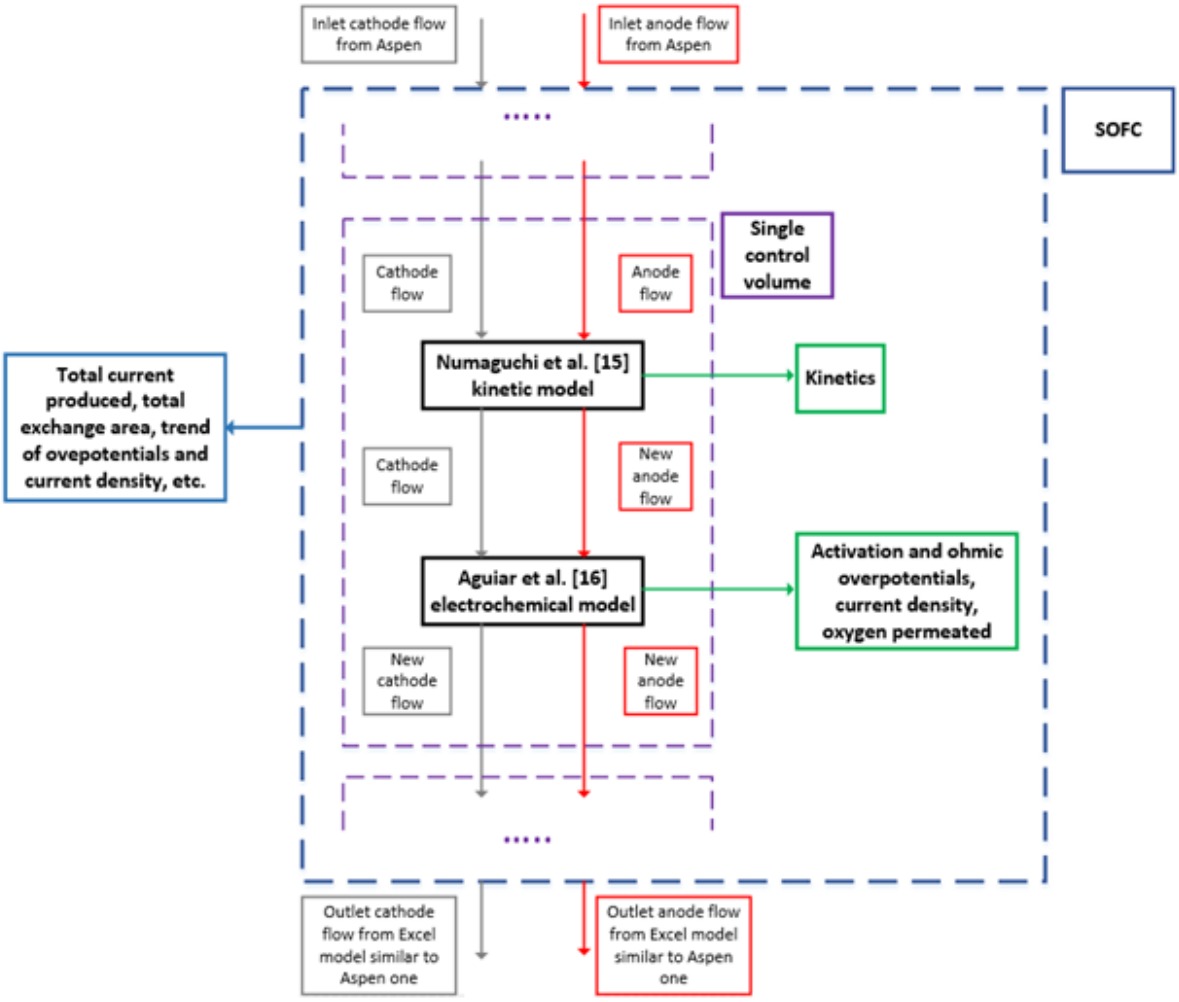

Figure 40: Summary scheme of the model used for the SOFC analysis.

7.2 Results

The SOFC Excel model was used to analyse the SOFC in the three different systems of Chapter 5: the benchmark case SOFC + combustor, the two integrated systems SOFC + CLC 'H-R' and 'C-R' configuration.
In Table 23, the main results of this analysis are shown. Table 24 shows the comparison between the Aspen model results and the Excel model results regarding the anode outlet composition. In Figures 41, the trends of compositions through the anode channel are shown.

Item	**No CO_2 capture**	**With CO_2 capture**	
	Benchmark case	**H-R**	**C-R**
A [m^2]	20125	22286	26680
I [MA]	72.681	78.002	77.912
$\dot{n}_{O_{2,permeated}}$ [kmol/s] (Aspen)	0.18831	0.20211	0.20188
$\dot{n}_{O_{2,permeated}}$ [kmol/s] (Excel)	0.18832	0.20231	0.20191
$i_{average}$ [A/m^2]	3610.0	3496.2	2915.4
i_{max} [A/m^2]	4917.9	5022.8	5498.5

Table 23: Main results regarding the SOFC analysis for the three base cases of Chapter 5 .

Anode	**n [kmol/s]**	**CH_4**	**CO_2**	**H_2O**	**H_2**	**CO**
Benchmark case						
Inlet	1,36500	0.06012	0.24598	0.29355	0.31500	0.08216
Outlet (Aspen)	1.52900	0	0.23889	0.43546	0.21509	0.10769
Outlet (Excel)	1.52897	0.00008	0.23456	0.43796	0.21257	0.11201
H-R						
Inlet	0.98620	0.09357	0.26024	0.31163	0.27355	0.05764
Outlet (Aspen)	1.17100	0	0.26387	0.48430	0.16626	0.08271
Outlet (Excel)	1.17071	0.00002	0.26040	0.48814	0.16242	0.08618
C-R						
Inlet	0.55800	0.18434	0.27766	0.38106	0.14068	0.01237
Outlet (Aspen)	0.76400	0	0.30626	0.56858	0.08199	0.04032
Outlet (Excel)	0.76372	0	0.30422	0.57143	0.07914	0.04237

Table 24: Properties of the inlet and outlet anode streams for the three base cases of Chapter 5.

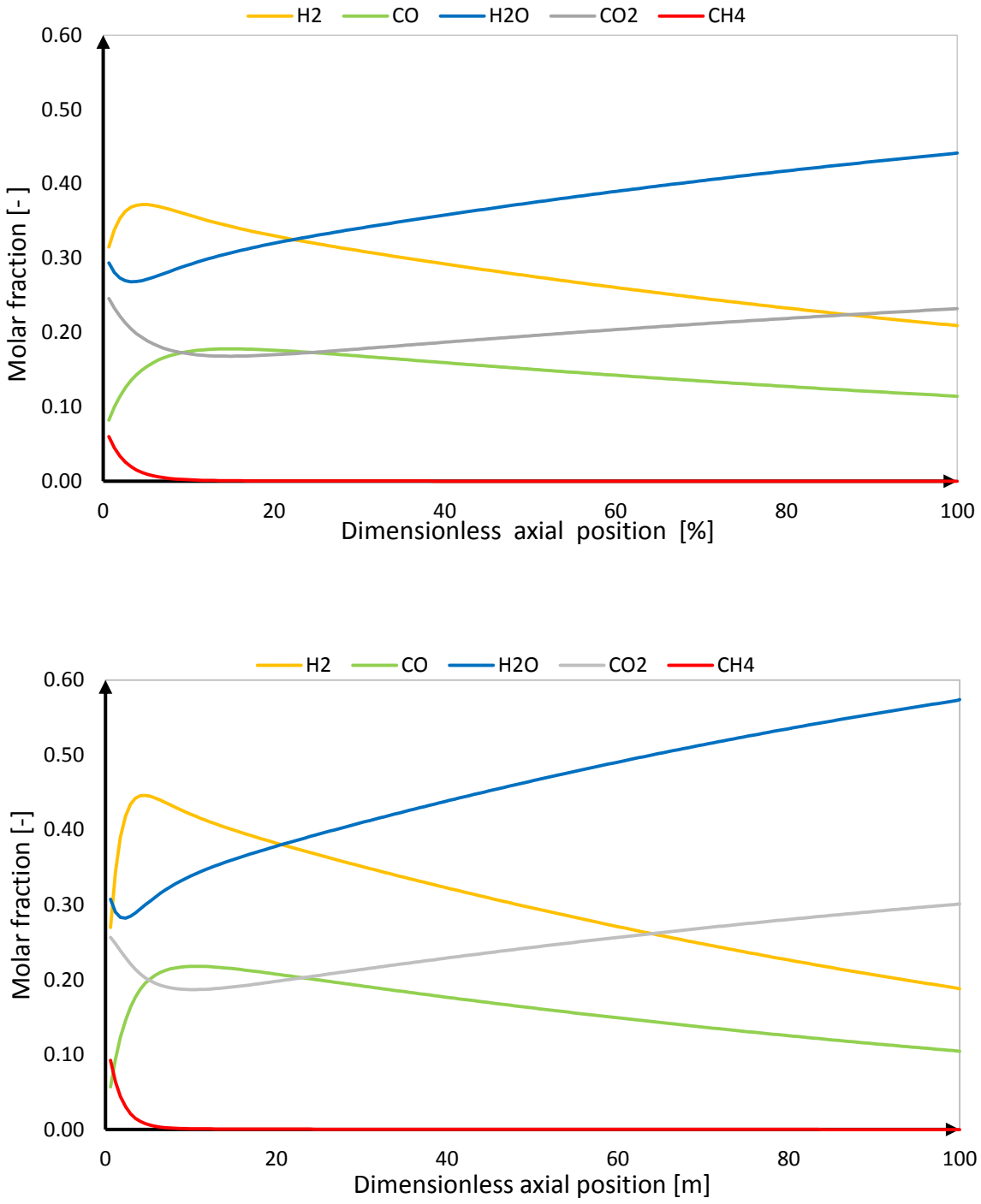

Figure 41: Trend of the molar composition through the anode channel. a) Benchmark case; b) 'H-R' case; c) 'C-R' case.

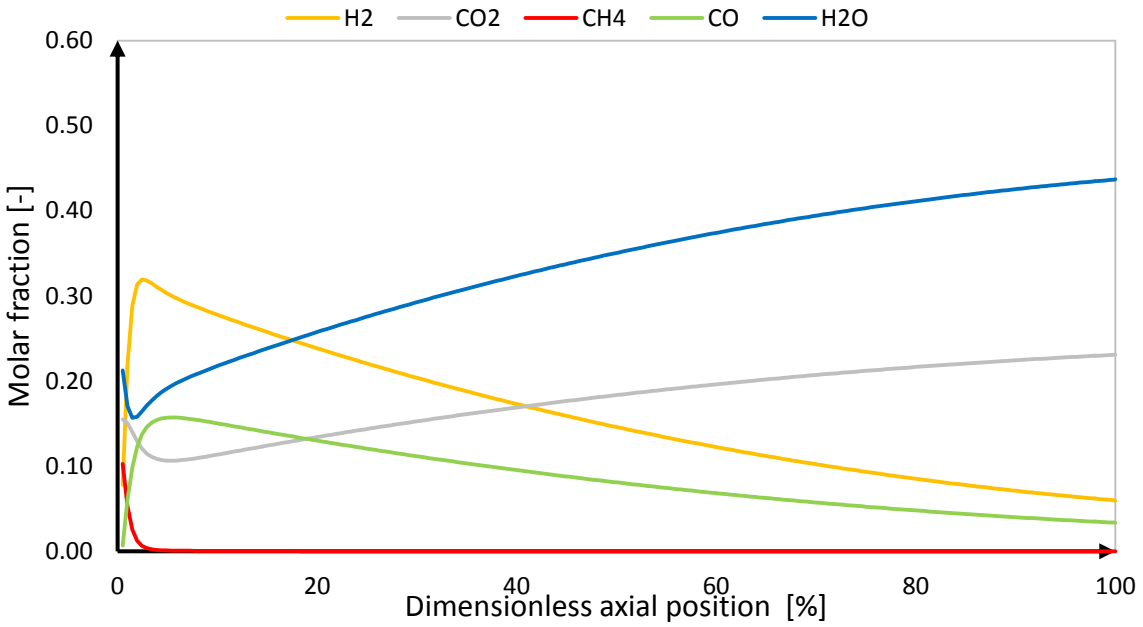

It is possible to make some considerations regarding these results:

- the exchange areas could seem excessive but fuel cell is a modular technology. For the commercial SOFC presented in Chapter 4 (made by CFCL), the component is obtained using 51 different layers in parallel. More layers allow to compact the necessary exchange area. Therefore, to obtain the areas of this work, using the same number of layers of the commercial SOFC, it is necessary an area of approximately 390-530 m^2 for each layer, that is 19.5-23 m for side for a square area case. This size is reasonable for a large-size power plant;
- the modularity is an advantage for the performance because it allows to reach, theoretically, comparable results with plants of different size. But, at the same time, it is a big disadvantage from an economic point of view because it is not possible to take delight of scale effect. Furthermore, nowadays, for SOFC technology, the biggest limit for a large-size application is the feasibility of a cell with so many layers in parallel: the structure could break easily due to thermal and mechanical stress;
- the results of Aspen model and Excel model fit very good, therefore the Excel model can be considered very reliable. There is a more evident difference between the two models regarding the amount of H_2 and CO at the anode outlet. In the Aspen model, less hydrogen reacts, vice versa regarding CO. In the Excel model, the opposite. This difference is not so remarkable and depends on the different method of calculation (correlations for the Excel model and minimization of the Gibbs free energy of the reactants for the Aspen model);
- the C-R case needs higher exchange area and higher current density. The cause is that the reactions are slower because, at the inlet, higher is the amount of products (H_2O and CO_2) with equal operating temperature;
- the H-R case needs bigger exchange area and higher current density than the benchmark case because, for the H-R case, higher is the fuel utilization of the SOFC;

- the methane is consumed very fast because the SR reaction is fast: the kinetic model (Numaguchi and Kikuchi model, Paragraph 2.2.1) confirms its velocity;
- in general, the trend of compositions at anode side is the same, qualitatively, for every case. In particular, the benchmark case and the H-R case are very similar due to the same kind of recycle and equal S/C at the pre-reformer inlet. The little differences of C-R case are due to the different composition at the inlet and the consequent different velocity of the reactions.

Thanks to the Excel model, it is possible to obtain the trend of voltage losses and the trend of the current density through the SOFC.
Figure 42 shows the trend of voltage losses for the benchmark case while Figure 43 the trend of the current density. The trends related to H-R case and C-R case will be the same qualitatively because their trends of compositions and their operating conditions are similar in comparison to the benchmark case.

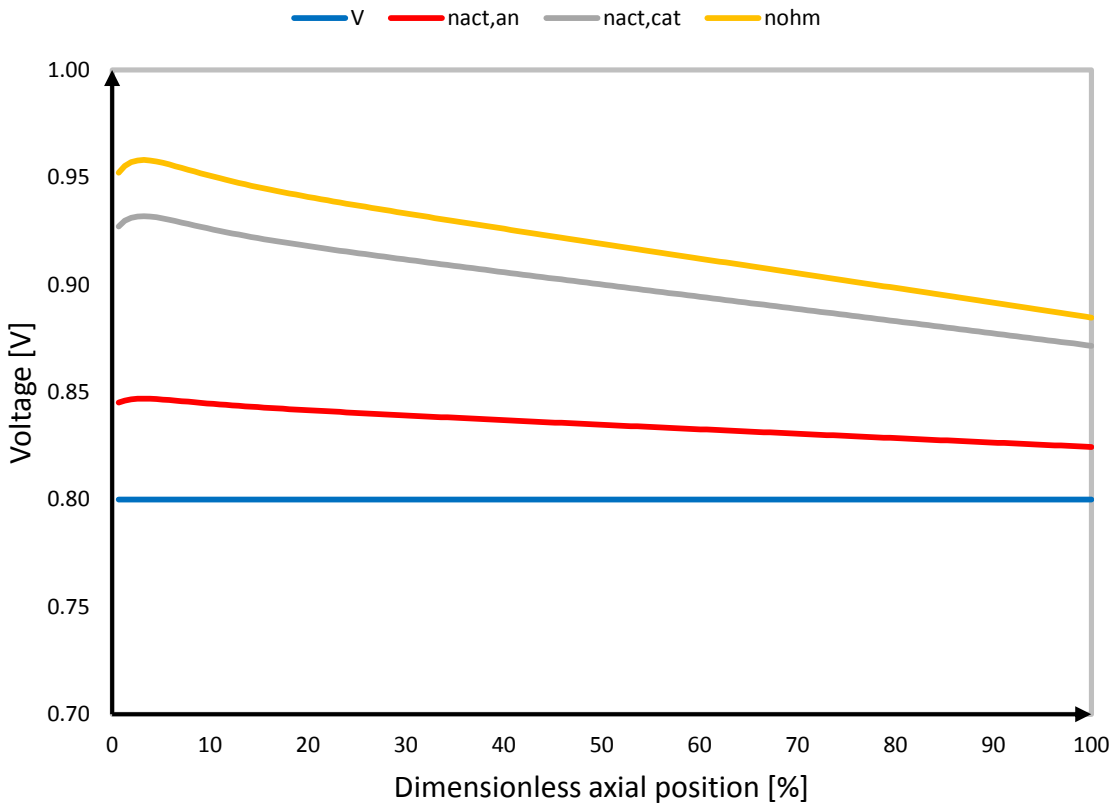

Figure 42: Trend of voltage losses in benchmark case. Blue line: operating cell voltage imposed. Red line: voltage level if added the activation overpotentials of anode side. Grey level: voltage level if added also the overpotentials of cathode side. Yellow line: voltage level if added also the ohmic overpotentials, equal to the maximum cell voltage achievable in a real application (different respect the Nernst voltage).

The most of the losses are related to the activation overpotentials at the cathode side, which are linked to the conversion of O_2 in ions. The level cell voltage is the highest after that SRM occurred. At this point, every single loss reaches its maximum value. Then, towards SOFC outlet, every loss decreases with linear trend because the current density is gradually

lower and lower is the maximum achievable voltage ($V_{OC,cell}$). Table 25 shows a summary of the values of the voltage losses.

Item	No CO_2 capture	With CO_2 capture	
	Benchmark case	**H-R**	**C-R**
Average			
$\eta_{act,an}$	0.03505	0.03398	0.02840
$\eta_{act,cat}$	0.06546	0.06359	0.05346
η_{ohm}	0.01917	0.02667	0.01548
η_{tot}	0.11971	0.12424	0.09734
Max			
$\eta_{act,an}$	0.04698	0.04790	0.05203
$\eta_{act,cat}$	0.08500	0.08642	0.09268
η_{ohm}	0.02612	0.01857	0.02920

Table 25: Main values regading the SOFC voltage losses in the three base cases of Chapter 5.

The activation overpotentials of cathode side are the highest and the loss with more variability in comparison to its maximum value. The total losses of benchmark case and H-R case are similar while the C-R total losses result lower.

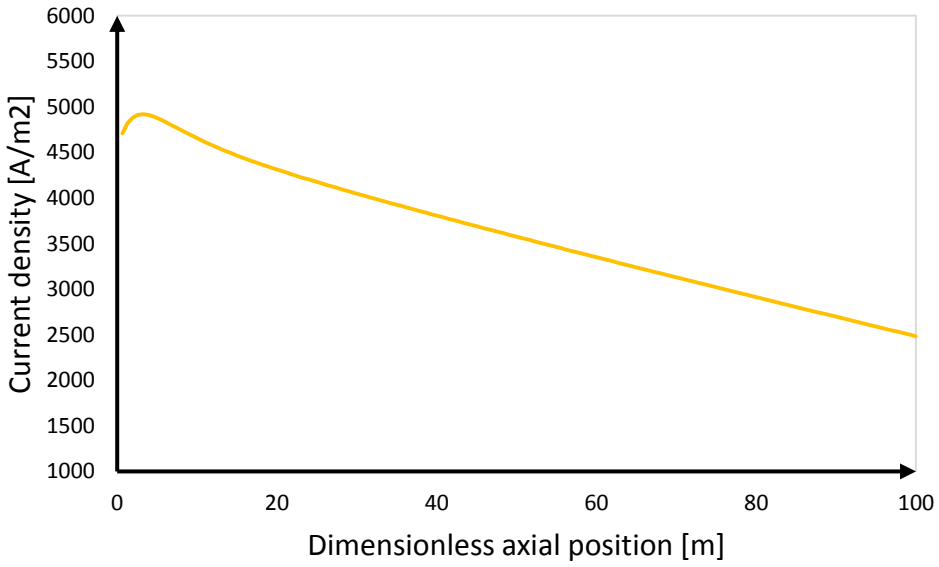

Figure 43: Trend of current density in the benchmark case.

In the beginning, the current density increases and reaches a maximum level. Then, the current density decreases with linear trend because some hydrogen reacts and the available hydrogen for the oxidation becomes lower. The maximum level of current density (reported for each case in Table 23) is achieved after SRM reaction and the trend of current density reflects the trend of the overpotentials. The reason of these maximum values is the highest level of hydrogen achieved after the SRM (confirmed by Figure 41): the more is

the hydrogen, the higher is the $V_{OC,cell}$, the higher are the overpotentials (with constant operating cell voltage) and the higher is the current density.

7.3 Influence of SOFC operating conditions

7.3.1 Effect of cell voltage

If the operating cell voltage changes, there will be changes in the exchange area. The analysis regarding the influence of the operating cell voltage on the SOFC was made only for the cases with CO_2 capture because the influence of SOFC operating conditions on the benchmark case is equal to the 'H-R' case (same kind of recycle). The voltages considered are 0.7 V and 0.75 V. Tables 26 show the results regarding 0.7 V while Tables 27 show the results regarding 0.75 V.

0.7 V	**With CO_2 capture**	
	H-R	**C-R**
A [m^2]	9047	9692
I [MA]	69.946	69.373
$\dot{n}_{O_{2,permeated}}$ [kmol/s] (Aspen)	0.18124	0.18079
$\dot{n}_{O_{2,permeated}}$ [kmol/s] (Excel)	0.18142	0.17995
$i_{average}$ [A/m^2]	7726.2	7145.2
i_{max} [A/m^2]	8743.1	9651.8

Anode	**n [kmol/s]**	**CH_4**	**CO_2**	**H_2O**	**H_2**	**CO**
H-R						
Inlet	1.72946	0.04213	0.23652	0.28607	0.33506	0.09746
Outlet (Aspen)	1.87506	0.00003	0.22596	0.41054	0.24001	0.12062
Outlet (Excel)	1.87272	0.00008	0.22109	0.41584	0.23468	0.12547
C-R						
Inlet	0.55843	0.18434	0.27766	0.38106	0.14068	0.01237
Outlet (Aspen)	0.76431	0	0.28788	0.53180	0.11877	0.05870
Outlet (Excel)	0.76431	0	0.28208	0.53487	0.11570	0.06504

Table 26: Results regarding 0.7 V. a) Influence on the exchange area and the current density; b) the comparison between Aspen and Excel model regarding the molar compositions at the outlet.

0.75 V	**With CO_2 capture**	
	H-R	**C-R**
A [m^2]	13371	14758
I [MA]	73.777	73.594
$\dot{n}_{O_{2,permeated}}$ [kmol/s] (Aspen)	0.19116	0.19069
$\dot{n}_{O_{2,permeated}}$ [kmol/s] (Excel)	0.19098	0.19079

$i_{average}$ [A/m^2]	5516.3	4978.7
i_{max} [A/m^2]	6756.1	7448.6

Anode	n [kmol/s]	CH_4	CO_2	H_2O	H_2	CO
H-R						
Inlet	1.26108	0.06722	0.24934	0.29697	0.30662	0.07662
Outlet (Aspen)	1.43058	0.00002	0.24406	0.44554	0.20502	0.10253
Outlet (Excel)	1.43050	0.00004	0.23935	0.45005	0.20049	0.10722
C-R						
Inlet	0.55843	0.18434	0.27766	0.38106	0.14068	0.01237
Outlet (Aspen)	0.76431	0	0.29653	0.54905	0.10152	0.05006
Outlet (Excel)	0.76431	0	0.29250	0.55334	0.09723	0.05409

Table 27: Results regarding 0.75 V. a) Influence on the exchange area and the current density; b) the comparison between Aspen and Excel model regarding the molar compositions at the outlet.

Figure 44 shows the trend of exchange area in relation to the operating cell voltage.

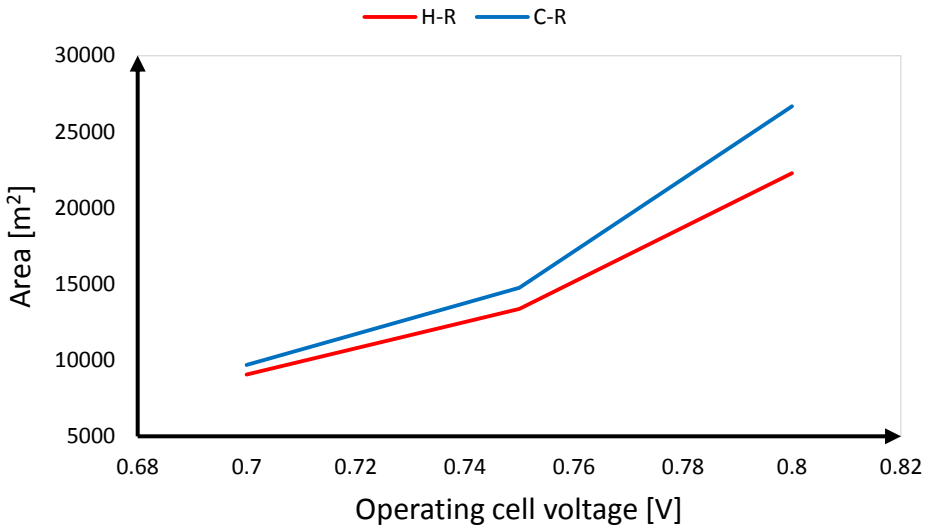

Figure 44: Trend of exchange area in relation to the operating cell voltage.

The results confirm what was expected and the results are reliable because the Aspen model and the Excel model fit very well regarding the outlet compositions. A reduction of cell voltage involves an increase of average current density due to the Ohm's law. In turn, an increase of average current density involves a reduction of the exchange area necessary to reach the total current produced by the SOFC and calculated by the Aspen model. In Figure 44, it is possible to see the strong influence of operating cell voltage on the exchange area. For example, the exchange area decreases of 25-30% passing from 0.8 V to 0.75 V. Another factor that causes a reduction of the exchange area is the total fuel utilization: the lower is the operating cell voltage, the lower is the achievable total fuel utilization and the lower is the total current and, consequently, the exchange area.
In Figure 44, it is possible to observe that the exchange area of C-R case is always higher in comparison to the exchange area of H-R case but the two exchange areas are gradually

closer. The reason could be that the recycle from the anode outlet is influenced by the total fuel utilization and it reduces the positive consequences of a reduction of cell voltage.

	H-R		C-R	
Item	**0.7**	**0.75**	**0.7**	**0.75**
Average				
$\eta_{act,an}$	0.07004	0.05209	0.06526	0.04723
$\eta_{act,cat}$	0.11804	0.09260	0.11123	0.08478
η_{ohm}	0.04103	0.02930	0.03795	0.02644
η_{tot}	0.22911	0.17398	0.21443	0.15845

Table 28: 8 Influence of operating cell voltage on the overpotentials.

In Table 28, it is possible to see that an increase of operating cell voltage involves an increment of the overpotentials. The activation overpotentials of cathode side are always the highestwhile the C-R case has always lower losses. The difference compared to the H-R case increases with the reduction of the operating cell voltage.
From a qualitative point of view, the trend of overpotentials and the trend of current density will be the same in every case compared to the trend shown in Figure 42 and 43.

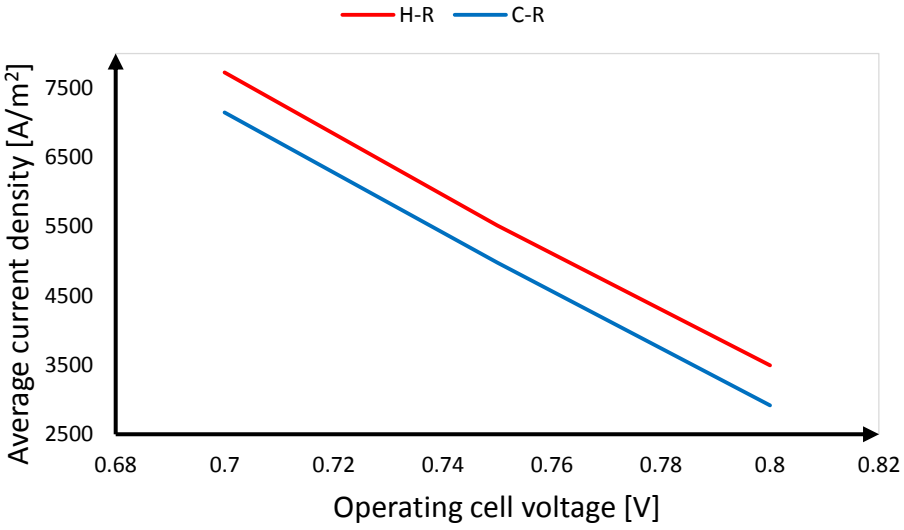

Figure 45: Influence of operating cell voltage on the average current density.

Figure 45 shows the linear influence of the operating cell voltage on the average current density, as expected by the Ohm's law: the higher is the voltage, the lower is the current.

In general, this sensitivity analysis has been demonstrated that a reduction of cell voltage involves a strong reduction of exchange area and, consequently, of the SOFC cost. At the same time, a reduction of cell voltage involves a reduction of the plant performance (Paragraph 6.1.1). A specific economic analysis could give the best operating condition from both points of view, economic and energetic.

A specific discussion has to be made regarding the 0.86 V case. It was demonstrated that it is not possible to make a SOFC with these operating conditions and this configuration

operating at 0.86 V. In fact, with a planar co-flow SOFC and the outlet composition resulted at anode and cathode side outlet, $V_{OC,cell}$ will be approximately 0.849 V for the benchmark case and H-R case and 0.815 V for C-R case. Each $V_{OC,cell}$ is lower than 0.86 V.

In Paragraph 6.1.1, it was demonstrated that an increment of operating cell voltage to 0.86 V involves strong improvement of the plant performance. It will be necessary to change the SOFC configuration to reach this value of operating cell voltage. For example, Campanari et al. [18] have made a study regarding the simulation of a finite volume 3D planar SOFC with different flow configurations. In Figure 46, the results of [18] regarding the current are shown.

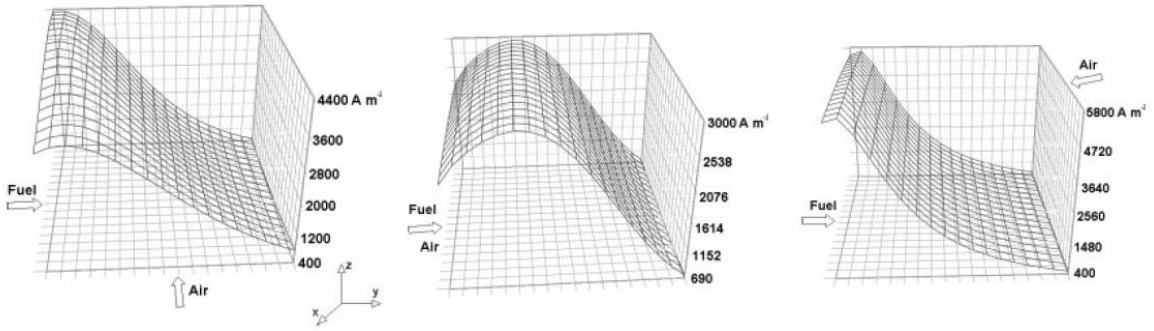

Figure 46: Results of [18] about current density profiles in a finite volume 3D planar SOFC. a) Cross-flow configuration; b) co-flow case; c) counter-flow case.

The three flow configuration analysed in [18] are cross-flow, co-flow and counter-flow. Campanari et al. operate with the following SOFC operating conditions: 0.7 V, atmospheric pressure, outlet temperature of approximately 950 °C, different fuel utilization depending on the configuration (0.8÷0.85) and fuel mass flow of 0.5 mol/h. The operating conditions of this work are different but the results of [18] can still be considered from a qualitative point of view. In Figure 46, it is possible to see how co-flow case presents the lowest current density. A change in the flow configuration could make achievable an operating cell voltage of 0.86 V.

It was not possible to build a SOFC model for the other two flow configurations in order to confirm this supposition. In fact, it would be necessary a specific study regarding the concentrations: the evolution of the compositions through the anode and the cathode side is not simultaneous. In counter-flow configuration, the outlet anode composition is in correspondence of the inlet (not outlet) cathode composition.
An alternative solution to apply 0.86 V with a planar and co-flow SOFC configuration is to reduce the fuel utilization but it involves a reduction of the performance (to be evaluated).

In return, the 3D current density trend shown in Figure 46 is the same trend obtained for the base cases of this work (Figure 43), another proof of the reliability of the Excel model.

7.3.2 Effect of S/C

If the S/C ratio imposed at the inlet of the pre-reformer changes, there will be changes in the exchange area. The analysis regarding the influence of S/C on the SOFC was made

only for the cases with CO_2 capture for the same reason of the cell voltage case. The additional S/C considered are 2.5 and 3.
Tables 29 show the results regarding S/C = 2.5 while Tables 30 show the results regarding S/C = 3.

S/C = 2.5	**With CO_2 capture**	
	H-R	**C-R**
A [m^2]	23711	30895
I [MA]	78.059	78.968
$\dot{n}_{O_{2,permeated}}$ [kmol/s] (Aspen)	0.20226	0.20461
$\dot{n}_{O_{2,permeated}}$ [kmol/s] (Excel)	0.20231	0.20462
$i_{average}$ [A/m^2]	3288.8	2553.5
i_{max} [A/m^2]	4490.1	4888.7

Anode	**n [kmol/s]**	**CH_4**	**CO_2**	**H_2O**	**H_2**	**CO**
H-R						
Inlet	1.35871	0.05697	0.26516	0.32839	0.28236	0.06392
Outlet (Aspen)	1.51351	0.00001	0.26416	0.48482	0.16575	0.08243
Outlet (Excel)	1.51344	0.00002	0.26057	0.48851	0.16206	0.08560
C-R						
Inlet	0.66300	0.15021	0.28872	0.40807	0.13752	0.01178
Outlet (Aspen)	0.86200	0	0.31297	0.58209	0.06849	0.03362
Outlet (Excel)	0.86217	0	0.31104	0.58393	0.06664	0.03554

Table 29: Results regarding S/C=2.5. a) Influence on the exchange area and the current density; b) the comparison between Aspen and Excel model regarding the molar compositions at the outlet.

S/C = 3	**With CO_2 capture**	
	H-R	**C-R**
A [m^2]	24788	36242
I [MA]	78.013	80.023
$\dot{n}_{O_{2,permeated}}$ [kmol/s] (Aspen)	0.20214	0.20735
$\dot{n}_{O_{2,permeated}}$ [kmol/s] (Excel)	0.20228	0.20740
$i_{average}$ [A/m^2]	3133.6	2206.8
i_{max} [A/m^2]	4129.1	4463.8

Anode	**n [kmol/s]**	**CH_4**	**CO_2**	**H_2O**	**H_2**	**CO**
H-R						
Inlet	1.86782	0.03160	0.26749	0.34330	0.28519	0.06939
Outlet (Aspen)	1.98584	0.00001	0.26393	0.48442	0.16615	0.08264
Outlet (Excel)	1.98581	0.00002	0.26038	0.48814	0.16243	0.08619
C-R						
Inlet	0.76712	0.12550	0.29670	0.42807	0.13479	0.01138

Outlet (Aspen)	0.95968	0	0.31829	0.59285	0.05772	0.02829
Outlet (Excel)	0.95967	0	0.31689	0.59438	0.05619	0.02970

Table 30: Results regarding S/C=3.0. a) Influence on the exchange area and the current density; b) the comparison between Aspen and Excel model regarding the molar compositions at the outlet.

Figure 47 shows the trend of SOFC exchange area in relation to the imposed S/C.

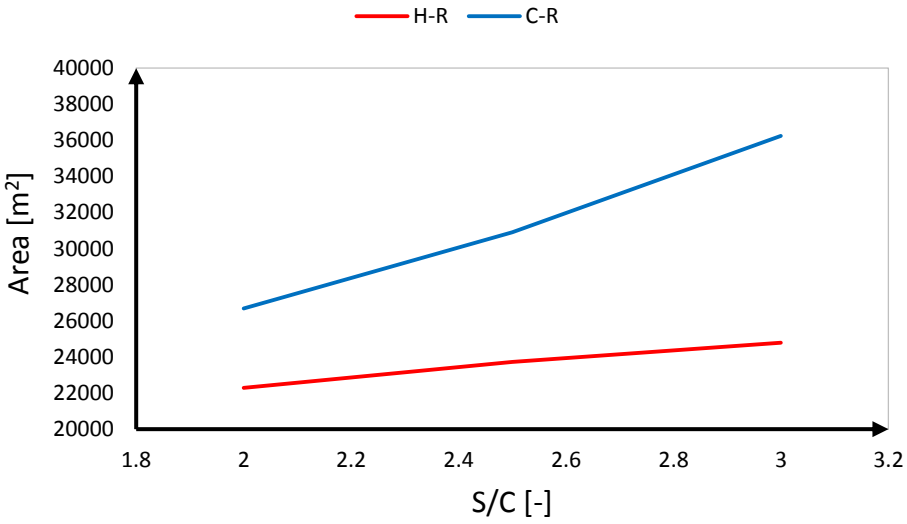

Figure 47: Trend of SOFC exchange area in relation to the S/C imposed.

The higher is the imposed S/C, the higher is the amount of products at the SOFC inlet and the more slowly are the reactions through the SOFC and, consequently, the necessary exchange area. This is the main result, a result reliable because the models fit very well (Tables 29b and 30b).
The influence of S/C on the area is stronger for C-R case (Figure 47), weak for H-R case.
In Paragraph 6.1.2, for H-R case, it was verified that there is no influence of S/C on the performance of the SOFC but only on its operating conditions (higher inlet temperature, higher fuel utilization of single passage and higher split factor). This could be the reason of the weak influence of the S/C in H-R case.
On the other hand, for the C-R case, the influence of S/C is strong because it involves an higher amount of products (H_2O and CO_2) at the anode inlet. More products at anode inlet involve in reactions more slowly and, consequently, in bigger exchange area with a big increase of the SOFC cost. In Paragraph 6.1.2, it was demonstrated that a higher S/C involves little improvement of the plant performance for C-R case. Probably, the choice to increase the S/C is not justified from an economic point of view. A specific economic analysis would be useful to find the best solution from both points of view, economic and energetic.

	H-R		C-R	
Item	**2.5**	**3.0**	**2.5**	**3.0**
Average				
$\eta_{act,an}$	0.03207	0.03063	0.02497	0.02404
$\eta_{act,cat}$	0.06042	0.05798	0.04740	0.04584
η_{ohm}	0.01747	0.01664	0.01356	0.01303

η_{tot}	0.10996	0.10525	0.08593	0.08291

Table 31: Influence of S/C on the overpotentials.

Table 31 shows the influence of S/C on the overpotentials. The higher is S/C, the lower are the overpotentials. The overpotentials are always lower for C-R case in comparison to the H-R case and the activation overpotentials for the cathode side are always the highest kind of overpotentials. The changes are similar for every loss and case.
The only difference is regarding the activation overpotentials of the anode side: the change in C-R case is significantly higher in comparison to the H-R case. It could be related to the different kind of recycle. In particular, in H-R case, an increase of S/C involves an increment of SOFC fuel inlet temperature and a reduction of the 'single passage' fuel utilization (Paragraph 6.1.2).

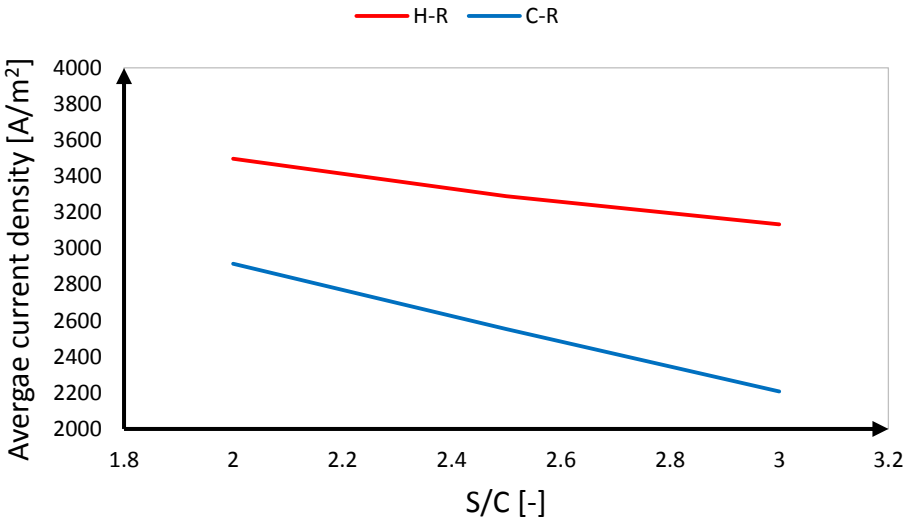

Figure 48: Influence of S/C on average current density.

Figure 7.12 shows that an increment of S/C involves an increase of the average current density, stronger for C-R case. This result was expected after the results shown in Figure 47 regarding the relation between the exchange area and S/C.

Chapter 8

Models for small-size power generation

After having analysed the large-size power generation case in the previous chapters, it will be presented a different proposal of integration of IT-SOFC and CLC finalized to small-size power generation. Large-size solutions are more interesting for the future application since more useful to solve the problem of electricity requirement and the energy production in an efficient way. But a small-size solution could be interesting because this size is closer to the current state-of-art of the considered technologies (SOFC and CLC); at the moment, technologies not ready and quite far for large-size application.
In the large-size case, it was demonstrated the importance of thermal integration and waste energy recovery. Steam Rankine Cycle is a power generation technology not performing in small-size application: in a steam turbine, the increase of water density during the expansion involves problems due to the increment of volumetric flow rate. For a small-size application, it is necessary to find a more fitting technology.

8.1 Organic Rankine Cycle (ORC)

Organic Rankine Cycle (ORC) is a revisiting of the traditional Stem Rankine Cycle. ORC uses organic and heavy fluid in order to use energetic sources at lower temperature (e.g. waste heat or renewable sources) in economic and efficient way. The types of usable fluid are many and their fundamental properties are two: molecular complexity and molecular mass.

The first property indicates the geometrical complexity of the molecule. It increases with the number of atoms and their non-linear distribution. It is possible to quantify the molecular complexity in different ways. The two most important methods are the specific heat at constant pressure (c_p) and the gradient of the saturation vapour curve in Andrew's diagram (σ). Equations 8.1 express their definitions.

$$c_p = \left(\frac{\partial h}{\partial T}\right)_p \qquad \sigma = \frac{T_c}{R}\left(\frac{dT}{ds}\right)_{T_{eva,ref}} \tag{8.1}$$

It is possible to identify three main intervals depending on σ value:

- σ < - 4 for simple molecule (wet fluids);
- σ > 4 for complex molecule (dry molecule);
- - 4 < σ < 4 for isentropic fluids.

Different σ involves different saturation curve (Figure 49).

This first simple property shows a very important particularity of the complex molecules: the retrograde saturation curve. It allows a dry expansion, without formation of liquid drops. In this way, all the problems of erosion and regarding fluid dynamic are reduced.

These problems are very strong in traditional low pressure steam turbine where vapor quality at the end of expansion can be also 85%.

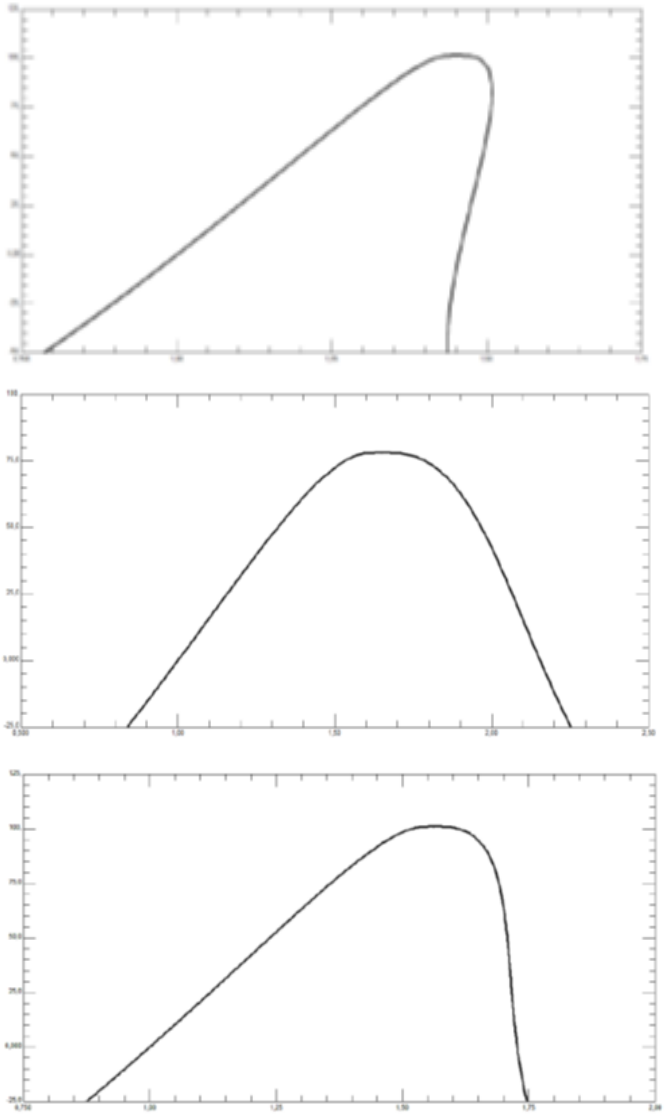

Figure 49: Different saturation curve depending on the molecular complexity. a) Wet fluids; b) dry fluids; c) isentropic fluids.

Another influence of molecular complexity is regarding the critical temperature ($\boldsymbol{T_c}$). The relation between these two properties is quite complex but, in general, an increase of $\boldsymbol{T_c}$ involves an easier design of supercritical cycle where the heat exchange between hot source and cycle occurs with variable temperature and, consequently, in a way less dissipative [57]. On the other hand, higher complexity involves strongly lower critic expansion ratio ($\boldsymbol{\beta_c}$). It involves an accurate design of the turbine because transonic conditions are often generated. Equation 8.2 defines the critic expansion ratio$\boldsymbol{\beta_c}$.

$$\beta_c = \left(\frac{2}{\gamma+1}\right)^{\frac{\gamma}{\gamma-1}} \tag{8.2}$$

The second property presented before, the molecular mass, has an influence on celerity and specific enthalpies.
Celerity (a) decreases with higher molecular mass (M_m). Consequently**,** there will be more probably transonic condition in the turbine, in particular if the temperature is low as in the heat recovery systems.
An higher molecular mass involves a limited enthalpy change during the expansion: it allows to have less charged stages and a lower number of stages in the turbo machinery, with a technological and economic advantage. Also the heat of evaporation is lower with a consequent reduction of the total heat necessary to evaporate the fluid. Equations 8.3 show all the relations useful to understand the considerations done.

$$a = \sqrt{\gamma \frac{R}{M_m} T} \qquad \Delta h_{is} = \frac{1}{M_m} \frac{R}{\vartheta} \left(\beta^{\vartheta} - 1\right)$$

$$\Delta h_{eva} = A\ R\ T_c \frac{1}{M_m} \tag{8.3}$$

8.2 The models

In Table 32, all the assumptions of the models for small-size power generation are shown.

Ambient conditions	
Temperature [°C]	15.0
Pressure [bar]	1.013
Relative Humidity [%]	60.0
Natural Gas	
Molar composition [%vol]	CH_4: 89.0, CO_2: 2.0, C_2H_6: 7.0, C_3H_8: 1.0, N_2: 0.89, C_4H_{10}: 0.11
LHV [MJ/kg]	46.482
Feed network pressure [bar]	20.0
SOFC	
Minimum air inlet temperature [°C]	735.0
Minimum fuel inlet temperature [°C]	600.0
Anode and cathode outlet temperature [°C]	800.0
Cell voltage [V]	0.80
Minimum O_2 molar fraction at SOFC outlet [%v/v]	5.0
Air and fuel channels pressure losses [%]	3.0
Pressure drop of air filter [bar]	0.01
Heat loss [% of fuel LHV]	5.0
DC/AC electrical efficiency [%]	97.0
ORC	
Evaporation pressure [bar]	30.0
Maximum steam temperature [°C]	300.0
Pressure drop in economiser [%]	20.0
Gas pressure drop in recovery boiler [bar]	0.05
Minimum condensing pressure [bar]	0.219
Maximum inlet temperature at condenser [°C]	80.0
Minimum outlet temperature at condenser [°C]	65.0
Turbine isentropic efficiency [%]	65.0
Pump hydraulic efficiency [%]	85.0
Turbine mechanical efficiency [%]	99.60
Generator electric efficiency [%]	98.50

Pre-reformer	
Pre-reformer inlet S/C ratio* [-]	2.0
Low Temperature Sulphur removal	
Operating temperature [°C]	15.0
Fuel pressure loss Δp/pin [%]	3.0
Heat Exchangers	
Hot and cold side $\Delta p/p_{in}$ [%]	2.0
LT and HT air regenerators $\Delta p/p_{in}$ [%]	3.0
Heat losses [% of heat transferred]	0.7
Minimum gas - evaporating water ΔT (pinch-point)[°C]	10.0
Minimum ΔT in gas - water heat exchangers [°C]	15.0
Minimum ΔT in gas - gas heat exchangers [°C]	30.0
Minimum ΔT in liquid – evaporating/condensing liquid exchangers [°C]	2.0
CLC	
Minimum air inlet temperature at AR [°C]	400.0
SOFC exhaust gas inlet temperature [°C]	800.0
Minimum outlet temperature from AR [°C]	735.0
Maximum fuel reactor outlet temperature [°C]	800.0
Maximum GS factor [kg/s/m^2]	20.0
Gas pressure drop in FR and AR [bar]	0.15
Minimum exhaust temperature at stack [°C]	80.0
Minimum exhaust pressure at stack [bar]	1.013
Air fan isentropic efficiency [%]	94.0
Air fan mechanical-electrical efficiency [%]	80.0
Auxiliaries for heat rejection [% of heat rejected]	0.8
CO_2 compression and storage	
Minimum CO_2 pressure to storage [bar]	110.0
Maximum pressure ratio/intercooled compressor stage [-]	2.0
CO_2 pressure at compressor outlet [bar]	80.0
Intercooled compressor stage isentropic efficiency [%]	82.0
Intercooled compressor stage mechanical efficiency [%]	94.0
Temperature at outlet of each cooling stage [°C]	30.0
Pressure drop in each cooling stage [% of p at inlet]	2.0
Pump isentropic efficiency [%]	75.0
Pump mechanical efficiency [%]	95.0
Minimum CO_2 dry purity [%v/v]	95.0

Table 32: Main assumptions for the models finalized to small-size power-production.

Some considerations regarding the assumptions are necessary:

- the most of the assumptions have as reference the ones of the models for large-size power generation;
- the SOFC assumptions are the same of large-size cases if not the heat loss, higher in the small-size cases, increased from 2% to 5%;
- the CLC operating conditions and their limits are the same of the large-size cases. In particular, copper is used as OC with a mixture of 40 wt% of CuO and 60 wt% of ZrO_2;
- the ORC operating condition are the ones of the ORC produced by Triogen [59]. Triogen is one of the most important ORC manufacturers. Figure 50 shows the plant layout of the technology used by Triogen.

The working fluid of ORC is Toluene. The maximum pressure achieved is 30 bar while the pressure of low pressure part is approximately 4 bar. The organic fluid reaches the

maximum temperature of 300 °C, approximately the saturation temperature at 30 bar: in an ORC, it is not necessary to superheat the fluid to have a more efficient cycle because the most efficient working condition is the saturated cycle. It is a consequent of the different saturation curve of an organic fluid. In the ORC proposed by Triogen, a recuperator is added in order to pre-heat the fluid before the evaporator and have a more efficient cycle. This component is common in ORC application. The condenser allows to produce warm water between 55 °C and 80 °C. For this reason, the minimum temperature of Toluene in the cycle has to be not lower than 65 °C, in order to respect the limit about the minimum difference of temperature in the specific kind of heat transfer (liquid-liquid 10 °C). The turbine outlet pressure is calculated by the Aspen model in order to respect the temperature limit in the condenser.

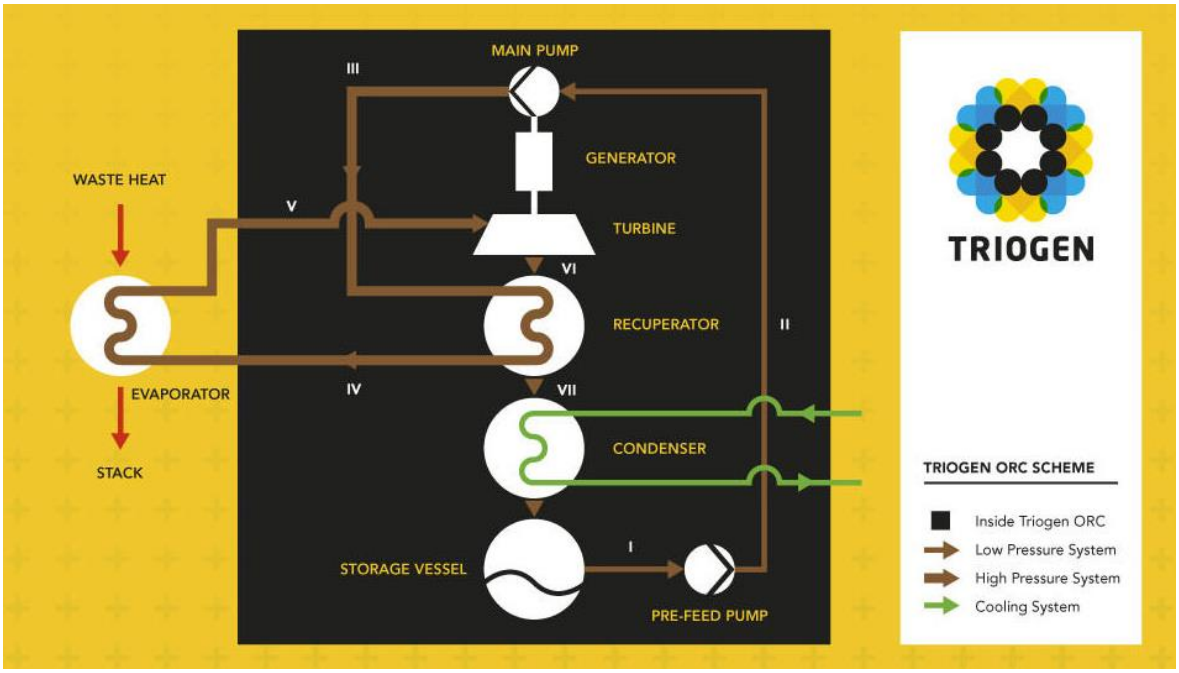

Figure 50: Plant layout of the ORC produced by Triogen [59].

The solution proposed by Triogen does not need an heat carrier (e.g. thermal oil or hot water) and the heat transfer is direct between the exhaust gas and the working fluid: it is a double advantage because involves less components with economic saving and higher efficiency, as well as a simpler plant layout and more safe management of the plant. Triogen ORC is appropriate for cogeneration and does not need an evaporative cooling tower. It is adapt for heat sources of higher temperature than 350 °C (perfect in the case of this wok) and, in general, produces 60 kW – 165 kW with total energy efficiency not higher than 20%. Furthermore, it is easy to install and transport.
For the values of isentropic efficiency of the turbo machinery, the reference is [60].

The models proposed in this work are three, depending on the sizing done by setting the feed of natural gas.

- Two plants are dimensioned on the CO_2 production. As seen in Chapter 1, CO_2 can be considered a useful product from an economic point of view. The main reference is the company Union Engineering, one of the world leaders in CO_2 technology for

purification and liquefaction of high quality CO_2 [61]. In particular, the reference is the Union Engineering plant called EBU, finalized to import CO_2 from boilers fired with various fossil fuels. The minimum standard size for this plant is 145 kg/h, measured as liquid food-grade CO_2 produced. This amount corresponds to a natural gas input of approximately 0.015 kg/s. One plant will be without ORC and the other one with ORC, in order to evaluate the ORC influence on performance and its convenience;

- The third plant is dimensioned, approximately, on the smallest standard ORC available by Triogen (60 kW).

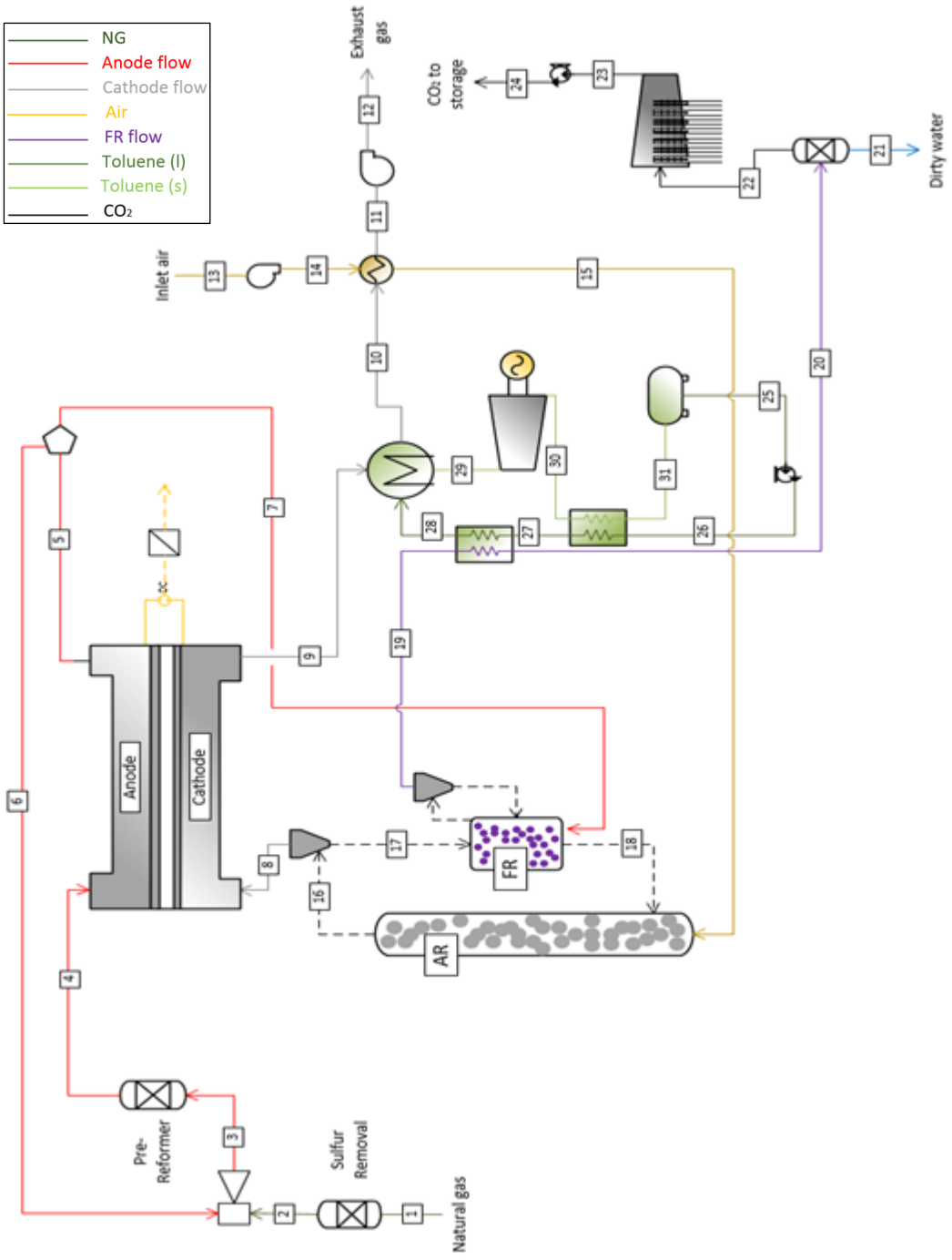

Figure 51: Layout of the system SOFC + CLC + ORC for small-size application.

Figure 51 shows the complete scheme of the model proposed for small-size power production and CO_2 generation with integration of SOFC, CLC and ORC. For the configuration without ORC, the bottoming cycle is replaced by two heat exchangers in order to cool the exhaust gas #9 and #19. In this way, some heat will be available for cogeneration.

8.3 Performance comparison

Tables 33 show the main results regarding the three models for small-size power generation and the relative energy balances. Tables 34 show the results of the relative SOFC Excel models.
In Appendix H, it is possible to find all the streams properties of the plant with ORC dimensioned on the CO_2 production.

Item	No ORC	Yes ORC	
		CO_2	ORC
$P_{el,\,net}$ [kW]	435.879	472.709	657.233
$P_{el,\,net,\,no\ CO_2}$ [MW]	448.950	485.840	634.722
η [%]	59.276	66.405	66.432
$\eta_{no\ CO_2}$[%]	61.112	68.249	68.276
U_{fuel} [%] (single pass)	66.920	66.920	66.795
Gs $\left[\frac{kg}{s\,m^2}\right]$	10.352	10.352	10.321
A $[m^2]$	0.280	0.280	0.368

Item	No ORC	Yes ORC	
		CO_2	ORC
Fuel Inlet [kW]	711.860	711.860	929.640
SOFC net power [kW]	449.966	449.966	617.575
ORC net power [kW]	-	50.293	66.051
Q [kW]	275.829	221.674	290.418
CO_2 compressor [kW]	-12.812	-12.812	-16.810
FD fan [kW]	-12.727	-12.727	-16.607
ORC pumps [kW]	-	-2.726	-3.580
CO_2 pump [kW]	-12.811	-12.811	-0.337
Condensation heat [kW]	159.038	89.732	117.136
Exhaust heat [kW]	116.791	-	-
ORC heat [kW]	-	131.942	173.282

Table 33: Main performance parameters for the three small-size models and relative energy balances. 'CO_2' is relative to the plant dimensioned on the CO_2 production while 'ORC' to the plant dimensioned on the ORC power output.

A [m^2]	179.9
I [MA]	579.854
$\dot{n}_{O_{2,permeated}}$ [kmol/s] (Aspen)	1.50244
$\dot{n}_{O_{2,permeated}}$ [kmol/s] (Excel)	1.50379
$i_{average}$ [A/m^2]	3222.3
i_{max} [A/m^2]	5124.4

	$\eta_{act,an}$	$\eta_{act,cat}$	η_{ohm}	η_{tot}
Average	0.03138	0.05896	0.01711	0.10745
Max	0.04879	0.08779	0.02721	0.16379

Table 34: Results regarding the SOFC Excel model for the small-size power plants (plant dimensioned on the CO_2 production).

It is possible to make some considerations about the results:

- the improvement of the plant performance due to the ORC is relevant. At the same time, the waste heat available is not so reduced;
- the ORC small-size plant dimensioned on the CO_2 output produces less electricity than the smallest ORC of Triogen [59];
- the total energy efficiency of the small-size plants is not so lower in comparison to the total energy efficiency of the large-size plants (see Table 2), approximately 0.5 points. This result confirms the advantage of a modular technology like SOFC: it is possible to achieve almost the same performance with different plant size. The little difference is more attributable to the energy recovery and not to the SOFC itself;
- the SOFC analysis was made only for the case dimensioned on CO_2 production because the difference in comparison to the case dimensioned on ORC is not so meaningful and because this analysis was made only in order to compare the small-size SOFC with the large-size case;
- another confirmation of the SOFC modularity is result regarding the exchange area. If the SOFC exchange area of the small-size case was calculated using a linear proportion in relation to the power output starting from the results of the H-R large-size case (Table 23), the exchange area would be approximately 166 m^2. The difference in comparison to the exchange area calculated by the Excel model is about 7%, not so much considering the high difference of order of magnitude;
- to obtain the SOFC exchange area calculated for the small-size system (179.9 m^2), using the same number of layers of the commercial SOFC (51), it is necessary an area of approximately 3.53 m^2 for each layer, that is 1.88 m for side for a square area case. This size is reasonable for a small-size power plant
- the values for the overpotentials are similar to the ones of the large-size case (Table 25).

Chapter 9

Conclusion & Recommendations

Reduction of greenhouse gas emissions is one of the most important challenges that the power industry will face in the next decades [3]. Solid Oxide Fuel Cells (SOFCs) are electrochemical devices able to convert a fuel into electricity, promoting a direct oxy-combustion in which the anode exhaust is a CO_2-rich stream that can be separated and sent to the final storage. SOFCs act as an air separation device in which O_2 migrates from cathode to anode generating electricity and therefore several configurations have been proposed for CO_2 capture [3]. However, the SOFC voltage drops to zero if the fuel is completely consumed at the anode therefore some unburnt species are always present in the anode off-gas. In the recent years, integration of CO_2 capture technologies has been presented using natural gas and coal as primary feedstock [62-65]. The majority of these studies consider hybrid cycles, where high temperature fuel cells are integrated with a simple or modified Brayton cycle, in some cases adding a bottoming cycle (e.g. based on steam or ORC). Natural gas integrated SOFC plants have demonstrated to reach already more than 60% electric efficiency, even at few kW scale [44]. Moreover, when applied to electric power generation, SOFC hybrid cycles (hundreds MW plants) can reach an impressive electrical efficiency (up to 75-78%) approaching the theoretical efficiency.

Recently Campanari et al. [41] have presented a revised study on natural gas hybrid cycles using advanced SOFC operated at 800°C with fuel utilization of 85% and cell voltage of 0.86 V reflecting the best available technology of different manufacturers [42]. In this case, the anode off-gas and the O_2 depleted air from the cathode outlet are burnt in a combustor to provide the heat duty to air – preheating up to the cathode inlet temperature (>730°C). In [41], in order to implement the CO_2 capture technology, it is proposed a system in which the anode off-gas is first sent to a HT-WGS to consume CO (more than 80%) increasing the CO_2 gas fraction and the resulting syngas is then sent to a CO_2 cryogenic unit to recover the H_2 in the gas stream (35% content vol. dry basis) and separate the CO_2 at high purity (98.8%).

In order to find out more efficient SOFC hybrid cycle with CO_2 capture technology, this work has proposed the integration of Chemical Looping Combustion (CLC) at atmospheric pressure for both large and small scale applications. Large scale application plant is designed according to the work from Campanari et al. [41], where the fuel power input has been fixed to 100 MWth (based on natural gas LHV) and atmospheric SOFC is operated at 800°C with NG. On the other hand, a cell voltage of 0.8 V has been considered. The interconnected fluidized bed reactors for the CLC work at mild conditions (500-800°C) and 1 bar. The CLC process is assumed to be operated at the chemical equilibrium and the oxygen carrier considered is a Cu-based material (CuO) with Zirconia (ZrO_2) as support material (60% wt. basis). Cu_2O/Cu are considered during the reduction. For the simulation of the interconnected fluidized beds, the maximum solid circulation of 20 $kg/s/m^2$ is considered. Two configurations have been proposed depending on the kind of recycle: the 'Hot-Recycle' (H-R) configuration, if the recycle is from the anode outlet; the 'Cold-

Recycle' (C-R) configuration, if the recycle is from the Fuel Reactor (FR) CLC outlet. The recycle is necessary to provide the steam for the WGS and SMR reactions.

In all the solutions proposed by Campanari et al. [41] as those proposed in this work, all the hot gases exiting the modules are sent to a heat recovery system to producing intermediate pressure steam (T = 400°C, p = 40 bar) for additional power generation. The bottoming cycle turns out to be a medium-scale steam cycle similar to waste-to-energy Rankine cycles.

Plant Performance			Cell Voltage 0.8 V			Cell voltage 0.86 V			
		Hybrid SOFC	SOFC	SOFC	Hybrid SOFC[41]	Hybrid SOFC[41]	SOFC	SOFC
CO_2 capture			CLC cold-rec	CLC hot-rec	-	WGS+ cryogenic	CLC cold-rec	CLC hot-rec
Natural Gas, inlet	MW_{th}	100	100	100	100	100	100	100
SOFC, AC power	MW_E	56.40	60.50	60.53	68.06	68.06	69.8	70.0
cell voltage	V	0.8	0.8	0.8	0.86	0.86	0.86	0.86
Fuel Utilization, U_f		75.7%	81.3%	81.3%	85.0%	85.0%	87.3%	87.5%
Air Utilization, O_{ox}		69.7%	38.0%	39.5%	21.8%	20%	58.7%	62.3%
Steam Turbine	MW_E	12.42	10.84	10.69	8.06	7.68	7.90	7.70
aux FD Fan	MW_E	-0.10	-2.29	-2.22			-1.59	-1.51
aux water pumps	MW_E	-0.09	-0.08	-0.08	-0.91	-4.24	-0.06	-0.06
aux CO_2 compressors	MW_E		-1.85	-1.85			-1.85	-1.85
aux CO_2/H_2O rec blower	MW_E		-0.18	-			-0.18	
Gross electric power	MW_E	68.82	71.34	71.22	76.12	75.74	77.7	77.7
Net electric power	MW_E	68.20	66.76	66.91	75.2	71.49	73.90	74.1
net el. efficiency, LHV	%	68.2%	66.7%	66.8%	75.2%	71.5%	73.9%	74.1%
CO_2 specific emissions, E_{CO2}	kg MWh^{-1}	301.92	0	0	273.59	48.86	0.00	0.00
CCR	%	-	100%	100%	-	82%	100%	100%
SPECCA	MJ kg_{CO2}^{-1}	-	0.38	0.34	-	1.11	0.31	0.30

The integrated SOFC+CLC proposed in this work reach a net electrical efficiency of 66.7% with SPECCA of 0.34-0.38 $MJ_{LHV}/kgCO_2$. Compared to the conventional hybrid cycle without CO_2 capture, the efficiency penalty is exclusively associated to the CO_2 compression up to 110 bar for the final storage. When comparing hybrid SOFC integrated with CO_2 capture technology (CLC vs WGS/cryogenic separation), the net electric efficiency increases up to 2 percentage points. Moreover, the carbon capture rate (CCR) is 100% in case of CLC while only 82% can be achieved in case of cryogenic separation due to the presence of some CO and CO_2 in the cryogenic off-gas. In terms of specific primary energy consumption for CO_2 avoided (SPECCA), the combination of SOFC and CLC is more advantageous (0.3 vs 1.11 $MJ/kgCO_2$). Very similar performances are obtained by varying the SOFC humidification system (cold and hot recycle) and the little efficiency penalty of C-R configuration is due to the recycle blower consumption. However, due to the off-gas recirculation, the anode-SOFC inlet flow rate increases from 12.72 kg/s to 20.61 kg/s. The choice between the two types of recycle depends on the criticality of the ejector design at high temperature and the availability of pressurized natural gas.

In case of higher cell voltage (0.86 V) is considered, the efficiency rises of 6 percentage points showing also a reduction in SPECCA compared with hybrid cycle with cryogenic CO_2 separation (0.3 vs 1.1 MJLHV/kgCO2) due to the combination of high CCR (+18%) and higher electric efficiency (+2.5%).

A sensitivity analysis has been carried out for the principal operating conditions of SOFC and CLC in order to analyse their influence on the performance of the system and find out the best possible operating conditions.

The cell voltage plays an important role in the overall performance of the plant due to the high power share associated to the SOFC. In fact, increasing the cell voltage, more electricity is produced from the SOFC and higher is the total energy efficiency (e.g. from 0.8 V to 0.86 V, +7.2 percentage points). At increased cell voltage, higher fuel utilization is required to keep the SOFC at 800°C. Increasing the cell voltage, less heat is available at the electrode and therefore higher fuel conversion is required. Furthermore, the higher is the cell voltage, the less is the weight of the steam cycle on the power output.

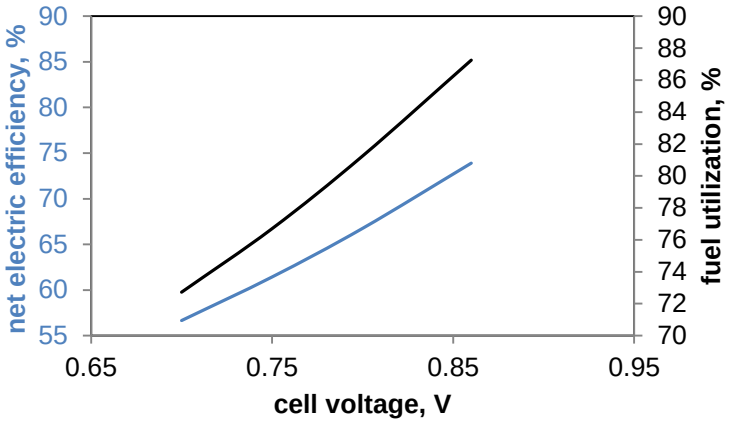

The increase of the S/C does not penalize the performance of the thermodynamic cycle since the natural gas humidification is not carried out using steam from the steam cycle but either the off-gas (hot recycle) or the FR exhausts (cold recycle) recirculation.
In case of C-R configuration, an increase of S/C from 2 to 3 corresponds to an increase in the overall net electric efficiency from 66.76% to 68.07%. Due to the higher amount of gasses at the anode side, the U_f slightly increases (from 81% to 83.4%) in order to maintain the fuel cell at 800 °C increasing the SOFC power production as well as the CO_2-H_2O blower consumption (+20%).
In case of H-R, since everything occurs within the SOFC module, the system performance does not change. However, due to the higher amount of H_2O required at the anode inlet, the fuel flow rate increases (up to 39.5 kg/s at S/C equal to 3) as well as the SOFC inlet temperature (from S/C = 2 to S/C = 3, from 668.5 °C to 727.7 °C).

The solid circulation between the AR and FR is used to control the temperature of the air at the cathode inlet. The higher is the solid circulation rate (Gs), the closer are the temperature of the gases leaving the AR and FR In case of Cu-based OC, the reduction is a fairly strong exothermic reaction and the temperature at the fuel reactor is always higher than in the air reactor. Therefore, high solid circulation is always required in order to reach the temperature higher than 730°C at the AR outlet.

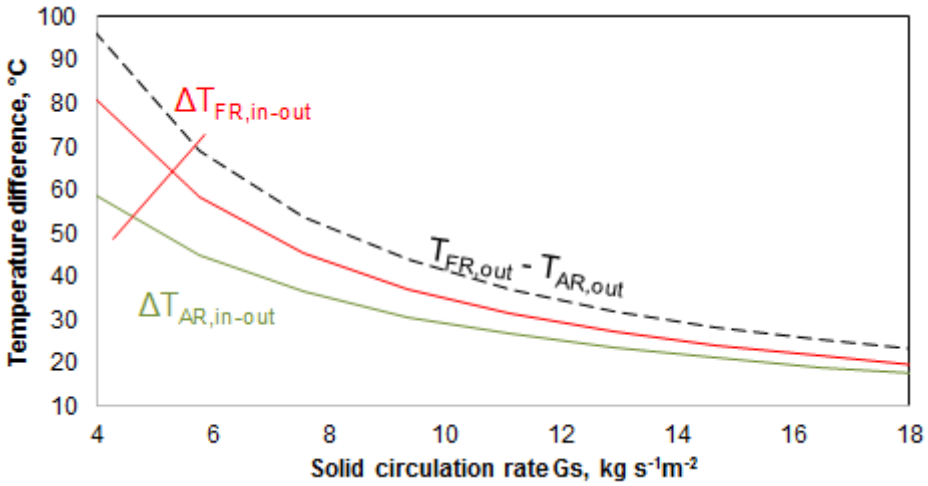

In addition to Cu-based material, Fe and Ni based materials have been considered as OCs. Zirconia (ZrO_2) has always been assumed as support material (60% wt. basis). In case of Fe-based OC, all the different Fe species have been considered in the equilibrium (Fe_2O_3, Fe_3O_4, FeO and Fe but only Fe_2O_3/Fe_3O_4 pair is present because of low temperature) while, in case of Ni-based OC, only Ni/NiO species participate to the redox reactions.
By using Cu-based OC, high solid circulation (about 20 kg/s/m^2) is required to heat-up the air stream to the SOFC inlet temperature. When using Fe-based OC, the amount of solid to circulate between AR and FR can decrease also to 200 kg/s (corresponding to 3.94 kg/s/m^2) while, in case of Ni, the amount of solid required is 886.5 kg/s (corresponding to 17.4 kg/s/m^2). These results are a consequence of the different features of AR and FR reactions. In particular, in case of Ni-based and Fe-based, the reduction is stronger in comparison to the Cu-based (see Appendix B).
It was also modelled an integrated SOFC-CLC system using the mixture Fe_2O_3 (0.6 wt%) – Al_2O_3 (0.4) as OC-support. The total energy efficiency of the H-R and C-R configuration increase of 0.1 percentage points with a strong reduction of the solid circulation rate (from 20 kg/s/m^2 to 10 kg/s/m^2).
Based on this sensitivity analysis, the pair Fe_3O_4/Fe_2O_3 OC results to be the best option in order to decrease the CLC reactors size and cost. However, the kinetics of Ni and Cu based OC is usually faster than in the case of Fe-based, especially at intermediate temperature (500-800°C) which is the operating range of the hybrid SOFC-CLC. Therefore the selection of the OC and the reactor design needs to be properly carried out through a specific economic, energetic and fluid dynamic analysis.

The improvement of the steam cycle operating conditions (from 400 °C and 40 bar without RH to 560 °C and 160 bar with RH) involves a very important improvement of the total system performance: the net power output relative to the steam cycle rises of 24% and the total energy efficiency η of 3.83 percentage points. Furthermore, the vapour fraction at steam turbine outlet increases from 85% to 96%. This is an important advantage for the design of the steam turbine.

A co-current mono-dimensional SOFC model has been implemented in order to analyse all the SOFC features (area, trend of compositions, average current density, overpotentials) and confirm the SOFC future feasibility.

The model is based on the following simplified assumptions:

- all the kinetics and material properties are assumed calculated at constant temperature;
- the kinetics model for the heterogeneous reactions of steam methane reforming and water gas shift is based on Numaguchi and Kikuchi equations [15];
- only current from the H_2 oxidation is considered according to the electrochemical model proposed in Aguiar et al. [16];
- concentration overpotentials in the cell are neglected as well as the mass transfer limitations from the bulk to the electrode.

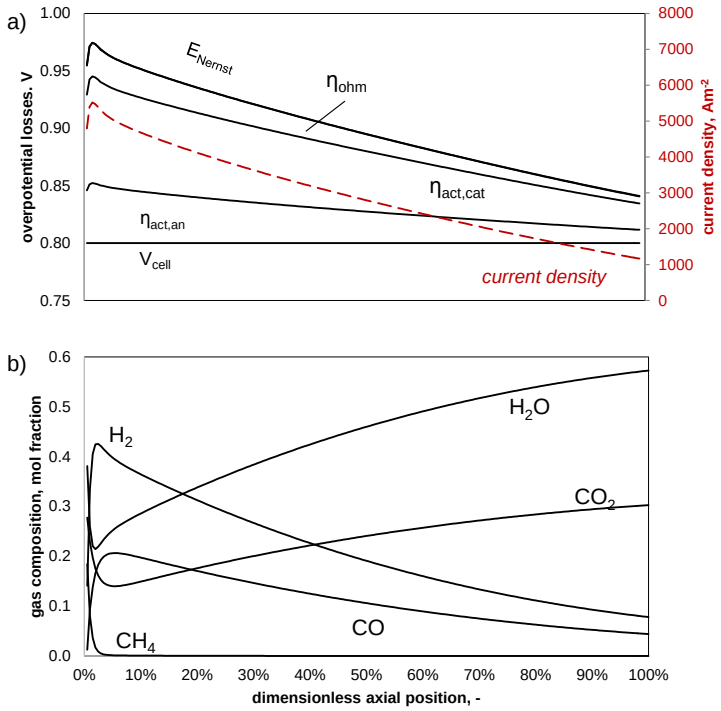

Item	No CO_2 capture	With CO_2 capture	
	Benchmark case	H-R	C-R
A [m^2]	20125	22286	26680
I [MA]	72.681	78.002	77.912
$i_{average}$ [A/m^2]	3610.0	3496.2	2915.4

The trends and the values fit very well with the literature results [14] [18]. The exchange areas could seem excessive but fuel cell is a modular technology. A commercial SOFC [42] is obtained using 51 different layers in parallel. More layers allow to compact the necessary exchange area. Therefore, to obtain the areas of this work, using the same number of layers of the commercial SOFC, it is necessary an area of approximately 390-530 m^2 for each layer, that is 19.5-23 m for side for a square area case. This size is reasonable for a large-size power plant.

An additional analysis has been made regarding the effect of the operating conditions on the SOFC exchange area.

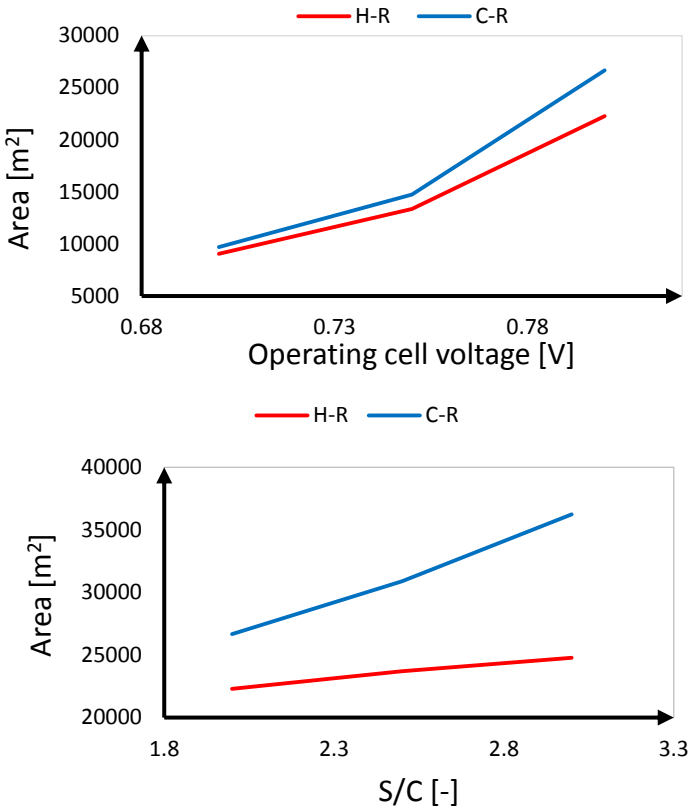

The lower is the SOFC exchange area, the lower is the average current density.

It has been demonstrated that it is not possible to make a planar co-flow SOFC with 0.86 V. A solution to apply 0.86 V with a planar and co-flow SOFC configuration is to reduce the fuel utilization but it involves a reduction of the performance (to be evaluated). Alternatively, it would be possible to apply a counter-flow or a cross-flow configuration that are able to increase the average current density in equal inputs.
It was not possible to build a SOFC model for the other two flow configurations in order to confirm this supposition. In fact, it would be necessary a specific study regarding the concentrations: the evolution of the compositions through the anode and the cathode side is not simultaneous. For example, in counter-flow configuration, the outlet anode composition is in correspondence of the inlet (not outlet) cathode composition.

An additional economic and fluid dynamic analysis might be useful to further confirm the SOFC future feasibility.

The integrated SOFC plant with CLC shows very promising performance at small scale where all the single technologies have been already developed with the intention of producing pure CO_2 for other processes and applications.
SOFCs have been commercialize in the last years in the range of 100-1000 kW power size from CHP applications. For CLC, the demonstration as already reached 1 MWth scale [68]. Therefore, the combination of both systems can also be considered for small scale application as in the case of CO_2 production plant (typically higher than 145 kg/h [61]). In this case, a different arrangement has been considered for the heat recovery. An organic Rankine cycle (ORC) has been adopted for the heat recovery of the system (using Toluene

as operating fluid, as in the case of Triogen generator [59]). The SOFC power output is 450 kWel while the ORC provides about 50 kWel (based on turbine isentropic efficiency of 85% inlet turbine pressure of 32 bar and maximum turbine inlet temperature of 300°C) which are produced from the overall heat duty of 183.6 kWth. Such system can also be considered without ORC producing IP-LP steam for industrial processes. The total energy efficiency is not so lower in comparison to the total energy efficiency of the large-size plants, approximately a difference 0.5 percentage points. This result confirms the advantage of a modular technology like SOFC: it is possible to achieve almost the same performance with different plant size. The SOFC exchange area is 179.9 m^2 and, using the same number of layers of the commercial SOFC [51], it is necessary an area of approximately 3.53 m^2 for each layer, that is 1.88 m for side for a square area case. This size is reasonable for a small-size power plant.

Appendix A
Features of the three periods of EU ETS and trend of CO_2 price during the years

	I° (2005-2007)	II° (2008-2012)	III° (2013-2020)
Sectors concerned	Energy and industry process (combustion plants > 20 MW)	Those of I° period, with more harmonized indications	Those of II° period plus aviation and petrochemical and other greenhouse gases (N_2O and perfluorocarbons)
Assigning permissions	Free (max 5% by auction) or based on a national allocation plan (NAP) approved by the European Commission	Free (max 10% by auction)	More than 50% by auction (88% based on historical emissions; 10% based on PIL/pro-capite; 2% for countries that have reduced their emission by 20% in 2005 respect 1990); 100% by auction for electricity generators; 100% free for industries with the risk of 'carbon leakage'
Credits	CER	CER and ERU	CER and ERU (max 50%)
Other	•	First period of Kyoto fulfillment; entry of Bulgaria, Romania and other extra-UE countries	Objective: reduction of emissions by 21% in 2020 respect 2005
Penalties	40 €/tonnCO_2 (emitted over allowances surrendered)	100 €/tonnCO2 (emitted over allowances surrendered)	100 €/tonnCO2 (emitted over allowances surrendered)

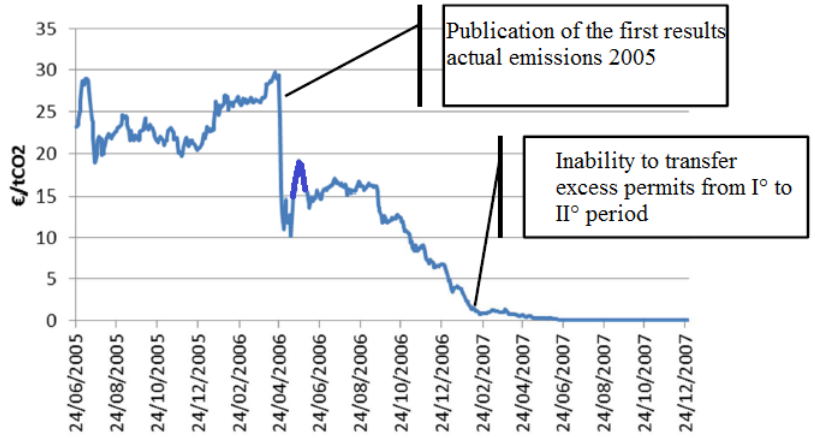

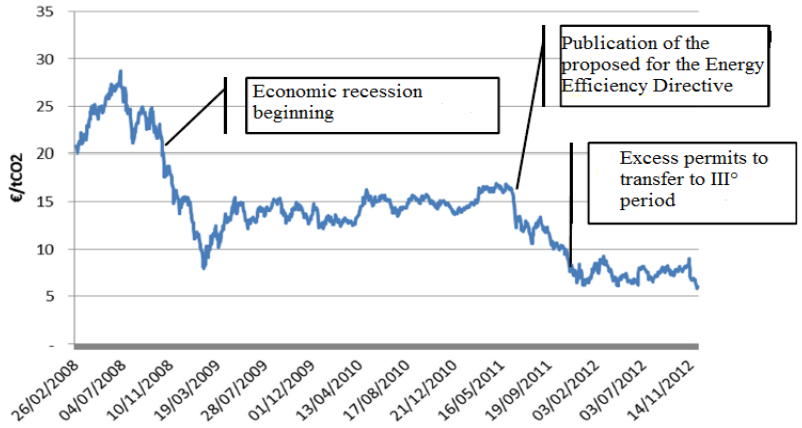

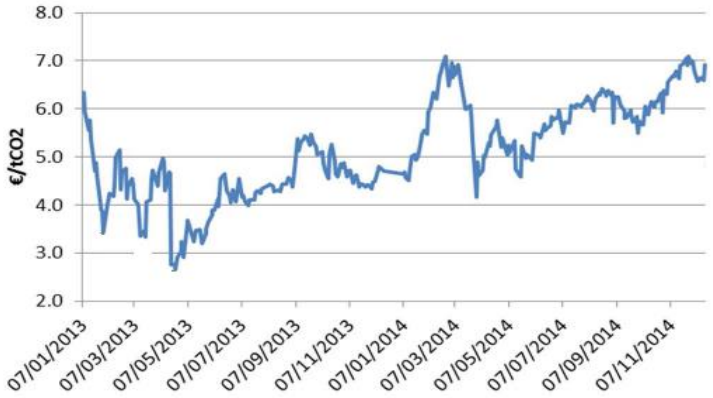

The three graphs show the trend of CO_2 price during the years of EU ETS. The first graph is related to the I° period (2005-2007), the graph in the middle is related to the II° period (2008-2012) and the last is related to the III° period (2013-present).

The reference of this Appendix is [5].

Appendix B
Summary of the CLC most studied OCs and their features

Material type	Support type	Oxygen Carrier	Melting points [°C]	Oxygen ratio	Reaction enthalpy at 1000°C [kJ/mol reactant gas]				
					CO	**H_2**	**CH_4**	**C**	**O_2**
Ni based	α-Al_2O_3,γ-Al_2O_3, Al_2O_3, $NiAl_2O_4$, $NiAl_2O_4$-MgO, $MgAl_2O_4$, Bentonite, ZrO_2-MgO	NiO/Ni	1455°C	0.214	-47	-15	134	75	-468
Cu based	α-Al_2O_3,γ-Al_2O, $MgAl_2O_4$	CuO/Cu	1085°C	0.201	-134	-101	-212	-99	-296
Cu based	Al_2O_3,γ-Al_2O, Sepiolite, $MgAl_2O_4$, Bentonite, ZrO_2, TiO_2, SiO_2	CuO/Cu_2O	1235°C	0.112	-151	-119	-283	-135	-260
Fe based	Al_2O_3, ZrO_2, Bentonite	Fe_2O_3/Fe_3O_4	1565°C	0.033	-42	-10	154	84	-479
Mn based	ZrO_2-MgO	Mn_2O_3/MnO	1347°C	0.101	-102	-70	-85	-36	-359
Mn based	SiO_2	Mn_2O_3/Mn_3O_4	1347°C	0.034	-192	-160	-446	-217	-179
Ilmenite ($FeTiO_3$)	-	Fe_2O_3/FeO	1565°C	0.1	-4.7	27.5	304	158	-554

Appendix C
IT-SOFC of latest generation proposed by CFCL – Assumptions and results [41]

Assumptions for the simulation model of the latest generation IT-SOFC proposed by CFCL.

Ambient conditions	
Temperature [°C]	15.0
Pressure [bar]	1.013
Relative Humidity [%]	60.0
Natural Gas chemical properties	
Molar composition [%mol]	CH_4: 89.0, CO_2: 2.0, C_2H_6: 7.0, C_3H_8: 1.0, N_2: 0.89, C_4H_{10}: 0.11
LHV [MJ/kg]	46.482
Fuel LHV power input [MW_{th}]	100.0
SOFC	
Minimum air inlet temperature [°C]	735.0
Anode and cathode outlet temperature [°C]	800.0
Cell voltage [V]	0.86
Fuel utilization factor (overall) [%]	85.0
Minimum O_2 molar fraction at SOFC outlet [%mol]	5.0
Air and fuel channels pressure losses [%]	3.0
Heat loss [% of fuel LHV]	2.0
DC/AC electrical efficiency [%]	97.0
Inter-Cooled Recuperative Gas Turbine (IC-RGT)	
Inlet air filter pressure loss [%]	1.0
LP Compressor pressure ratio [-]	2.068
HP Compressor pressure ratio [-]	2.0
HP/LP Compressors polytropic efficiency [%]	89.7/88.9
Combustor pressure losses [%]	3.0
Turbine polytropic efficiency [%]	92.3
Mechanical efficiency of compressor/turbine [%]	99.7
Generator electric efficiency [%]	98.0
Maximum TIT [°C]	950.0
GT rotating speed [rpm]	8000
Steam Cycle	
Evaporation pressure [bar]	40.0
Maximum steam temperature [°C]	400.0
Subcooling ΔT at evaporator drum inlet [°C]	5.0
Pressure drop at steam turbine inlet [%]	5.0
Pressure drop in steam super-heater	3.5
Pressure drop in evaporator [%]	0.0
Pressure drop in economiser [%]	20.0
Temperature drop in superheater to turbine piping [°C]	2.0
Condensing pressure [bar]	0.048
Turbine isentropic efficiency [%]	91.5 [67]
Feed water pump hydraulic efficiency [%]	85.0
Turbine mechanical efficiency [%]	99.6
Generator electric efficiency [%]	98.5
Pre-reformer	
Pre-reformer inlet S/C ratio* [-]	2.0
Low Temperature Sulphur removal	
Operating temperature [°C]	15.0
Fuel pressure loss $\Delta p/p_{in}$ [%]	3.0

Heat Exchangers	
Hot and cold side $\Delta p/p_{in}$ [%]	2.0
LT and HT air regenerators $\Delta p/p_{in}$ [%]	3.0
Heat losses [% of heat transferred]	0.7
Minimum gas-evaporating water ΔT (pinch-point) [°C]	10
Minimum ΔT in gas—water heat exchangers [°C]	15
Minimum ΔT in gas—gas heat exchangers [°C]	30
Miscellaneous	
Minimum combustor outlet O_2 molar fraction [%mol]	1.5
Minimum exhaust temperature at stack [°C]	80.0
Air fan isentropic efficiency [%]	80.0
Air fan mechanical-electrical efficiency [%]	94.0
Electric auxiliaries for heat rejection [% of heat rejected]	0.8

*S/C value has been calculated vs. reactive carbon-based molecules (i.e. total carbon except CO_2)

Results obtained by the model built with Aspen to simulate the CFCL system (numbers of the streams reported in Figure 21) [41]

Stream	T	P	G	m	Composition [%mol]								
	[°C]	[bar]	[mol s^{-1}]	[kg s^{-1}]	Ar	CH_4	C+	CO	CO_2	H_2	H_2O	N_2	O_2
1	15.0	1.2	3.08E-03	5.30E-05	-	91.2	4.5	-	-	-	-	4.3	-
2	350.0	1.2	1.01E-02	1.74E-04	-	29.2	-	1.4	-	2.9	65.1	1.3	-
3	20.0	1.2	8.35E-02	2.41E-03	0.9	-	-	-	0.0	-	1.0	77.3	20.7
4	500.0	1.1	1.01E-02	1.74E-04	-	29.2	-	1.4	-	2.9	65.1	1.3	-
5	735.0	1.1	8.35E-02	2.41E-03	0.9	-	-	-	0.0	-	1.0	77.3	20.7
6	771.9	1.1	1.60E-02	3.40E-04	-	-	-	2.0	17.3	9.5	70.4	0.8	-
7	771.9	1.1	7.83E-02	2.24E-03	1.0	-	-	-	0.0	-	1.1	82.4	15.5
8	911.6	1.1	9.33E-02	2.58E-03	0.8	-	-	-	3.3	-	14.6	69.3	12.0
9	830.0	1.0	1.04E-01	2.89E-03	0.8	-	-	-	3.0	-	13.2	70.1	12.9
10	125.6	1.0	1.04E-01	2.89E-03	0.8	-	-	-	3.0	-	13.2	70.1	12.9
11	15.0	1.2	6.72E-03	1.21E-04	-	-	-	-	-	-	100	-	-
12	615.7	1.2	6.72E-03	1.21E-04	-	-	-	-	-	-	100	-	-
13	20.0	1.2	1.08E-02	3.10E-04	0.9	-	-	-	0.0	-	1.0	77.3	20.7

Appendix D
Comparison between the benchmark plant of Campanari et al. [41] and the same plant built using AspenPlus

In the following tables, the assumptions and the all the streams properties related to the results achieved by Campanari et al. [41] are shown. The layout is the same for all the models presented in this Appendix and it is shown in the Figure below.

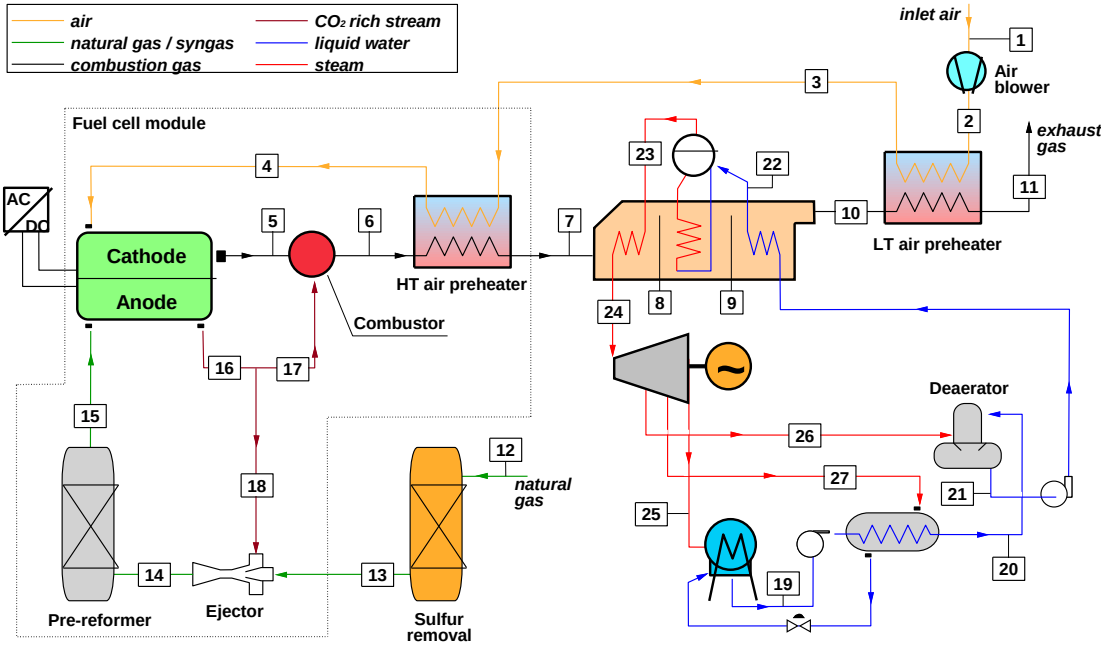

Ambient conditions	
Temperature [°C]	15.0
Pressure [bar]	1.013
Relative Humidity [%]	60.0
Natural Gas chemical properties	
Molar composition [%mol]	CH_4: 89.0, CO_2: 2.0, C_2H_6: 7.0, C_3H_8: 1.0, N_2: 0.89, C_4H_{10}: 0.11
LHV [MJ/kg]	46.482
Fuel LHV power input [MW_{th}]	100.0
SOFC	
Minimum air inlet temperature [°C]	735.0
Anode and cathode outlet temperature [°C]	800.0
Cell voltage [V]	0.86
Fuel utilisation factor (overall) [%]	85.0
Minimum O_2 molar fraction at SOFC outlet [%mol]	5.0
Air and fuel channels pressure losses [%]	3.0
Heat loss [% of fuel LHV]	2.0
DC/AC electrical efficiency [%]	97.0
Steam Cycle	
Evaporation pressure [bar]	40.0
Maximum steam temperature [°C]	400.0

Subcooling ΔT at evaporator drum inlet [°C]	5.0
Pressure drop at steam turbine inlet [%]	5.0
Pressure drop in steam super-heater	3.5
Pressure drop in evaporator [%]	0.0
Pressure drop in economiser [%]	20.0
Temperature drop in superheater to turbine piping [°C]	2.0
Condensing pressure [bar]	0.048
Turbine isentropic efficiency [%]	91.5 [67]
Feed water pump hydraulic efficiency [%]	85.0
Turbine mechanical efficiency [%]	99.6
Generator electric efficiency [%]	98.5
Pre-reformer	
Pre-reformer inlet S/C ratio* [-]	2.0
Low Temperature Sulphur removal	
Operating temperature [°C]	15.0
Fuel pressure loss $\Delta p/p_{in}$ [%]	3.0
Heat Exchangers	
Hot and cold side $\Delta p/p_{in}$ [%]	2.0
LT and HT air regenerators $\Delta p/p_{in}$ [%]	3.0
Heat losses [% of heat transferred]	0.7
Minimum gas-evaporating water ΔT (pinch-point) [°C]	10
Minimum ΔT in gas—water heat exchangers [°C]	15
Minimum ΔT in gas—gas heat exchangers [°C]	30
Miscellaneous	
Minimum combustor outlet O_2 molar fraction [%mol] Minimum	1.5
exhaust temperature at stack [°C]	80.0
Air fan isentropic efficiency [%]	80.0
Air fan mechanical-electrical efficiency [%]	94.0
Electric auxiliaries for heat rejection [% of heat rejected]	0.8

	T	p	n	m	m*LHV	Composition [%mol]								
Stream	[°C]	[bar]	[mol s-1]	[kg s-1]	[MW]	Ar	CH4	CO	CO2	C+	H2	H2O	N2	O2
1	15.0	1.000	1302.2	37.6	-	0.92	-	-	0.03	-	-	1.03	77.28	20.73
2	34.3	1.200	1302.2	37.6	-	0.92	-	-	0.03	-	-	1.03	77.28	20.73
3	131.0	1.190	1302.2	37.6	-	0.92	-	-	0.03	-	-	1.03	77.28	20.73
4	753.8	1.160	1302.2	37.6	-	0.92	-	-	0.03	-	-	1.03	77.28	20.73
5	799.9	1.120	1090.8	30.8	-	1.10	-	-	0.04	-	-	1.24	92.26	5.37
6	1155.8	1.090	1427.2	39.7	-	0.84	-	-	9.10	-	-	17.98	70.59	1.50
7	679.1	1.050	1427.2	39.7	-	0.84	-	-	9.10	-	-	17.98	70.59	1.50
8	600.3	1.040	1427.2	39.7	-	0.84	-	-	9.10	-	-	17.98	70.59	1.50
9	263.5	1.040	1427.2	39.7	-	0.84	-	-	9.10	-	-	17.98	70.59	1.50
10	166.8	1.020	1427.2	39.7	-	0.84	-	-	9.10	-	-	17.98	70.59	1.50
11	80.0	1.010	1427.2	39.7	-	0.84	-	-	9.10	-	-	17.98	70.59	1.50
12	15.0	20.000	119.4	2.2	100.0	-	89.00	-	2.00	8.11	-	-	0.89	-
13	15.0	19.400	119.4	2.2	100.0	-	89.00	-	2.00	8.11	-	-	0.89	-
14	651.9	1.200	781.1	17.9	133.5	-	13.61	5.07	24.59	1.24	11.81	43.30	0.38	-
15	520.6	1.160	841.0	17.9	137.7	-	11.55	4.45	26.66	-	24.16	32.83	0.35	-
16	799.9	1.130	1035.3	24.7	52.5	-	-	5.99	28.67	-	13.94	51.11	0.28	-
17	799.9	1.130	373.6	8.9	18.9	-	-	5.99	28.67	-	13.94	51.11	0.28	-
18	799.9	1.130	661.7	15.8	33.5	-	-	5.99	28.67	-	13.94	51.11	0.28	-
19	32.3	0.048	482.9	8.7	-	-	-	-	-	-	-	100.00	-	-
20	104.1	5.600	483.5	8.7	-	-	-	-	-	-	-	100.00	-	-
21	139.9	3.600	517.3	9.3	-	-	-	-	-	-	-	100.00	-	-
22	245.4	40.000	517.1	9.3	-	-	-	-	-	-	-	100.00	-	-
23	250.4	40.000	517.1	9.3	-	-	-	-	-	-	-	100.00	-	-
24	398.0	36.670	517.1	9.3	-	-	-	-	-	-	-	100.00	-	-
25	32.2	0.048	403.1	7.3	-	-	-	-	-	-	-	100.00	-	-
26	148.7	3.790	34.1	0.6	-	-	-	-	-	-	-	100.00	-	-
27	108.6	1.370	60.0	1.1	-	-	-	-	-	-	-	100.00	-	-

In the following tables, the results of the Aspen model with the same assumptions of Campanari et al. [41] are shown.

	T	p	n	m	Composition [%mol]								
Stream	[°C]	[bar]	[kmol s-1]	[kg s-1]	Ar	CH4	CO	CO2	C+	H2	H2O	N2	O2
1	15.0	1.013	1.303	37.6	0.92	-	-	0.03	-	-	1.03	77.28	20.73
2	32.8	1.200	1.303	37.6	0.92	-	-	0.03	-	-	1.03	77.28	20.73
3	131.0	1.180	1.303	37.6	0.92	-	-	0.03	-	-	1.03	77.28	20.73
4	753.8	1.150	1.303	37.6	0.92	-	-	0.03	-	-	1.03	77.28	20.73
5	800.0	1.120	1.092	30.8	1.10	-	-	0.04	-	-	1.24	92.26	5.37
6	1158.4	1.090	1.428	39.8	0.84	-	-	9.10	-	-	17.98	70.59	1.50
7	679.2	1.050	1.428	39.8	0.84	-	-	9.10	-	-	17.98	70.59	1.50
8	616.4	1.040	1.428	39.8	0.84	-	-	9.10	-	-	17.98	70.59	1.50
9	277.8	1.040	1.428	39.8	0.84	-	-	9.10	-	-	17.98	70.59	1.50
10	164.6	1.020	1.428	39.8	0.84	-	-	9.10	-	-	17.98	70.59	1.50
11	80.0	1.010	1.428	39.8	0.84	-	-	9.10	-	-	17.98	70.59	1.50
12	15.0	20.000	0.119	2.2	-	89.00	-	2.00	8.11	-	-	0.89	-
13	15.0	19.400	0.119	2.2	-	89.00	-	2.00	8.11	-	-	0.89	-
14	649.4	1.200	0.781	17.9	-	13.60	5.40	24.10	1.40	11.30	43.80	0.40	-
15	517.9	1.160	0.841	17.9	-	11.60	4.40	26.70	-	24.50	32.50	0.30	-
16	800.0	1.130	1.034	24.7	-	-	6.60	28.00	0.10	13.30	51.70	0.30	-
17	800.0	1.130	0.374	8.9	-	-	6.60	28.00	0.10	13.30	51.70	0.30	-
18	800.0	1.130	0.662	15.8	-	-	6.60	28.00	0.10	13.30	51.70	0.30	-
19	35.3	0.048	0.472	8.6	-	-	-	-	-	-	100.00	-	-
20	104.1	5.600	0.472	8.6	-	-	-	-	-	-	100.00	-	-
21	140.0	3.600	0.507	9.2	-	-	-	-	-	-	100.00	-	-
22	245.4	40.000	0.507	9.2	-	-	-	-	-	-	100.00	-	-
23	250.4	40.000	0.507	9.2	-	-	-	-	-	-	100.00	-	-
24	398.5	36.670	0.507	9.2	-	-	-	-	-	-	100.00	-	-
25	35.3	0.048	0.472	7.5	-	-	-	-	-	-	100.00	-	-
26	161.5	3.790	0.035	0.6	-	-	-	-	-	-	100.00	-	-
27	110.4	1.370	0.057	1.0	-	-	-	-	-	-	100.00	-	-

In order to achieve the same temperatures in every points (as well as possible), it was necessary to make a modification of the SOFC heat losses, assumed equal to the 2% of the thermal input (100 MW_{th}). In order to use the exact operating conditions of [41] for the fuel and oxidant utilization and for the recycle split fraction, the heat losses have been increased from 2 MW to approximately 2.77 MW. The differences are mainly due to the difference of calculation between Aspen Plus and GS, the software used for the work of the article [41]. Furthermore, some values presented in the article are approximated.

It was built also an Aspen model of the benchmark case with 0.86 V using 2 MW of heat losses. The air temperature at SOFC inlet has been decreased to 735 °C (the minimum limit) in order to use more fuel in the SOFC and recover a part of the heat losses, useful to cool the SOFC and oxidize more fuel at equal outlet temperature.

Below, the comparison of the performance parameters and the energy balances.

Item	[41]	2.77 MW	2 MW
$P_{el,net}$ [MW]	75.200	75.022	75.309
η [%]	75.200	75.022	75.309
Recycle split fraction [%]	~ 64.000	64.000	63.784
U_{fuel} [%] (overall)	~ 85.000	85.008	85.086
U_{fuel} [%] (single pass)	~ 67.200	67.200	67.386
U_{ox}[%] (single pass)	78.300	78.148	78.306
e [g_{CO_2}/MJ_{el}]	75.988	76.627	75.972
e [g_{CO_2}/MWh]	273.590	275.857	273.499

	[41]	2.77 MW	2 MW
Fuel Inlet [MW]	100.000	100.000	100.000
SOFC net power [MW]	68.060	68.043	68.106
Steam cycle net power [MW]	8.060	7.594	7.623
FD fan [MW]	-0.719	-0.719	-0.719
Water pumps [MW]	-0.063	-0.063	-0.065
Condensation heat [MW]	16.456	16.513	16.993
Auxiliaries work for heat rejection [MW]	-0.132	-0.132	-0.136
Tot auxiliaries electric power [MW]	-0.911	-0.914	-0.920

Based on this comparison, the Aspen model respects all the assumptions and it is built in a solid way. In particular, the most important result is the comparison of the performance parameters: electric power output, total energy efficiency and emissions. These parameters fit very well each other.

In the large-size models of this work, it is used 2 MW as SOFC heat losses, the exact value of 2% of the thermal energy input.

Appendix E
Benchmark case (reference plant with 0.8 V)

The complete plant layout is shown in the Appendix D. The results for the performance parameters and the energy balance are shown in Table 2 and 3. Below, all the streams properties of the model are shown.

	T	p	n	m	Composition [%mol]								
Stream	[°C]	[bar]	[kmol s-1]	[kg s-1]	Ar	CH4	CO	CO2	C+	H2	H2O	N2	O2
1	15.0	1.013	1.303	37.6	0.92	-	-	0.03	-	-	1.03	77.28	20.73
2	32.8	1.200	1.303	37.6	0.92	-	-	0.03	-	-	1.03	77.28	20.73
3	131.0	1.180	1.303	37.6	0.92	-	-	0.03	-	-	1.03	77.28	20.73
4	735.0	1.150	1.303	37.6	0.92	-	-	0.03	-	-	1.03	77.28	20.73
5	800.0	1.120	1.092	30.8	1.10	-	-	0.04	-	-	1.24	92.26	5.37
6	1371.5	1.090	1.428	39.7	0.84	-	-	9.10	-	-	18.00	70.61	1.50
7	923.2	1.050	1.428	39.7	0.84	-	-	9.10	-	-	18.00	70.61	1.50
8	832.5	1.040	1.428	39.7	0.84	-	-	9.10	-	-	18.00	70.61	1.50
9	334.8	1.040	1.428	39.7	0.84	-	-	9.10	-	-	18.00	70.61	1.50
10	164.6	1.020	1.428	39.7	0.84	-	-	9.10	-	-	18.00	70.61	1.50
11	80.0	1.010	1.428	39.7	0.84	-	-	9.10	-	-	18.00	70.61	1.50
12	15.0	20.000	0.119	2.2	-	89.00	-	2.00	8.11	-	-	0.89	-
13	15.0	19.400	0.119	2.2	-	89.00	-	2.00	8.11	-	-	0.89	-
14	701.1	1.200	1.275	27.4	-	8.30	9.80	21.80	0.80	19.50	39.50	0.30	-
15	570.7	1.160	1.275	27.4	-	6.00	8.20	24.60	-	31.50	29.40	0.30	-
16	800.0	1.130	1.529	33.5	-	-	10.80	23.90	0.10	21.50	43.50	0.30	-
17	800.0	1.130	0.374	8.2	-	-	10.80	23.90	0.10	21.50	43.50	0.30	-
18	800.0	1.130	1.155	25.3	-	-	10.80	23.90	0.10	21.50	43.50	0.30	-
19	35.3	0.048	0.716	12.9	-	-	-	-	-	-	100.00	-	-
20	104.1	5.600	0.716	12.9	-	-	-	-	-	-	100.00	-	-
21	140.0	3.600	0.769	13.9	-	-	-	-	-	-	100.00	-	-
22	245.4	40.000	0.769	13.9	-	-	-	-	-	-	100.00	-	-
23	250.4	40.000	0.769	13.9	-	-	-	-	-	-	100.00	-	-
24	398.5	36.670	0.769	13.9	-	-	-	-	-	-	100.00	-	-
25	35.3	0.048	0.628	11.3	-	-	-	-	-	-	100.00	-	-
26	152.2	3.790	0.053	1.0	-	-	-	-	-	-	100.00	-	-
27	110.4	1.370	0.088	1.6	-	-	-	-	-	-	100.00	-	-

Appendix F
SOFC + CLC – Hot Recycle

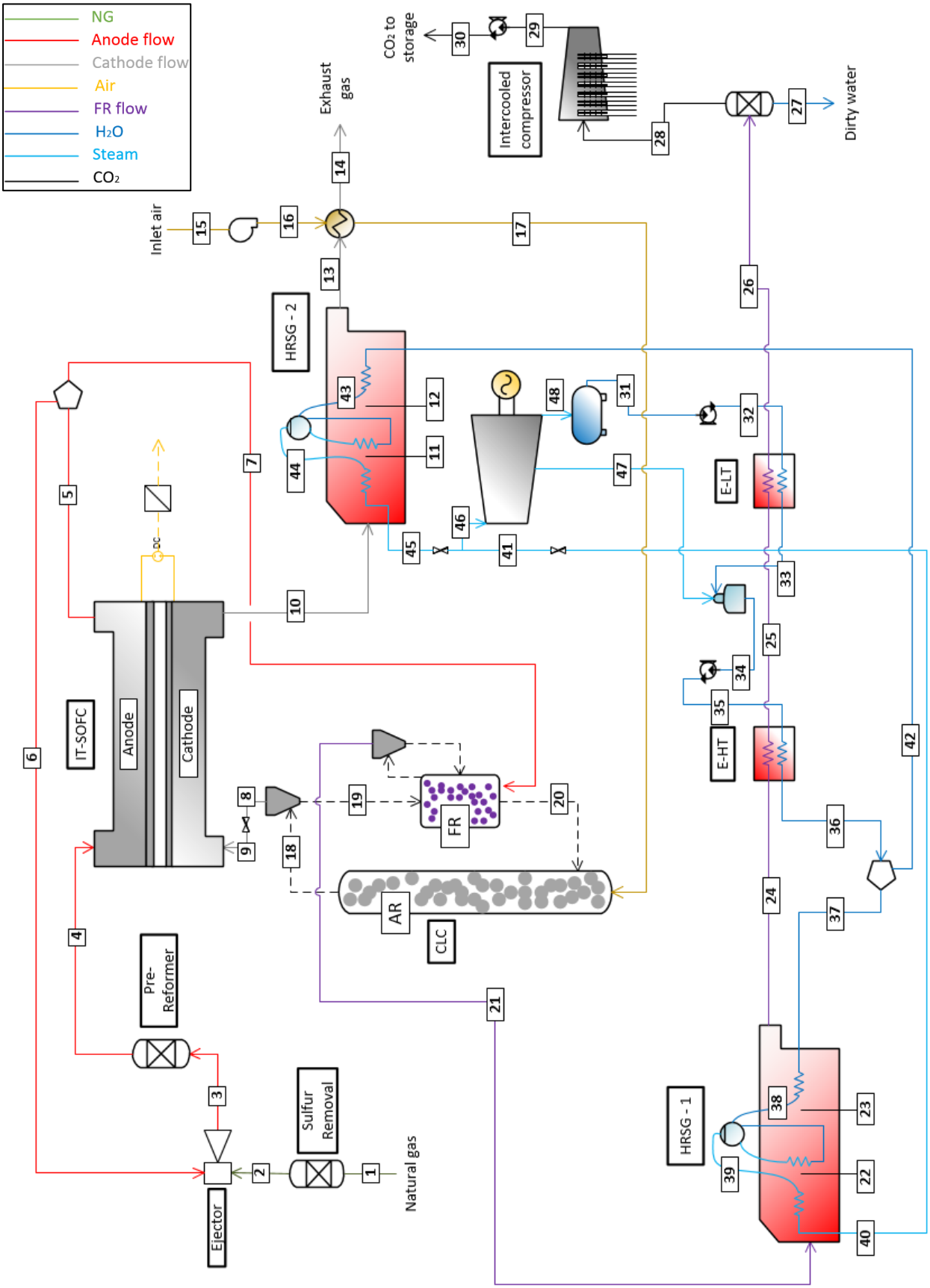

	T	***p***	***N***	***m***		***Composition, %mol***								
#	°C	bar	kmol/s	kg/s	**CH_4**	**C_{2+}**	**CO_2**	**H_2O**	**$H_2O(l)$**	**N_2**	**O_2**	**H_2**	**CO**	**Ar**
1	15.0	20.0	0.119	2.151	89.0	8.1	2.0	-	-	0.9	-	-	-	-
2	14.8	19.6	0.119	2.151	89.0	8.1	2.0	-	-	0.9	-	-	-	-
3	668.5	1.12	0.917	20.541	11.6	1.0	23.2	42.1	-	0.4	-	14.5	7.2	-
4	538.0	1.12	0.986	20.541	9.4	-	26.0	48.4	-	0.3	-	27.4	5.8	-
5	800.0	1.12	1.171	11.934	6ppm	-	26.4	48.4	-	0.3	-	16.6	8.3	-
6	800.0	1.12	0.797	18.390	6ppm	-	26.4	48.4	-	0.3	-	16.6	8.3	-
7	800.0	1.12	0.374	8.619	6ppm	-	26.4	48.4	-	0.3	-	16.6	8.3	-
8	735.0	1.13	2.647	76.230	-	-	407ppm	1.0	-	78.6	19.3	-	-	0.9
9	735.0	1.12	2.647	76.230	-	-	407ppm	1.0	-	78.6	19.3	-	-	0.9
10	800.0	1.09	2.445	69.763	-	-	441ppm	1.1	-	85.1	12.7	-	-	1.0
11	760.1	1.09	2.445	69.763	-	-	441ppm	1.1	-	85.1	12.7	-	-	1.0
12	558.4	1.09	2.445	69.763	-	-	441ppm	1.1	-	85.1	12.7	-	-	1.0
13	527.1	1.04	2.445	69.763	-	-	441ppm	1.1	-	85.1	12.7	-	-	1.0
14	80.0	1.02	2.445	69.763	-	-	441ppm	1.1	-	85.1	12.7	-	-	1.0
15	15.0	1.01	2.694	77.719	-	-	400ppm	1.0	-	77.3	20.7	-	-	0.9
16	41.5	1.30	2.694	77.719	-	-	400ppm	1.0	-	77.3	20.7	-	-	0.9
17	450.0	1.28	2.694	77.719	-	-	400ppm	1.0	-	77.3	20.7	-	-	0.9
18	735.0	1.13	12.168	1038.1	-	-	89ppm	0.2	-	17.1	4.6	-	-	0.2
21	756.1	1.13	0.374	10.107	-	-	34.7	65.1	-	0.3	3ppm	-	-	-
22	699.9	1.13	0.374	10.107	-	-	34.7	65.1	-	0.3	3ppm	-	-	-
23	420.7	1.13	0.374	10.107	-	-	34.7	65.1	-	0.3	3ppm	-	-	-
24	400.0	1.08	0.374	10.107	-	-	34.7	65.1	-	0.3	3ppm	-	-	-
25	165.0	1.08	0.374	10.107	-	-	34.7	65.1	-	0.3	3ppm	-	-	-
26	88.9	1.08	0.374	10.107	-	-	34.7	47.6	17.5	0.3	3ppm	-	-	-
27	30.0	1.08	0.239	4.299	-	-	-	-	100.0	-	-	-	-	-
28	30.0	1.08	0.135	5.808	-	-	95.9	3.3	-	0.8	8ppm	-	-	-
29	30.0	80.0	0.135	5.808	-	-	95.9	3.3	-	0.8	8ppm	-	-	-
30	37.7	110.0	0.135	5.808	-	-	95.9	3.3	-	0.8	8ppm	-	-	-
31	32.2	0.048	0.599	10.80	-	-	-	-	-	100.0	-	-	-	-
32	32.2	5.60	0.599	10.80	-	-	-	-	-	100.0	-	-	-	-
33	110.0	5.60	0.599	10.80	-	-	-	-	-	100.0	-	-	-	-
34	140.0	3.79	0.637	11.47	-	-	-	-	-	100.0	-	-	-	-
35	140.6	50.00	0.637	11.47	-	-	-	-	-	100.0	-	-	-	-
36	202.0	40.00	0.637	11.47	-	-	-	-	-	100.0	-	-	-	-
37	202.0	40.00	0.134	2.422	-	-	-	-	-	100.0	-	-	-	-
38	245.4	40.00	0.134	2.422	-	-	-	-	-	100.0	-	-	-	-
39	250.4	40.00	0.134	2.422	-	-	-	-	100.0	-	-	-	-	-
40	400.0	38.60	0.134	2.422	-	-	-	-	100.0	-	-	-	-	-
41	398.5	36.67	0.134	2.422	-	-	-	-	100.0	-	-	-	-	-
42	202.0	40.00	0.502	9.050	-	-	-	-	-	100.0	-	-	-	-
43	245.4	40.00	0.502	9.050	-	-	-	-	-	100.0	-	-	-	-
44	250.4	40.00	0.502	9.050	-	-	-	-	100.0	-	-	-	-	-
45	400.0	38.60	0.502	9.050	-	-	-	-	100.0	-	-	-	-	-
46	398.5	36.67	0.637	11.47	-	-	-	-	100.0	-	-	-	-	-
47	152.2	3.79	0.037	0.673	-	-	-	-	100.0	-	-	-	-	-
48	32.2	0.048	0.599	10.80	-	-	-	-	100.0	-	-	-	-	-
18	735.0	1.13	12.168	1038.1		*molar fraction* CuO 39.8%; ZrO_2 38.5%								
19	735.0	1.28	9.521	961.86		*weight fraction*: CuO 40%; ZrO_2 60%								
20	756.1	1.28	9.428	960.40		*weight fraction*: CuO 38.6%; Cu_2O 1.4%; ZrO_2 60%								

Appendix G
SOFC + CLC – Cold Recycle

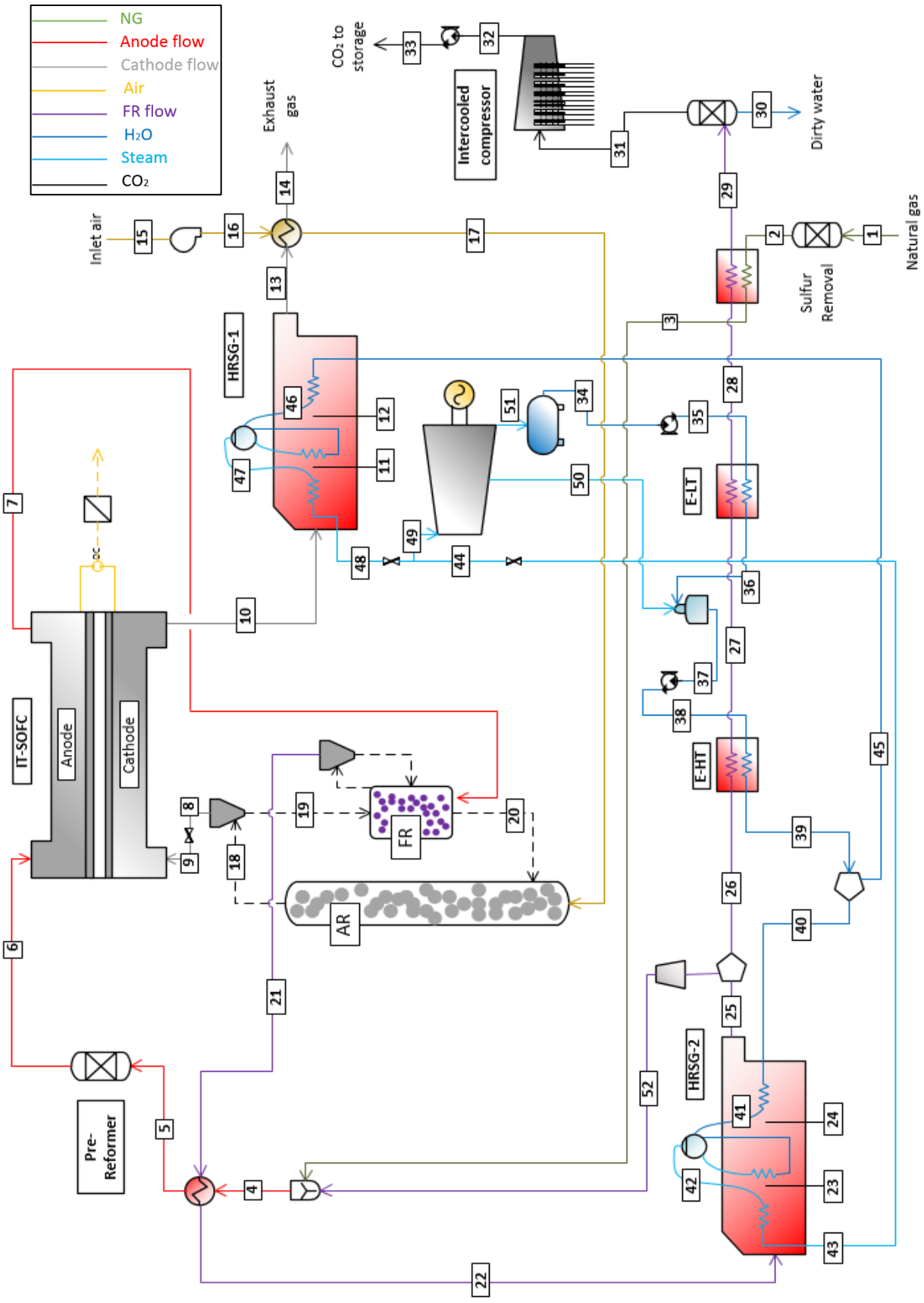

	T	***p***	***N***	***m***		***Composition, %mol***								
#	°C	bar	kmol/s	kg/s	**CH_4**	**C_{2+}**	**CO_2**	**H_2O**	**$H_2O(l)$**	**N_2**	**O_2**	**H_2**	**CO**	**Ar**
1	15.0	20.0	0.119	2.151	89.0	8.1	2.0	-	-	0.9	-	-	-	-
2	14.8	19.6	0.119	2.151	89.0	8.1	2.0	-	-	0.9	-	-	-	-
3	85.0	19.4	0.119	2.151	89.0	8.1	2.0	-	-	0.9	-	-	-	-
4	323.0	1.15	0.510	12.722	20.8	2.0	27.0	49.8	-	0.4	-	-	-	-
5	600.0	1.13	0.510	12.722	20.8	2.0	27.0	49.8	-	0.4	-	-	-	-
6	442.3	1.13	0.558	12.722	18.4	-	27.8	38.1	-	0.4	-	14.1	1.2	-
7	800.0	1.10	0.764	19.181	278ppm	-	30.6	56.9	-	0.3	-	8.2	4.0	-
8	734.6	1.13	2.744	79.015	-	-	407ppm	1.0	-	78.6	19.4	-	-	0.9
9	734.6	1.12	2.744	79.015	-	-	407ppm	1.0	-	78.6	19.4	-	-	0.9
10	800.0	1.09	2.542	72.555	-	-	439ppm	1.1	-	84.8	13.0	-	-	1.0
11	760.7	1.09	2.542	72.555	-	-	439ppm	1.1	-	84.8	13.0	-	-	1.0
12	551.7	1.09	2.542	72.555	-	-	439ppm	1.1	-	84.8	13.0	-	-	1.0
13	525.6	1.04	2.542	72.555	-	-	439ppm	1.1	-	84.8	13.0	-	-	1.0
14	80.0	1.02	2.542	72.555	-	-	439ppm	1.1	-	84.8	13.0	-	-	1.0
15	15.0	1.01	2.790	80.511	-	-	400ppm	1.0	-	77.3	20.7	-	-	0.9
16	41.5	1.30	2.790	80.511	-	-	400ppm	1.0	-	77.3	20.7	-	-	0.9
17	450.0	1.28	2.790	80.511	-	-	400ppm	1.0	-	77.3	20.7	-	-	0.9
18	734.6	1.13	11.944	1008.6	-	-	93ppm	0.2	-	18.1	4.5	-	-	0.2
21	757.7	1.13	0.764	20.677	-	-	34.7	65.1	-	0.3	3ppm	-	-	-
22	563.6	1.13	0.764	20.677	-	-	34.7	65.1	-	0.3	3ppm	-	-	-
23	595.6	1.13	0.764	20.677	-	-	34.7	65.1	-	0.3	3ppm	-	-	-
24	377.3	1.13	0.764	20.677	-	-	34.7	65.1	-	0.3	3ppm	-	-	-
25	400.0	1.08	0.764	20.677	-	-	34.7	65.1	-	0.3	3ppm	-	-	-
26	400.0	1.08	0.374	10.107	-	-	34.7	65.1	-	0.3	3ppm	-	-	-
27	165.0	1.08	0.374	10.107	-	-	34.7	65.1	-	0.3	3ppm	-	-	-
28	88.9	1.08	0.374	10.107	-	-	34.7	47.2	17.9	0.3	3ppm	-	-	-
29	87.9	1.06	0.374	10.107	-	-	34.7	45.2	19.9	0.3	3ppm	-	-	-
30	30.0	1.06	0.239	4.297	-	-	-	-	100.0	-	-	-	-	-
31	30.0	1.06	0.135	5.810	-	-	95.9	3.4	-	0.8	8ppm	-	-	-
32	30.0	80.0	0.135	5.810	-	-	95.9	3.4	-	0.8	8ppm	-	-	-
33	37.7	110.0	0.135	5.808	-	-	95.9	3.4	-	0.8	8ppm	-	-	-
34	32.2	0.048	0.609	10.97	-	-	-	-	-	100.0	-	-	-	-
35	32.2	5.60	0.609	10.97	-	-	-	-	-	100.0	-	-	-	-
36	110.0	5.60	0.609	10.97	-	-	-	-	-	100.0	-	-	-	-
37	140.0	3.79	0.647	11.65	-	-	-	-	-	100.0	-	-	-	-
38	140.6	50.00	0.647	11.65	-	-	-	-	-	100.0	-	-	-	-
39	201.2	40.00	0.647	11.65	-	-	-	-	-	100.0	-	-	-	-
40	201.2	40.00	0.122	2.204	-	-	-	-	-	100.0	-	-	-	-
41	245.4	40.00	0.122	2.204	-	-	-	-	-	100.0	-	-	-	-
42	250.4	40.00	0.122	2.204	-	-	-	-	100.0	-	-	-	-	-
43	400.0	38.60	0.122	2.204	-	-	-	-	100.0	-	-	-	-	-
44	398.5	36.67	0.122	2.204	-	-	-	-	100.0	-	-	-	-	-
45	201.2	40.00	0.524	9.443	-	-	-	-	-	100.0	-	-	-	-
46	245.4	40.00	0.524	9.443	-	-	-	-	-	100.0	-	-	-	-
47	250.4	40.00	0.524	9.443	-	-	-	-	100.0	-	-	-	-	-
48	400.0	38.60	0.524	9.443	-	-	-	-	100.0	-	-	-	-	-
49	398.5	36.67	0.647	11.65	-	-	-	-	100.0	-	-	-	-	-
50	152.2	3.79	0.038	0.683	-	-	-	-	100.0	-	-	-	-	-
51	32.2	0.048	0.609	10.97	-	-	-	-	100.0	-	-	-	-	-
18	734.6	1.13	11.944	1008.6		*molar fraction:* CuO 39.1%; ZrO_2 37.9%								
19	734.6	1.28	9.521	928.04		*weight fraction*: CuO 40%; ZrO_2 60%								
20	757.7	1.28	9.428	929.53		*weight fraction*: CuO 38.6%; Cu_2O 1.4%; ZrO_2 60%								

Appendix H
SOFC + CLC – Small-size

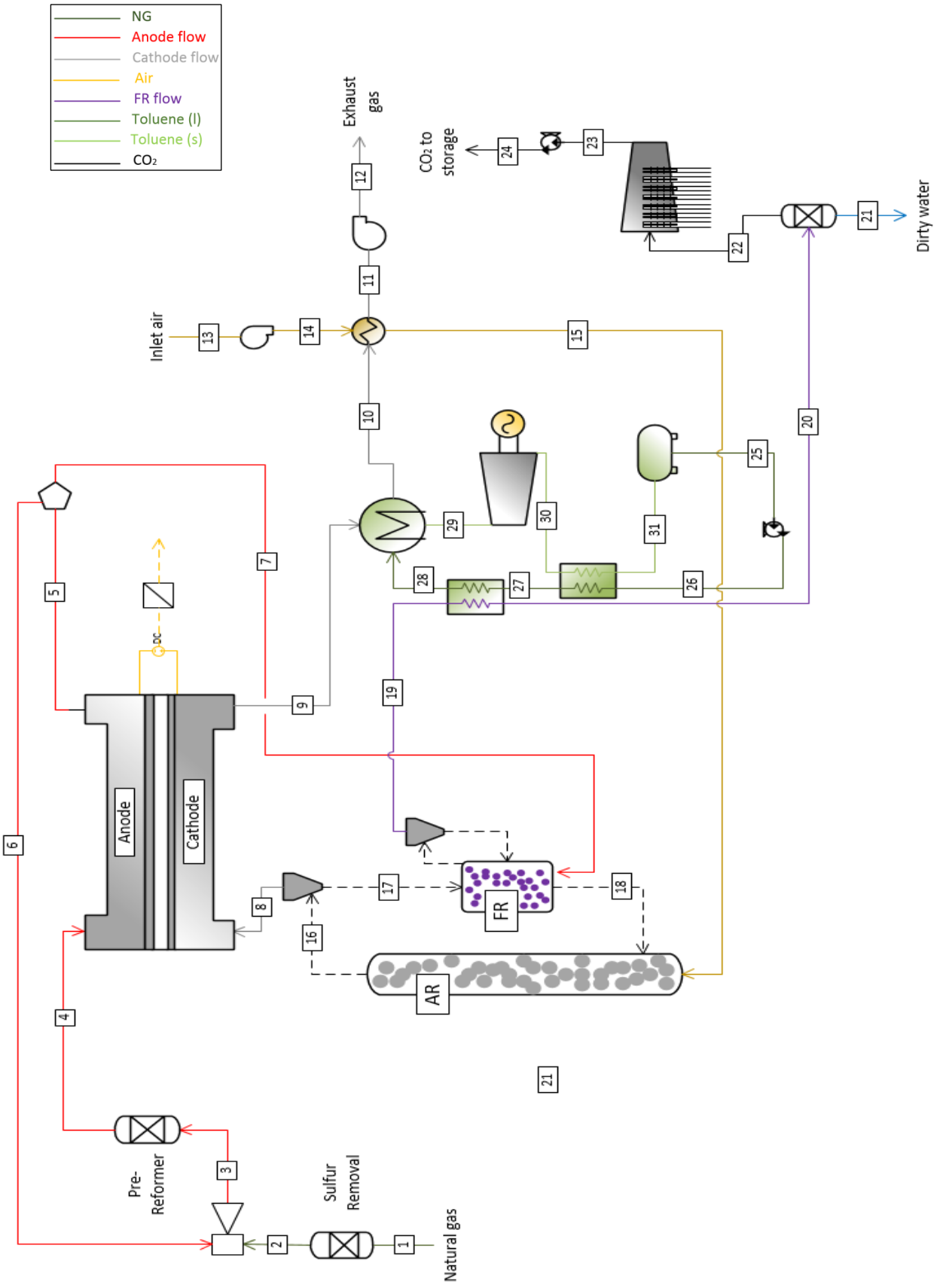

	T	***p***	***N***	***m***	***Composition, %mol***									
#	°C	bar	kmol/s	kg/s	**CH_4**	**C_{2+}**	**CO_2**	**H_2O**	**Tol.**	**N_2**	**O_2**	**H_2**	**CO**	**Ar**
1	15.0	20.0	0.001	0.015	89.0	8.1	2.0	-	-	0.9	-	-	-	-
2	14.8	19.6	0.001	0.015	89.0	8.1	2.0	-	-	0.9	-	-	-	-
3	650.1	1.12	0.006	0.128	13.6	1.0	24.0	43.7	-	0.4	-	11.4	5.7	-
4	518.6	1.12	0.006	0.128	11.4	-	26.7	32.5	-	0.3	-	24.6	4.5	-
5	800.0	1.12	0.007	0.176	2ppm	-	28.0	51.6	-	0.3	-	13.4	6.7	-
6	800.0	1.12	0.005	0.113	2ppm	-	28.0	51.6	-	0.3	-	13.4	6.7	-
7	800.0	1.12	0.003	0.128	2ppm	-	28.0	51.6	-	0.3	-	13.4	6.7	-
8a	735.0	1.13	0.015	0.435	-	-	407ppm	1.0	-	78.6	19.3	-	-	0.9
8b	735.0	1.12	0.015	0.435	-	-	407ppm	1.0	-	78.6	19.3	-	-	0.9
9	800.0	1.09	0.014	0.387	-	-	441ppm	1.1	-	87.3	10.4	-	-	1.0
10	538.7	1.04	0.014	0.387	-	-	441ppm	1.1	-	87.3	10.4	-	-	1.0
11	80.0	1.02	0.014	0.387	-	-	441ppm	1.1	-	87.3	10.4	-	-	1.0
12	80.0	1.02	0.014	0.387	-	-	441ppm	1.1	-	87.3	10.4	-	-	1.0
13	15.0	1.01	0.015	0.435	-	-	400ppm	1.0	-	77.3	20.7	-	-	0.9
14	41.5	1.30	0.015	0.435	-	-	400ppm	1.0	-	77.3	20.7	-	-	0.9
15	450.0	1.28	0.015	0.435	-	-	400ppm	1.0	-	77.3	20.7	-	-	0.9
16	735.0	1.28	0.435	3.335	-	-	140ppm	0.4	-	27.1	6.7	-	-	0.3
19	774.2	1.13	0.003	0.072	-	-	34.7	65.1	-	0.3	5ppm	-	-	-
20	156.6	1.11	0.003	0.072	-	-	34.7	65.1	-	0.3	5ppm	-	-	-
21	30.0	1.08	0.002	0.031	-	-	-	100.0*	-	-	-	-	-	-
22	30.0	1.08	0.001	0.041	-	-	96.0	3.2	-	0.8	13ppm	-	-	-
23	30.0	80.0	0.001	0.041	-	-	96.0	3.2	-	0.8	13ppm	-	-	-
24	37.7	110.0	0.001	0.041	-	-	96.0	3.2	-	0.8	13ppm	-	-	-
25	65.0	0.219	0.004	0.326	-	-	-	-	100.0*	-	-	-	-	-
26	65.3	4.00	0.004	0.326	-	-	-	-	100.0*	-	-	-	-	-
27a	138.0	3.92	0.004	0.326	-	-	-	-	100.0*	-	-	-	-	-
27b	140.8	37.5	0.004	0.326	-	-	-	-	100.0*	-	-	-	-	-
28	232.6	30.0	0.004	0.326	-	-	-	-	100.0*	-	-	-	-	-
29	300.0	30.0	0.004	0.326	-	-	-	-	100.0	-	-	-	-	-
30	171.5	0.223	0.004	0.326	-	-	-	-	100.0	-	-	-	-	-
31	80.0	0.219	0.004	0.326	-	-	-	-	100.0	-	-	-	-	-
16	735.0	1.28	0.435	3.335	*molar fraction* CuO 33.3%; ZrO_2 32.2%									
17	735.0	1.28	9.521	961.86	*weight fraction*: CuO 40%; ZrO_2 60%									
18	756.1	1.28	9.428	960.40	*weight fraction*: CuO 38.6%; Cu_2O 1.4%; ZrO_2 60%									

List of Figures

List of Tables

List of Abbreviations

AAU	Assigned Amount Unit
ASU	Air Separation Unit
AR	Air Reactor
ATR	Auto Thermal Reforming
CCA	Cost of CO_2 Avoided
CCR	Carbon Capture Ratio
CCS	Carbon Capture and Storage
CDM	Clean Development Mechanism
CER	Certified Emission Reduction
CLC	Chemical Looping Combustion
CLR	Chemical Looping Reforming
DEA	Diethanolamine
DIR	Direct Internal Reforming
ECO	Economizer
EOR	Enhanced Oil Recovery
ERU	Emission Reduction Unit
EU	European Union
EU ETS	The EU Emissions Trading System
EVA	Evaporator
FBMR	Fluidized Bed Membrane Reactor
FTR	Fired Tubular Reforming
FR	Fuel Reactor
HRSG	Heat Recovery Steam Generator
HT	High Temperature
IEA	International Energy Agency
IGCC	Integrated Gasification Combined Cycle
IIR	Indirect Internal Reforming
IP	Intermediate Pressure
IPCC	Intergovernmental Panel on Climate Change
IT	Intermediate Temperature
JI	Joint Implementation
LHV	Low Heating Value
LP	Low Pressure
LT	Low Temperature
MDEA	Methyl-di-ethanolamine
MEA	Methyl-ethanolamine
NG	Natural Gas
OC	Oxygen Carrier
OECD	Organization for Economic Co-operation and Development
PEM	Proton Exchange Membrane
PH	Pre-Heater
ppmv	Part Per Million in Volume
ppm	Part Per Milion
PSA	Pressure Swing Adsorption

S/C	Steam to Carbon ratio
SH	Super Heating
SMR	Steam Methane Reforming
SPECCA	Equivalent Specific Primary Energy Consumption for CO_2 Avoided
SOFC	Solid Oxide Fuel Cell
WGS	Water gas shift
WMO	World Meteorological Organization
TPES	Total Primary Energy Supplies
UN	United Nations
UNFCC	United Nations Framework Convention on Climate Change

References

[1] Intergovernmental Panel On Climate Change, “IPCC Fourth Assessment Report: Climate Change 2007”, 2007.

[2] Intergovernmental Panel On Climate Change, “IPCC Fifth Assessment Report: Climate Change 2013”, 2013.

[3] http://www.iea.org/

[4] A. Galliani, “L’energia primaria: fonti e fabbisogni,” Politecnico di Milano, 2015.

[5] A. Galliani, “Il protocollo di Kyoto e gli obiettivi europei 2020. Il ruolo delle fonti rinnovabili e dell’efficienza energetica,” Politecnico di Milano, 2015.

[6] A. Galliani, “Il sistema europeo di scambio dei permessi di emissione (EU Emission Trading System),” Politecnico di Milano, 2015.

[7] G. Groppi, “Assorbimento,” Politecnico di Milano, 2014.

[8] P. Chiesa, “Tecnologie per la generazione di elettricitá e di idrogeno in centrali con emissioni fortemente ridotte di anidride carbonica,” Politecnico di Milano, 2015.

[9] A. Galliani, “Strumenti di promozione dell’efficienza energetica,” Politecnico di Milano, 2015.

[10] S. Douvartzides, F. Coutelieris, P. Tsiakaras, “Exergy analysis of a solid oxide fuel cell power plant fed by either ethanol or methane,” *Journal of Power Sources*, vol. 131, pp. 224-230, 2004.

[11] E. Pedrocchi, A. Galliani, *Analisi exergetica*. Polipress, 2014.

[12] E. Achenbach, E. Riensche, “Methane steam reforming kinetics for solid oxide fuel cells,” *Journal of Power Sources*, vol. 52, pp. 283-288, 1994.

[13] J. Divisek, L. Haart, P. Holtappels, “The kinetics of electrochemical reactions on high temperature fuel cell electrodes,” *Journal of Power Sources*, vol. 49, pp. 257-270, 1994.

[14] V. Spallina, L. Mastropasqua, P. Iora, M. C. Romano, S. Campanari, “Assessment of finite volume modeling approaches for intermediate temperature solid oxide fuel cells working with CO-rich syngas fuels,” *International Journal of Hydrogen Energy*, vol. 40, pp. 15012-15031, 2015.

[15] T. Numaguchi, K. Kikuchi, “Intrinsic kinetics and design simulation in a complex reaction network; steam-methane reforming,” *Chemical Engineering Science*, vol. 43, pp. 2295-2301, 1988.

[16] P. Aguiar, C. Adjiman, N. Brandon, "Anode-supported intermediate temperature direct internal reforming solid oxide fuel cell. I: Model-based steady-state performance," *Journal of Power Sources*, vol. 138, pp. 120-136, 2004.

[17] R. Suwanwarangkul, E. Croiset, E. Entchev, S. Charojrochkul, M. D. Pritzker, M. W. Fowler, "Experimental and modeling study of solid oxide fuel cell operating with syngas fuel," *Journal of Power Sources*, vol. 161, pp. 308-322, 2006.

[18] S. Campanari, P. Iora, "Comparison of finite volume SOFC models for the simulation of a planar cell geometry," *Fuel Cells*, vol. 5, pp. 34-51, 2005.

[19] S. Campanari, P. Iora, "Definition and sensitivity analysis of a finite volume SOFC model for a tubular cell geometry," *Journal of Power Sources*, vol. 132, pp. 113-126, 2004.

[20] M. Boder, R. Dittmeyer, "Catalytic of conventional SOFC anodes with a view to reducing their activity for direct internal reforming of natural gas," *Journal of Power Sources*, vol. 155, pp. 13-22, 2006.

[21] H. Z. Martin, C. E. Heminger, *United States Patent Office*, n∘ 2665199, 10th December 1946.

[22] W. K. Lewis, E. R. Gilliland, "Carbon-steam reaction at low temperatures," *Reactions of Carbon – Part of Symposium on Properties and Reactions of Carbon presented before the Division of Gas and Fuel Chemistry*, 122nd meeting, 1950.

[23] K. F. Knoche, H. J. Richter, ''Reversibility of combustion processes'', 1983.

[24] M. Ishida, D. Zheng, T. Akehata, "Evaluation of a chemical-looping-combustion power-generation system by graphic exergy analysis," *Energy*, vol. 12, pp. 147-154, 1987.

[25] M. Hossan, H. de Lasa, "Chemical-looping combustion (CLC) for inherent CO_2 separations – a review," *Chemical Engineering Science*, vol. 63, pp. 4433-4451, 2008.

[26] V. Spallina, "Chemical Looping Technologies: state of the art and future perspectives," TU/Eindhoven, 2016.

[27] T. Mattisson, M. Johansson, A. Lyngfelt, "The use of NiO as an oxygen carrier in chemical-looping combustion," *Fuel*, vol. 85, pp. 736-747, 2006.

[28] J. Bolhár-Nordenkampf, T. Proll, P. Kolbitsch, H. Hofbauer, "Performance of a NiO-based oxygen carrier for chemical looping combustion and reforming in a 120 kW unit," *Energy Procedia*, vol. 1, pp. 19-25, 2009.

[29] M. Ishida, H. Jin, "A novel chemical looping combustor without NO_x formation," *Research notes – Tokyo University of Technology*, vol. 5885, pp. 2469-2472, 1996.

[30] F. He, H. Wang, Y. Dai, "Application of Fe_2O_3/Al_2O_3 composite particles as oxygen carrier of chemical looping combustion," *Journal of Natural Gas Chemistry,* vol. 16, pp. 155-161, 2007.

[31] Q. Zafar, T Mattisson, B. Gevert, "Redox investigation of some oxides of transition-state metals Ni, Cu, Fe and supported on SiO_2 and $MgAl_2O_4$," *Energy & Fuels*, vol. 20, pp. 34-44, 2006.

[32] B. Corbella, J. Palacios, "Titania-supported Iron oxide as oxygen carrier for chemical-looping combustion of methane," *Fuel*, vol. 86, pp. 113-122, 2007.

[33] Q. Zafar, T Mattisson, B. Gevert, "Integrated Hydrogen and power production with CO_2 capture using chemical-looping reforming redox reactivity of particles of CuO, Mn_2O_3, NiO and Fe_2O_3 using SiO_2 as support," *Industrial & Engineering Chemistry Research*, vol. 2, pp. 3485-3496, 2005.

[34] T. Mattisson, F. Garcia-Labiano, B. Kronberger, A. Lyngfelt, J. Adanez, H. Hofbauer, "Chemical-looping combustion using syngas as fuel," *International Journal of Greenhouse Gas Control*, vol. 1, pp. 158-169, 2007.

[35] L. F. De Diego, F. Garcia-Labiano, J. Adanez, P. Gayan, A. Abad, B. M. Corbella, J. M. Palacios, "Development of Cu-based oxygen carriers for chemical-looping combustion," *Fuel*, vol. 83, pp. 1749-1757, 2004.

[36] M. M. Azis, E. Jerndal, H. Leion, T. Mattisson, A. Lyngfelt, "On the evaluation of synthetic and natural ilmenite using syngas as fuel in chemical-looping combustion (CLC)," *Chemical Engineering Research and Design*, vol. 88, pp. 1505-1514, 2010.

[37] H. Leion, A. Lyngfelt, M. Johansson, E. Jerndal, T. Mattisson, "The use of ilmenite as an oxygen carrier in chemical-looping combustion," *Chemical Engineering Research and Design*, vol. 86, pp. 1017-1026, 2008.

[38] B. Kronberger, A. Lyngfelt, G. Lo, H. Hofbauer, "Design and Fluid Dynamic Analysis of a Bench-Scale Combustion System with CO Separation – Chemical-Looping Combustion," *Industrial Engineering Chemistry Research*, vol. 44, pp. 546-556, 2005.

[39] J. Adanez, L. Diego, P. Gayan, J. M. Palacios, A. Abad, "Selection of Oxygen Carriers for Chemical-Looping Combustion Selection of Oxygen Carriers for Chemical-Looping Combustion," *Energy & Fuels*, vol. 18, pp. 371-377, 2004.

[40] Ø. Brandvoll, O. Bolland, "Inherent CO_2 Capture Using Chemical Looping Combustion in a Natural Gas Fired Power Cycle," *Journal of Engineering for Gas Turbines and Power*, vol. 126, pp. 316-321, 2004.

[41] S. Campanari, M. Gazzani, L. Mastropasqua, P. Chiesa, M. C. Romano, "Predicting the ultimate potential of natural gas SOFC power cycles with CO_2 capture," 2016.

[42] http://www.fuelcellenergy.com/, 2015.

[43] K. Foger, T. Rowe "Ultra-High-Efficiency Residential Power System", 3rd European Fuel Cell Technology Applications Conference, Rome, Dec. 2009.

[44] L. Mastropasqua, S. Campanari, P. Iora, M. C. Romano "Simulation of intermediate-temperature SOFC for 60%+ efficiency distributed generation", Proc. of ASME 2015 Power and Energy Conversion Conference, PowerEnergy 2015-49373, USA, June 2015.

[45] S. Consonni, F. Viganó, "Waste gasification vs. conventional Waste-To-Energy: A comparative evaluation of two commercial technologies," *Waste Management*, vol. 32, pp. 653-666, 2012.

[46] T. Elmer, M. Worall, S.Wu, S. B. Riffat "Emission and economic performance assessment of a solid oxide fuel cell micro-combined heat and power system in a domestic building" *Applied Thermal Engineering*, vol. 90, pp. 1082-1089, April 2015.

[47] D. Pandolfo, "Techno-economic analysis of innovative systems of hydrogen production from natural gas with membrane reactors and low CO2 emissions," Politecnico di Milano, 2014.

[48] G. O. Alptekin, A. Jayaraman, M. Dubovik, M. Schaefer, W. Mike, K. Bradley "Natural Gas Desulfurization for Fuel Cell Applications by Adsorption," 2008.

[49] M. Johansson, T. Mattisson, A. Lyngfelt "Comparison of oxygen carriers for Chemical-Looping combustion," *Thermal Science*, vol. 10, pp. 93-107, 2006.

[50] I. Martinez, M. C. Romano, P. Chiesa, G. Grasa, R. Murillo "Hydrogen production through sorption enhanced steam reforming of natural gas: Thermodynamic plant assessment," *International Journal of Hydrogen Energy*, vol. 38, pp. 15180-15199, 2013.

[51] T. Takeguchi, Y. Kani, T. Yano, R. Kikuchi, K. Eguchi, K. Tsujimoto, Y. Uchida, A. Ueno, K. Omoshiki, M. Aizawa "Study on steam reforming of CH4 and C2 hydrocarbons and carbon deposition on Ni-YSZ cermets," *Journal of Power Sources*, pp. 588-595, 1989.

[52] R. W. Breault, V. K. Mathur "High-velocity Fluidized Bed Hydrodynamic Modeling. 1. Fundamental Studies of Pressure Drop," *Ind. Eng. Chem. Res.*, vol. 112, pp. 684-688, 2002.

[53] J. Adanez, A. Abad, F. Garcia-Labiano, P. Gayan, L. De Diego "Progress in chemical-looping combustion and reforming technologies," *Progress in Energy and Combustion Science*, vol. 38, pp. 215-282, 2012.

[54] T. Mattisson, M. Johansson, A. Lyngfelt "The use of NiO as an Oxygen Carrier in Chemical-Looping Combustion," *Fuel*, vol. 85, pp. 736-747, 2006.

[55] M. Johansson "Screening of oxygen-carrier particles based on iron-, manganese-, copper- and nickel oxides for use in chemical-looping technologies," 2007.

[56] P. Colonna "Organic Rankine Cycle Power Systems: from the concept to current technology, applications and an outlook to the future," *Journal of Engineering for Gas Turbine and Power*, vol. 137, 2015.

[57] S. Zamblera, "Ottimizzazione di forma di pale di turbina centrifuga ORC mediante l'impiego di algoritmi evolutivi," Politecnico di Milano, 2015.

[58] G. Manzolini, "Biomass – Conversion processes," Politecnico di Milano, 2014.

[59] www.triogen.nl

[60] N. Palestra, R. Vescovo "Applicazione di Cicli ORC a Recuperi Termici da Processi Industriali," E.ON Energia Spa, Turboden Srl, 2009.

[61] www.union.dk

[62] E. Liese "Comparison of Preanode and Postanode Carbon Dioxide Separation for IGFC Systems," *Journal of Gas Turbines Power*, 2010.

[63] M. C. Romano, V. Spallina, S. Campanari "Integrating IT-SOFC and gasification combined cycle with methanation reactor and hydrogen firing for near zero-emission power generation from coal," *Energy Procedia*, 2011.

[64] V. Spallina, M. C. Romano, S. Campanari, G. Lozza "A SOFC-Based Integrated Gasification Fuel Cell Cycle With CO2 Capture," *Journal of Gas Turbines Power*, 2010.

[65] M. Li, A.D. Rao, J. Brouwer, G.S. Samuelsen "Design of highly efficient coal-based integrated gasification fuel cell power plants," *Journal of Power Sources*, 2010.

[66] M.C. Romano, S. Campanari, V. Spallina, G. Lozza "Thermodynamic Analysis and Optimization of IT-SOFC-Based Integrated Coal Gasification Fuel Cell Power Plants," *Journal of Fuel Cell*, 2011.

[67] S. Chen, N. Lior, W. Xiang "Coal gasification integration with solid oxide fuel cell and chemical looping combustion for high-efficiency power generation with inherent CO_2 capture," *Apply Energy*, 2015.

[68] P. Ohlemüller, J.P. Busch, M. Reitz, J. Ströhle, B. Epple "Chemical-Looping Combustion of Hard Coal: Autothermal Operation of a 1 MW th Pilot Plant," *Journal of Energy*, 2016.

[69] S. Quoilin, M. Broek, S. Declaye, P. Dewallef, V. Lemort "Techno-economic survey of organic rankine cycle (ORC) systems," *Reneawable Sustain Energy*, 2013.

[70] V. Spallina, P. Nocerino, M. C. Romano, M. van Sint Annaland, S. Campanari, F. Gallucci "Integration of Solid Oxide Fuel Cell and Chemical Looping Combustion for efficient power production with CO_2 capture," *4th International Conference on Chemical Looping*, 26th - 28th September 2016, Southeast University of Nanjing, China.